

620.51
P97He
1091

SCHOOL OF CIVIL ENGINEERING

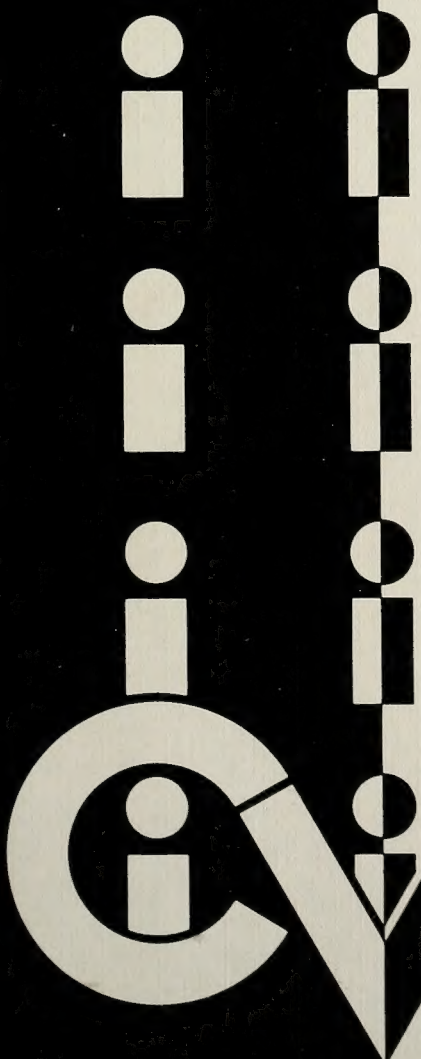
INDIANA DEPARTMENT OF HIGHWAYS

JOINT HIGHWAY RESEARCH PROJECT

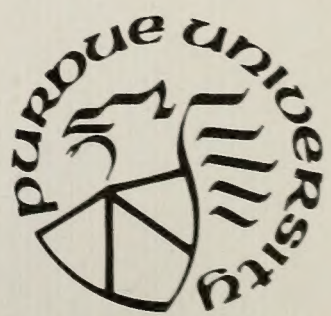
FHWA/IN/JHRP-82-1

STRENGTH OF FIELD COMPACTED
CLAYEY EMBANKMENTS

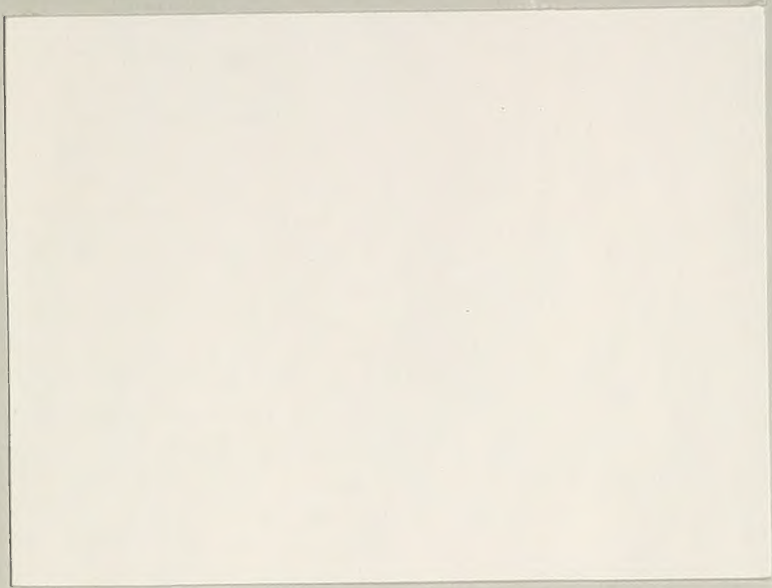
Y. Liang and C. W. Lovell



8



PURDUE UNIVERSITY



{

JOINT HIGHWAY RESEARCH PROJECT

FHWA/IN/JHRP-82-1

STRENGTH OF FIELD COMPACTED
CLAYEY EMBANKMENTS

Y. Liang and C. W. Lovell

Interim Report

STRENGTH OF FIELD COMPACTED CLAYEY EMBANKMENTS

To: H. L. Michael, Director
Joint Highway Research Project

February 2, 1982

Project: C-36-5M

From: C. W. Lovell, Research Engineer
Joint Highway Research Project

File: 6-6-13

Attached is an Interim Report on the HPR Part II Study titled "Improving Embankment Design and Performance". This is Interim Report No. 10 and is titled "Strength of Field Compacted Clayey Embankments". It is authored by Y. Liang and C. W. Lovell of our staff.

The report describes the shearing behavior of field-compacted St. Croix clay. The experimental test parameters were related to the compaction variables and statistically valid prediction equations were produced. The laboratory-compacted and field-compacted relationships are functions of the same variable; therefore they can be simply related.

The Report is presented for acceptance as partial fulfillment of the objectives of the HPR Project of which it is a part. Review by all sponsors will result in a final copy which will be published.

Respectfully submitted,

C. W. Lovell/nw

C. W. Lovell
Research Engineer

CWL/nw

cc:	A. G. Altschaeffl	M. J. Gutzwiller	C. F. Scholer
	J. M. Bell	G. K. Hallock	K. C. Sinha
	W. L. Dolch	J. F. McLaughlin	C. A. Venable
	R. L. Eskew	R. D. Miles	L. E. Wood
	G. D. Gibson	P. L. Owens	E. J. Yoder
	W. H. Goetz	G. T. Satterly	S. R. Yoder

Interim Report

STRENGTH OF FIELD COMPACTED CLAYEY EMBANKMENTS

by

Yueh Liang
Graduate Instructor in Research

and

C. W. Lovell
Professor of Civil Engineering

Joint Highway Research Project

Project No.: C-36-5M

File No.: 6-6-13

Prepared as a Part of an Investigation

Conducted by

Joint Highway Research Project
Engineering Experiment Station
Purdue University

in cooperation with the

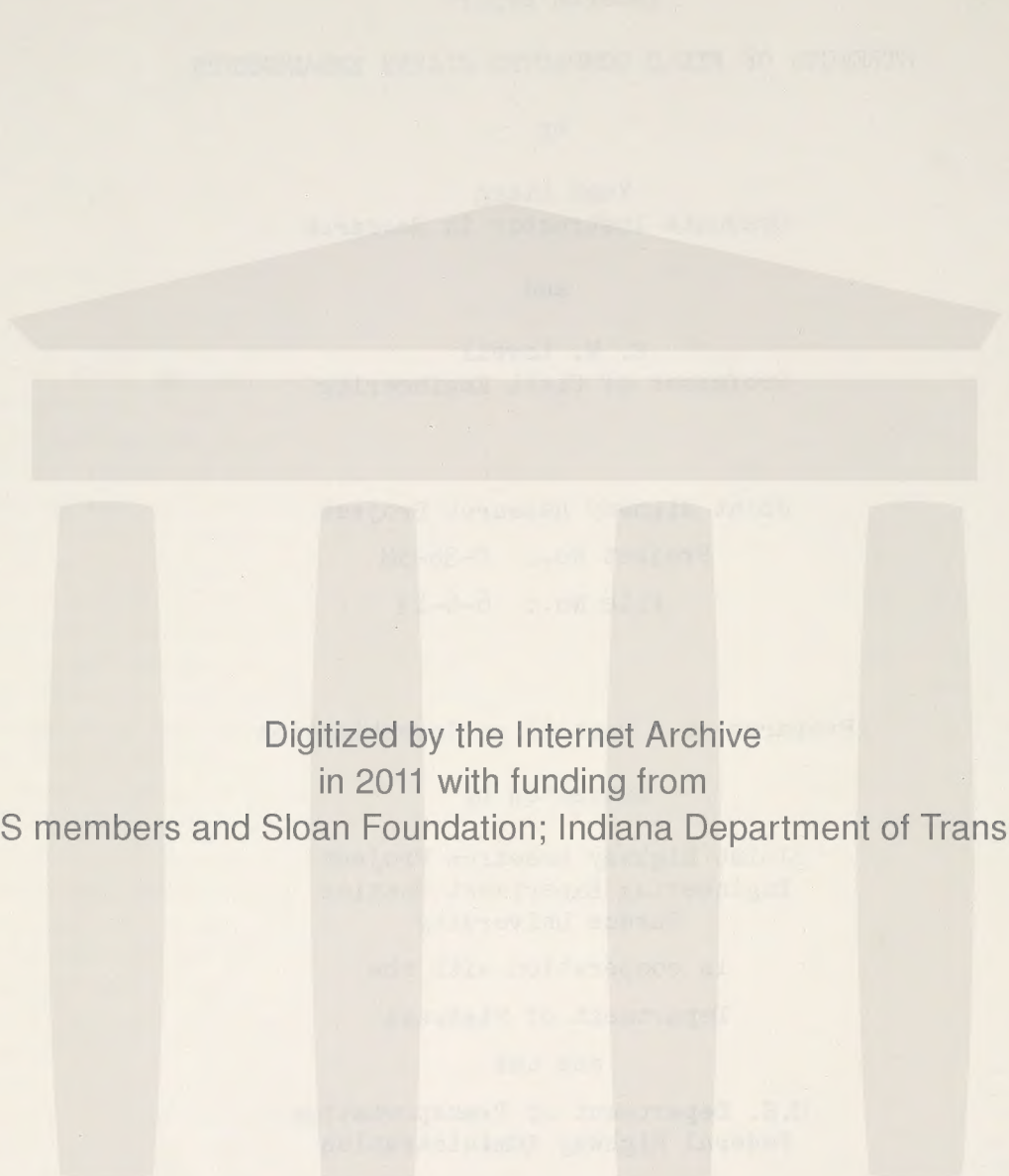
Department of Highways

and the

U.S. Department of Transportation
Federal Highway Administration

The contents of this report reflect the views of the authors who are responsible for the facts and the accuracy of the data presented herein. The contents do not necessarily reflect the official views or policies of the Federal Highway Administration. This report does not constitute a standard, specification, or regulation.

Purdue University
West Lafayette, Indiana
February 2, 1982



Digitized by the Internet Archive
in 2011 with funding from

LYRASIS members and Sloan Foundation; Indiana Department of Transportation

TECHNICAL REPORT STANDARD TITLE PAGE

1. Report No. FHWA/IN/JHRP-82/1	2. Government Accession No.	3. Recipient's Catalog No.	
4. Title and Subtitle STRENGTH OF FIELD COMPACTED CLAYEY EMBANKMENTS		5. Report Date February 2, 1982	
7. Author(s) Y. Liang and C. W. Lovell		6. Performing Organization Code	
9. Performing Organization Name and Address Joint Highway Research Project Civil Engineering Building Purdue University West Lafayette, Indiana 47907		10. Work Unit No.	
12. Sponsoring Agency Name and Address* Indiana Department of Highways State Office Building 100 North Senate Avenue Indianapolis, Indiana 46204		11. Contract or Grant No. HPR-1(19) Part II	
15. Supplementary Notes Prepared in cooperation with the U.S. Department of Transportation, Federal Highway Administration. Part of the study titled "Improving Embankment Design and Performance".		13. Type of Report and Period Covered Interim Report Field Compacted Phase	
16. Abstract The shearing behavior of a plastic Indiana clay (St. Croix) was studied for both laboratory and field compaction. This interim report deals with the field compacted phase. The strength tests were performed by unconsolidated undrained (UU) and saturated consolidated-undrained (CU) triaxials. These were run at various confining pressures to approximate the end of construction and long term conditions at several embankment depths. Statistical analyses were performed to establish the best predictive models for dry density, as-compacted strength, volume change due to saturation and consolidation, Skempton's A parameter at failure and the effective stress strength parameter (c' and ϕ'), in terms of the field compaction variables. Predictions of field compacted relationships from laboratory tests can be accomplished for soils which are somewhat different by applying a translation factor based upon the ratio of standard Proctor optimum moisture contents.			
17. Key Words field compaction, as-compacted strength, effective stress shear parameters, clay, volume change, lab. vs. field relations	18. Distribution Statement No restrictions. This document is available to the public through the National Technical Information Service, Springfield, Virginia 22161.		
19. Security Classif. (of this report) Unclassified	20. Security Classif. (of this page) Unclassified	21. No. of Pages 212	22. Price

ACKNOWLEDGMENTS

Special thanks are extended to Professor R. D. Holtz for his valuable counsel and helpful review of the manuscript. The kind encouragement provided by Professor A. G. Altschaeffl is much appreciated.

Thanks are also extended to Professor E. C. Ting for his service on the Advisory Committee. Thanks are due to Professor George McCabe for his help and advice in developing the statistical analysis used in this study.

Dr. R. A. Abeysekera is specially thanked for his laboratory assistance and valuable suggestions for improvement. Special thanks go to Dr. P. S. Lin for his assistance as a research partner.

The author is grateful for the financial support provided by the Joint Highway Research Project of Purdue University, the Indiana Department of Highways, and the Federal Highway Administration.

Mrs. Ziza Saleeb and Mr. Tim Gilbert did the drafting work. Nancy Warren typed the final manuscript. Thanks are extended to all of them.

TABLE OF CONTENTS

	Page
LIST OF TABLES	vi
LIST OF FIGURES	ix
LIST OF ABBREVIATIONS AND SYMBOLS	xxi
HIGHLIGHT SUMMARY	xxiv
INTRODUCTION	1
1- LITERATURE REVIEW	3
1-1 Theories for the Mechanics of Compaction	3
1-2 Shear Strength of Compacted Fine Grained Soils	8
1-2-1 Effective Stress in Saturated Soil	11
1-2-2 Effective Stress in Unsaturated Soil	11
1-2-3 Stress-Strain Characteristics	18
1-2-4 Statistical Prediction Model for the Strength of Compacted Clay	22
1-3 Volume Change Characteristics	27
1-3-1 Volume Change of Partially Saturated Soil	27
1-3-2 Volume Change Due to Saturation	29
1-4 Pore Pressure Response During Undrained Shear	35
1-5 Comparison of Field and Laboratory Compacted Strength	45
2- APPARATUS AND EXPERIMENTAL PROCEDURE	57
2-1 Soil Studied	57
2-2 Field Compacted Samples	58

	Page
2-2-1 Test Pad Construction	58
2-2-2 Field Sampling	66
2-3 Experimental Design	69
2-4 Preparation of Specimens	71
2-5 Strain Rates for Triaxial Testing	75
2-6 Unconsolidated-Undrained Triaxial Compression Test	75
2-6-1 Test Apparatus	75
2-6-2 Test Procedure	76
2-7 Consolidated Undrained Triaxial Compression Test	85
2-7-1 Test Apparatus	85
2-7-2 Back Pressure Saturation	87
2-7-3 Consolidation	91
2-7-4 Undrained Shear	93
3. RESULTS AND DISCUSSION OF RESULTS	94
3-1 Analysis of Results	94
3-1-1 Field Compaction	94
3-1-2 Unconsolidation-Undrained Shear Strength	100
3-1-2.1 Stress-Strain Behavior	100
3-1-2.2 The $e_f \sqrt{S_f} - \log (q_c / 2)$ Relationship	121
3-1-3 Consolidated-Undrained Shear Strength	121
3-1-3.1 Volume Change Due to Saturation and Consolidation	130
3-1-3.2 Stress-Strain and Pore Water Pressure Response.	138

3-2 Statistical Analysis	146
3-2-1 Density Prediction Models	151
3-2-2 As-Compacted Strength Prediction Model	154
3-2-3 Prediction Model for Volume Change Due to Saturation and Consolidation	166
3-2-4 Prediction Model for Skempton's A Parameter at Failure	177
3-2-5 Prediction Model for the Effective Stress Parameters, \hat{c}' and $\hat{\phi}'$	182
3-3 Application of Results	195
4. CONCLUSIONS AND RECOMMENDATIONS	206
4-1 Conclusions	206
4-2 Recommendations for Future Research	209
BIBLIOGRAPHY	210
APPENDICES	
Appendix A - Results from UU Tests	219
Appendix B - Results from CIU Tests	255
Appendix C - \hat{p}'_f versus \hat{q}_f Failure Lines	291
Appendix D - List of Negative Number for Photographs	312

LIST OF TABLES

Table		Page
1-1	Effective Stress Equation for Partially Saturated Soils	19
1-2	Regression Results for a Laboratory Compacted Clayey Silt (from Essigmann, 1976 and Scott, 1977)	24
1-3	Regression Results from Field Compacted Samples of Silty Clay (from Price, 1978)	25
1-4a	Value of Parameter A_f (Lambe and Whitman, 1969)	42
1-4b	Value of Parameter B (Lambe and Whitman, 1969)	42
1-5	Characteristic Variables Pertaining to the Different Type of Field Compacting Equipment (After Wahls, et al., 1966)	46
1-6	Summary of Equations by Selig (1971)	47
2-1	Index Properties and Classification of St. Croix Clay	58
2-2	Field Compaction Equipment Specifications	63
2-3	Design for the Study of UU Strengths.	72
2-4	Design for the Study of CIU Strengths	73
3-1	The Variations of Water Content and Dry Density for Each Test Pad Compacted by the Rascal Type of Roller	95
3-2	The Variations of Water Content and Dry Density for Each Test Pad Compacted by the Caterpillar Type of Roller	96
3-3	Compaction Pressure	99
3-4	The Variation of Atterberg Limits (%) for Each Test Pad	101

Table		Page
3-5	Failure Conditions for Unconsolidated-Undrained Triaxial Tests	106
3-6	Values of OCR, Volumetric Strain at Failure and at End of Test	112
3-7	Volume Change Data	115
3-8	Back Pressure Required to Attain the Experimentally Observed Degree of Saturation	127
3-9	Volume Change Due to Saturation and Consolidation	131
3-10	Failure Conditions for Consolidated Undrained Triaxial Tests	142
3-11	Basic Compaction Variables for Dry Density	152
3-12	Statistical Data for Density Prediction	153
3-13	Basic Compaction Variables for As-Compacted Compressive Strength at Failure	158
3-14	Statistical Data for As-Compacted Strength Model	164
3-15	Basic Compaction Variables for Percent Volume Change Due to Saturation and Consolidation	169
3-16	Statistical Data of the Prediction Models for Percent Volume Change Due to Saturation and Consolidation	174
3-17	Basic Compaction Variables for Skempton's A Parameter at Failure	178
3-18	Statistical Data of the Prediction Model for Skempton's A Parameter at Failure	181
3-19	Regression Models for Pore Pressure and Soaked Strength at Failure	187
3-20	Basic Compaction Variables for the Effective Stress Strength Parameters	191

Table		Page
3-21	Statistical Data of the Prediction Model for Effective Stress Strength Parameters	193
3-22	Regression Results	196

LIST OF FIGURES

Figure	Page
1-1 X-Factor vs. Degree of Saturation (After Bishop and Henkel, 1962)	13
1-2 Relationship of Dry Density, Pore Water Pressure, and X-Factor to Molding Water Content (After Wahls, et al., 1966)	15
1-3 Influence of Molding Water Content on Stress-Strain Relationship for Compacted Kaolinite (from Seed and Chan, 1959)	21
1-4 Classification of Stress-Strain Curves (After Casagrande and Hirschfeld, 1962)	23
1-5 Volumetric Strain Behavior During an Unconsolidated-Undrained Triaxial Test (After Conlin, 1972)	30
1-6 Prediction of Percent Volume Change on Wetting (After DiBernardo, 1979)	33
1-7 Effect of Void Ratio on Percent Volume Change Model at a Constant Water Content (After Lin, 1981)	34
1-8 Prediction of Percent Volume Change Due to Saturation and Consolidation (After Johnson, 1979)	36
1-9 Contours of Percent Volume Change (After Abeysekera, 1978)	37
1-10 The Dependence of the Pore Pressure Parameter A on Stress History (After Bishop, 1960)	39
1-11 A_f versus Overconsolidation Ratio (After Henkel, 1956)	40
1-12a Relationship Between A_f and the Ratio of the Consolidation Pressure to the Preconsolidation Pressure (After Bjerrum, 1960) . . .	41

Figure	Page
1-12b Relationship Between A_f and Overconsolidation Ratio (After Simons, 1960)	41
1-13 Variation of A_f with $\log(P_c/\sigma'_c)$ for Compacted Specimens Having Different Initial Gradations and Molding Water Contents (After Abeysekera et al., 1978)	43
1-14 Prediction of Skempton's A Parameter at Failure for an Initial Saturation of 80% (After Johnson, 1979)	44
1-15 Comparison of Field and Laboratory Compaction and CBR (After WES, 1949)	50
1-16 Laboratory to Field Strength Correlation: Sheepfoot Roller, As-Compacted (After Price, 1978)	52
1-17 Laboratory to Field Strength Correlation: Rubber-Tired Roller, Soaked (After Price, 1978)	53
1-18 Laboratory to Field Strength Correlation: Rubber-Tired Roller, As-Compacted (After Price, 1978)	54
1-19 Compactive Prestress Models (After Lin, 1981)	56
2-1 Boring Profile (IDOH, Indiana Department of Highways)	59
2-2 Laboratory Impact Compaction Curves for Test Pad and Laboratory Study, St. Croix Clay	60
2-3 Test Pad Showing Pad Number, Water Content Level, and Compactor Type	62
2-4 Rascal Compaction Curves for Field Nuclear Gage Values (After Terdich, 1981)	64
2-5 Caterpillar Compaction Curves for Field Nuclear Gage Values (After Terdich, 1981)	65

Figure		Page
2-6	Typical Field Sample Label	67
2-7	Driving Assembly with Sampling Tube	68
2-8	Hydraulic Jack Used for Extrusion of Tube Samples	70
2-9	Volume Change Measuring Device	77
2-10	Calibration of Cell Expansion (After 10 min. Application of Confining Pressure)	79
2-11	Calibration of Triaxial Cell Expansion Under Creep (After Application of Cell Pressure for 25 min.)	80
2-12	Calibration for Volume Change Due to Temperature Change	81
2-13	Disassembled Triaxial Cell	86
2-14	Schematic of the Saturation- Consolidation System	88
2-15A	Back Pressure Required for Various Degrees of Saturation (After Lowe and Johnson, 1960)	89
2-15B	Time Needed to Saturate Sample by Using Back Pressure (After Black and Lee, 1973)	89
2-16	Plot of B Versus Back Pressure with Typical Sample Responses (After Chaney, 1980)	92
3-1	Correspondence Between Caterpillar Roller and Impact Method	97
3-2	Correspondence Between Rascal Roller and Impact Method	98
3-3	Dry Density-Water Content Relationship Before Test for UU Triaxial Test Specimens at 276 kpa Confinement	102

Figure	Page
3-4 Dry Density-Water Content Relationship Before Test for UU Triaxial Test Specimen at 138 kpa Confinement	103
3-5 Dry Density-Water Content Relationship Before Test for UU Triaxial Test Specimen at 69 kpa Confinement	104
3-6 Joint Region of Observations for UU Compression Strength Prediction Model	105
3-7 Axial Stress and Volumetric Strain Vs. Axial Strain for Samples R2B7, R1B1, R3B10, R5C9	109
3-8 OCR Vs. Volumetric Strain Due to Shear up to Failure	111
3-9 Water Content Vs. Volumetric Strain During Application of Confining Pressure for Caterpillar Samples	119
3-10 Water Content Vs. Volumetric Strain During Application of Confining Pressure for Rascal Samples	120
3-11 Void Ratio Times Square Root of Saturation at Failure Vs. Logarithm of One Half the Compression Strength	122
3-12 Caterpillar Dry Density-Water Content Relationship Before Test for CIU Triaxial Test Specimens	123
3-13 Rascal Dry Density-Water Content Relationship Before Test for CIU Triaxial Test Specimens	124
3-14 Joint Region of Observations for CIU Compression Strength Prediction Model	125
3-15 Percent Volume Change Upon Saturation Vs. Initial Void Ratio for All Samples	134
3-16 Caterpillar Percent Volume Change Upon Saturation and Consolidation Vs. Consolidation Pressure	136

Figure	Page
3-17 Rascal Percent Volume Change Upon Saturation and Consolidation Vs. Consolidation Pressure	137
3-18 CIU Results for Samples R3C2, C5B6, and R2B8	139
3-19 CIU Results for Samples C2C4, C3B2, and CLA3	140
3-20 CIU Results for Samples R2A5, RLBl0, and C4B6	141
3-21 CIU Results for Samples C4B6, C5C7	145
3-22 Caterpillar A_f Vs. Consolidation Pressure	147
3-23 Rascal A_f Vs. Consolidation Pressure	148
3-24 Joint Region of Observations for Dry Density Prediction Model	155
3-25 Wet-of-Optimum Dry Density Model	156
3-26 All Moistures Dry Density Models	157
3-27 Predicted Field As-Compacted Strength-Water Content Relationship at a Constant Initial Void Ratio	165
3-28 Predicted Laboratory As-Compacted Strength-Water Content Relationship at a Constant Initial Void Ratio	167
3-29 Predicted Compressive Strength-Dry Density Relationship at a Constant Confining Pressure	168
3-30 Prediction of Field Percent Volume Change Due to Saturation and Consolidation at a Constant Initial Void Ratio	175
3-31 Prediction of Laboratory Percent Volume Change Due to Saturation and Consolidation at a Constant Initial Void Ratio	176

Figure	Page
3-32 Field Skempton's A Parameter at Failure Versus OCR at a Constant Initial Saturation	183
3-33 Laboratory Skempton's A Parameter at Failure Versus OCR at a Constant Initial Saturation	184
3-34 Field Skempton's A Parameter at Failure Versus OCR at a Constant Initial Void Ratio	185
3-35 Laboratory Skempton's A Parameter at Failure Versus OCR at a Constant Void Ratio	186
3-36 \hat{p}_f' Versus \hat{q}_f Failure Line	189
3-37 \hat{p}_f' Versus \hat{q}_f Failure Line	190
3-38 Prediction of Field Effective Stress Strength Parameters, c' and ϕ'	194
4-1 The Predicted Dry Density for Field Compacted and Translated Laboratory Compacted Soils	201

Appendix
Figure

A1 Axial Stress and Volumetric Strain Vs. Axial Strain for Samples C1A2, C2A3, C3A7	219
A2 Axial Stress and Volumetric Strain Vs. Axial Strain for Samples C4A6, C5A2	220
A3 Axial Stress and Volumetric Strain Vs. Axial Strain for Samples C1B1, C2B3, C3B3	221
A4 Axial Stress and Volumetric Strain Vs. Axial Strain for Samples C4B8, C5B3	222
A5 Axial Stress and Volumetric Strain Vs. Axial Strain for Samples C1C5, C1C7	223

Appendix
Figure

Page

A6	Axial Stress and Volumetric Strain Vs. Axial Strain for Samples C4C1, C5C10, C5C3	224
A7	Axial Stress and Volumetric Strain Vs. Axial Strain for Samples R1A7, R2A8, R3A10	225
A8	Axial Stress and Volumetric Strain Vs. Axial Strain for Samples R4A7, R5A10	226
A9	Axial Stress and Volumetric Strain Vs. Axial Strain for Samples R1B1, R2B7, R3B10	227
A10	Axial Stress and Volumetric Strain Vs. Axial Strain for Samples R4B4, R5B3	228
A11	Axial Stress and Volumetric Strain Vs. Axial Strain for Samples R1C5, R2C5, R3C1	229
A12	Axial Stress and Volumetric Strain Vs. Axial Strain for Samples R4C9, R5C9	230
A13	Axial Stress and Volumetric Strain Vs. Axial Strain for Samples C1A4, C2A2, C3A1	231
A14	Axial Stress and Volumetric Strain Vs. Axial Strain for Samples C4A1, C5A10	232
A15	Axial Stress and Volumetric Strain Vs. Axial Strain for Samples C1B3, C2B9, C3B9	233
A16	Axial Stress and Volumetric Strain Vs. Axial Strain for Samples C4B2, C5B9	234
A17	Axial Stress and Volumetric Strain Vs. Axial Strain for Samples C1C4, C2C10, C3C2	235
A18	Axial Stress and Volumetric Strain Vs. Axial Strain for Samples C4C9, C5C1	236
A19	Axial Stress and Volumetric Strain Vs. Axial Strain for Samples R1A2, R2A3, R3A9	237

Appendix Figure		Page
A20	Axial Stress and Volumetric Strain Vs. Axial Strain for Samples R4A2, R5A3	238
A21	Axial Stress and Volumetric Strain Vs. Axial Strain for Samples R1B9, R2B2, R3B5	239
A22	Axial Stress and Volumetric Strain Vs. Axial Strain for Samples R4B6, R5B8	240
A23	Axial Stress and Volumetric Strain Vs. Axial Strain for Samples R1C8, R2C6, R3C3	241
A24	Axial Stress and Volumetric Strain Vs. Axial Strain for Samples R4C7, R5C1	242
A25	Axial Stress and Volumetric Strain Vs. Axial Strain for Samples C1A1, C2A6, C3A3	243
A26	Axial Stress and Volumetric Strain Vs. Axial Strain for Samples C4A8, C5A1	244
A27	Axial Stress and Volumetric Strain Vs. Axial Strain for Samples C1B2, C2B2, C3B8	245
A28	Axial Stress and Volumetric Strain Vs. Axial Strain for Samples C4B10, C5B10	246
A29	Axial Stress and Volumetric Strain Vs. Axial Strain for Samples C2C6, C3C8	247
A30	Axial Stress and Volumetric Strain Vs. Axial Strain for Samples C4C10, C5C4	248
A31	Axial Stress and Volumetric Strain Vs. Axial Strain for Samples R2A10, R3A1	249
A32	Axial Stress and Volumetric Strain Vs. Axial Strain for Samples R4A4, R5A2	250
A33	Axial Stress and Volumetric Strain Vs. Axial Strain for Samples R2B10, R3B6	251
A34	Axial Stress and Volumetric Strain Vs. Axial Strain for Samples R4B7, R5B9	252

Appendix Figure		Page
A35	Axial Stress and Volumetric Strain Vs. Axial Strain for Samples R1C9, R2C4, R3C10	253
A36	Axial Stress and Volumetric Strain Vs. Axial Strain for Samples R4C8, R5C8	254
B1	Results from <u>CIU</u> Triaxial Test for Samples C1A3, C2A1	255
B2	Results from <u>CIU</u> Triaxial Test for Samples C3A9, C4A9	256
B3	Results from <u>CIU</u> Triaxial Test for Samples C2B5, C5B8	257
B4	Results from <u>CIU</u> Triaxial Test for Samples C4B6, C5B8	258
B5	Results from <u>CIU</u> Triaxial Test for Samples C2C4, C3C6	259
B6	Results from <u>CIU</u> Triaxial Test for Samples C4C6, C5C7	260
B7	Results from <u>CIU</u> Triaxial Test for Samples R1A4, R2A5	261
B8	Results from <u>CIU</u> Triaxial Test for Samples R3A2, R5A8	262
B9	Results from <u>CIU</u> Triaxial Test for Samples R1B10, R2B9	263
B10	Results from <u>CIU</u> Triaxial Test for Samples R3B3, R5B4	264
B11	Results from <u>CIU</u> Triaxial Test for Samples R2C3, R3C5	265
B12	Results from <u>CIU</u> Triaxial Test for Samples R4C6, R5C4	266
B13	Results from <u>CIU</u> Triaxial Test for Samples C2A5, C3A1	267
B14	Results from <u>CIU</u> Triaxial Test for Samples C4A5, C5A7	268

**Appendix
Figure**

Page

B15	Results from <u>CIU</u> Triaxial Test for Samples C1B8, C3B6	269
B16	Results from <u>CIU</u> Triaxial Test for Samples C4B5, C5B4	270
B17	Results from <u>CIU</u> Triaxial Test for Samples C2C1, C3C1	271
B18	Results from <u>CIU</u> Triaxial Test for Samples C4C7, C5C8	272
B19	Results from <u>CIU</u> Triaxial Test for Samples R2A1, R3A3	273
B20	Results from <u>CIU</u> Triaxial Test for Samples R4A6, R5A7	274
B21	Results from <u>CIU</u> Triaxial Test for Samples R2B3, R3B7	275
B22	Results from <u>CIU</u> Triaxial Test for Samples R4B9, R5B2	276
B23	Results from <u>CIU</u> Triaxial Test for Samples R2C9, R3C9	277
B24	Results from <u>CIU</u> Triaxial Test for Samples R4C1, R5C6	278
B25	Results from <u>CIU</u> Triaxial Test for Samples C1A9, C3A5	279
B26	Results from <u>CIU</u> Triaxial Test for Samples C4A4, C5A5	280
B27	Results from <u>CIU</u> Triaxial Test for Samples C1B10, C2B7	281
B28	Results from <u>CIU</u> Triaxial Test for Samples C4B9, C5B6	282
B29	Results from <u>CIU</u> Triaxial Test for Samples C1C9, C2C3	283
B30	Results from <u>CIU</u> Triaxial Test for Samples C3C10, C4C5	284

Appendix Figure	Page
B31 Results from CIU Triaxial Test for Samples R1A3, R2A7	285
B32 Results from CIU Triaxial Test for Samples R3A5, R5A6	286
B33 Results from CIU Triaxial Test for Samples R2B8, R3B8	287
B34 Results from CIU Triaxial Test for Samples R4B1, R5B6	288
B35 Results from CIU Triaxial Test for Samples R3C2, R5C3	289
B36 Results from CIU Triaxial Test for Samples R1C3, R1C10	290
C1 \hat{p}_f' vs. \hat{q}_f Failure Line for Sample C2A	291
C2 \hat{p}_f' vs. \hat{q}_f Failure Line for Sample C3A	292
C3 \hat{p}_f' vs. \hat{q}_f Failure Line for Sample C4A	293
C4 \hat{p}_f' vs. \hat{q}_f Failure Line for Sample C5A	294
C5 \hat{p}_f' vs. \hat{q}_f Failure Line for Sample C2B	295
C6 \hat{p}_f' vs. \hat{q}_f Failure Line for Sample C3B	296
C7 \hat{p}_f' vs. \hat{q}_f Failure Line for Sample C4B	297
C8 \hat{p}_f' vs. \hat{q}_f Failure Line for Sample C5B	298
C9 \hat{p}_f' vs. \hat{q}_f Failure Line for Sample C4C	299
C10 \hat{p}_f' vs. \hat{q}_f Failure Line for Sample C5C	300
C11 \hat{p}_f' vs. \hat{q}_f Failure Line for Sample R1A	301

Appendix Figure	Page
C12 \hat{p}_f' vs. \hat{q}_f Failure Line for Sample R2A	302
C13 \hat{p}_f' vs. \hat{q}_f Failure Line for Sample R3A	303
C14 \hat{p}_f' vs. \hat{q}_f Failure Line for Sample R4A	304
C15 \hat{p}_f' vs. \hat{q}_f Failure Line for Sample R5A	305
C16 \hat{p}_f' vs. \hat{q}_f Failure Line for Sample R2B	306
C17 \hat{p}_f' vs. \hat{q}_f Failure Line for Sample R3B	307
C18 \hat{p}_f' vs. \hat{q}_f Failure Line for Sample R4B	308
C19 \hat{p}_f' vs. \hat{q}_f Failure Line for Sample R5B	309
C20 \hat{p}_f' vs. \hat{q}_f Failure Line for Sample R4C	310
C21 \hat{p}_f' vs. \hat{q}_f Failure Line for Sample R5C	311

LIST OF ABBREVIATIONS AND SYMBOLS

AASHTO -	American Association of State Highway and Transportation Officials
<u>CIU</u> -	Isotropically consolidated undrained triaxial shear test with pore pressure measurements
IDOH -	Indiana Department of Highways
MIT -	Massachusetts Institute of Technology
OCR -	Overconsolidation ratio
SPSS -	Statistical Package for the Social Sciences
UU -	Unconsolidated undrained triaxial shear test
WES -	Waterways Experiment Station
A -	Skempton's A parameter
A_f -	A parameter at failure
\hat{A}_f -	Estimated A parameter at failure
b -	Regression parameter
B -	Skempton's B parameter
c' -	Effective stress strength intercept
\hat{c}' -	Estimated effective stress strength intercept
e_o -	Initial void ratio
e_f -	Final void ratio
Δe -	$(e_o - e_f)$
G_s -	Specific gravity of soil solids
H -	Henry's coefficient of solubility
K_o -	Coefficient of earth pressure at rest

log -	Base 10 logarithm
n -	Porosity
p'_f -	Mean effective normal stress at failure = $(\sigma'_1 + \sigma'_3)_f / 2$
P_c -	Compactor foot pressure
\hat{p}_s -	Estimated compactive prestress
q_c -	Compressive strength (stress difference at failure)
\hat{q}_c -	Estimated compressive strength
q_f -	Shear Stress at failure = $(\sigma_1 - \sigma_3)_f / 2$
\hat{q}_u^s -	Estimated compressive strength for saturated soil
ϕ' -	Effective stress strength angle
$\hat{\phi}'$ -	Estimated effective stress strength angle
ρ_d -	Dry density
$\hat{\rho}_d$ -	Estimated dry density
ρ_w -	Density of water, 1000 kg/m ³
R^2 -	Coefficient of multiple determination
R_a^2 -	Adjusted R^2
S_i -	Initial degree of saturation (%)
S_f -	Final degree of saturation (%)
σ -	Total normal stress
σ' -	Effective normal stress
σ_1 -	Major principal stress
σ'_1 -	Effective major principal stress
σ_3 -	Minor principal stress
σ'_3 -	Effective minor principal stress
σ_c -	Confining pressure
σ'_c -	Consolidation pressure (isotropic)
$(\sigma_1 - \sigma_3)_f$ -	Deviator stress at failure

τ -	Shear stress
Δu_T -	Theoretical back pressure
Δu_E -	Experimental back pressure
Δu -	Pore pressure change during shear
Δu_f -	Pore pressure at failure
$\Delta V/V_0$ (%) -	Percent volume change (volumetric strain) due to saturation and consolidation
$\hat{\Delta V}/V_0$ (%) -	Estimated percent volume change due to saturation and consolidation
u_w -	Pore water pressure
u_c -	capillary pressure
u_a -	pore air pressure
w -	Water content
w_f -	Final water content
ϵ_v -	Volumetric strain
ϵ_1 -	Axial compressive strain
ϵ_3 -	Lateral strain
μ -	Poisson's ratio

HIGHLIGHT SUMMARY

The purpose of this study was to investigate the relationships among the compaction variables (dry density, water content, and compaction energy) and the shearing behavior of a field compacted St. Croix clay. The strength tests were performed by unconsolidated-undrained (UU) and saturated consolidated-undrained ($\overline{\text{CIU}}$) triaxials. These were run at various confining pressures to approximate the end of construction and long term conditions at several embankment depths. Samples for the triaxial tests were taken from the ten test pads, which had been compacted to three levels of effort, at five levels of water content, and by two kinds of rollers.

The results of field as-compacted strength from UU tests showed that an increase in strength results from an increase in density or a decrease in water content. The strength also increased with confining pressure until a near-saturation condition was reached in the sample. A regression model for field as-compacted strength was thus developed in terms of the water content, dry density, and confining pressure.

The effective stress strength parameters were evaluated for various compaction conditions through the performance of saturated consolidated undrained triaxial tests with pore water pressure measurements. The results of the testing program showed that the effective stress strength

parameters, c' and ϕ' , are functions of compaction water content and initial void ratio. For a constant value of initial void ratio, as the water content increases, c' increases and ϕ' decreases. The values of volumetric strain due to saturation and consolidation, and Skempton's A parameter at failure demonstrated dependency on the water content, dry density, energy level, and confinement for this field compacted soil.

Comparison of the prediction models for as-compacted and saturated undrained strength of a field compacted medium plastic St. Croix clay were made with prediction models previously developed for a laboratory compacted highly plastic St. Croix clay. The coupling of the relations for field compaction with those previously established for laboratory compaction is also reported here.

INTRODUCTION

The general purpose of compaction is to improve one or more engineering properties of the given material and hence, to improve the performance of the material in a given application. For the project entitled "Improvement of Embankment Design", the engineering properties of both laboratory and field compacted soil were investigated and the results were correlated with the compaction variables. Where the laboratory-compacted and field-compacted relationships are functions of the same variable, they can be simply related. This means that the behavior of laboratory compacted soil can be used to predict the behavior of field compacted soil.

The safety of a compacted clay embankment against shear failure is assessed at two critical times: (a) end of construction, and (b) in the long term. For the former time the fill material exists in the as-compacted condition. For the long term case, the embankment material is assumed to become fully saturated under the confinement of the embankment. The as-compacted strength was measured in unconsolidated undrained triaxial tests. The saturated undrained strength for the long term case was measured in consolidated undrained triaxial tests with pore pressure measurements.

The objectives of this particular task within the study were accomplished in the following steps.

- (a) Samples were acquired from the St. Croix test pads which had been compacted at five levels of water content, three levels of energy, and by two types of rollers.
- (b) Laboratory tests were run for as-compacted strength, volume change on saturation and saturated undrained strength on the samples procured from the test pads.
- (c) The experimental test parameters were related to the compaction variables and statistically valid prediction equations were produced.
- (d) Prediction models for field compacted parameters were related to laboratory compacted data for a similar soil. Where the relationships are simply related, it is possible to predict field compacted behavior from tests on laboratory compacted samples.

Prediction equations were produced for dry density (ρ_d), as-compacted strength (\hat{q}_c), percent volume change due to saturation and consolidation ($\Delta\hat{V}/V_0$, %), Skempton's A parameter at failure (A_f) and the effective stress strength parameters (c' and ϕ'), in terms of the field compaction variables.

1- LITERATURE REVIEW

1-1 Theories for the Mechanics of Compaction

Compaction is the most direct and economical method of improving the physical properties of the material. The extent to which a soil mass can be made to occupy a smaller volume depends mainly on the type of soil, the moisture conditions, method of compaction, and the compaction energy.

The pioneering work of Proctor in the 1930's clarified the mechanism of compaction and demonstrated the unique relation between water content and density which could be achieved by a particular compactive effort. Proctor's theory states that the continual addition of water to a very dry soil produces two effects, capillarity and lubrication. In the very dry state, the addition of water reduces the density due to the reduction of capillary force which allows the particles to spring apart, but further addition of water produces a lubrication effect which increases the density. The relative influence of capillarity and lubrication depends on the type of soil. The decrease in density that results from the reduction in capillary force is relatively small compared to the increase in density due to the lubrication effect. His concept of fabric dealt with particle spacing, rather than degree of particle orientation.

Hogentogler's (1936) theory suggests four stages of wetting that influence the density: hydration, lubrication, swell and saturation.

These stages occur as a result of the variation in the character of moisture films. The water during the hydration stage is absorbed by the soil particles and the remainder is attached to the surface of the soil particle. During the lubrication stage, the water acts as a lubricant allowing the soil particles to slide past each other more easily, thus increasing the density. At water contents greater than the lubrication limit, the additional water merely acts to push the soil particles apart which causes the soil to swell. This is the swelling stage. During the saturation stage, the remaining air is displaced and the soil becomes truly saturated.

Lambe's (1958) structural theory uses the physical-chemical nature of clay to explain its structural and engineering behavior. In his theory the sizes and shapes of particles play an important role in determining the structure of a particular soil. Some soils may show an extreme variation of structure with increase in molding water. Compaction at low water contents results in a high concentration of electrolyte, which prevents the diffuse double layer of ions surrounding each clay particle from fully developing. The double layer depression leads to low inter-particle repulsion, resulting in a tendency towards flocculation of the colloids and a consequent low degree of clay particle orientation in the compacted soil. This type of structure has been termed a "flocculated" arrangement of soil particles. As the molding water content is increased, Lambe postulates that the electrolyte concentration is reduced, resulting in an expansion of the double layer, increased repulsion between particles and a low degree of flocculation. This causes a more orderly arrangement of particles during application of compactive effort and therefore a higher density. Further increase

in water content above the optimum moisture content increases this effect, and tends to produce a dispersed arrangement of particles, but the double layers are large enough to reduce the concentration of soil particles per unit of volume. This causes a decrease in dry density. The surface chemistry theories utilized in Lambe's theory apply principally to clay minerals; therefore, it would seem that his theory is limited in that it could not be used to explain the compaction behavior of soils composed primarily of sand or silt.

Seed and Chan (1961) presented considerable additional data which confirmed and extended the concept that the strength, deformation, and many other properties of compacted clay were greatly dependent upon the structure of the soil, as well as on the water content and density.

Olson's (1963) effective stress theory marks the first attempt at explaining the compaction process in terms of changes in effective stress, pore water pressure, and shearing deformations in the soil. Olson explained the shape of the compaction curve as follows. For compaction at low water content, increases in moisture increase the degree of saturation which results in higher pore air pressures and pore water pressures. This weakens the soil by reducing the effective stresses between the particles. He believed the negative pore water pressures in samples dry-of-optimum caused large effective stresses that could resist penetration of the compaction foot. As the moisture content is increased, the greater amount of water increased pore pressure and lowered the effective stresses. This left the soil unable to resist foot penetration. So, large foot penetrations occurred on the wet side of optimum and resulted in a more dispersed structure.

Barden and Sides (1970) made an experimental investigation of engineering behavior of a compacted, partly saturated lean clay and offered a deformable aggregate model to explain the compaction process. Their results indicate that the soil structure is markedly affected by the compaction moisture content. At low compaction moisture content, the macropeds have high strength and are able to resist the compaction pressure without much distortion. Thus, during compaction, the macropeds are displaced but little distorted, as the size of the interpedal air void is reduced. Further increase in the compaction moisture content causes the macropeds to become even weaker, and during compaction they are somewhat distorted to fill the macropores which tend to disappear. At this compaction moisture content the dry density reaches a maximum. Further increase in compaction moisture content causes the dry density to decrease as the water layers between the soil particles increase in thickness.

Hodek (1972) verified his deformable aggregate theory by investigating the particle orientation and strength of kaolin aggregates of varying moisture content and size. In his theory as water content increased, the aggregates became weaker, more deformable, and squeezed into each other to form a more oriented fabric normal to the direction of the compacting force. Thus, his study showed that the particles in the aggregates increased in orientation with higher water content and compactive efforts. Also, the compacted energy required to achieve a given density decreases as the moisture content increases.

The size and distribution of pore space of compacted clay fabric has also been studied considerably. Diamond (1971) employed pore size distribution techniques, scanning electron microscopy, and X-ray

diffraction to study the fabric of impact compacted kaolinite and illite. For samples compacted dry-of-optimum, scanning electron microscopy showed distinct soil domains several microns in diameter with intervening voids of similar diameter. The domains were indistinguishable and the voids were closed for samples compacted wet-of-optimum. Bhasin (1975) found that the distributions of the pore sizes for soil at equal porosities wet- and dry-of-optimum were very different, the dry sample having larger pores than the wet one. Also, as compactive effort increased at a constant water content dry-of-optimum, the quantity of larger pores was vastly reduced. For the samples wet-of-optimum, increases in compactive effort had little effect on the porosity or pore distribution. Sridharan, Altschaeffl and Diamond (1971) reported that the reduction in void ratio obtained by increasing compaction effort is absorbed primarily by the large pores. Ahmed, Lovell, and Wood (1974) also showed that compaction to a constant water content and density by impact and kneading compaction methods had little effect on the pore size distribution. Reed (1977) and Garcia-Bengochea (1978) found that only when a high enough percentage of kaolin was present in their silt-kaolin mixes did the deformable aggregate model seem to be valid.

Hodek and Lovell (1978 and 1979) have proposed a model and a mechanism which explains the achievement of compacted density for kaolinite. They studied certain properties of the soil aggregates before compaction. The size and distribution of aggregates play an important role in the compaction process. During compaction, the densification occurs due to aggregate rearrangement not requiring deformation, aggregate rearrangement initiated by slight yielding, the deformation of aggregates into the shape of available voids, and the reduction of possible intra-aggregate air voids. Accordingly, the type of compaction

and aggregate size distribution establish the water continuity condition within the soil, and once the air voids are no longer inter-connected, little densification occurs regardless of the input effort.

White (1980) conducted pore size distribution measurements on the St. Croix clay used in this study. He attacked the prediction problem by investigating a possible source of the differences soil fabric between the laboratory and field compacted soil. He concluded that the fabric of the laboratory compacted soil was significantly different from that of the field compacted soil. The difference was more pronounced at water contents on the dry side of optimum and on the wet side; near optimum the differences were less pronounced. White also pointed out that laboratory compaction by impact and kneading procedures produced the same fabric. Differences in fabric existed on the dry side between the Rascal and the Caterpillar field compacted samples.

In conclusion, it appears that none of the compaction theories alone adequately explains the complete compaction process. That is, none of the theories are sufficiently general to cover all types of soils and all types of compaction processes. Nevertheless, each of them is of value in that each proposes a unique explanation for the effect of water on the dry density that can be produced by the compaction process.

1-2 Shear Strength of Compacted Fine Grained Soils

The engineering behavior of a compacted cohesive soil is primarily controlled by molding water content, degree of saturation, method of compaction, and compactive effort. These factors control the type of structure that is produced during the compaction process, which in turn influences the manner of development of pore pressures during the

undrained application of shearing stresses. It is well known that the development of pore pressure during shear is important in determining the shear resistance offered by a soil. The shear strength of soil is generally expressed by the Mohr-Coulomb equation:

$$s = c' + \sigma' \tan \phi' \quad (1-1)$$

Where s is the shear stress on the failure plane at failure, σ' is the effective normal stress on the failure plane at failure, c' is the strength intercept, and ϕ' is the strength angle. When full drainage in a saturated sample is allowed to take place during the consolidation and compression shear test, or when developed pore pressure are evaluated, the shear strength can be expressed as a function of effective normal stress (σ'). If pore pressures are developed during the test, and these pore pressures are not evaluated, the strength is expressed only as a function of total normal stress (σ).

In summarizing the results of the Harvard-MIT-WES cooperative tri-axial shear research program, Rutledge (1947) observed that for saturated normally consolidated clays there was a unique relation between the shear strength and the water content at failure. The water content at failure was also found to be one of the primary factors governing the strength of partially saturated clays, along with the confining pressure, soil density and degree of saturation. Further data were added by Leonards (1955), who illustrated the importance of void ratio at failure on the strength of partially saturated compacted clays. Leonards found a unique relationship only for specimens having constant initial conditions of void ratio and water content.

Seed and Chan (1959) showed that the method of compaction and the molding water content used to obtain a given dry density had a pronounced effect on the relative strength developed at low strains for soil compacted wet-of-optimum but hardly any effect for soils compacted dry-of-optimum. For samples compacted wet-of-optimum to any given density and water content, particle orientation and shrinkage tend to decrease, and strength at low strains tends to increase in the following order of compaction methods: kneading, impact, vibratory, static. Neither the method of compaction nor the molding water content had any significant influence on the relative strength at large strains. Lee and Haley (1968) showed that under very high confining pressures, samples with a flocculated fabric remained stronger than samples with an oriented fabric. However, due to the volume changes which occurred during consolidation, the strength after soaking and consolidation at high pressures were very little different for soils prepared by different compaction methods. DaCruz (1963) found the differences could be accounted for by including degree of saturation and void ratio, i.e., $e\sqrt{S_r}$. These values at failure when plotted against the $\log \left[\frac{1}{2} (\sigma_1 - \sigma_3)_f \right]$ showed a linear relationship for all compacted samples of his residual clay. Seed and Hirschfeld (1960) concluded that the strength characteristics of compacted clays are largely determined by the same principles that control the strength of undisturbed and remolded clays. It was recognized that the shearing resistance of a partially saturated compacted soil was controlled by effective stress, but was not as well defined as for saturated soil. Measuring the pore water and pore air pressures in a partial saturated clay remains a problem.

1-2-1 Effective Stress in Saturated Soil

Since the effective stress controls changes in volume and strength of soils, it is desirable, to evaluate soil strength in terms of effective stress. Effective stress in saturated soils has been found to follow the Terzaghi equation $\sigma' = \sigma - u$ where σ is total stress, σ' is effective stress, and u is the pore pressure. The validity of this effective stress equation has been justified by experimental evidence. Skempton (1960) has attempted a somewhat rigorous, theoretical approach and concluded that the above equation " ... has the status of an excellent approximation in the special case of saturated soils".

1-2-2 Effective Stress in Partially Saturated Soil

Generally, effective stress in partially saturated soil cannot conform to the Terzaghi equation, because the pressure in the air and water phases of the soil are not equal. This pressure difference arises due to the presence of capillary menisci in the water. These menisci cause tension in the water that results in negative pore water pressure. The water pressure will be less than that of the pore air pressure unless the air is occluded.

A number of studies have attempted to extend the principle of effective stress to the case of partly saturated soils. Hilf (1956) recognized that Terzaghi's equation was not adequate to describe the effective stress in an unsaturated soil and proposed the equation:

$$\sigma = \sigma' + u_a + u_c \quad (1-2)$$

Where u_a is the pore air pressure and u_c is the capillary pressure ($u_c = u_a - u_w$). If the applied stress and the pore air pressure are taken

equal to zero, Hilf's equation degenerates to $\sigma' = -u_w$. This expression was significant in pointing out the existence of negative water pressures. Croney, et al. (1958), Jennings (1960) and Aitchison (1960) all proposed modified forms of the effective stress equation to account for the two-phase nature of the pore fluid in a partly saturated soil. These equations (1-3a,b,c) are shown in Table 1-1.

Bishop et al. (1960) proposed a more general form of the equation for defining effective stress in problems involving the partially saturated state:

$$\sigma' = \sigma - u_a + \chi(u_a - u_w) \quad (1-4)$$

Where χ is a parameter between 0 and 1 that varies with degree of saturation. Therefore, in order to evaluate the effective stress in an unsaturated soil it is necessary to have a knowledge of both the pore-air and pore-water pressures, as well as the χ -factor. Bishop and Henkel (1962) presented the relationships between χ -factor and degree of saturation for four soils as shown in Fig. 1-1. However, it should be noted that the χ -factor is not necessarily the same in equations of effective stress for volume change and shear strength. It is also a function of suction, water content, surface charge on particles, electrolyte composition, particle arrangement, stress path, etc. (Aitchison, 1965). Olson and Langfelder (1965) have presented data to show that the relationship between water content and negative pore water pressure follows a hyperbolic type curve. They further showed that for a given compaction procedure, the as-compacted pore water pressure becomes increasingly negative at any water content as the specific surface of a soil increases. Wahls, et al. (1966) assumed that pore air pressures dissipate

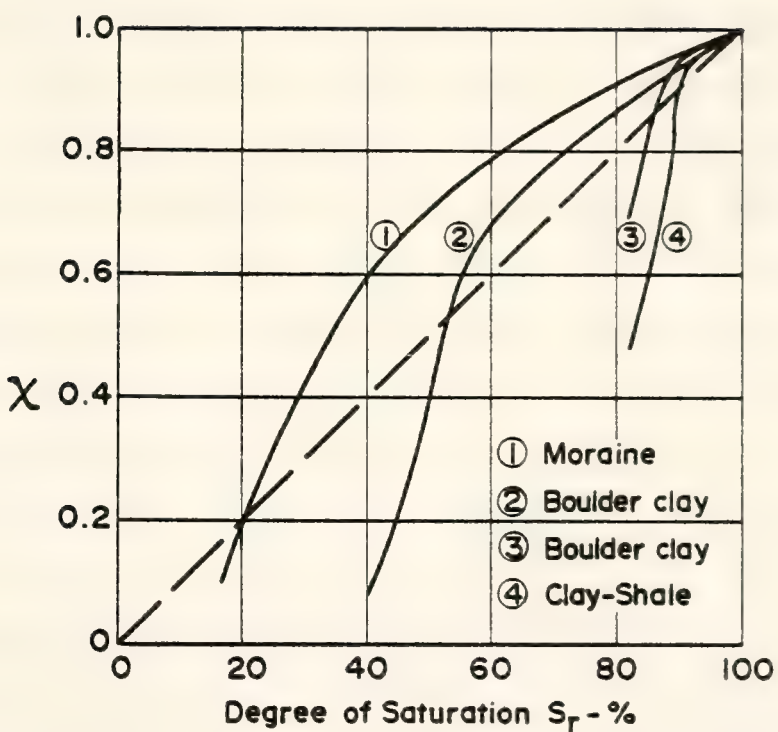


Figure I-1 χ -Factor vs. Degree of Saturation (After Bishop and Henkel, 1962)

quite rapidly because of high air permeability; accordingly the pore air pressures may be taken to be zero and Equation (1-4) reduces to:

$$\sigma' = \sigma - \chi u_w \quad (1-5)$$

They further assumed that when the total stress is constant, the effective stress, σ' , is a linear function of the product χu_w . The relationship between the χ -factor, degree of saturation, dry density, negative pore water pressure and molding water content is presented as Fig. 1-2. Referring to Fig. 1-2, it is seen that on the dry side of optimum, u_w becomes less negative but χ also increases, therefore the strength may decrease or increase. This implies that increase in dry density does not necessarily result in increased strength. On the wet side of optimum, u_w continues to be increasingly less negative and χ is essentially constant. This implies that the strength must decrease on the wet side of optimum. A number of triaxial tests on silty clay performed at MIT (1963), at constant void ratio and structure, but different water contents, showed poor applicability of Equation (1-4) to shear strength. The MIT report considered the principle of effective stress to be valuable to shear strength, but the internal and external stresses would have to be correlated to an effective stress that would contribute to the value of χ .

Lambe (1960) generalized an equation for effective stress which considered an internal stress exerted between adjacent particles of a particular soil mass:

$$\sigma = \bar{\sigma} a_m + u_a a_a + u_w a_w + R - A \quad (1-6)$$

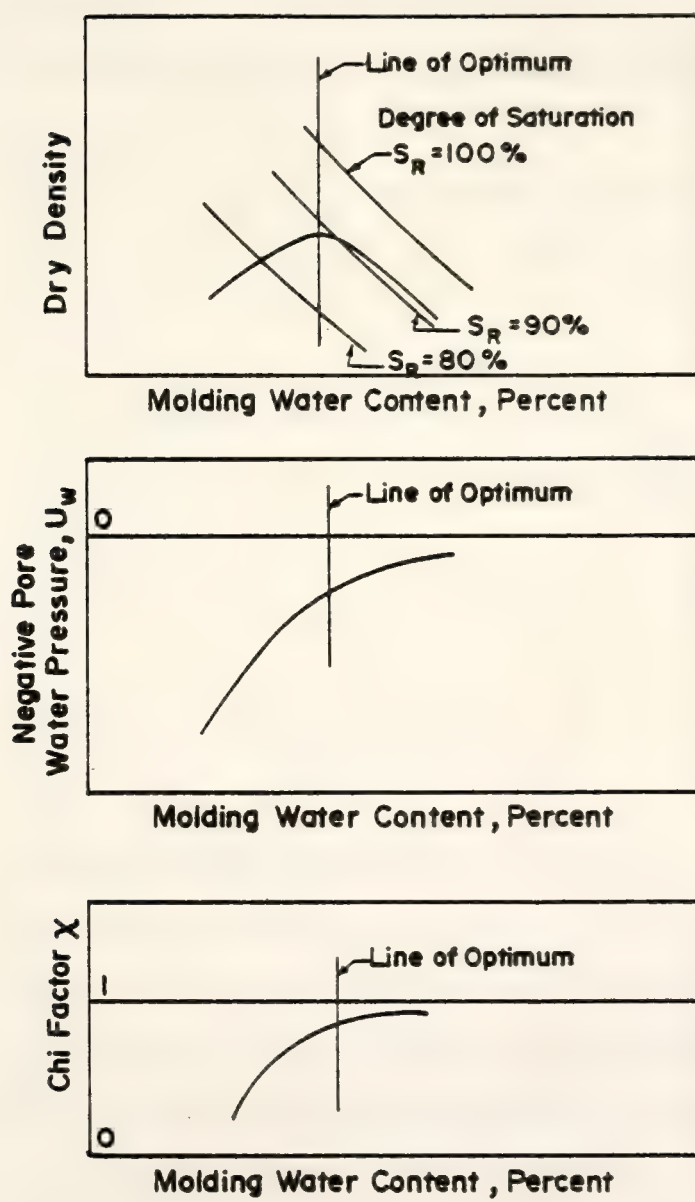


Figure 1-2 Relationship of Dry Density, Pore Water Pressure, and χ -Factor to Molding Water Content (After Wahls, et al., 1966)

Where σ = total stress

$\bar{\sigma}$ = intergranular stress of mineral-mineral contact

a_m = percent of total area in mineral-mineral contact

u_a = pressure of air in air-mineral contact

a_a = percent of total area in air-mineral contact

u_w = pressure in water

a_w = percent of total area in water-mineral contact

R = total interparticle electrical repulsion divided by total
interparticle area

A = total interparticle electrical attraction divided by
total interparticle area

The limitations to the use of this equation (1-6) lie in the eval-
uation of its terms.

Sridharan (1968) used a similar equation for effective stress, \bar{c} ,

$$\bar{c} = \sigma - (\bar{u}_a + \bar{u}_w) - R + A \quad (1-7)$$

where σ = total stress

\bar{u}_a = effective pore air pressure

\bar{u}_w = effective pore water pressure

R = net repulsive pressure due to particle electrical forces.

A = net attractive pressure due to particle electrical forces.

He related the net interparticle contact stress to shear strength s, by

$$s = f(\bar{c}) + c \quad (1-8)$$

where c was a constant. Sridharan found that the variation in attrac-
tive and repulsive forces with degree of saturation appears to control
the variation in strength up to about a 35% degree of saturation.

Beyond this, the variation in strength is primarily influenced by variation in negative pore pressures. Clay type is the major influence in defining the electrical forces and negative pore water pressures in the relationship.

Aitchison (1973) related matrix and solute suctions to the effective stress by:

$$\sigma' = \sigma + x_m \rho_m'' + x_s \rho_s'' \quad (1-9)$$

Where σ = total applied stress

$$\rho_m'' = \text{matrix suction} = u_a - u_w$$

$$\rho_s'' = \text{solute suction}$$

x_m, x_s = factors ranging from zero to one which are dependent upon stress paths.

Fredlund and Morgenstern (1977) applied multiphase continuum mechanics, involving force equilibrium equations for each phase, to describe effective stress in unsaturated soils. They considered that the air-water interface or "contractile skin" was a fourth phase in the soil-air-water system. Two independent stress matrices are as follows:

$$\begin{bmatrix} \sigma_x - u_w & \tau_{yx} & \tau_{zx} \\ \tau_{xy} & \sigma_y - u_w & \tau_{zy} \\ \tau_{xz} & \tau_{yz} & \sigma_z - u_w \end{bmatrix}$$

and

$$\begin{bmatrix} u_a - u_w & 0 & 0 \\ 0 & u_a - u_w & 0 \\ 0 & 0 & u_a - u_w \end{bmatrix} \quad (1-10)$$

They also pointed out that any two of three possible normal stress variables can be used to define the stress state. Possible combinations

are: (1) $(\sigma - u_w)$ and $(u_a - u_w)$; (2) $(\sigma - u_a)$ and $(u_a - u_w)$; and (3) $(\sigma - u_a)$ and $(\sigma - u_w)$.

A summary of the effective stress equations for partially saturated soils as discussed above is shown in Table 1-1.

While it is well recognized that the effective stress concept approach to the evaluation of the strength of unsaturated soil would be highly desirable, this approach is generally not used at the present. This is because of the experimental difficulties involved in determining the shear strength in terms of effective stress. Also none of the above models of effective stress in partially saturated soils has been found to be fully applicable.

1-2-3 Stress-Strain Characteristics

Seed and Chan (1959) showed some typical stress-strain curves of "as-compacted" soils in Figure 1-3. It will be seen that as the samples with the lower water contents and the flocculated structure, in conjunction with highly negative pore water pressures, have much steeper stress-strain curves and develop their maximum strength at low strains, as for curves 1 and 2. Samples with the higher water contents, lower density and more oriented fabric have much flatter stress-strain curves and continue to increase in strength at very high strains, as in curves 3, 4, 5, 6. The variations of stress-strain behavior depend on amount and type of soil fraction, density, compaction method, water content and degree of saturation, and minor principal stress. Similar stress-strain curves of as-compacted soil were observed by Price (1978) and Weitzel (1980). The dry-of-optimum samples were stiffer and the sample at the lowest water content was quite brittle. As water content increases from dry-of-optimum the soil aggregates become weaker and more plastic, so they yield

TABLE 1-1 Effective Stress Equation for Partially Saturated Soils

Reference	Equation	
Hilf (1956)	$\sigma' = \sigma - u_a - u_c$	(1-2)
Croney, et al. (1958)	$\sigma' = \sigma - \beta' u_w$	(1-3a)
Jennings (1960)	$\sigma' = \sigma + \beta \rho''$	(1-3b)
Aitchison (1960)	$\sigma' = \sigma + \chi \rho''$	(1-3c)
Bishop (1960)	$\sigma' = \sigma - u_a + \chi(u_a - u_w)$	(1-4)
Lamb (1960)	$\sigma = \bar{\sigma} a_m + u_a a_a + u_w a_w + R - A$	(1-6)
Sridharan (1968)	$\bar{\sigma} = \sigma - (\bar{u}_a + \bar{u}_w) - R + A$	(1-7)
Aitchison (1973)	$\sigma' = \sigma + x_m \rho_m'' + x_s \rho_s''$	(1-9)
Fredlund and Morgenstern (1977)	$\begin{bmatrix} \sigma_x - u_x & \tau_{yx} & \tau_{zx} \\ \tau_{xy} & \sigma_y - u_w & \tau_{zy} \\ \tau_{xy} & \tau_{yz} & \sigma_z - u_w \end{bmatrix} \begin{bmatrix} u_a - u_w & 0 & 0 \\ 0 & u_a - u_w & 0 \\ 0 & 0 & u_a - u_w \end{bmatrix}$	(1-10)

TABLE 1-1 (Continued)

Description of Variables	
u_a = pressure in air	u_c = capillary pressure
u_w = pore water pressure	σ' = effective stress
σ = total stress	ρ'' = pressure deficiency
$\bar{\sigma}$ = intergranular or contact stress between particles	
x = parameter related to degree of saturation	
x_m = effective stress parameter for matrix suction	
x_s = effective stress parameter for solute suction	
ψ = parameter with values ranging from zero to one	
β = statistical factor of same type as contact area (should be measured experimentally in each case).	
β' = holding or bonding factor which is a measure of number of bonds under tension effective in contributing to soil strength.	
R = net repulsive pressure due to particle electrical forces	
A = net attractive pressure due to particle electrical forces	
P_m'', P_s'' = matrix and solute suction	
\bar{u}_a = effective pore air pressure	
\bar{u}_w = effective pore water pressure	
$\bar{\sigma}$ = effective stress	
a_m = percent of total area in mineral-mineral contact	
a_a = percent of total area in air-mineral contact	
a_w = percent of total area in water-mineral contact	

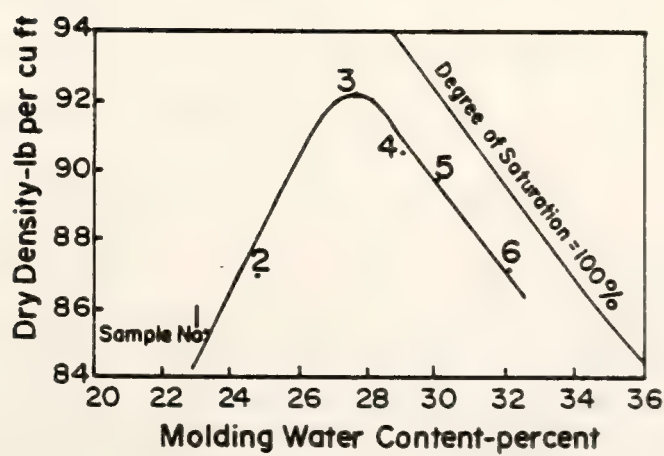
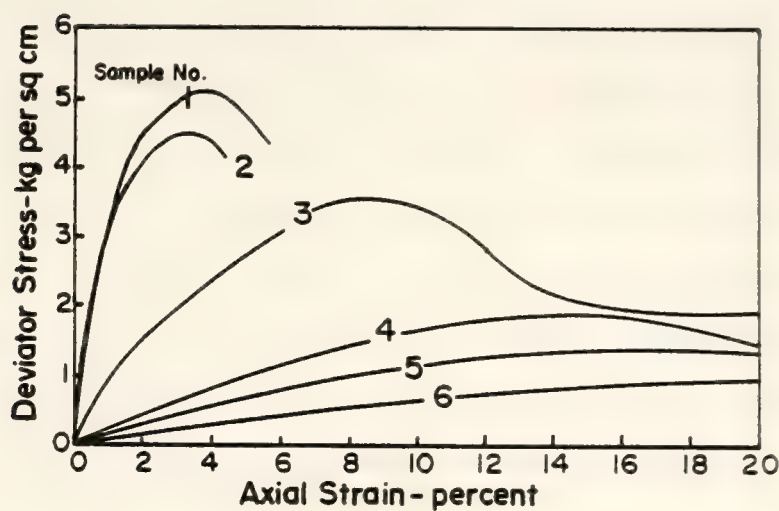


Figure I-3 Influence of Molding Water Content on Stress-Strain Relationship for Compacted Kaolinite (From Seed and Chan, 1959)

more before the shear resistance between them is exceeded. Casagrande and Hirschfeld (1962) also proposed a classification system for the shapes of stress-strain curves which is shown in Figure 1-4. The subdivisions within each type (a,b,c) indicate whether resistance increases, stays constant or decreases following yield. Johnson (1979) showed that the stress-strain curves from CIU tests on St. Croix clay were classified as either Type I or Type II, as defined in the system presented by Casagrande and Hirschfeld. Type I and Type II curves are well-rounded curves with the possible exception of an initial straight line section which terminates before half the maximum shear stress is attained.

1-2-4 Statistical Prediction Models for the Strength of Compacted Clay

Peterson (1975) performed regression analysis on the data from unconfined compression tests. The prediction equation of the unconfined compressive strength (\hat{q}_u) of a laboratory kneading compacted silty clay included density (ρ_d) and water content cubed (w^3):

$$\hat{q}_u = -91.16 + 1.56 \rho_d - 0.0187 w^3 \quad (1-11)$$

Essigmann (1976) and Scott (1977) also performed unconfined compression tests on a laboratory impact compacted silty clay. Table 1-2 shows the prediction regression equations for as-compacted and soaked strength. Price (1978) developed prediction equations similar to those of Scott and Essigmann, but by a slightly different approach. Tests run by Price were on field compacted samples, both as-compacted and saturated. The results of the statistical analysis are presented in Table 1-3. Weitzel (1979) determined the statistical as-compacted (UU) strength model of St. Croix clay compacted in the laboratory. The strength prediction model dry-of-optimum includes variables of water content, dry

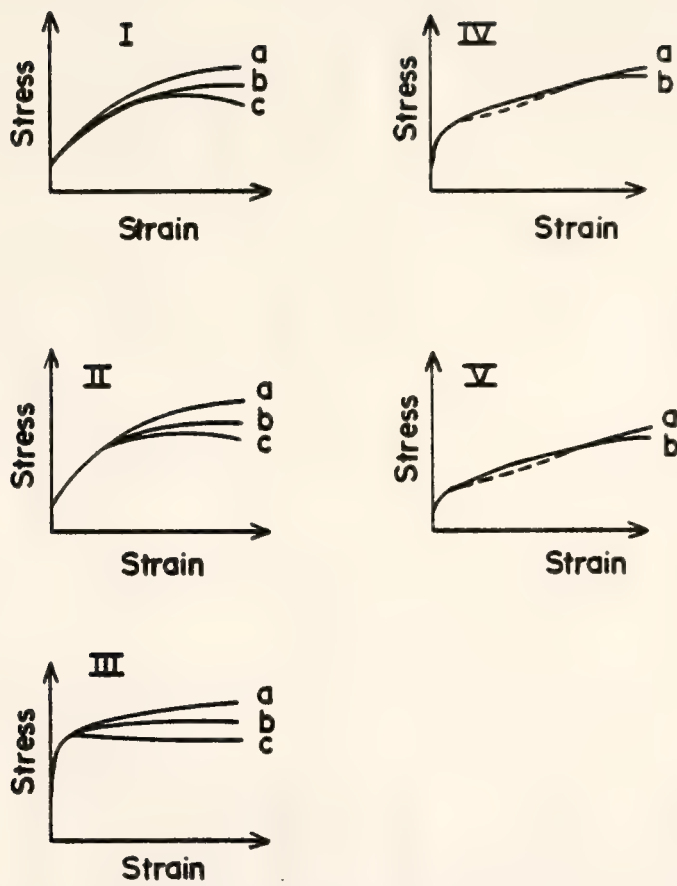


Figure 1-4 Classification of Stress-Strain Curves (After Casagrande and Hirschfeld, 1962)

TABLE 1-2 Regression Results for a Laboratory Compacted Clayey Silt
from Essigmann, 1976 and Scott, 1977

Dependent Variable	Moisture Range	Regression Relationship	R ²
As-compacted Unconfined Strength	All Moistures	$\hat{q}_u = 4.12 \rho_d - 0.049 \rho_d w - 393.3$	0.889
	Dry of Optimum	$\hat{q}_u = 4.14 \rho_d - 0.047 \rho_d w - 396.2$	0.888
	Wet of Optimum	$\hat{q}_u = 3.10 \rho_d - 0.073 \rho_d w - 231.8$	0.943
Soaked Strength	All Moisture	$\hat{q}_u^s = 26.184 w - 0.178 \rho_d^2 + 0.00106 \rho_d^3$ $- 0.000078 w^2 \rho_d^2 + 591.79$	0.553
	Dry of Optimum	$\hat{q}_u^s = -13.19 E^2 + 0.000679 \rho_d^2 E^2 +$ $0.0385 w^2 E^2 + 3.53$	0.715
	Wet of Optimum	$\hat{q}_u^s = -4.71 w + 69.427$	0.605

ρ_d = dry unit weight,pcf

\hat{q}_u^s = estimated soaked strength, psi

w = water content, %

E = energy ratio

\hat{q}_u = estimated unconfined compressive strength, psi

TABLE 1-3 Regression Results from Field Compacted Samples of Silty Clay (from Price 1978)

Roller Type/ Soil Condition	Dependent Variable	Regression Relationship	R^2
Sheepsfoot / As-compacted	Unconfined Strength	$\hat{q}_u = -2.058 w + 0.585 E + 0.353 \rho_d + 16.99$	0.419
Rubber Tired/ As-compacted	Unconfined Strength	$\hat{q}_u = -2.224 w - 0.155 E + 0.0734 \rho_d + 51.91$	0.29
Sheepsfoot / Soaked	Unconfined Strength	No Significant Models	
Rubber Tired/ Soaked	Unconfined Strength	$\hat{q}_u = 1.189 w + 0.195 E + 0.968 \rho_d - 118.37$	0.659

 ρ_d = dry unit weight, pcf

w = water content, %

E = compactive effect (No. of passes)

 \hat{q}_u = estimate unconfined compressive strength

density, degree of saturation and confining pressure. On the wet side, the logarithm of strength decreases linearly with initial void ratio. The prediction equations for as compacted strength confined and undrained are:

(a) Compressive strength, dry-of-optimum:

$$\hat{q}_c = -1784.8 + 3.1 \rho_d \sqrt{s_i} / w + 84.0 (1 - s_i/100) \sqrt{\sigma_3}$$

$$R^2 = 0.98 \quad (1-12)$$

(b) Compressive strength, wet-of-optimum:

$$\log(\hat{q}_c) = 1.70/e_o; R^2 = 0.99 \quad (1-13)$$

where ρ_d = dry density, kg/m^3

w = water content, %

σ_3 = confining pressure, kPa

e_o = initial void ratio

s_i = initial degree of saturation, %

\hat{q}_c = estimated compressive strength, kPa

R^2 = coefficient of determination

For the long term shearing behavior, Lovell and Johnson (1980) developed the relationships between the compaction conditions and the long term effective stress strength parameters for the St. Croix clay. The statistical prediction models for effective stress strength parameters, $\hat{\phi}'$ and \hat{c}' are

$$\hat{\phi}' = 20.1^\circ \pm 1.3^\circ \quad (1-14)$$

and

$$\hat{c}' = 1.71 - 3.83 w \log e_o \quad (1-15)$$

where \hat{c}' = estimated value of the effective stress strength intercept (kPa)

w = water content, %

e_o = initial void ratio

The multiple coefficient of determination (R^2) value of 0.63 is low but acceptable.

1-3 Volume Change Characteristics

1-3-1 Volume Change of Partically Saturated Soil

Coleman (1962) proposed a simple and consistent equation for volumetric strain applicable to the triaxial test.

$$\frac{-dv}{v} = -C_1 d(u_w - u_a) + C_2 \cdot d(\sigma - u_a) + C_3 d(\sigma_1 - \sigma_3) \quad (1-16)$$

where σ_1 = axial total stress

σ_3 = lateral total stress

$$\sigma = \frac{1}{3} (\sigma_1 + 2\sigma_3)$$

u_w = pore-water pressure

u_a = pore-air pressure

C_1, C_2, C_3 = compressibility factors in x, y, z direction

For isotropic loading, σ is the all around stress and

$$\frac{-dv}{v} = C_a d(u_w - u_a) + C_t d(\sigma - u_a) \quad (1-17)$$

where C_a = compressibility of the soil structure with respect

$$\text{to a change in } (u_a - u_w) = 3/H_1$$

H_1 = an elastic modulus with respect to a change in $(u_a - u_w)$

C_t = compressibility of the soil structure with respect to a change in $(\sigma - u_w)$

$$= 3 \frac{1 - 2\mu}{E}$$

μ = Poisson's ratio

E = elastic modulus with respect to a change in $(\sigma - u_w)$.

Matyas and Radhakrishna (1968) confirmed the findings of Jennings and Burland (1962) that the principle of effective stress is inadequate to explain the volumetric behavior of partially saturated soils subjected to different stress paths. They found that the volumetric strain could be expressed as a direct function of two independent stress components, applied stress and suction, rather than in terms of a single effective stress. Barden (1969) introduced the form of equation (1-16) for the case of one-dimensional compression. The relevant equation became:

$$\frac{-dv}{v} = C_1 d(\sigma - u_a) + C_2 d(u_a - u_w) \quad (1-18)$$

where the coefficients C_1 and C_2 are functions only of the current stresses. He also found that the general transition from a flocculent structure on the dry side of optimum to a oriented structure on the wet side results in a very different compression behavior for clays compacted dry and wet of optimum. Fredlund and Morgenstern (1976) proposed two volume change relations for unsaturated soils from a semi-empirical standpoint. The first equation is for the deformation of the soil fabric.

$$\begin{aligned} \epsilon_v &= \frac{1}{v} \cdot \frac{\partial v}{\partial(\sigma - u_a)} \cdot d(\sigma - u_a) \\ &\quad + \frac{1}{v} \cdot \frac{\partial v}{\partial(u_a - u_w)} \cdot d(u_a - u_w) \end{aligned} \quad (1-19)$$

where $\epsilon_v = \Delta V/V = \text{volumetric strain}$

$v = \text{unit volume}$

$\frac{1}{v} \cdot \frac{\partial v}{\partial(\sigma - u_w)} = \text{compressibility of the soil structure when } d(u_a - u_w) \text{ is zero.}$

$\frac{1}{v} \cdot \frac{\partial v}{\partial(u_a - u_w)} = \text{compressibility of the soil structure when } d(\sigma - u_w) \text{ is zero.}$

The second equation is for the change in volume of water in the element.

$$Q_w = \frac{1}{v} \cdot \frac{\partial v_w}{\partial(\sigma - u_a)} \cdot d(\sigma - u_a) + \frac{1}{v} \frac{\partial v_w}{\partial(u_a - u_w)} \cdot d(u_a - u_w) \quad (1-20)$$

where v_w = volume of water in the element

$\frac{1}{v} \cdot \frac{\partial v_w}{\partial(\sigma - u_w)}$ = slope of the water volume vs. $(\sigma - u_w)$ plot
when $d(u_a - u_w)$ is zero.

$\frac{1}{v} \cdot \frac{\partial v_w}{\partial(u_a - u_w)}$ = slope of the water volume vs. $(u_a - u_w)$ plot
when $d(\sigma - u_w)$ is zero.

Conlin (1972) measured volume change both during application of confining pressure and throughout shear in his UU triaxial tests on a highly plastic clay. The general trends are shown in Figure 1-5. It can be seen that the volumetric strain due to confining pressure increased with water content up to optimum. But the total volumetric strain decreased as water content increased because of the increased saturation. Also the volumetric strain increased with increasing confining pressure at constant water content.

1-3-2 Volume Change due to Saturation

This volume change of compacted clay is associated with a change in water content rather than a change in applied stress. The volume changes which result could be either increases (swell) or decreases (settlement), depending upon the level of confinement and the compaction variables. Ladd (1960) indicates that the swelling behavior of a compacted clay is governed primarily by composition of clay, compaction conditions, chemical

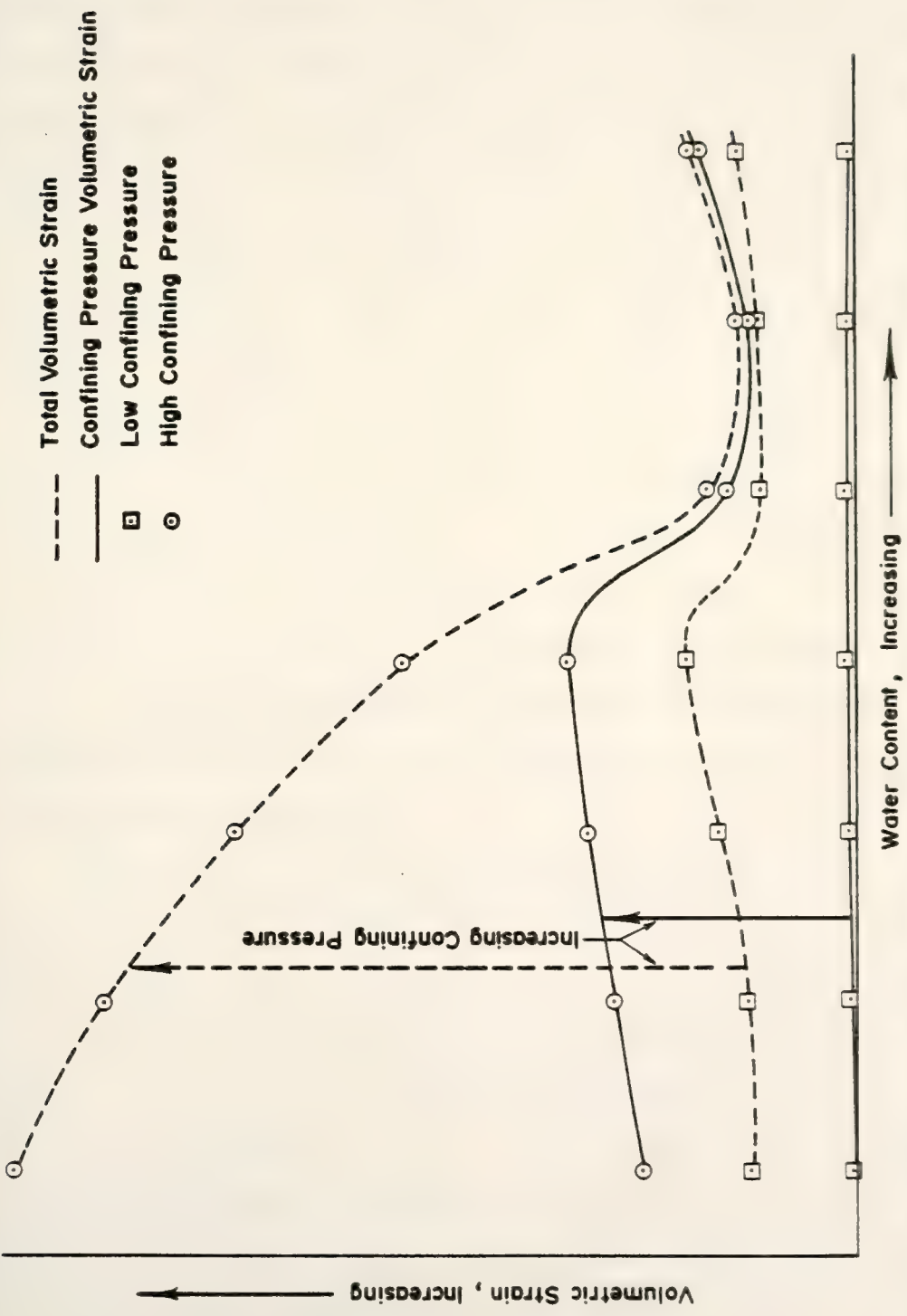


Figure 1-5 Volumetric Strain Behavior During an Unconsolidated - Undrained Triaxial Test
(After Conlin, 1972)

properties of the pore fluid, confining pressure applied during swelling and time allowed for swelling. He concludes that the osmotic repulsive forces play an important role in the swelling of compacted clays for samples which are compacted wet of optimum. However, for dry of optimum samples, swelling is influenced by factors in addition to osmotic pressure. Seed, Mitchell, and Chan (1960) compared the amounts of swell for samples of a sandy clay compacted dry and wet of optimum by static and kneading compaction. They concluded that specimens compacted dry of optimum exhibited greater swelling tendencies and swelled to higher water contents than specimens at the same dry density compacted wet of optimum. Seed, Woodward, and Lundgren (1962) also showed that low water contents and high dry densities caused compacted clays to swell the most. Swelling decreased with increasing confining pressure. DiBernardo (1979) found that one-dimensional volume change on saturation of St. Croix clay compacted in the laboratory was a function of as-compacted water content and nominal compaction pressure. His statistical prediction equation is

$$\hat{\frac{\Delta V}{V_o}} (\%) = 25.47 - 0.872 w - 0.0048 P_c^2; R^2 = 0.86 \quad (1-21)$$

where V_o = as-compacted volume

ΔV = the volume change from the as-compacted
to the fully saturated condition under a
surcharge load.

$\hat{\Delta V/V_o}$ = estimated volumetric strain (%)

w = as-compacted water content (%)

P_c = nominal compaction pressure (kN/m^2)

This relationship for one-dimensional percent volume change on satura-

tion is plotted in Figure 1-6. For a given water content, as the compaction pressure is increased, there is less tendency toward settlement and more toward swell. Similar trends are established for increasing water content at a constant compaction pressure.

Lin (1981) developed the statistical volume change model of St. Croix clay compacted in the field by both Caterpillar and Rascal model vibratory rollers. He further developed a correlation between a similar soil compacted in the laboratory and the field compacted soil. Lin's one-dimensional percent volume change model is

$$\hat{\frac{\Delta V}{V_o}} (\%) = -2.26 + 0.400 e_o \cdot P_o^{\frac{1}{2}} - 0.00026 w \cdot P_o; R^2 = 0.79 \quad (1-22)$$

Where e_o = void ratio

P_o = equivalent embankment pressure

w = water content (%)

Figure (1-7) shows the comparison of Lin's laboratory and field volume change models at a constant water content (14%). Both curves indicate that increasing the initial void ratio reduces the swelling tendency, and as the equivalent embankment pressure increases, the volumetric strain eventually becomes settlement. Lovell and Johnson (1980) developed a statistical prediction equation for percent volume change due to saturation and consolidation on triaxial samples, relating the compaction variables to the properties of the compacted soil. The samples were formed in the laboratory with a kneading compactor. The prediction equation is a function of as-compacted dry density (ρ_d), initial degree of saturation (S_i), and isotropic consolidation pressure (σ_c').

$$\hat{\frac{\Delta V}{V_o}} (\%) = 28.48 - 0.0000136 \rho_d^2 + 0.0077 S_i \sqrt{\sigma_c'}; R^2 = 0.95 \quad (1-23)$$

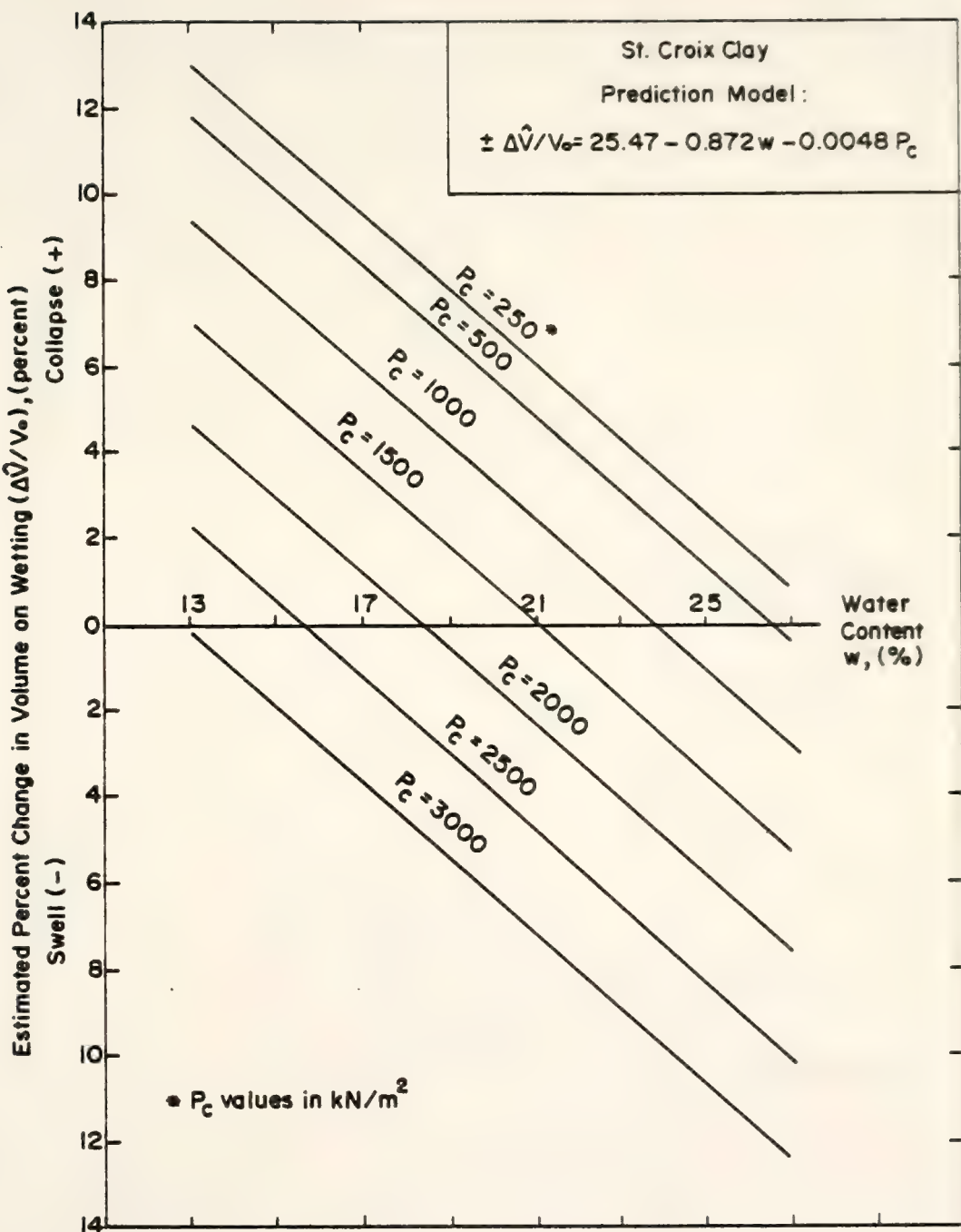


Figure I-6 Prediction of Percent Volume Change on Wetting (After DiBernardo, 1979)

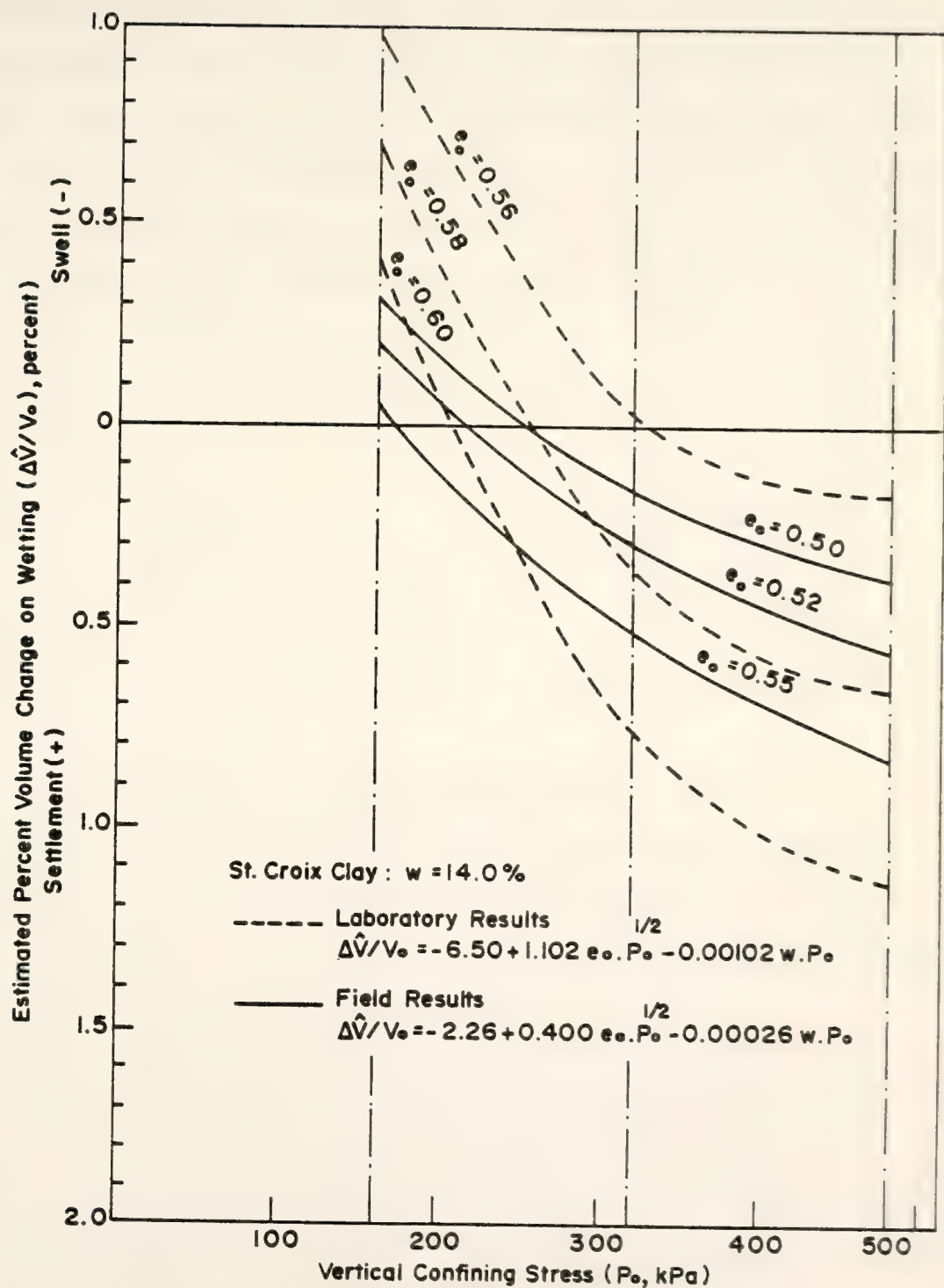


Figure I-7 Effect of Void Ratio on Percent Volume Change Model at a Constant Water Content (After Lin, 1981)

The relationship between predicted percent volume change due to saturation and consolidation and dry density for an initial saturation of 80% is shown in Figure 1-8. The figure shows that for a constant value of saturation, $\hat{\Delta V}/V_0$ decreases as dry density increases. It also shows that for constant values of dry density and initial degree of saturation, $\hat{\Delta V}/V_0$ increases as the consolidation pressure increases.

From the above review, it can be seen that the volume change due to wetting of compacted clay is a function of the as-compacted void ratio, the water content, and the confining pressure (or the surcharge pressure for oedometer specimens). The volume change characteristics of triaxial specimens of compacted shale on saturation were studied by Abeysekera (1978). Figure 1-9 shows contours of percentage of volume change in terms of the as-compacted void ratio and the consolidation pressures.

1-4 Pore Pressure Response During Undrained Shear

For a change in stress under undrained conditions the change in pore pressure (Δu) may be expressed (Skempton, 1954) as

$$\Delta u = B \left[\Delta \sigma_3 + A(\Delta \sigma_1 - \Delta \sigma_3) \right] \quad (1-24)$$

where $\Delta \sigma_1$ = change in major principal stress

$\Delta \sigma_3$ = change in minor principal stress

B = an empirical coefficient related to the degree of saturation and sample stiffness.

A = an empirical coefficient which describes the pore pressure response to shear stress.

Under undrained shear, normally consolidated and lightly overconsolidated clays tend to densify when loaded and to develop positive pore water pressure. Highly overconsolidated clays tend to dilate

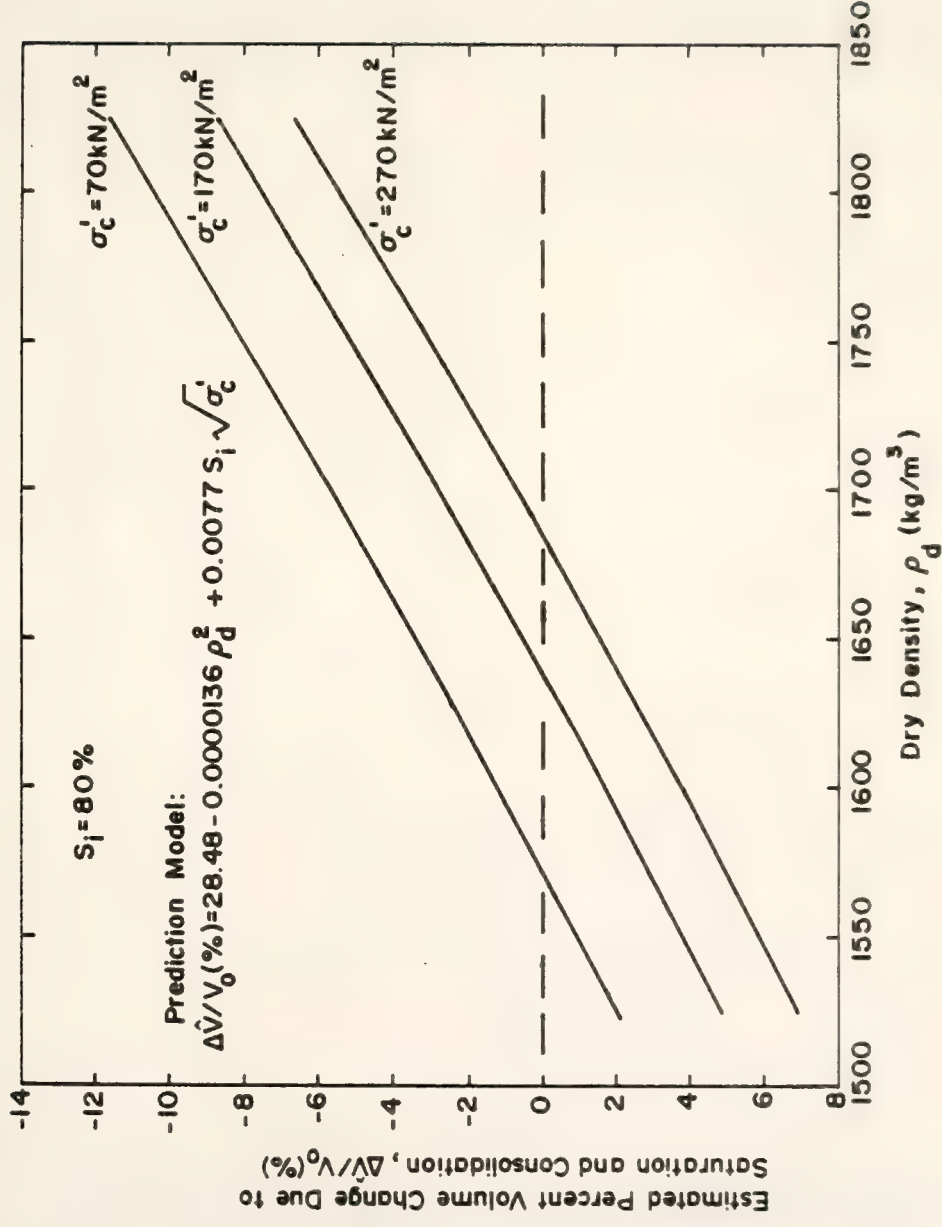


Figure I-8 Prediction of Percent Volume Change Due to Saturation and Consolidation
 (After Johnson, 1979)

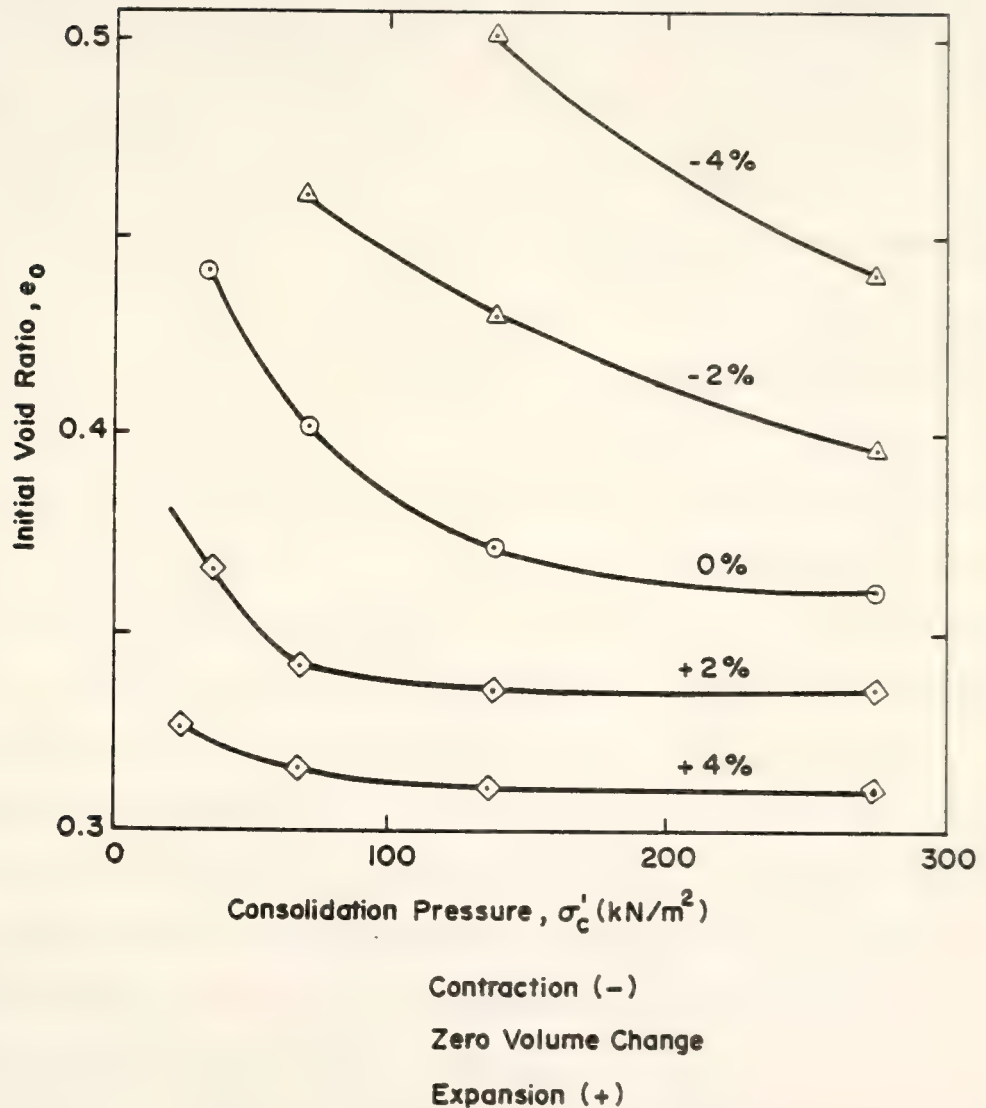


Figure I-9 Contours of Percent Volume Change (After Abeysekera, 1978)

when loaded and to develop negative pore water pressure. This is illustrated in Figure (1-10) where the A values for normally and overconsolidated clay are given (Bishop, 1960). Triaxial compression tests show that for fully saturated soils $B = 1$ (within practical limits of accuracy), and that the values of A at failure are very dependent on the OCR. Henkel (1956), Bjerrum (1960), and Simons (1960) also presented data which showed that the magnitude of the A parameter at failure is a function of OCR. Figures 1-11, 12a, 12b show results obtained from Henkel, Bjerrum, and Simons. Lambe and Whitman (1969) collected typical values for the A factor, as shown in Table 1-4. The tabulated values show that the A parameter at failure can range from 2 to 3 for very loose sand to -0.5 for heavily overconsolidated clay. Abeysekera et al (1978) proposed that the value of the A parameter at failure, shown in Figure 1-13, is a function of the ratio of the compaction pressure to the consolidation pressure (P_c / σ'_c), which is analogous to the overconsolidation ratio, OCR, for a compacted shale. They also found that for a given value of (P_c / σ'_c), the higher values of A_f were observed at the lower molding water contents. Johnson (1979) developed a prediction for Skempton's A parameter for St. Croix compacted clay at failure as follows

$$\hat{A}_f = 1.79 - 0.00011 \rho_d \sqrt{S_i} + 1.28 \sigma'_c / \rho_d; R^2 = 0.71 \quad (1-25)$$

where \hat{A}_f = estimated value of Skempton's A parameter at failure

ρ_d = as-compacted dry density (kg/m^3)

S_i = initial degree of saturation (%)

σ'_c = isotropic consolidation pressure (kN/m^2)

Figure 1-14 shows for constant values of initial degree of saturation that an increase in dry density produces a decrease in \hat{A}_f . It also

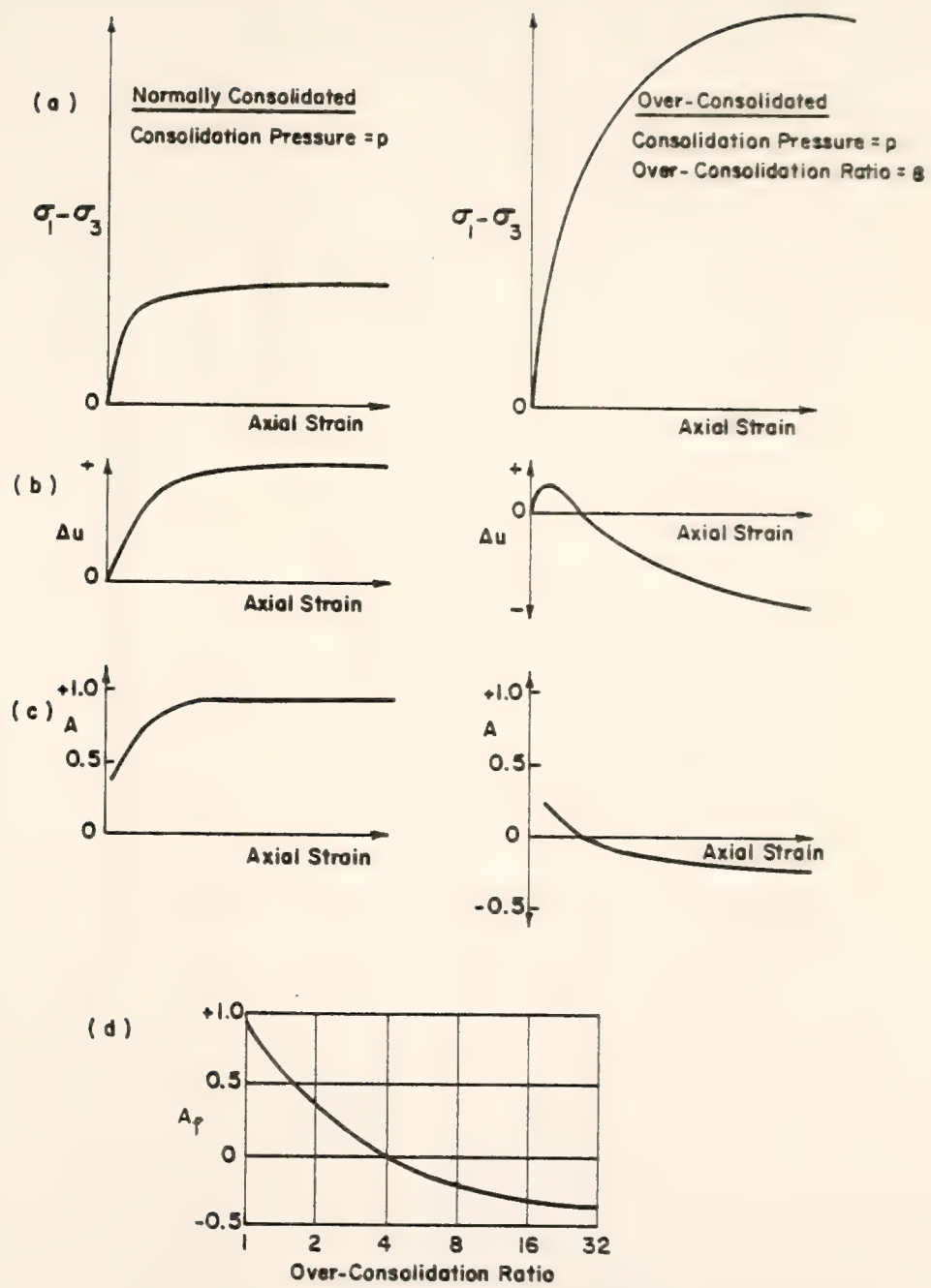


Figure I-10 The Dependence of the Pore Pressure Parameter A on Stress History (After Bishop, 1960)

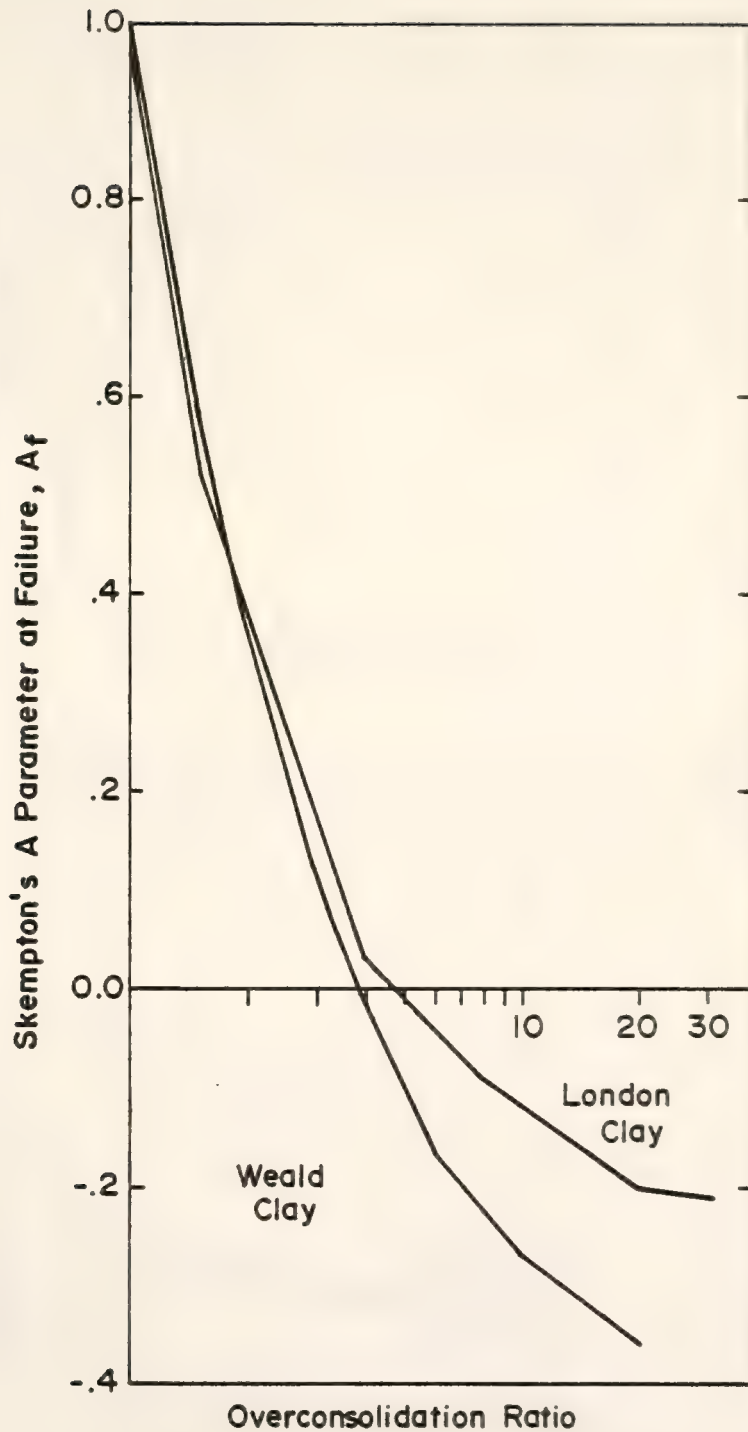


Figure I-II A_f Versus Overconsolidation Ratio (After Henkel, 1956)

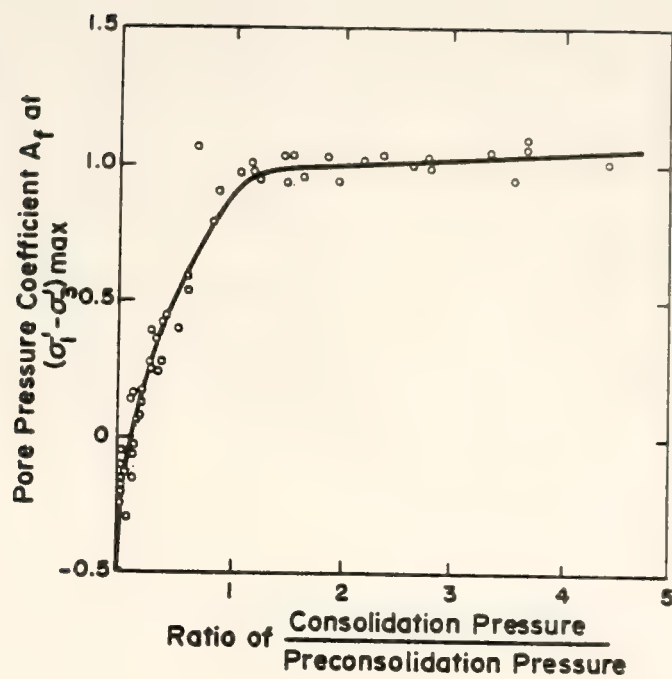


Figure I-12a Relationship Between A_f and the Ratio of the Consolidation Pressure to the Preconsolidation Pressure (After Bjerrum ,1960)

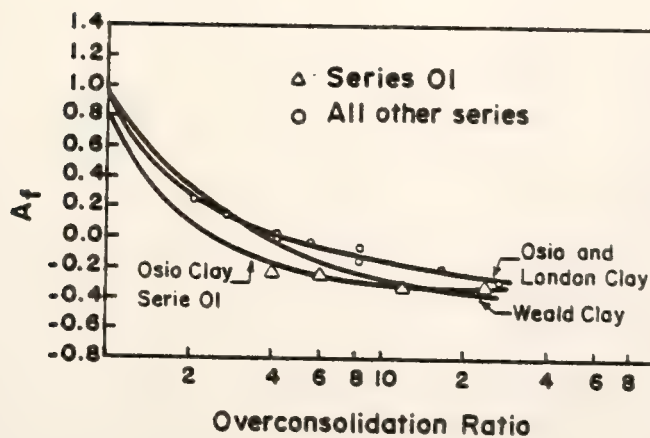


Figure I-12b Relationship Between A_f and Overconsolidation Ratio (After Simons ,1960)

TABLE 1-4a Value of Parameter A_f (Lambe and Whitman, 1969)

Material ($S_r = 100\%$)	A_f
Very loose fine sand	2 to 3
Sensitive clay	1.5 to 2.5
Normally consolidated clay	0.7 to 1.3
Lightly overconsolidated clay	0.3 to 0.7
Heavily overconsolidated clay	-0.5 to 0

Table 1-4b Value of Parameter B (Lambe and Whitman, 1969)

Material	$S_r (\%)$	B
Sandstone	100	0.286
Granite	100	0.342
Marble	100	0.550
Concrete	100	0.582
Dense Sand	100	0.9921
Loose Sand	100	0.9984
London Clay (OC)	100	0.9981
Gosport Clay (NC)	100	0.9998
Vicksburg Buckshot Clay	100	0.990
Kawasaki Clay	100	0.9988 to 0.9996
Boulder Clay	93	0.69
	87	0.33
	76	0.10

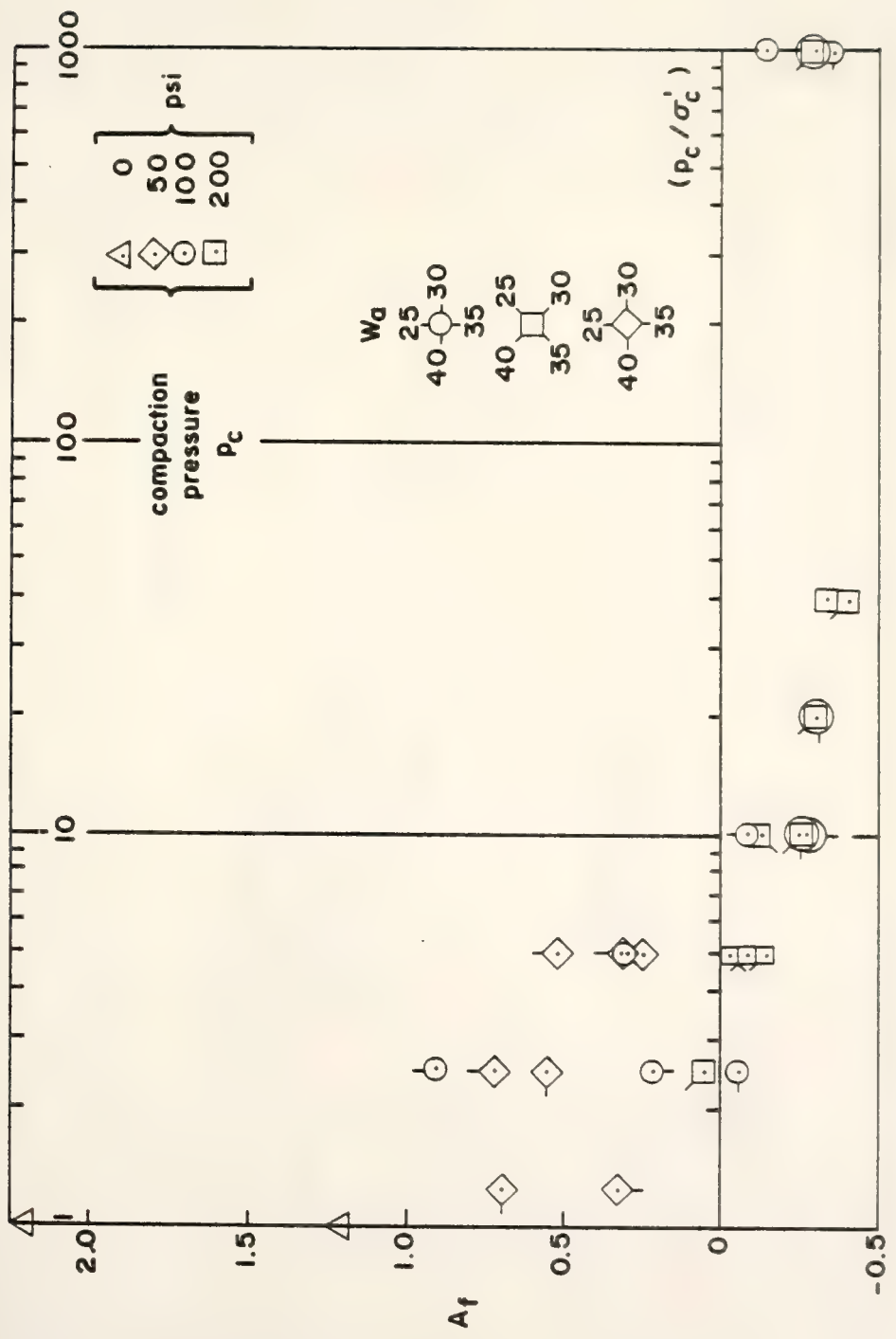


Figure I-13 Variation of A_f with $\log(p_c / \sigma'_c)$ for Compacted Specimens Having Different Initial Gradations and Molding Water Contents (After Abeysekera et al, 1978)

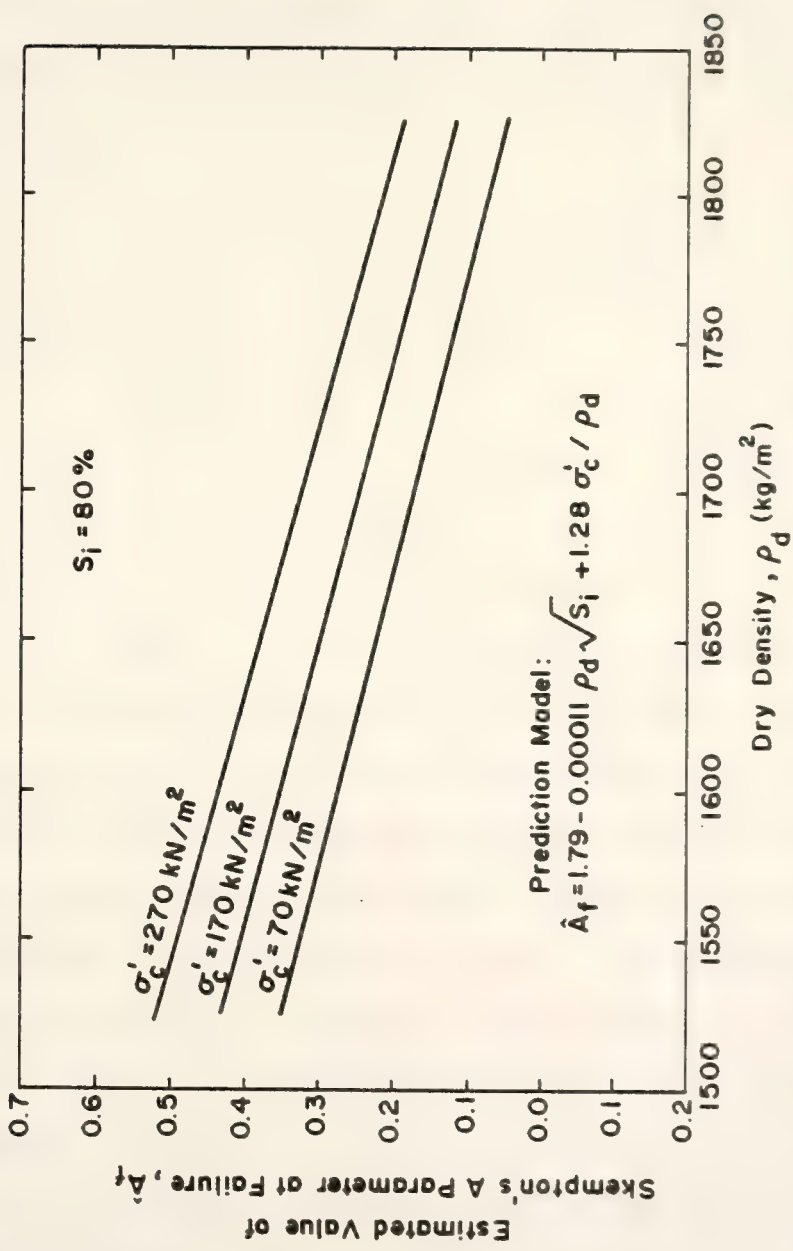


Figure 1-14 Prediction of Skempton's A Parameter at Failure for an Initial Saturation of 80%
(After Johnson, 1979)

shows that an increase in consolidation pressure, representative of decrease in OCR, results in an increase in A_f . Essentially the relationship between A_f and OCR is unique for a given saturated remolded clay. But for compacted samples with different initial gradations and molding water contents, the relationship between A_f and OCR may not be unique.

1-5 Comparison of Field and Laboratory Compacted Strengths

Several compaction methods have been studied in the laboratory. In general, the compaction types used are static, impact, kneading and vibratory. The factors that influence laboratory compaction are compaction type, size and shape of mold, support for the mold, method of preparing the sample and compacting the soil, method of determining moisture content and degradation during compaction.

Field compaction of soils has been accomplished through the use of smooth wheel rollers, tamping-type rollers, pneumatic rollers, vibratory compactors, and track-type tractors, and tampers. The principal factors that influence field compaction are soil type, moisture conditions, compactive effort, speed, type of compaction equipment, thickness of lift, climatic conditions, and etc. The characteristic variables pertaining to each type of field compaction equipment are listed in Table 1-5. For the purpose of predicting field compactor performance, Selig (1971) developed a set of equations, as shown in Table 1-6, for defining compactive effort of the four following basic classes of roller: smooth wheel, pneumatic, tamping, and vibratory. Equations were derived for the compactive effort per unit volume of soil, production rate in volume of soil compacted per unit time, and horsepower required to provide the towing force at a desired speed.

TABLE 1-5 Characteristic Variables Pertaining to the Different Type of Field Compacting Equipment (After Wahls, et al., 1966)

Type of Field Compactor	Characteristic Variables*
Smooth-wheel power rollers	gross weight, diameter of rolls, width of rolls, and compression (lb/in. of roller)
Pneumatic-tired rollers	gross weight, roller dimensions, type roller, tire inflation pressure, contact pressure, contact area
Tamping-type rollers (sheepsfoot, segmented)	gross weight, type of foot, number of feet/drum, area of foot, foot contact area in percent of total area of cylinder generated, length of feet, dimensions of drum, contact pressure
Vibratory compactors (base plate type)	gross weight, weight of each vibrating unit, contact area of base plate, unit contact pressure, frequency, amplitude, dynamic force, speed of travel
Vibratory compactors (roller type)	gross weight, roller weights, dimensions of roller, frequency, amplitude, speed of travel
Track-type tractors	gross weight, width of track, contact pressures, speed of travel
Tampers	weight, area of base plate, height of jump

* The table includes both independent and dependent variables.

TABLE 1-6 Summary of Equations by Selig (1971)

<u>Horsepower, H</u>	<u>Roller</u>	<u>Expression</u>
All types		$H = 27 \times 10^{-4} f W S, \text{ or}$ $= 1.38 \times 10^{-5} RE$

TABLE 1-6 (Continued)

Symbols and Dimensions

A = Contact area of tamping foot, sq ft

B = Roller width, ft

b = Width of tire, ft

c = Foot area correction factor, > 1.0

D = Roller drum diameter, ft

d = Center-to-center tire spacing, ft

E = Compactive effort per unit volume, ft-lb/cu ft

f = Coefficient of compaction, ($f = k \cdot t/p$)

H = Horsepower

H_v = Horsepower of vibrator engine

$h = n \cdot b$ for $d > 2b$

$= B = b + (n - 1) \cdot d$ for $d < 2b$

k_o = Overlap correction factor, < 1.0

ℓ = Tamping foot length, ft

N = Number of tamping feet

n = Number of tires

P = Number of passes

R = Production rate, cu yd/hr

S = Forward speed, mph

t = Compacted lift thickness, ft

W = Total weight, lb

k = Compaction constant, pass/ft

These equations may be the best available to estimate roller performance.

Generally, field compacted shear strength characteristics are inferred from tests run on laboratory compacted specimens at the same moisture and density. However, the compaction method also has an influence on the fabric of the soil which, in turn, has an influence on the shear strength for a given water content and dry density. Therefore, the field compacted strengths may not be identical with the laboratory compacted ones.

The Waterways Experiment Station (1949) conducted comprehensive laboratory and field investigations on a compacted Vicksburg silty clay. Typical data which present the molding water content - dry density - strength relationships are presented in Figure 1-15. It may be seen from Figure 1-15A and 1-15C that the strength of the laboratory compacted samples are quite different from the strength of the field compacted samples for both the soaked and the unsoaked conditions. Because the moisture-density conditions are also in general quite different, it is difficult to isolate the effect of the method of compaction. However, in the soaked case, the strength of the laboratory sample is still higher than the field compacted sample up to a water content of about 20%. For the unsoaked materials, the strength of the laboratory sample is lower than the field compacted samples for water contents above about 17%. It also can be seen that an increase in density may or may not produce an increase in shearing resistance. For the soaked CBR values on the dry side of optimum, it appears that there is a continuous increase in strength until approximately the optimum is reached. However, for the unsoaked material, the maximum strength appears to be obtained at the driest water content. These observations

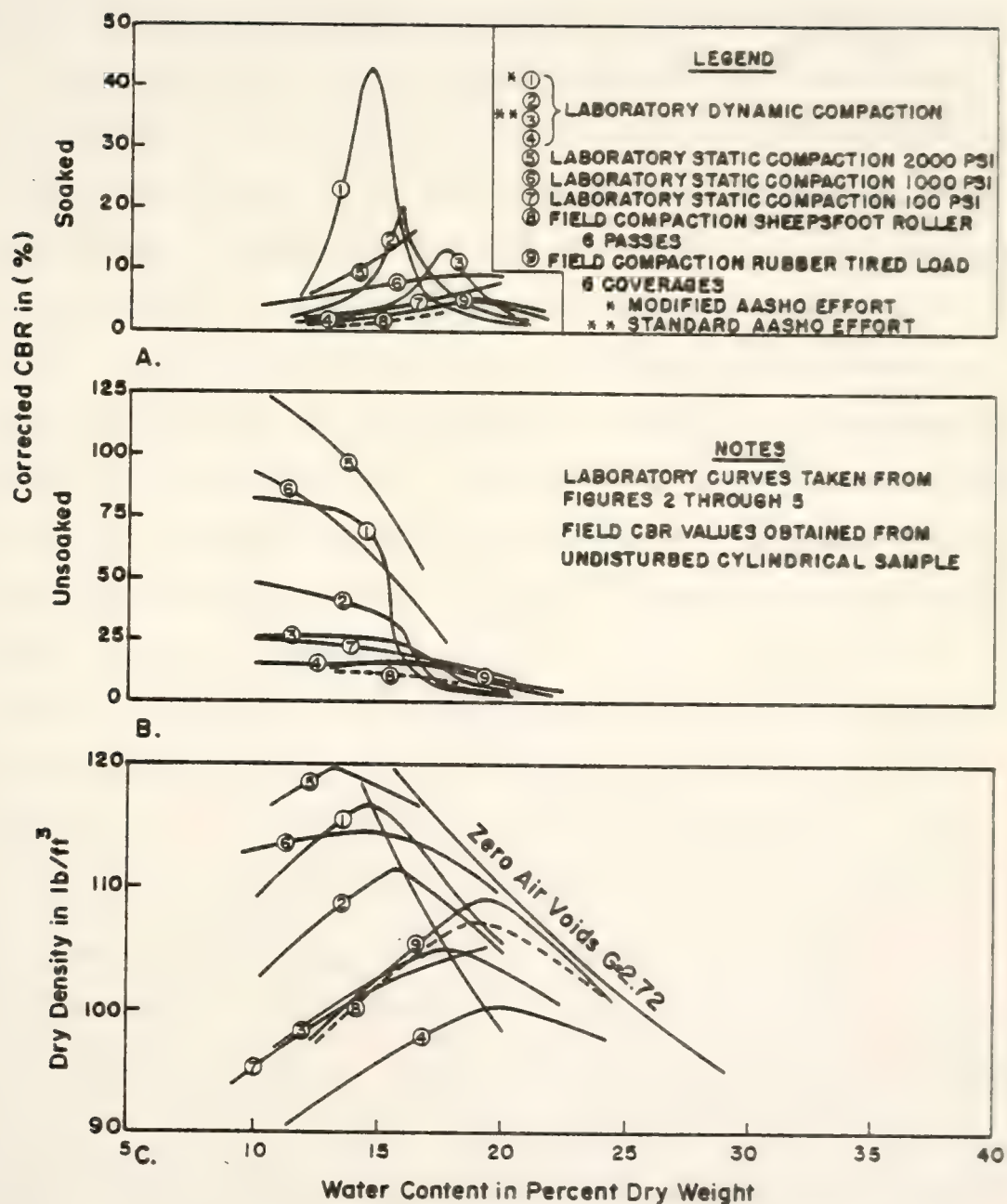


Figure I-15 Comparison of Field and Laboratory Compaction and CBR. (After WES, 1949)

are in agreement with the previously mentioned concept of the influence of soil structure on the shear strength of compacted cohesive soils.

Holtz and Ellis (1964) performed a series of triaxial shear tests on specimens of lean clay soil which were compacted by heavy sheepsfoot rollers, and compacted in the laboratory by impact and kneading compaction methods. Their results show that the strengths of soils compacted by the standard laboratory and the field methods are close to each other. Peterson (1975) collected compaction data from published and unpublished sources. Additional data were obtained from an embankment being constructed by the IDOH. Regression equations were then developed to explain the laboratory strength relationship. Next, these laboratory relationships were statistically tested as predictors of field performance. Peterson noted that a reasonable correlation exists between laboratory as-compacted and field as-compacted strength. Essigmann (1976) and Scott (1977) developed a technique to predict the expected variability of both the dry density and the unconfined shear strength for a clayey silt tested in the as-compacted and the soaked conditions. Their results indicate that the variations in dry density and strength are dependent upon both the compaction process and the soil conditions at the time of compaction. Price (1978) performed a statistical examination of a glacial silty-clay soil compacted in the field by either a rubber-tired roller or a sheepsfoot roller. He also used the results obtained by Essigmann (1976) and Scott (1977) (who developed similar relationships for a laboratory compacted soil) to develop a prediction method for field-compacted strengths. The field and laboratory strength regression models are presented in Figure 1-16, 17, 18 for the as-compacted and soaked soil conditions. He concluded that field strength

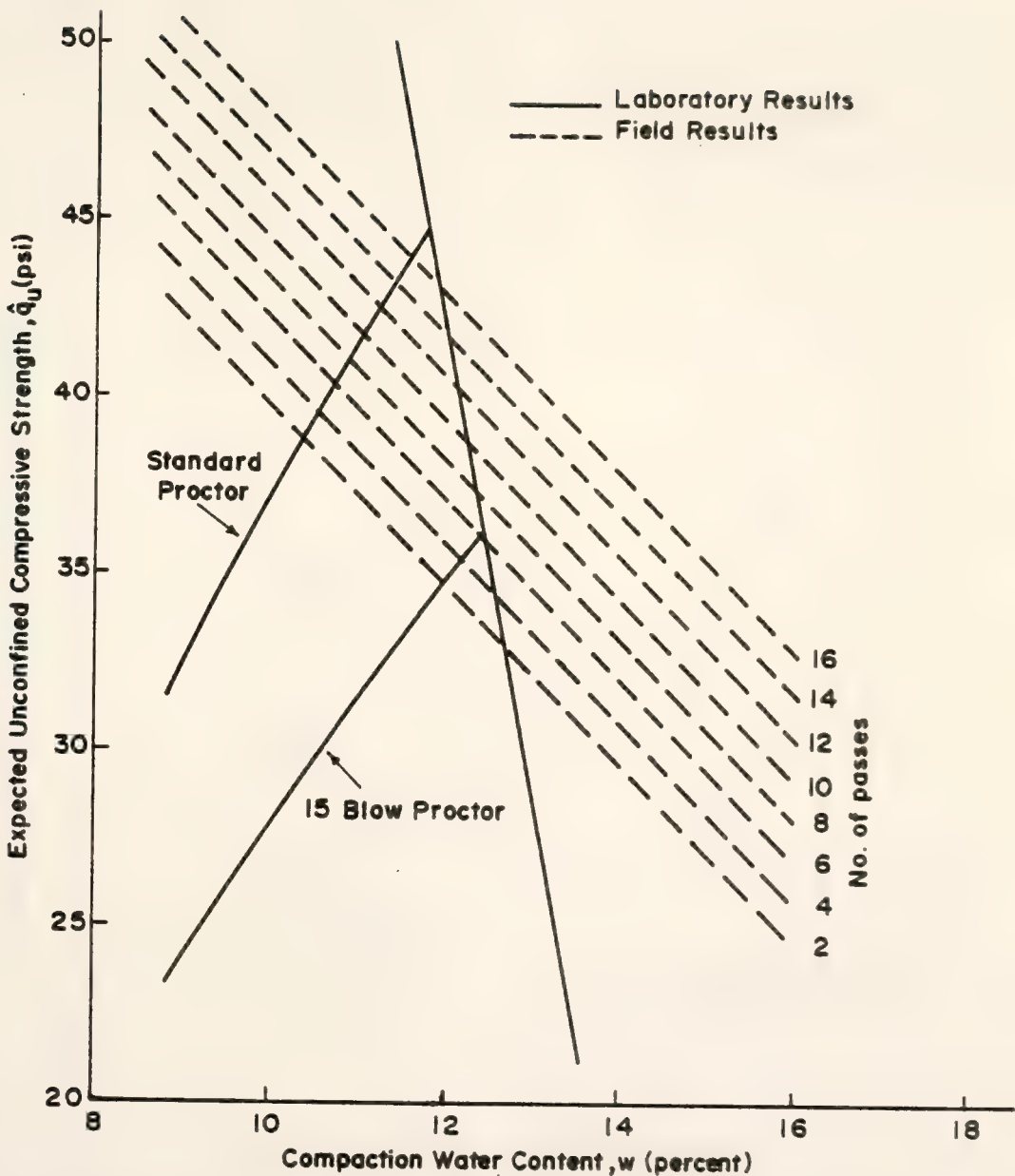


Figure I-16 Laboratory to Field Strength Correlation: Sheepsfoot Roller, As-Compacted (After Price, 1978)

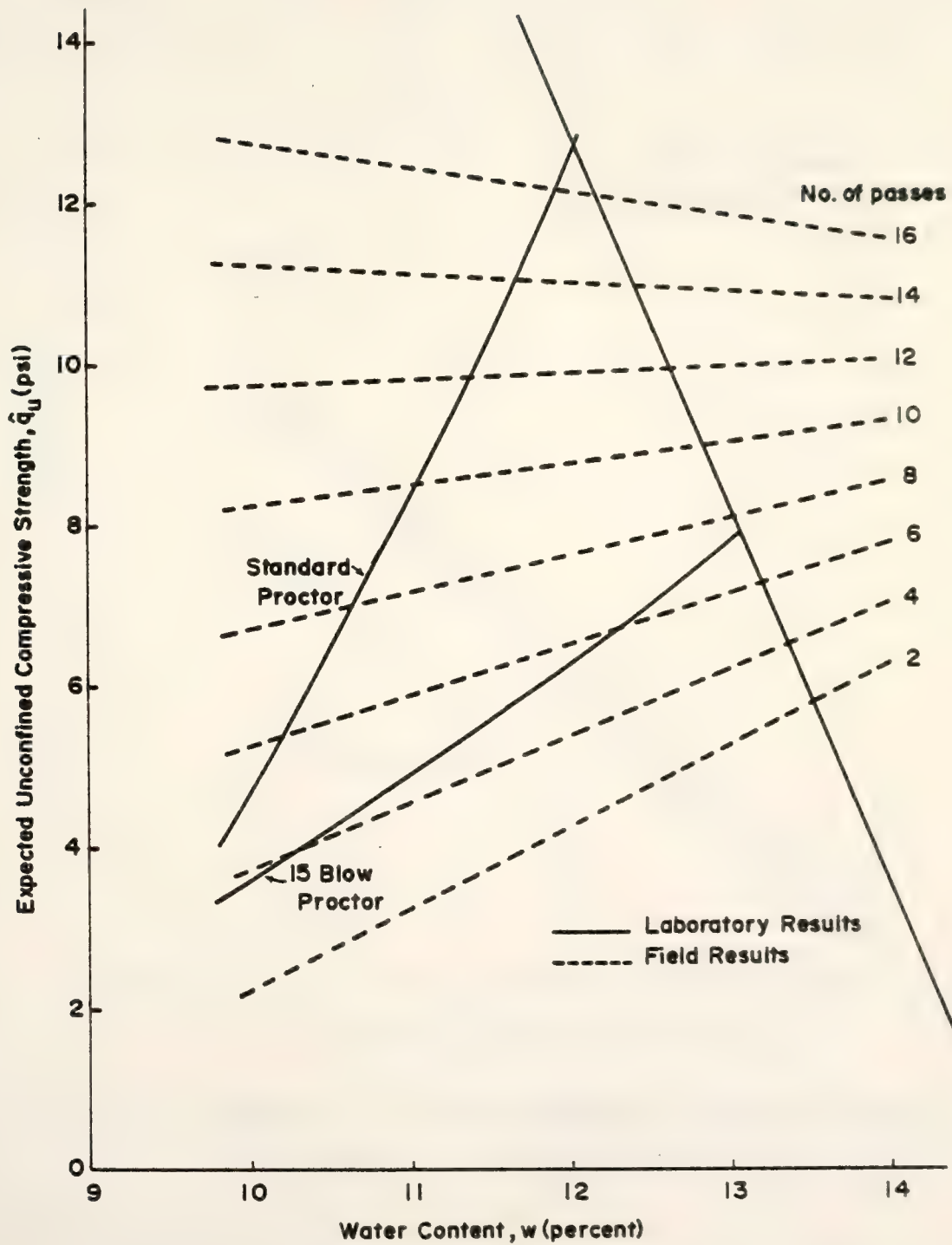


Figure I-17 Laboratory to Field Strength Correlation : Rubber-Tired Roller, Soaked (After Price, 1978)

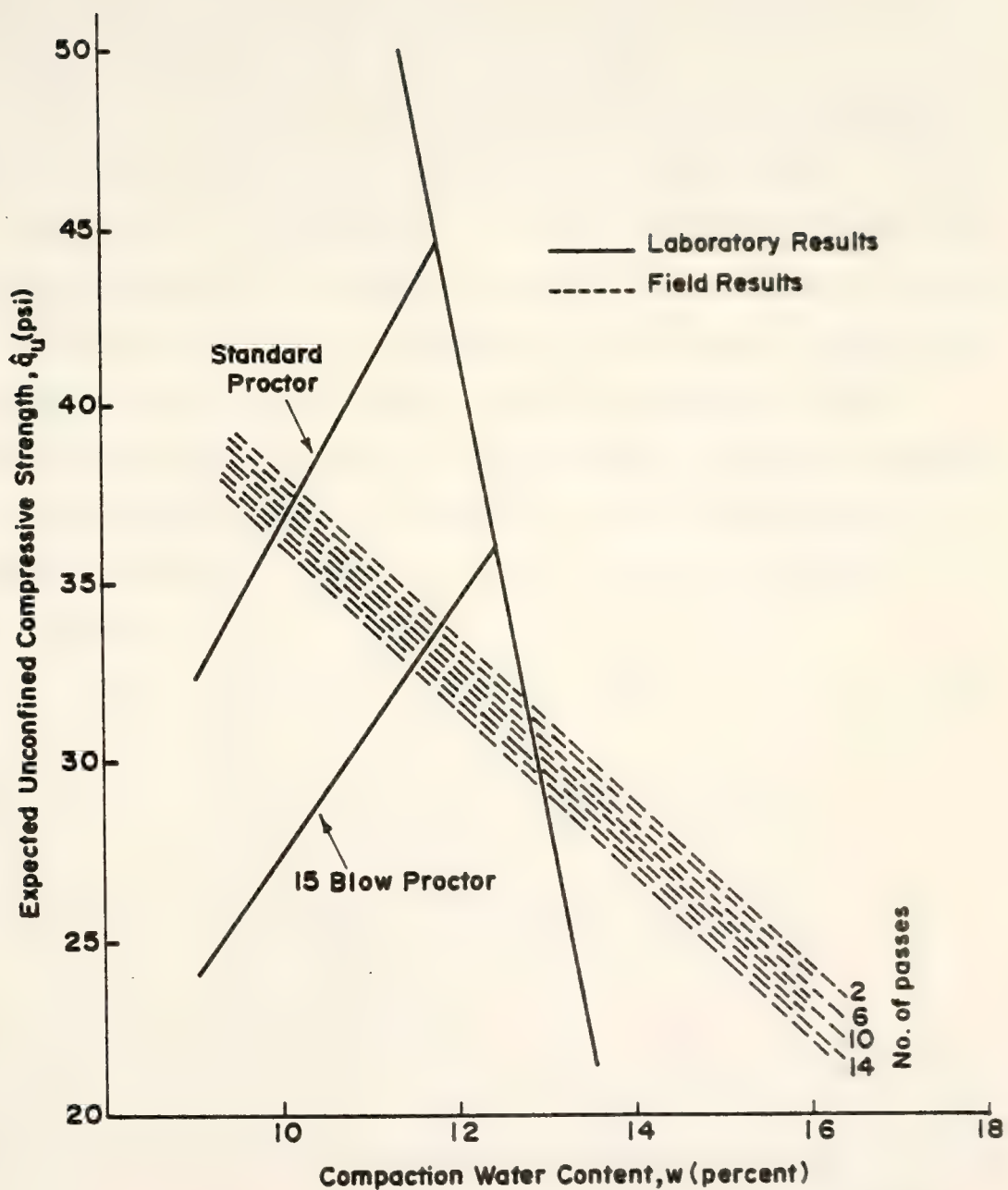


Figure I-18 Laboratory to Field Strength Correlation : Rubber-Tired Roller, As-Compacted (After Price, 1978)

response could be predicted by laboratory testing, particularly if a simple graphic superposition technique were used.

Lin (1981) developed the compactive prestress regression models for the laboratory and field as-compacted soil shown in Figure 1-19. It is observed that for a given water content, the estimated compactive prestress increases with increasing compaction pressure for both laboratory and field compacted St. Croix clay. If the compaction pressure is held constant, an increase in water content will result in a lower value of compactive prestress. He also developed a predictive prestress relationship between similar laboratory and field compacted soils by using the ratios of the plasticity indexes (IR) of the two soils.

The equation is:

$$\hat{P}_s \text{ (field)} = 95.42 + 75.62 \text{ IR} + 0.547 \hat{P}_s \text{ (lab)} \quad (1-31)$$
$$R^2 = 0.80$$

where $\hat{P}_s \text{ (lab)}$ = estimated value of compactive prestress for laboratory compacted soil

$\hat{P}_s \text{ (field)}$ = estimated value of compactive prestress for field compacted soil

$$\text{IR} = I_p \text{ (field)} / I_p \text{ (lab)}$$

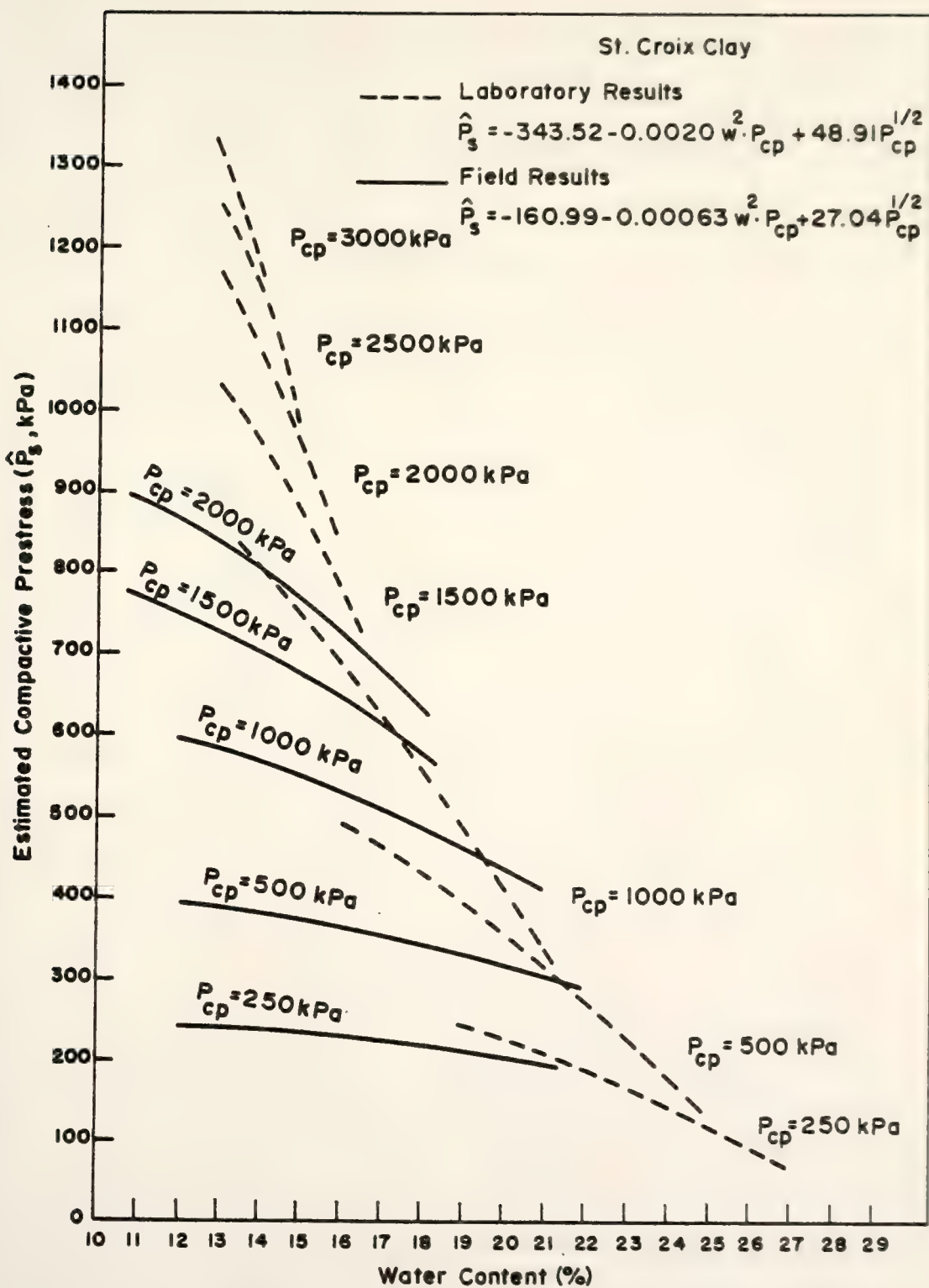


Figure I-19 Compactive Prestress Models (After Lin, 1981)

2- APPARATUS AND EXPERIMENTAL PROCEDURE

2-1 Soils Studied

The soils utilized for both the field and laboratory compaction studies were obtained from a cut and fill area in the relocation project of State Road 37, about four miles south of St. Croix, Indiana. They were shale and sandstone residuals of tan color with gray and red mottling. Numerous friable sandstone rocks were present throughout the mass, and some of the gray mottled areas of the soil had a shaly structure. The results of classification tests on both the field and the laboratory compacted soils are shown in Table 2.1. The cause for the difference between the soils used for field and laboratory studies can be seen from boring logs (IDOH) shown in Figure 2-1. The soil taken for laboratory compaction was from greater depths (5.5 to 13.0 ft). The upper soils (0 to 5.5 ft) were to be used for the test pad base only, with the deeper soils being compacted in the pads proper. However, there was an inadvertent mixing of the two. The two soils are almost identical in appearance. Typical moisture-density curves for both laboratory and field test pad soils are shown in Figure 2-2. They were obtained by the impact compaction method. The test pad soil, with lower plasticity, had a higher density than the soil with higher plasticity. It can be seen that the efficiency of compaction decreased for all levels of water content as plasticity increased.

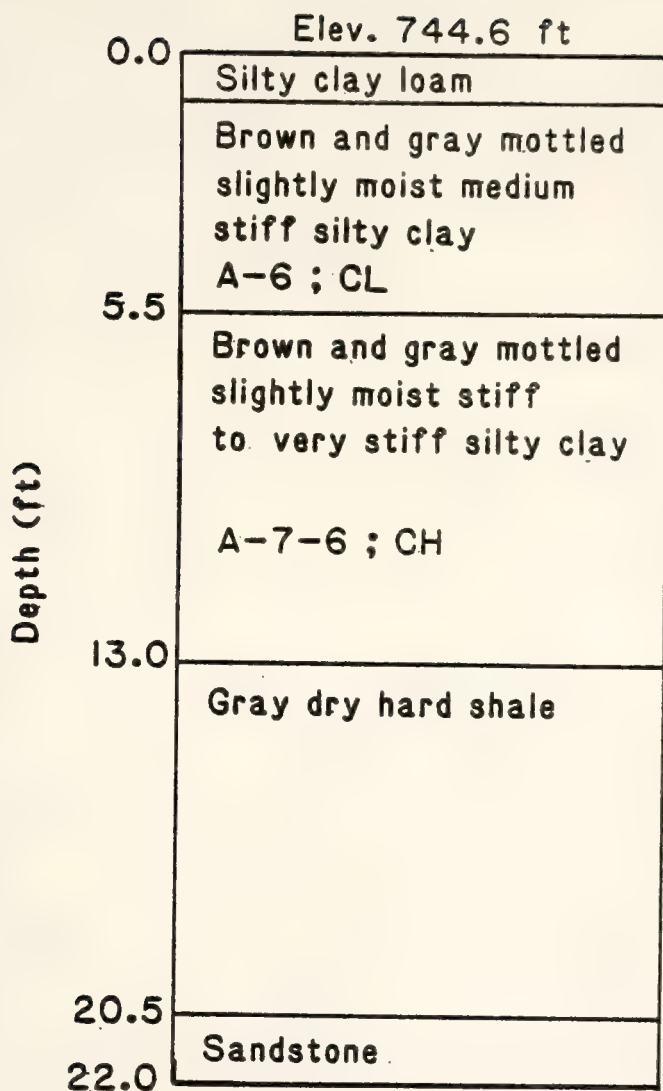
2-2 Field Compaction Samples

2-2-1 Test Pad Construction

Ten test pads were constructed in the fill area of the relocation

TABLE 2-1 Index Properties and Classification of St. Croix Clay

	Test Pad	Laboratory
Atterberg Limits (%)	w_L 40.0 (30.0, 53.2)	52
	w_p 18.4 (16.7, 21.3)	23
Mean (low, high)	I_p 21.9 (16.4, 29.0)	29
Shrinkage Limit, w_s (%)	11.8	12
Specific Gravity	2.79	2.80
Percent finer than 0.002 mm (Clay Content)	34	40
Skempton's Activity, A	0.65	0.73
Unified Soil Classification	CL	CH
AASHTO Classification	A-6	A-7-6



Boring No. 20

State Road 37

1005 - 50,35 ft Left

Figure 2-1 Boring Profile (IDOH, Indiana Department of Highways)

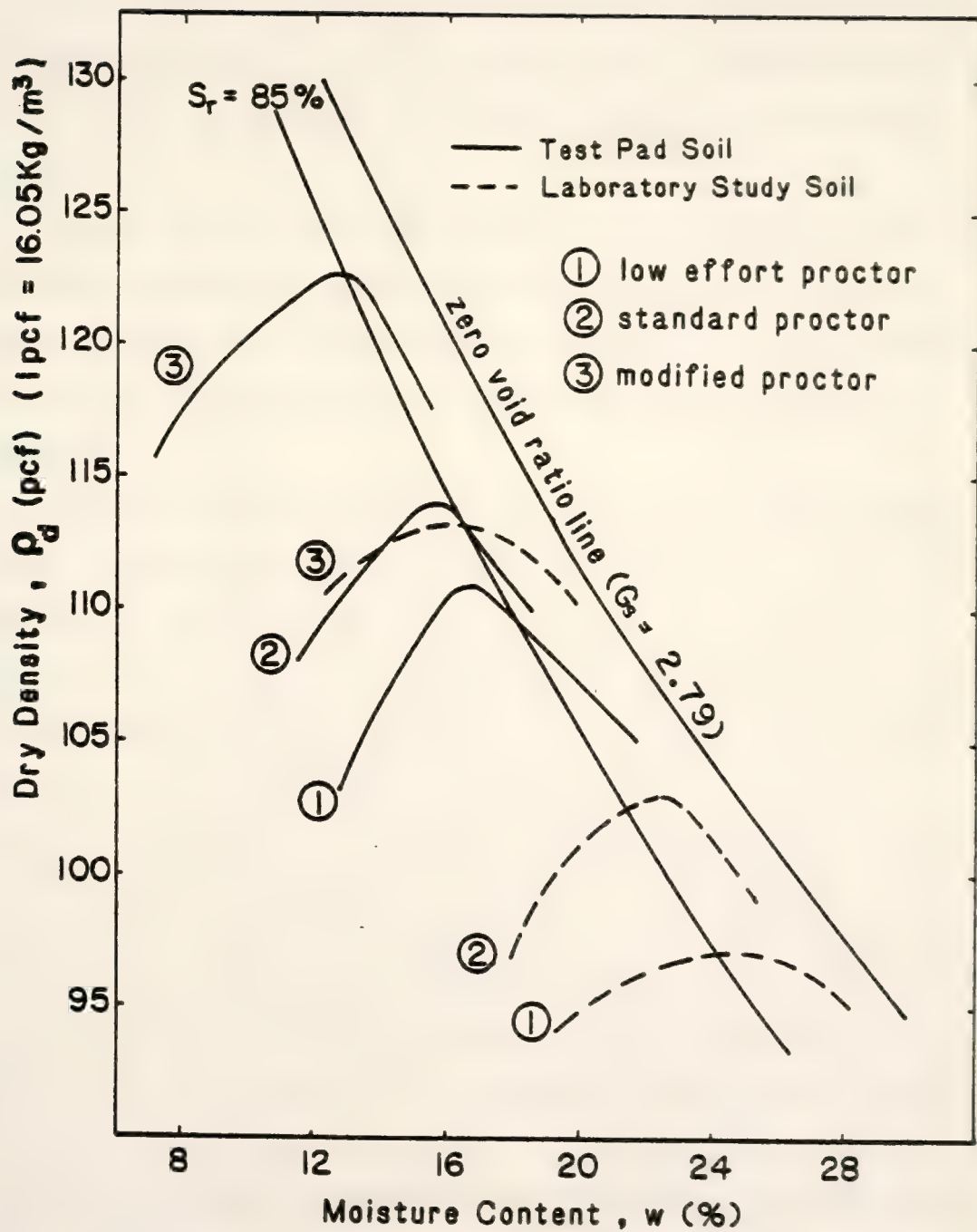


Figure 2-2 Impact Compaction Curves for Test Pad and Laboratory Study Soils

project of State Road 37 in June 1978. Each pad was 14 ft (4.3 m) wide by 116 ft (35.4 m) long. A subbase of varying thickness (4 to 5 ft or more) was constructed to provide a level base for the test pads. The pads were placed as 8 in. (20 cm) loose lifts. During the compaction process, water was sprinkled into the soil and the area was disked to aid mixing.

The ten test pads were laid out as shown in Figure 2-3. Five test pads were compacted by a RayGo Rascal model 420C vibratory drum compactor, and five pads were rolled with a Caterpillar model 825 tamping foot roller. The specifications of these two compactors are given in Table 2-2.

For each roller type, the five test pads were brought to different average water contents prior to compaction. The moisture contents were indicated by "1" to "5" from lowest to highest moisture level. Test pads 2, 3, 4, 7 and 6 were rolled by the Caterpillar roller; pads 1, 5, 8, 9 and 10 were rolled by the Rascal roller. Each test pad was sampled following the completion of 4, 8, and 16 passes of the compaction equipment over the pad. These samples were labeled "A", "B", and "C", respectively, for identification of energy levels. Equipment was operated at top speed in first gear for all passes and guided to prevent overlap at the interface of adjacent coverages. The same equipment operator was used for all compaction work. The Speedy Moisture Tester apparatus and nuclear density equipment were used to determine the field water contents and densities. Figures 2-4 and 2-5 show the moisture-density-energy curves from field nuclear gage values for the Caterpillar roller and Rascal roller, respectively. These plots indicate large variability within the compacted soil mass. The scatter could be produced by

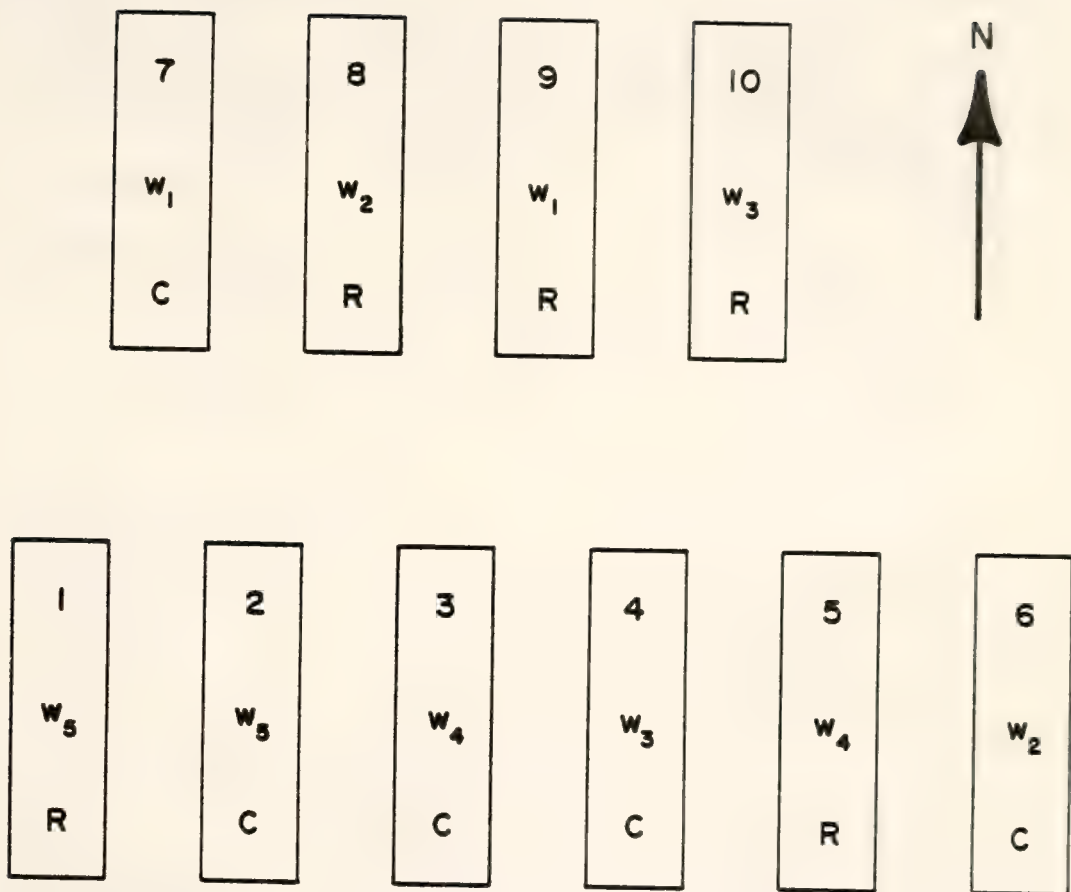


Figure 2-3 Test Pad Showing Pad Number, Water Content Level, and Compactor Type

TABLE 2-2 Field Compaction Equipment Specifications

Caterpillar Model 825

Dimensions

Length, with dozer	23 ft 4 in.	Each drum width	4 $\frac{1}{2}$ in.
Width, w/o clearers	11 ft 11 in.	Max. ballast	
w/o dozer	12 ft 6 in.	per wheel	244 U.S. Gal.
w/o dozer	13 ft 7 $\frac{1}{2}$ in.	Bulldozer dimensions	
Wheelbase	140 in.	Length	14 ft
		Height	40 $\frac{1}{2}$ in.
Weight, shipping		Maximum Speeds	
w/o dozer	59,000 lb	Gear	MPH
with dozer	63,000 lb	Forward	
No. of Drums	4	1	3.1
No. of Pads/Drums	65	2	7.0
		3	17.0

RayGo Rascal Model 420C

Dimensions

Length, with blade	18 ft 9 in.	No. of Drums	1
Width	9 ft	No. of Pads/Drums	140
Wheelbase	9 ft	Each drum width	8 $\frac{1}{4}$ in.
Weight	25,160 lb	Maximum Speeds	
Vibration Drive	Hydraulic, Direct Drive	Gear	MPH
Frequency	18 to 25 Hz	Forward	
Dynamic Force	32,000 lb	1	4
		2	6
		3	8

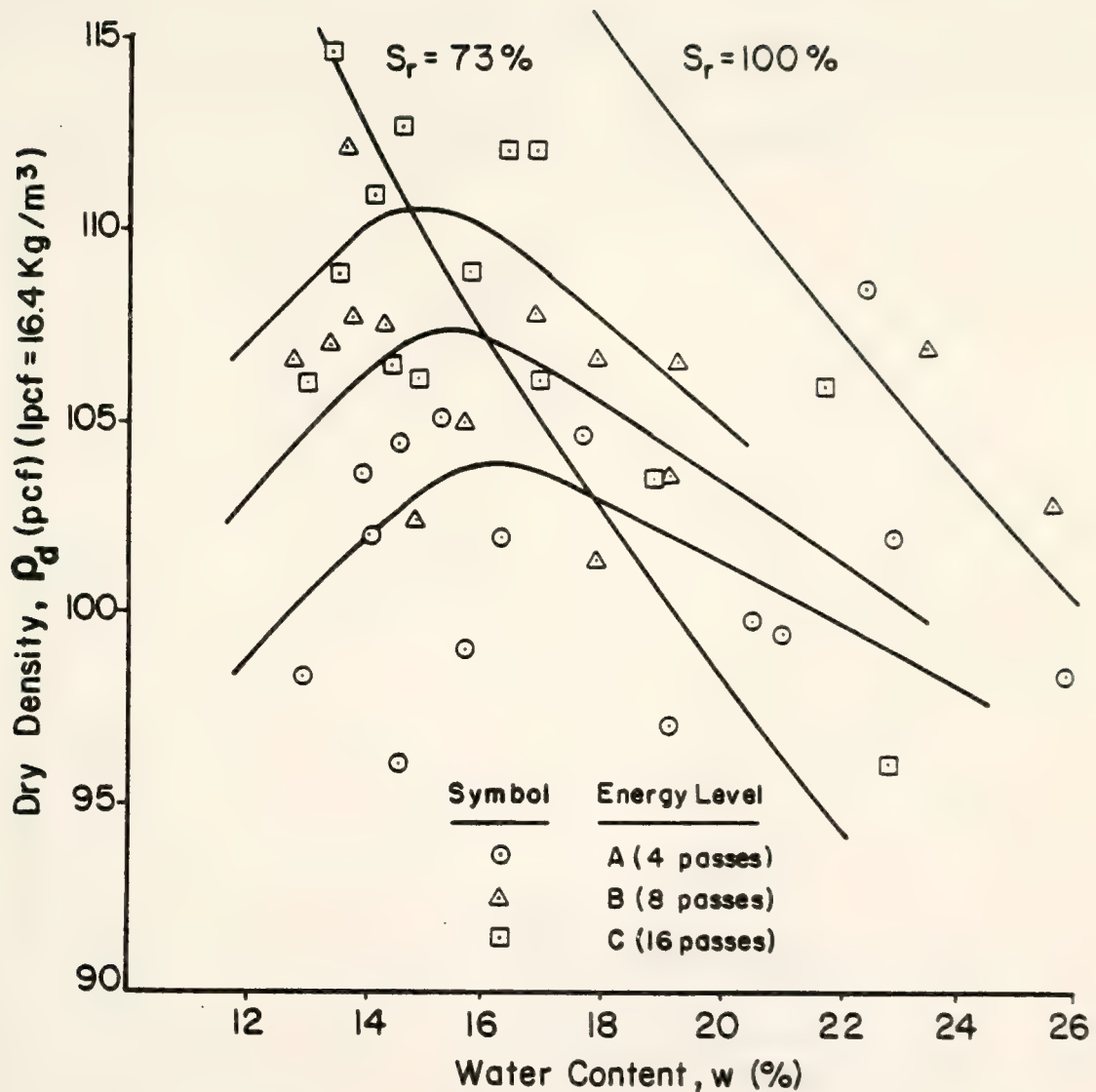


Figure 2-4 Rascal Compaction Curves for Field Nuclear Gage Values (After Terdich, 1981)

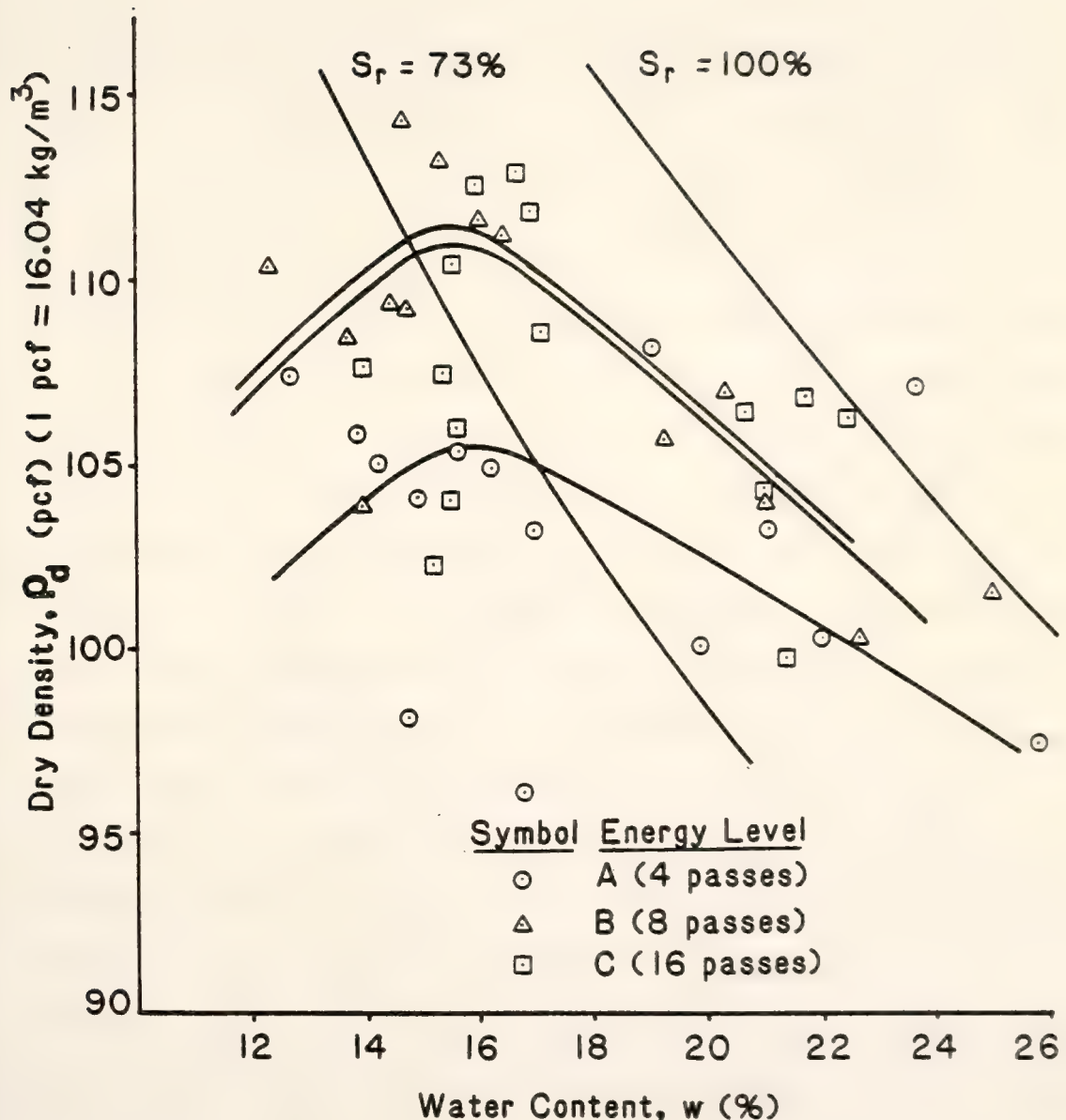


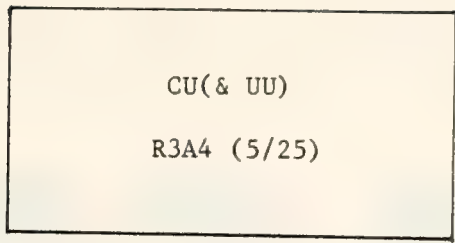
Figure 2-5 Caterpillar Compaction Curves for Field Nuclear Gage Values (After Terdich, 1981)

variations in compactive effort, soil type, and compaction water content. Sampling and testing can also introduce variability.

2-2-2 Field Sampling

After the required number of passes had been completed, field sampling of the test pad was started. Each pad was laid out in a 2 ft by 2 ft (0.6 m by 0.6 m) grid pattern, and each grid was marked with consecutively numbered stakes. The required number of 300 sampling tubes were lightly lubricated with silicone oil and were distributed to their proper locations, along with labels and plastic bags. The sample tubes for the strength tests were made from steel tubing with an internal diameter of 1.87 in (4.75 cm), an external diameter of 2 in (5.08 cm), and 7.0 in (17.78 cm) in length. The locations of sampling within each grid had been determined using a random number process. For this study, ten samples were taken for each combination of compactor type, water content level, and energy level. A total of 840 samples were collected for the entire project, of which 300 were taken for the work on strength. A typical sample label, and its explanation, is shown in Figure 2-6.

Sampling tubes were driven into the ground with a drop hammer at the specified grid location and at the bottom of a taper-foot depression made by the roller. The driving assembly, with tube, is shown in Figure 2-7. The 16.7 lb (7.6 kg) weight fell 28 in (71 cm) producing about 40 ft-lb (54 N-m) of energy per blow, with numerous blows (usually 10 to 25) being required to fully drive each tube. The total weight of driving assembly is 27.5 lb (12.5 kg), light enough to be operated by one person. After being driven, the tubes were dug out of the ground,



CU(& UU) - Behavior property to be studied

- R - Compactor type
- 3 - Water content level
- A - Energy level
- 4 - Sample number for the compaction
condition indicated above
- 5 - Grid location in the East-West
direction
- 25 - Grid location in the North-South
direction

Figure 2-6 Typical Field Sample Label



Figure 2-7 Driving Assembly with Sampling Tube

wrapped in plastic bags, labeled, and carefully transported to the extruding area. Samples were then extruded from the tubes using either an hydraulic jack, as shown in Figure 2-8, or an electrically driven loading press. Each sample was wrapped in plastic, covered with a cheesecloth, and coated with paraffin. They were then placed into plastic bags along with their labels, packed into 5 gallon metal cans and transported to the Geotechnical Engineering Laboratory at Purdue University.

Two factors which contributed to compaction water content variability during sampling were: (1) the wheather during sampling was warm (daily temperatures of 90^oF +); and (2) four to six hours elapsed from start to finish of sampling for a single test pad. Although efforts were made throughout the sampling program to mitigate moisture losses, some losses probably did occur.

2-3 Experimental Design

Laboratory studies for the strength of field compacted St. Croix clay consisted mainly of two sets of experiments.

The first set of experiments (UU tests) was to determine the as-compacted strength of field compacted clay. The independent variables were:

1. Moisture content - Five levels of moisture content were used for this study.
2. Type of compaction equipment - Two types of rollers were used; one was a RayGo Rascal model 420C padded vibratory drum compactor and the other was a Caterpillar model 825 tamping foot roller.

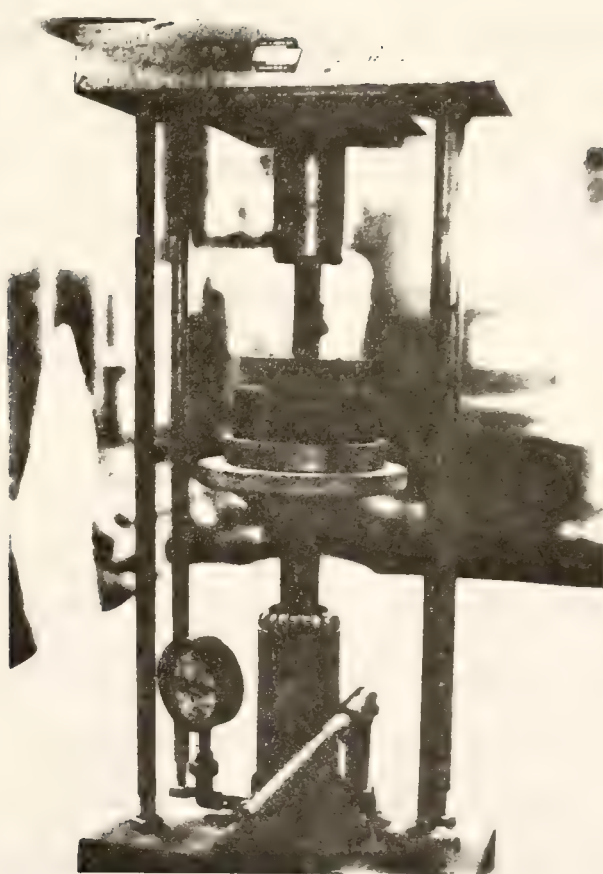


Figure 2-8 Hydraulic Jack Used for Extrusion of Tube Samples

3. Compaction energy level - Three levels of energy were used, viz., 4.8, and 16 passes of the roller.
4. Confining pressure - Three levels of confining pressure, viz., 10, 20 and 40 psi, approximating depths of 11.5 ft (3.5 m), 23 ft (7.0 m), and 46 ft (14 m) in the embankment, respectively.

A completely randomized factorial design was used (see Table 2-3).

This set of experiments required a total of 90 specimens.

The second set of experiments was to investigate the long term shear behavior (CIU) of field compacted clay. The independent variables were the same as for the first set, except moisture content was held to four levels. The experimental design is shown in Table 2-4. A total of 72 specimens were required.

2-4 Preparation of Specimens

The field samples had been wrapped in plastic, covered with cheese-cloth, and heavily coated with paraffin. Therefore, the first step in the trimming process for field samples was to remove the wax and cheese cloth covering. The samples were trimmed with a sharp pen knife, so that the lengths were approximately 106.7mm (4.2 in.). The ends were trimmed perpendicular to the axis of the sample cylinder. Any voids around the perimeter of the sample cylinder were filled with soil shavings. Sample number, field location, initial height and diameter, and wet weight were recorded for each sample. Also, other notes were made throughout the trimming process such as: color, defects, irregularities of shape, homogeneity, moisture content, and the location of rocks and voids. The initial water content was determined from the trimmings. Several samples were discarded during the trimming process. Samples of

TABLE 2-3 Design for the Study of UU Strengths

($2 \times 3 \times 3 \times 5 = 90$ factorial design)

Water Content	Confining Pressure (psi)	No. of Passes	Type of Roller	W ₁		W ₂		W ₃		W ₄		W ₅	
				10	20	40	10	20	40	10	20	40	10
			R	X	X	X	X	X	X	X	X	X	X
			C	X	X	X	X	X	X	X	X	X	X
		4	R	X	X	X	X	X	X	X	X	X	X
		4	C	X	X	X	X	X	X	X	X	X	X
	8	R	R	X	X	X	X	X	X	X	X	X	X
	8	R	C	X	X	X	X	X	X	X	X	X	X
	16	R	R	X	X	X	X	X	X	X	X	X	X
	16	R	C	X	X	X	X	X	X	X	X	X	X
	4	C	R	X	X	X	X	X	X	X	X	X	X
	4	C	C	X	X	X	X	X	X	X	X	X	X
	8	C	R	X	X	X	X	X	X	X	X	X	X
	8	C	C	X	X	X	X	X	X	X	X	X	X
	16	C	R	X	X	X	X	X	X	X	X	X	X
	16	C	C	X	X	X	X	X	X	X	X	X	X

Note: X One test per cell.

TABLE 2-4 Design for the Study of CIU Strengths

($2 \times 3 \times 3 \times 4 = 72$ factorial design)

	Water Content	Confining Pressure (psi)	No. of Passes	Type of Roller	W ₁				W ₂				W ₃				W ₄			
					10	20	40	10	20	40	10	20	40	10	20	40	10	20	40	
		4	X	X	X	X	X	X	X	X	X	X	X	X	X	X	X	X	X	
		8	X	X	X	X	X	X	X	X	X	X	X	X	X	X	X	X	X	
		16	X	X	X	X	X	X	X	X	X	X	X	X	X	X	X	X	X	
	R				4	X	X	X	X	X	X	X	X	X	X	X	X	X	X	
	C				8	X	X	X	X	X	X	X	X	X	X	X	X	X	X	
					16	X	X	X	X	X	X	X	X	X	X	X	X	X	X	

Note: X One test per cell.

low water content compacted with low energy were quite brittle and very difficult to trim. Some of these had insufficient height due to problems of the field sampling. Samples in the low and intermediate water content ranges sometimes showed distinct zones of differing water contents. This was due to the incomplete mixing of water into soil lumps which were at different initial water contents. Wet-side samples produced the longest and most uniform samples. Rock fragments were found in all samples, and some samples were destroyed because large rocks were present. Certain samples showed horizontal cracks, while others showed distinct horizontal interfaces between individual lumps of soil.

At the end of the trimming process, the UU test sample was placed on the base pedestal. The specimen then was encased in two thin rubber membranes which were sealed to the specimen cap and base by four rubber O-rings. The cap and base had a plane surface of contact with the specimen and were of the same diameter as the specimen.

For CIU tests, the samples were wrapped with longitudinal filter paper drains to accelerate back pressure saturation, consolidation, and pore pressure equalization (Bishop and Henkel, 1962). Saturation filter paper and porous stone discs having the same diameter as the specimen were placed between the specimen and the base and cap. Two membranes were used to protect against pinhole leaks. O-rings were used to provide a leak-proof seal between the rubber membranes and the loading caps and base pedestals. The triaxial chamber was then positioned, clamped and filled with distilled deaired water.

2-5 Strain Rate for Triaxial Testing

The rate of testing has a marked influence, in clay soils in particular, on the pore pressures observed during undrained shear. Whitman and Richardson (1962) indicated that a higher strain-rate increased the deviator stress and decreased the magnitude of the pore pressure change for normally-consolidated clay. It was necessary to select a strain rate which allowed pore water pressure equalization throughout the sample volume. A deformation rate of 0.106 mm (0.004 in.) per minute for both UU and CIU triaxial tests was chosen, which translates to approximately 0.09 percent strain per minute. This rate was the same as that used by Weitzel (1979) and Johnson (1979).

2-6 Unconsolidated-Undrained Triaxial Compression Test

The strength appropriate to the "short-term" or "as-compacted" condition is the undrained shear strength, or more precisely the unconsolidated-undrained (UU) shear strength. This strength is determined with no drainage, and hence no change in water content allowed. Also the UU strength is in terms of total stresses, since the excess pore water pressure during shear is not measured. The compressive strength of as-compacted soil is highly dependent on void ratio and degree of saturation. Because of the volume changes occurring during shear, these initial conditions also change. Therefore, it is desirable to measure the changes in volume.

2-6-1 Test Apparatus

The triaxial cell was manufactured by Geotest of Wheeling, Illinois. The bearings and the seal around the piston are designed for no leakage

of the confining fluid (water). A smooth base without drains was machined and fitted to the base of the cell. The volume change measuring device was designed by Chan (1967). It is basically a burette type of instrument that measures the quantity of water which flows into and out of the triaxial cell chamber due to changes in the sample volume. For accurate measurement in a burette, the internal diameter of the tube must be small. In this device, volume changes can be read to about 0.01% of the initial volume of the sample. The volume change in the tube is read by an oil-water interface. When the interface nears the end of the tube, the flow can be reversed by the turn of a single valve. This apparatus is shown in Figure 2-9.

Axial deformation was applied by a constant strain rate loading frame manufactured by Wykeham Farrance. Load was measured by a proving ring with a 1500 lb capacity. The sample deformation was measured with a dial gage of 0.001 in. sensitivity.

2-6-2 Test Procedure

For the purpose of minimizing errors of volume change measurements, silicon oil was placed between the cell piston and bushings, and the piston was left in the up position to prevent loss of oil. After the sample had been set up, the top of the cell was secured to the base, and the cell was filled with distilled water. Next, the cell was connected to the volume change measuring device. The pressure-controlling device was adjusted to the desired cell pressure and the pressure was applied to the cell fluid.

During an increase in cell pressure an expansion of the cell occurs, and this volume change must be deducted from the observed displacement

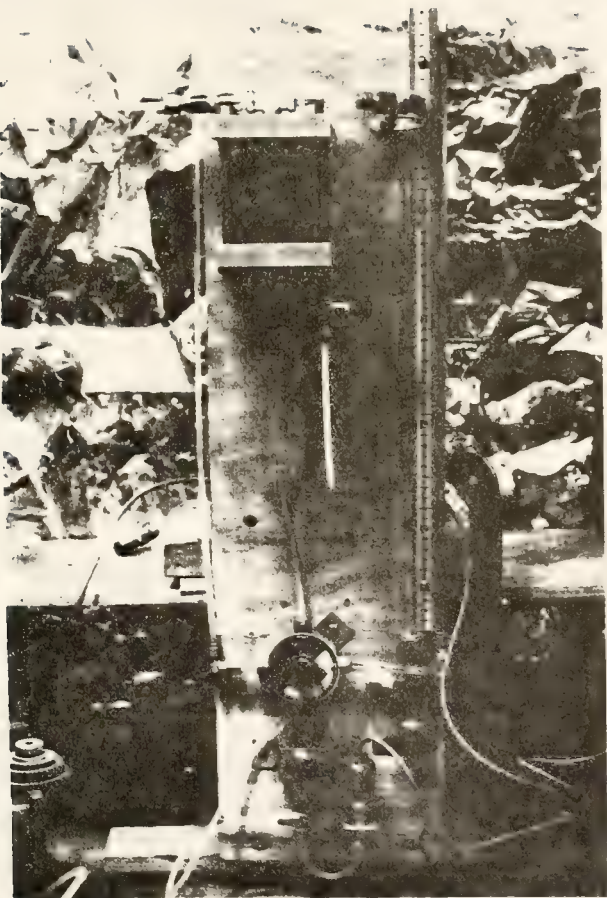


Figure 2-9 Volume Change Measuring Device

of water. The calibration curve for the cell expansion vs. confining pressure is shown in Figure 2-10. The cell expansion over most of the range of pressure was quite constant. The small diameter tube on the right of the meter stick in Figure 2-9 could not be used to measure this volume, since when the oil moved too quickly it would stick and separate. Therefore, the large diameter burette on the left of the meter stick in Figure 2-9 was used to measure volume change during application of the confining pressure.

During the four hours period of testing, the triaxial cell also underwent creep. The calibration curve for the cell creep volume change vs. time is shown in Figure 2-11. According to Yoshimi (1958), DiBernardo (1979), and Lin (1981), most of the volume change of as-compacted soil occurred within a few minutes after load application. Therefore, the volume change was measured after 10 min. of the application of confining pressure. Since most of the cell creep occurred in a short time, the piston was lowered to contact with the loading cap, and the large burette remained open to the cell for 14 min.. At the end of this time, the burette was closed and the valve to the fine measuring tube was carefully opened. The axial loading was started one minute later.

Errors of volume change may also be caused by changes in temperature. A calibration curve for temperature change is shown in Figure 2-12. While the testing was done in a fairly constant temperature area, the temperature could rise in the range of 0.2 to 0.6°C over a period of four hours, due to equipment and body heat. This resulted in only very minor volume change corrections.

During the application of axial load, readings of load, axial defor-

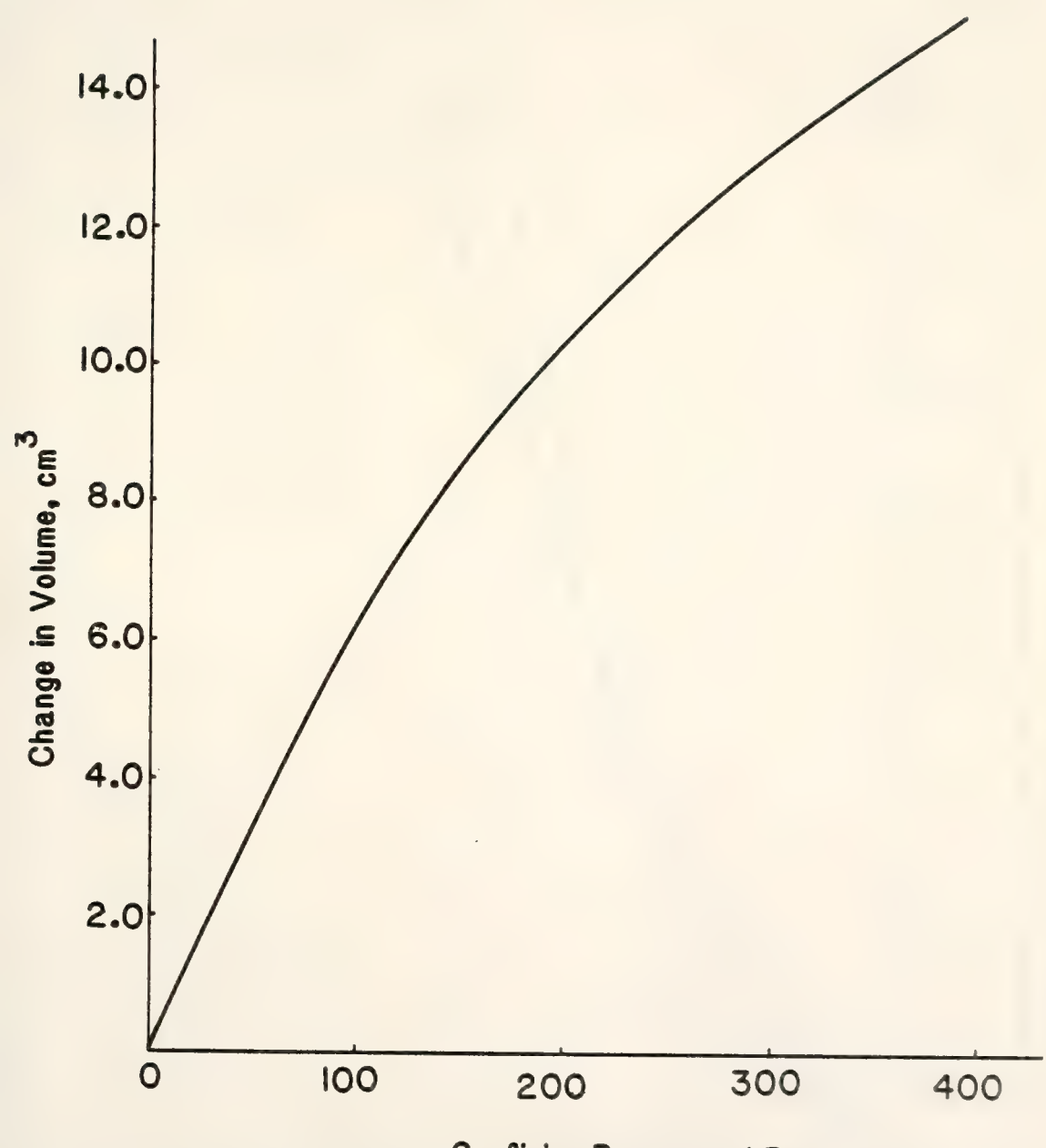


Figure 2-10 Calibration of Cell Expansion (After 10 Min.
Application of Confining Pressure)

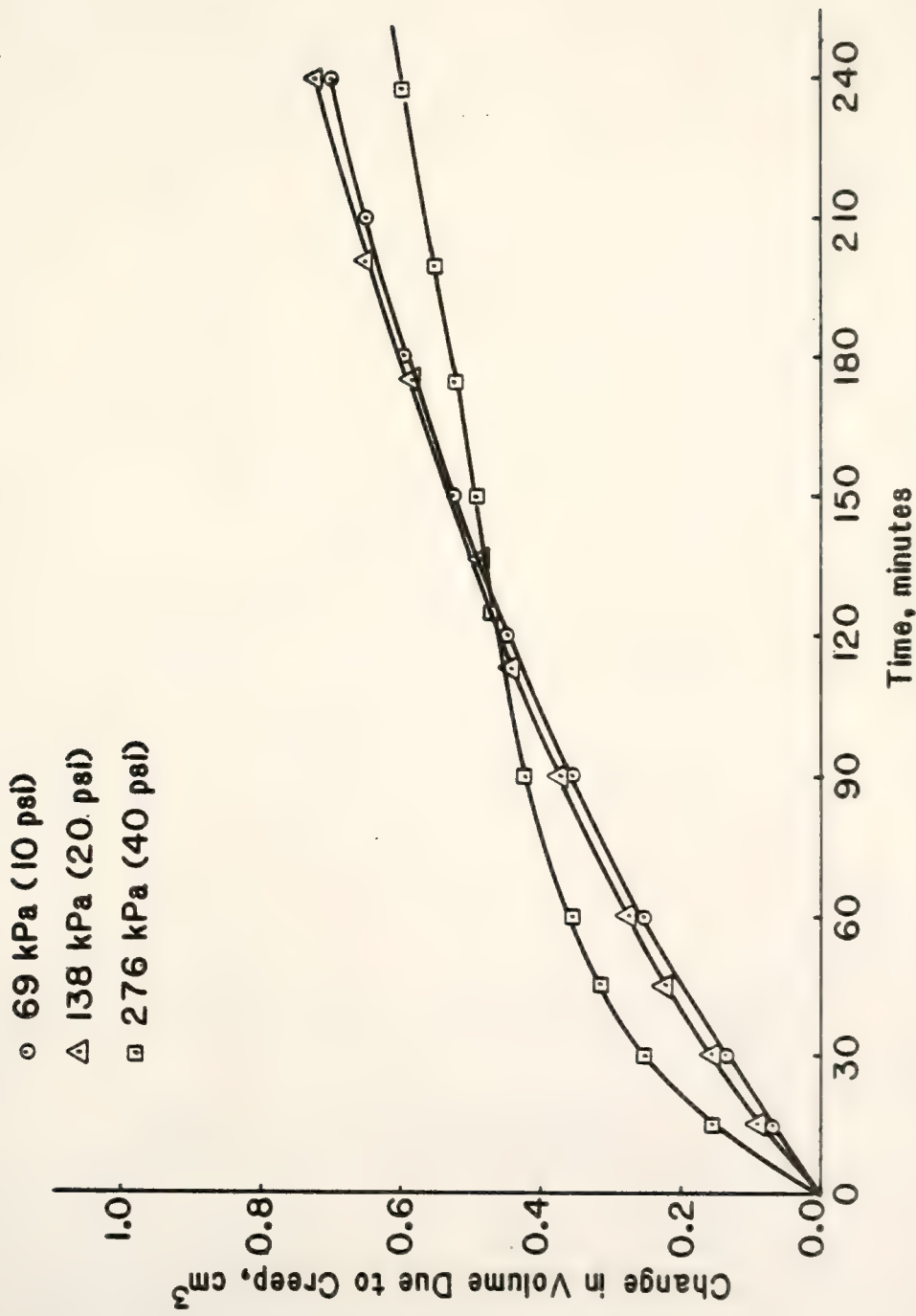


Figure 2-11 Calibration of Triaxial Cell Expansion Under Creep (After Application of Cell Pressure for 25 min.)

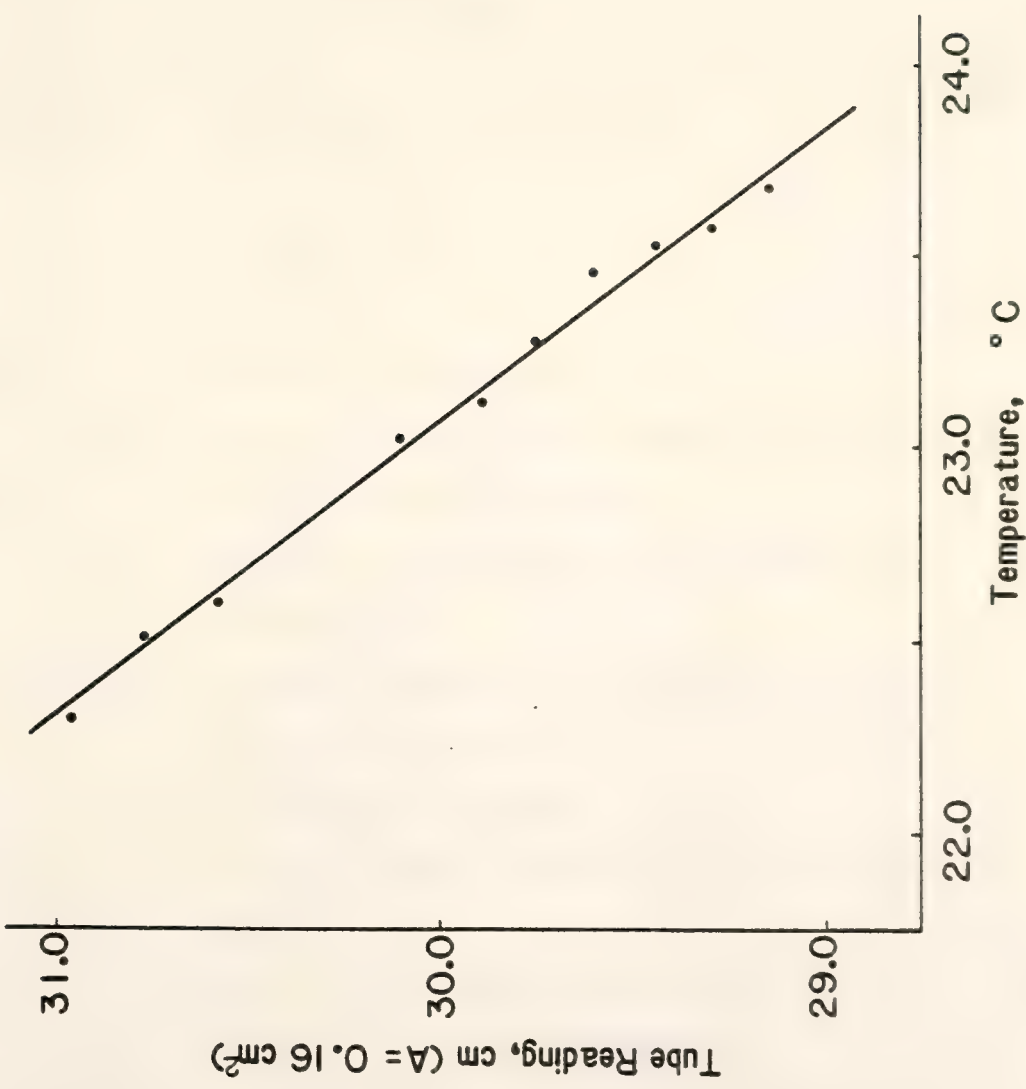


Figure 2-12 Calibration for Volume Change Due to Temperature Change

mation, volume change and temperature were recorded. Volume change readings were corrected using the calibrations for temperature, piston displacement, cell expansion, and creep. The volume change due to application of confining pressure was ΔV_c . The cross-sectional area after application of confining pressure, A_c , can be determined as follows:

$$A_c l_c + \Delta V_c = A_o l_o$$

then,

$$\begin{aligned} A_c &= \frac{A_o l_o - \Delta V_c}{l_c} = \frac{A_o (1 - \frac{\Delta V_c}{A_o l_o})}{\frac{l_o - (l_o - l_c)}{l_o}} \\ &= \frac{A_o (1 - v_c)}{1 - \epsilon_{lc}} \end{aligned} \quad (2-1)$$

where A_o = the initial cross-sectional area

$\Delta V_c = \Delta V_{cm} - \Delta V_{ce}$ = the corrected volume change due to application of confining pressure

ΔV_{cm} = the measured volume change due to application of confining pressure

ΔV_{ce} = the volume change due to cell expansion (calibration curve as shown in Figure 2-10)

l_o = the initial specimen length

l_c = the specimen length after application of confining pressure

$v_c = \Delta V_c / A_o l_o$ = the volumetric strain occurring during application of confining pressure

$\epsilon_{lc} = (l_o - l_c) / l_o$ = the axial strain occurring during application of confining pressure

If the specimen is elastic and isotropic, ϵ_{lc} is going to be $1/3 v_c$.

Then, Equation 2-1 becomes:

$$A_c = A_o \frac{(1 - v_c)}{(1 - v_c/3)} \quad (2-2)$$

The corrected volume change during shear can be computed from the equation:

$$\Delta V = \Delta V_m - \Delta V_e - \Delta V_p - \Delta V_T \quad (2-3)$$

where ΔV = the corrected volume change during shear

ΔV_m = the measured volume change during shear

ΔV_e = the volume change due to cell creep (as shown in Figure 2-11)

ΔV_p = the volume change due to piston displacement

ΔV_T = the volume change due to temperature change (as shown in Figure 2-12)

The average cross-section area, A, for a given applied axial load was determined as follows:

$$A = A_c \frac{(1 - v)}{(1 - \epsilon_1)} \quad (2-4)$$

where A_c = the cross-sectional area after application of confining pressure

v = the volumetric strain occurring during shear

ϵ_1 = the axial strain occurring during shear

Assuming linear elastic response, the variation of Poisson's ratio with axial strain also can be calculated from the expression:

$$\mu = \epsilon_3/\epsilon_1 = (1 - \epsilon_v/\epsilon_1)/2 \quad (2-5)$$

where μ = Poisson's ratio

ϵ_1 = axial strain

ϵ_3 = lateral strain

$\epsilon_v = \epsilon_1 + 2\epsilon_3$ = volumetric strain

This equation is valid for small strains. Values of the axial strain and the volumetric strain were determined from the experimental UU data.

The triaxial test was run until the sample reached failure or to 20 percent axial strain. After the completion of the test, the cell was drained and the sample removed.

For the determination of sample volume and final degree of saturation, a procedure used by Weitzel (1979) was followed. The sample was weighed in air on a Mettler P1210 balance (0.01 gm accuracy). Then the sample was hand-dipped in melted wax until it was thoroughly coated. The waxed sample was weighed in air and also weighed in water by suspending it in a basket attached to the balance. Knowing the specific gravity of the wax, 0.805, the volume of the sample was calculated using Archimedes' principle. The wax was then cut away and the sample was placed in a 105°C oven for water content determination. The final degree of saturation was calculated knowing the total weight, the total volume, the water content, and the specific gravity of solids. The equation is:

$$S_f = \left(\frac{V_w}{V_T - V_s} \right) \times 100\% \quad (2-6)$$

where V_T = total volume of the sample calculated by using
Archimedes principle

$V_s = W_s/G_s$ = volume of solids

W_s = weight of dry solids

V_w = final volume of water

S_f = final degree of saturation

Once the degree of saturation was known, the final void ratio was computed from the equation:

$$e_f = \frac{w_f \cdot G_s}{S_f} \quad (2-7)$$

where w_f = final water content, %

G_s = the specific gravity of solids

e_f = final void ratio

S_f = final degree of saturation, %

2-7 Consolidated Undrained Triaxial Compression Test

The effective stress strength parameters are utilized for analysis of long term stability. These parameters can be evaluated for various compaction conditions through the performance of consolidated undrained triaxial tests with pore pressure measurement. The consolidated undrained (CIU) test consists of three stages. The first stage is saturation by back pressure. The second stage is volume change of the saturated sample under isotropic confinement. The third stage is an axial compression test with no drainage permitted from the specimen and measurement of change in pore pressure during shear.

2-7-1 Test Apparatus

The high-pressure triaxial cell was manufactured by Geotest of Wheeling, Illinois. Figure 2-3 shows a disassembled triaxial cell. A standard laboratory loading device manufactured by Wykeham Farrance was employed to furnish the constant strain rate in the test. Two nitrogen gas cylinders and two Airco model 57-300 high pressure regulators with integral purge assembly were used successfully as the pressure supply in the test program. The cell pressure and back pressure were measured by two calibrated Tyco model AB pressure transducers with 1379 kPa (200 psi) capacity and 1 kPa (0.1 psi) sensitivity. These two trans-

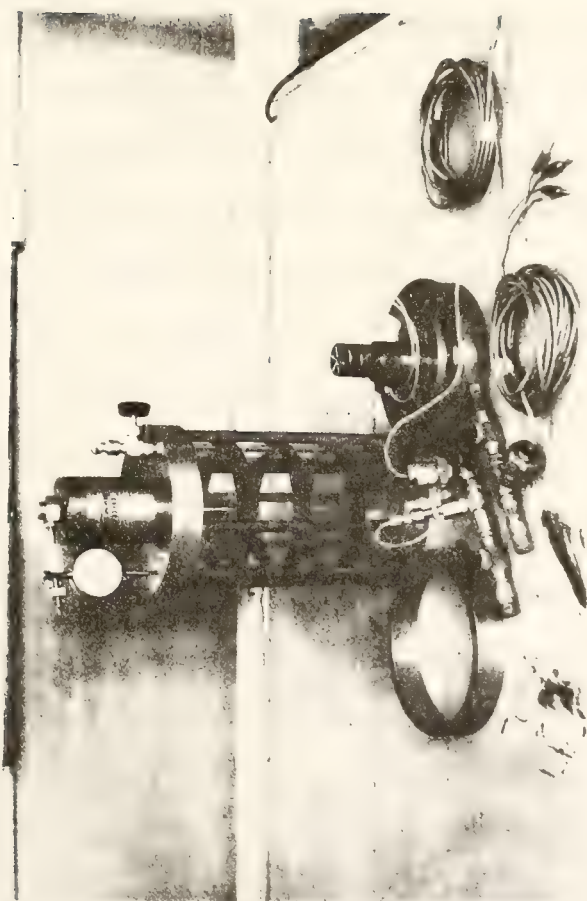


Figure 2-13 Disassembled Triaxial Cell

ducers were calibrated and monitored with Hewlett Packard model 3476A Digital Multimeters. Axial load was measured with a calibrated proving ring, while axial deformation was monitored with a dial gage (sensitivity of 0.0254 mm or 0.001 in.) attached to the loading piston.

2-7-2 Back Pressure Saturation

For the purpose of accurate and meaningful determinations of pore water pressure, the specimen must be completely saturated before the compression test is begun. During the saturation, even with extreme care, some air will almost always be trapped in the lines, between the membrane and the specimen, or within the specimen itself. Therefore, a back pressure is commonly used to dissolve the pore air completely into the surrounding pore water.

A schematic of the saturation and consolidation system is shown in Figure 2-14. Using a high back pressure will increase the saturation level of the specimen. Lowe and Johnson (1960), and Black and Lee (1973) presented guidelines for the appropriate back pressure and the time required to ensure various levels of saturation from different initial degree of saturation. These are shown in Figure 2-15A, B. Two back pressures 965 kPa (140 psi) and 896 kPa (130 psi) have been used for this study. The back pressure of 965 kPa was used for sample confining pressures of 69 kPa (10 psi) and the back pressure value of 896 kPa was applied for sample confining pressures of 138 and 276 kPa (20 and 40 psi).

To saturate the samples, a vacuum was applied to the loading cap back pressure line and deaired distilled water was allowed to enter the specimen through the bottom drainage line. Simultaneously, a cell pressure was applied such that the combined vacuum and cell pressure

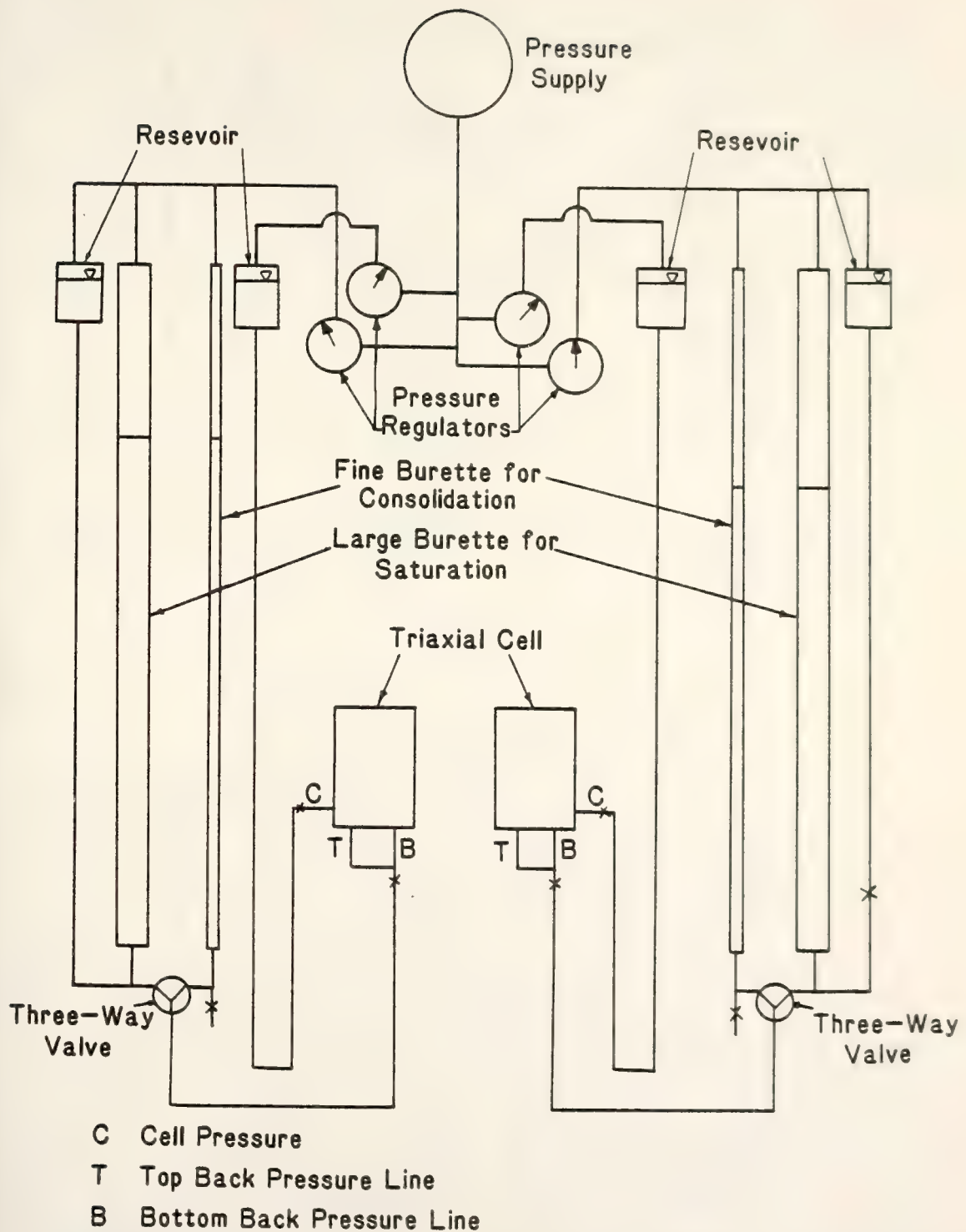


Figure 2-14 Schematic of the Saturation Consolidation System

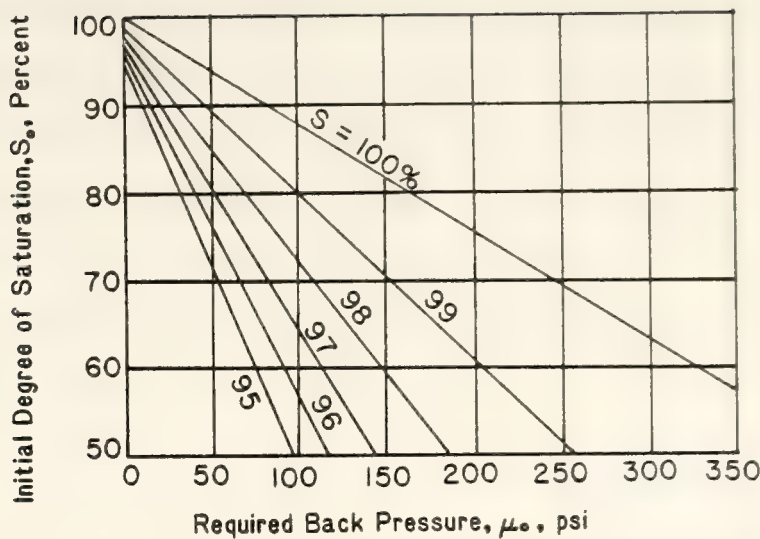


Figure 2-15A Back Pressure Required for Various Degrees of Saturation (After Lowe and Johnson, 1960)

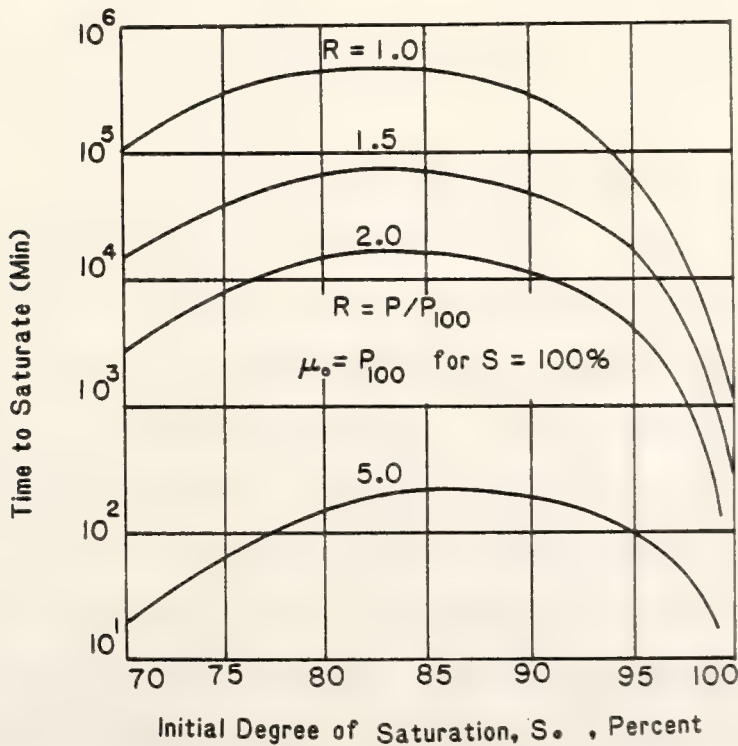


Figure 2-15B Time Needed to Saturate Sample by Using Back Pressure (After Black and Lee, 1973)

totalled less than 48 kPa (7 psi). A period of approximately 2 to 6 hours was allowed for the water to flow out of the top drainage line. When the flow was clear of air bubbles, the top drainage valve was closed. The vacuum line was then disconnected and replaced in the back pressure loop. Thereafter, the sample was progressively saturated by increasing the cell pressure and back pressure in equal increments, without excessive cyclic loading of the samples. The procedure described by Lowe and Johnson (1960) was followed. For the final consolidation pressure of 69 kPa (10 psi), the cell pressure and back pressure were incremented by 48 kPa (7 psi) at two hour intervals. A differential of 21 kPa (3 psi) was allowed between them. For the final consolidation pressure of 138 kPa (20 psi) or 276 kPa (40 psi), the cell pressure and back pressure were incremented by 69 kPa (10 psi) with two hour pressure equalization periods.

The method for checking saturation is based on the determination of the B parameter as presented by Skempton (1954). The B parameter is defined as the ratio of the change in pore water pressure in an undrained triaxial specimen to an incremental change in the cell pressure, and may be related to the degree of saturation. The B parameter has been shown by various authors (Skempton, 1954, Wissa, 1969, and Lade, 1977) to be a function of the soil's porosity, the compressibility of the soil structure and the pore water, the absolute pressure existing in the pore fluid, and the degree of saturation. The B parameter may be expressed as a function of these variables by using the equations below: (Skempton, 1954 or Lade, 1977)

$$B = \frac{1}{1 + n \frac{C_w}{C_s}} \quad (2-8)$$

where n = porosity of the sample

C_s = compressibility of soil skeleton

C_w = compressibility of water

or

$$B = \frac{1}{1 + n S_r (C_w/C_s) + (n/C_s P_a) (1 - S_r)} \quad (2-9)$$

where P_a = absolute pressure in the pore liquid

S_r = degree of saturation

According to these equations, B will decrease below unity for specimens that are either not fully saturated or very stiff.

The method for determining the level of saturation was suggested by Channey (1980). This check requires that the B value remain constant when plotted against increasing back pressure, as shown in Figure 2-16. In addition to the curve for the satisfactorily saturated case, two other typical curves are presented in Figure 2-16. One is for an unsaturated material and one is for a specimen that is experiencing membrane leaks.

2-7-3 Consolidation

After saturation had been achieved, generally within a period of 48 hours, the back pressure was maintained constant while the cell pressure was increased to give the desired consolidation pressure (69, 138, 276 kPa). The back pressure line was opened and the expulsion of water from each specimen into the fine burette was recorded. The consolidation process was continued until primary consolidation was complete and secondary compression was evidenced. The end of primary consolidation was determined by Casagrande's logarithm of time method (Lambe and Whitman, 1969) and required from 0.5 to 4 hours.

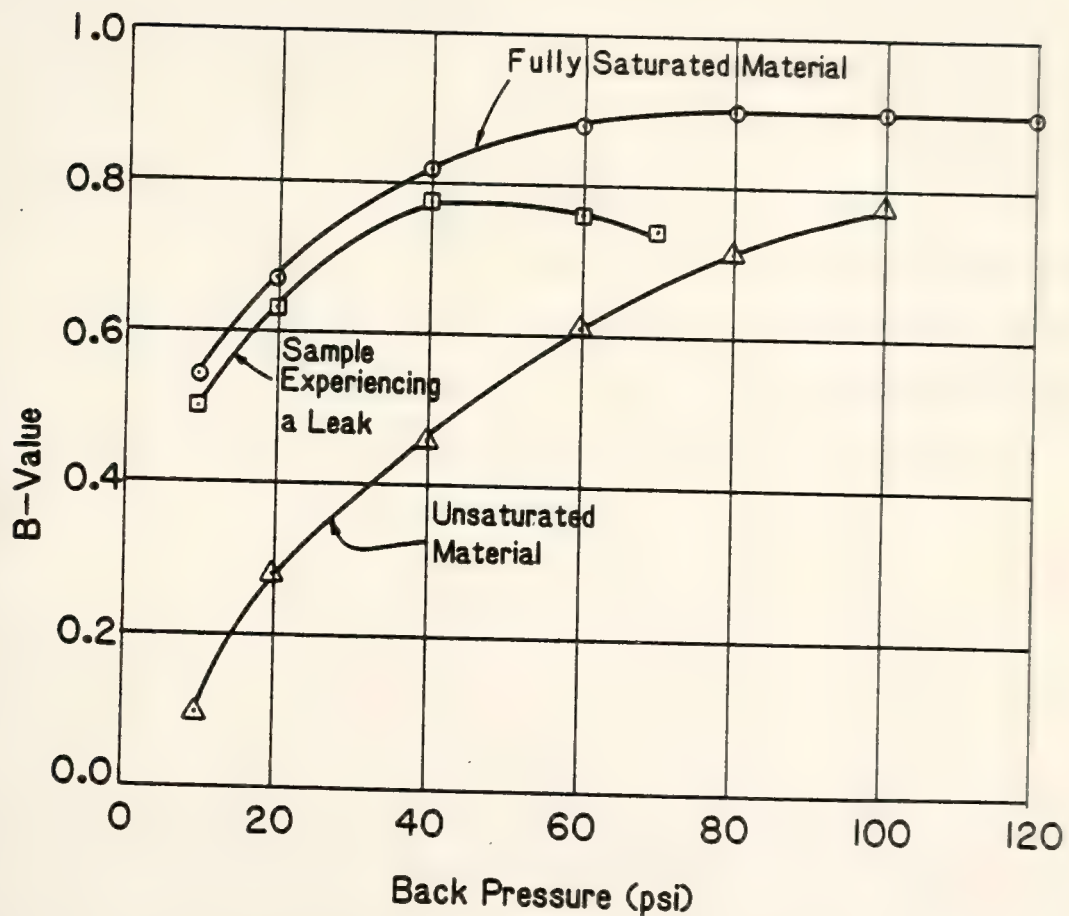


Figure 2-16 Plot of B Versus Back Pressure with Typical Sample Responses (After Chaney, 1980)

2-7-4 Undrained Shear

The valve to the back pressure line was closed following consolidation. Axial load due to water pressure on the piston and bushing friction was deducted from the measured load by taking the proving ring reading, just prior to contact of the piston and loading ball, as zero axial load. A deformation rate of 0.09 percent strain per minute was chosen. Axial compression was continued until the load reduced or to slightly beyond the estimated 20 percent axial strain. After the sample failed, the compression machine was shut off and reversed to remove the sample load. The chamber pressure was released and the cell was removed from the saturation and consolidation system. The sample was removed from the cell and weighed in air. The final degree of saturation and void ratio were determined by using equations 2-6 and 2-7, respectively.

3- RESULTS AND DISCUSSION OF RESULTS

3-1 Analysis of Results

3-1-1 Field Compaction

The values of moisture content and dry density for field compaction of St. Croix clay are tabulated in Table 3-1 and Table 3-2. The water contents and dry densities are the average values of the field samples compacted at the same nominal water content and nominal energy levels by the same roller type. These field sample values were chosen from the tests run in the swelling task (Terdich, 1981), the compressibility task (Lin, 1981), and this task (triaxial compression). The moisture-density-energy relations of the Caterpillar tamping roller and Rascal vibratory roller for three nominal energy levels: A (4 passes), B (8 passes), and C (16 passes) are shown in Figures 3-1 and 3-2. These figures show that the Caterpillar tamping roller is more efficient for this soil than the Rascal vibratory roller. The moisture-density-energy relations of St. Croix clay for laboratory compaction at Low Energy, Standard and Modified Proctor impact levels, shown in Figure 3-1 and Figure 3-2, are available from Terdich (1981). Soils used to define these laboratory impact compaction curves were obtained from test pads six and eight. The nominal compactive foot pressure (P_c) delivered to the soil during compaction by the laboratory kneading compactor, the Rascal vibratory roller and the Caterpillar tamping roller are shown in Table 3-3. The compactive foot pressure is used as a variable in the subsequent statistical analyses. The foot pressures of the Rascal roller and the Caterpillar roller were computed by using the Equations 1-28 and 1-29 from Table 1-6.

Dry density, moisture content and compaction energy are the compac-

TABLE 3-1 The Variations of Water Content and Dry Density
for Each Test Pad Compacted by the Rascal Type of Roller

Test Pad	No. of Passes	No. of Samples	Mean Moisture Content (%)	Standard Deviation of Moisture Content (%)	Mean Dry Density (kg/m ³)	Standard Deviation of Dry Density (kg/m ³)	Com-paction Factor of Dry Foot Pressure (kPa)
R1A	4	9	14.07	1.45	1740.0	55.8	780
R2A	4	13	15.48	2.02	1755.3	61.2	780
R3A	4	12	14.91	0.90	1754.0	57.4	780
R4A	4	13	17.36	2.24	1782.1	60.9	780
R5A	4	10	18.48	2.26	1756.7	57.9	780
R1B	8	7	15.27	1.93	1773.6	40.5	1038
R2B	8	13	14.77	1.23	1810.6	47.5	1038
R3B	8	12	14.31	1.42	1806.7	64.1	1038
R4B	8	12	17.03	1.81	1789.0	47.9	1038
R5B	8	10	18.12	2.09	1736.9	58.8	1038
R1C	16	9	14.18	1.57	1835.4	36.0	1525
R2C	16	14	14.07	0.84	1839.9	45.1	1525
R3C	16	10	15.4	2.34	1803.4	44.8	1525
R4C	16	11	16.38	1.91	1816.8	40.0	1525
R5C	16	10	19.18	2.47	1740.4	62.5	1525

TABLE 3-2 The Variation of Water Content and Dry Density for Each Test Pad Compacted by the Caterpillar Type of Roller

Test Pad	No. of Passes	No. of Samples	Mean Moisture Content (%)	Mean Dry Density (kg/m^3)	Standard Deviation of Moisture Content (%)	Mean Dry Density (kg/m^3)	Standard Deviation of Dry Density (kg/m^3)	Com- pression factor of Foot Pressure (kPa)
C1A	4	10	14.54	1771.2	1.44	82.5	797	797
C2A	4	11	15.47	1762.5	1.90	70.6	797	797
C3A	4	11	14.68	1784.3	0.81	65.8	797	797
C4A	4	13	18.51	1745.1	1.63	46.8	797	797
C5A	4	11	17.56	1768.6	1.44	42.0	797	797
C1B	8	11	13.48	1860.1	0.75	51.8	1204	1204
C2B	8	11	14.62	1847.3	1.30	48.2	1204	1204
C3B	8	10	14.06	1773.7	3.11	51.5	1204	1204
C4B	8	13	16.7	1795.2	1.28	41.2	1204	1204
C5B	8	10	17.27	1782.9	0.99	35.7	1204	1204
C1C	16	8	13.05	1877.4	1.23	27.8	1771	1771
C2C	16	13	14.35	1824.7	1.41	53.3	1771	1771
C3C	16	11	15.04	1815.5	2.53	74.3	1771	1771
C4C	16	14	17.51	1783.8	1.74	44.7	1771	1771
C5C	16	10	17.57	1791.3	2.67	59.4	1771	1771

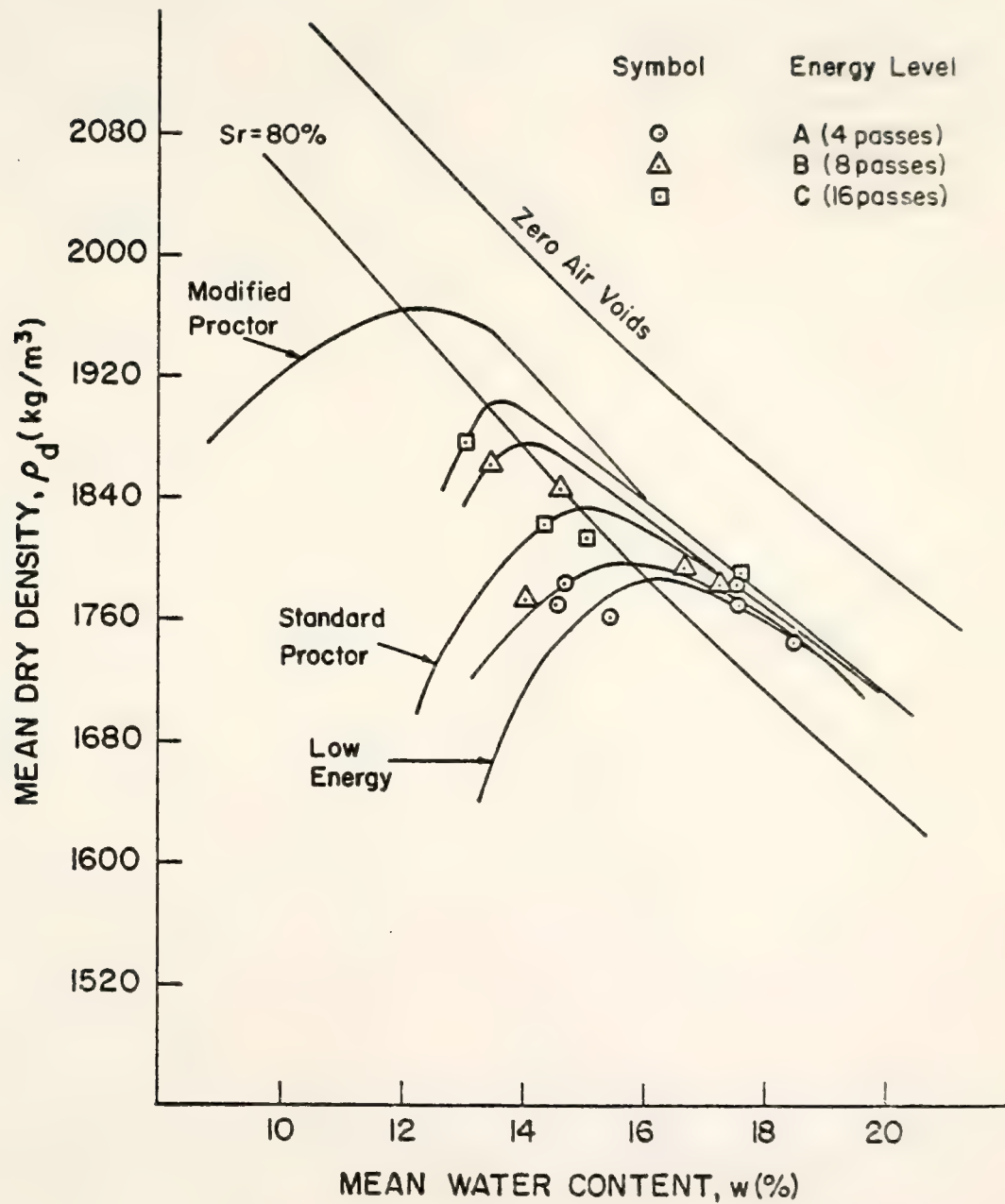


Figure 3-1 Correspondence Between Caterpillar Roller and Impact Method

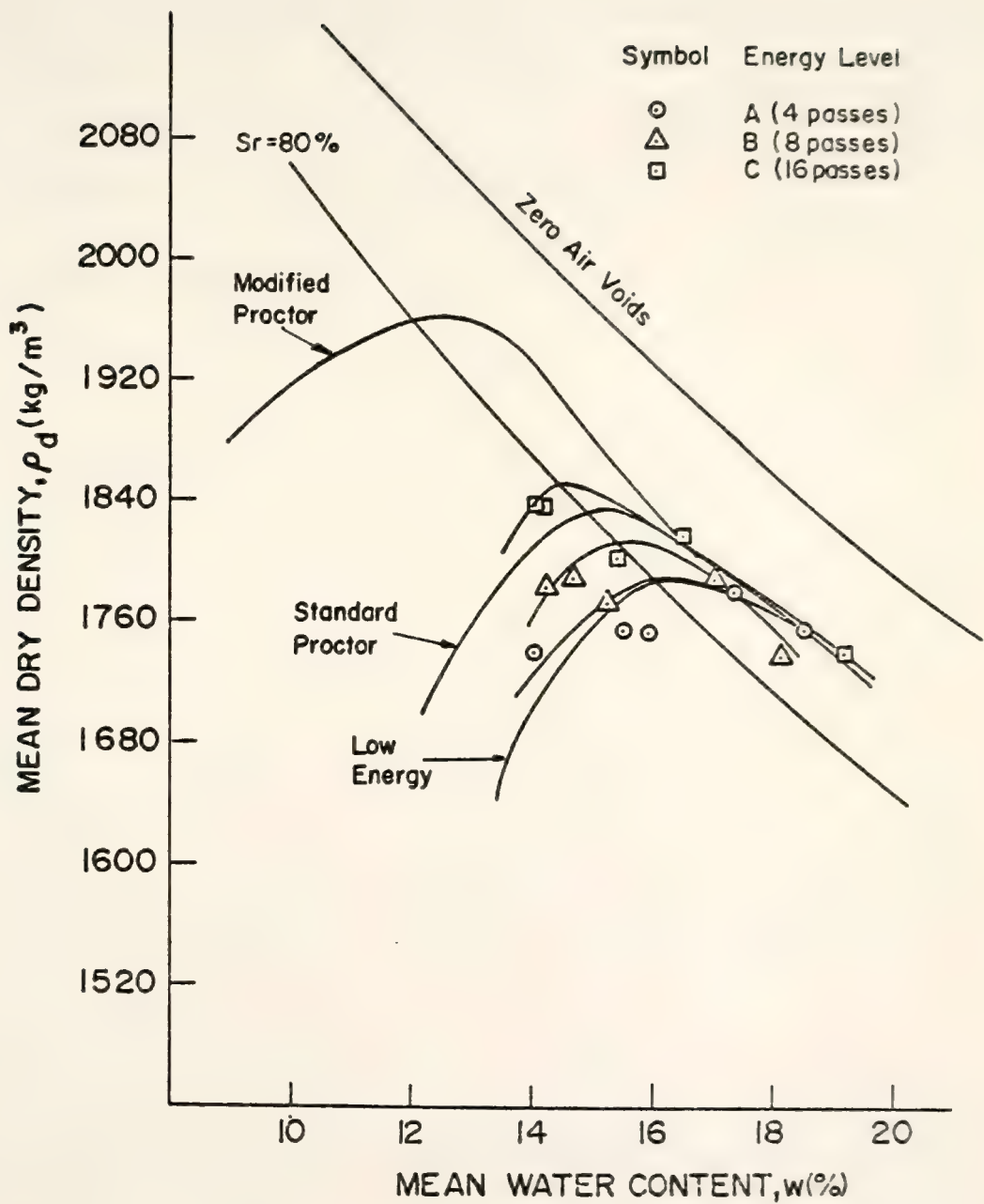


Figure 3-2 Correspondence Between Rascal Roller and Impact Method

TABLE 3-3 Compaction Pressures

Compactor Type	Quantity Measured	Compaction Pressures (kPa)
Kneading (Weitzel's data)	Gage Pressure (psi)	
	4	500
	7	950
	26	3050
Caterpillar	No. of Passes	
	4	797
	8	1204
	16	1771
Rascal	No. of Passes	
	4	780
	8	1038
	16	1525

tion variables. Initial degree of saturation (S_r , %) and initial void ratio (e_0) are calculated from the values of dry density, moisture content, and specific gravity of solids. The plasticities of the soil compacted in the laboratory and the soil compacted in the field were different, and the compaction efficiencies of the two soils at the same energy level were also different. The plasticity indexes are potentially useful in adjusting the relationships. Table 3-4 shows the variation of Atterberg limits for each test pad.

3-1-2 Unconsolidated-Undrained Shear Strength

The density-water content relationships for triaxial samples before testing are shown in Figures 3-3, 3-4, and 3-5. For comparison, the curves from laboratory impact compaction are superimposed on these figures. Figure 3-6 shows the joint region of water content and dry density values for the UU triaxial tests.

The results of failure conditions for UU triaxial tests are given in Table 3-5. The principal stress different at failure was defined at peak stress or the stress at approximately 20% axial strain.

3-1-2.1 Stress-Strain Behavior

Typical stress-strain curves for as-compacted soils in UU tests with 69 kpa confining pressure are shown in Figure 3-7. These results are quite similar to those of Seed and Chan (1959) shown in Figure 1-3. The samples with lower water contents and highly negative pore water pressures have much steeper stress-strain curves. Hence, less strain is required to mobilize the total shearing resistance. Samples with the higher water contents have flatter stress-strain curves and continue to

TABLE 3-4 The Variation of Atterberg
Limits (%) for Each Test Pad

Test Pads	Mean w_L	Standard Deviation w_L	Mean w_p	Standard Deviation w_p	Mean I_p	Standard Deviation I_p
C1	40.8	2.7	17.4	0.1	21.0	1.0
C2	40.8	6.4	18.6	1.5	23.3	1.6
C3	37.5	4.2	19.0	1.8	21.0	1.7
C4	42.2	2.0	19.3	1.9	22.3	0.6
C5	42.9	2.6	19.6	1.3	24.8	2.4
R1	36.0	1.2	17.7	1.1	18.1	1.1
R2	35.1	2.3	18.5	0.9	16.9	0.5
R3	38.8	1.3	17.8	0.8	20.4	1.9
R4	43.6	4.3	18.7	1.4	26.5	2.0
R5	41.9	3.7	18.1	0.5	24.5	1.4

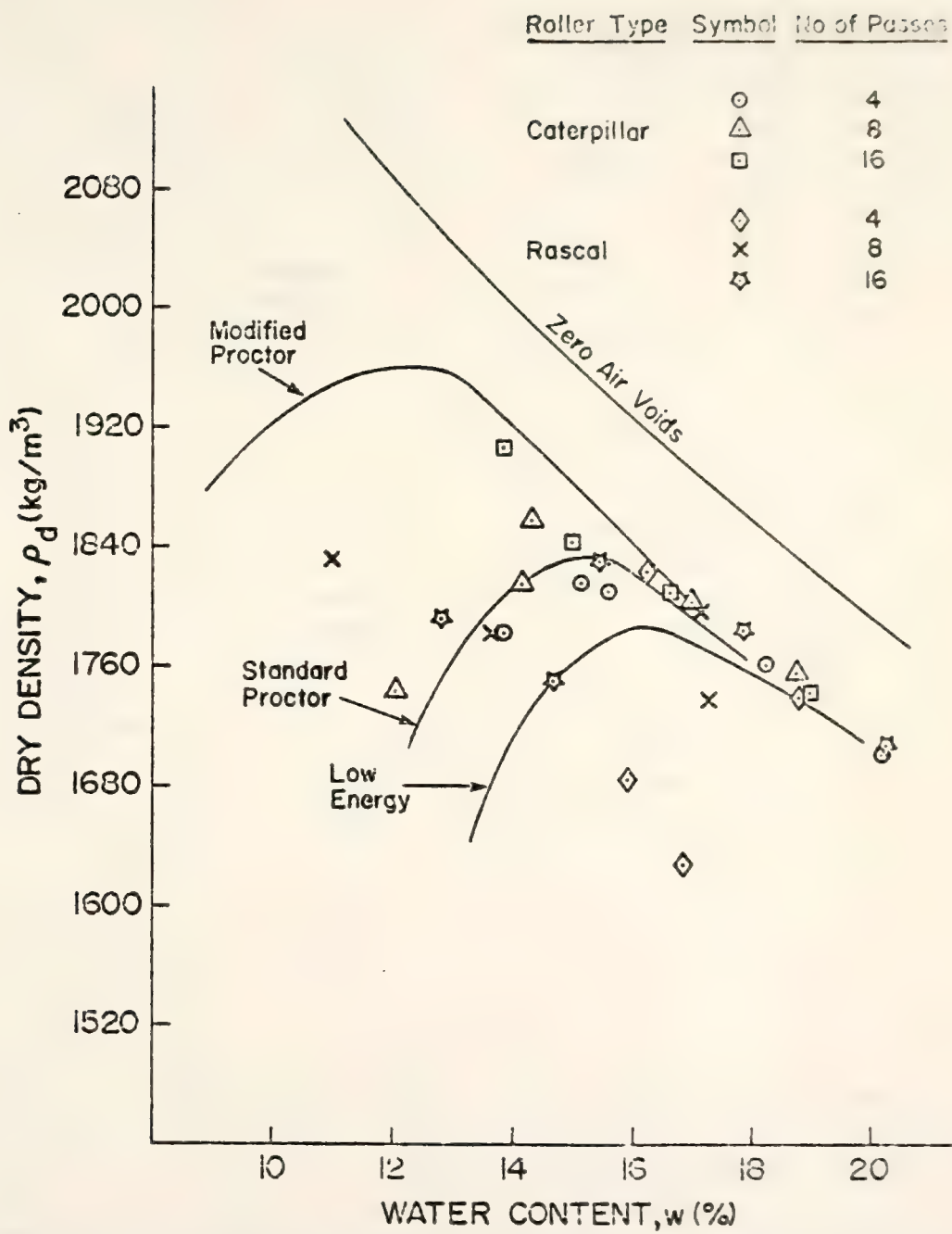


Figure 3-3 Dry Density - Water Content Relationship Before Test for UU Triaxial Test Specimens at 276 kPa Confinement

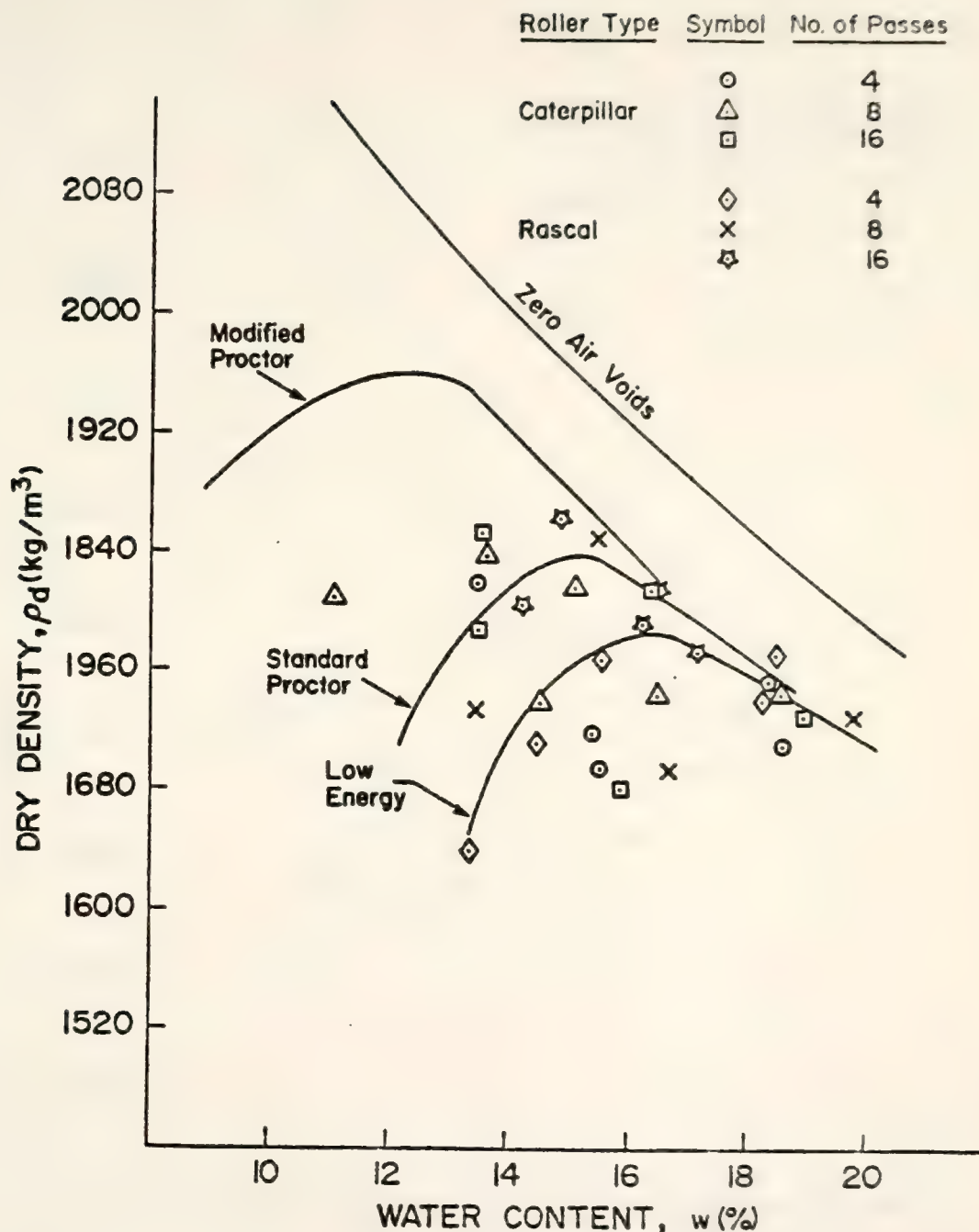


Figure 3-4 Dry Density-Water Content Relationship Before Test for UU Triaxial Test Specimens at 138 kPa Confinement

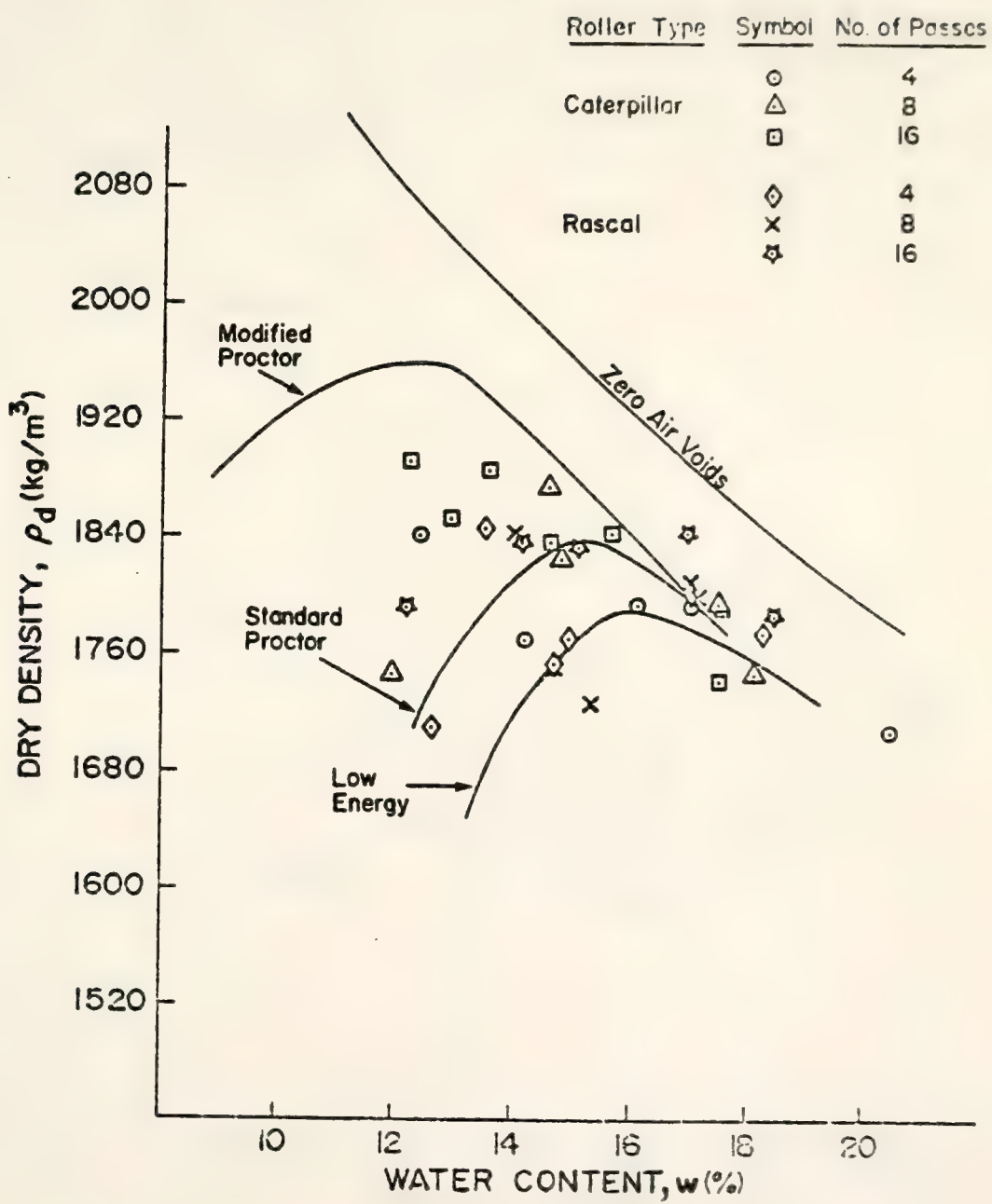


Figure 3-5 Dry Density-Water Content Relationship Before Test for UU Triaxial Test Specimens at 69 kPa Confinement

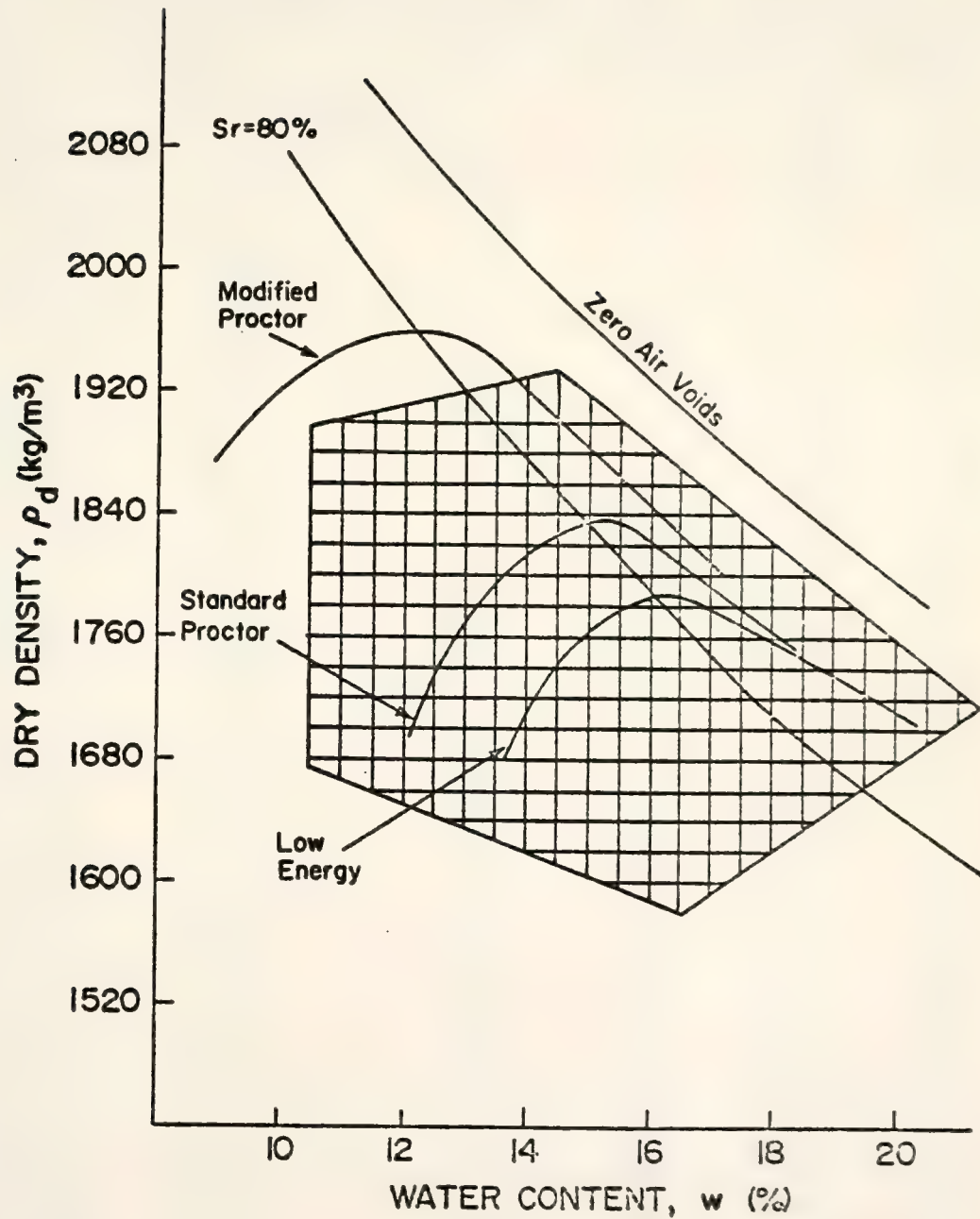


Figure 3-6 Joint Region of Observation for UU Compression Strength Prediction Model

TABLE 3-5 Failure Conditions for Unconsolidated-
Undrained Triaxial Tests

Sample No.	Principal Stress Different at Failure $(\sigma_1 - \sigma_3)_f$ (kPa)	Volumetric Strain Failure %	Axial Strain at Failure %	Final Void Ratio e_f	Poisson's Ratio at Failure μ_f
C1A1(276)	804.3	1.03	6.94	0.506	0.426
C2A6(276)	789.8	0.90	5.87	0.497	0.423
C3A3(276)	1005.6	1.67	7.17	0.504	0.384
C4A8(276)	235.6	0.67	16.29	0.57	0.480
C5A1(276)	378.3	1.02	9.42	0.527	0.446
C1B2(276)	1166.9	0.81	7.37	0.472	0.445
C2B2(276)	746.5	1.51	7.7	0.513	0.402
C3B8(276)	959.3	2.61	13.0	0.501	0.399
C4B10(376)	449.6	2.32	16.33	0.503	0.429
C5B10(276)	478.3	1.02	18.38	0.541	0.472
C2C6(276)	685.9	1.05	13.71	0.485	0.462
C3C8(276)	693.6	1.00	13.65	0.425	0.463
C4C10(276)	304.3	0.84	15.72	0.542	0.473
C5C4(276)	624.0	1.11	17.95	0.49	0.469
R2A10(276)	461.7	1.68	12.52	0.569	0.433
R3A1(276)	465.8	3.0	11.35	0.547	0.368
R4A4(276)	508.6	0.61	17.18	0.48	0.482
R5A2(276)	416.1	1.32	19.57	0.544	0.466
R2B10(276)	988.7	2.39	17.66	0.490	0.432
R3B6(276)	1138.8	1.70	10.36	0.465	0.418
R4B7(276)	390.4	1.02	8.9	0.50	0.442
R5B9(276)	532.6	2.07	19.66	0.524	0.447
R1C9(276)	1013.0	1.83	8.28	0.508	0.39
R2C4(276)	855.2	1.03	19.71	0.475	0.474
R3C10(276)	504.9	3.42	15.75	0.487	0.392
R4C8(276)	382.0	1.07	13.78	0.513	0.461
R5C8(276)	211.3	0.86	8.28	0.58	0.448

TABLE 3-5 (Continued)

Sample No.	Principal Stress Different at Failure $(\sigma_1 - \sigma_3)_f$ (kPa)	Volumetric Strain at Failure %	Axial Strain at Failure %	Final Void Ratio e_f	Poisson's Ratio at Failure μ_f
C1A4(138)	536.3	1.62	5.96	0.569	0.364
C2A2(138)	781.1	0.55	5.45	0.492	0.45
C3A10(138)	539.4	1.56	8.55	0.565	0.409
C4A1(138)	235.6	0.98	17.35	0.535	0.472
C5A10(138)	264.7	1.21	8.23	0.589	0.426
C1B3(138)	1152.3	0.47	2.754	0.473	0.414
C2B9(138)	691.1	0.76	7.16	0.566	0.447
C3B9(138)	650.1	1.42	5.67	0.471	0.375
C4B2(138)	195.3	0.99	8.53	0.548	0.442
C5B9(138)	472.9	1.43	19.11	0.536	0.463
C1C4(138)	1156.7	0.79	4.48	0.473	0.412
C2C10(138)	771.4	1.04	7.4	0.515	0.43
C3C2(138)	546.4	0.88	13.67	0.605	0.468
C4C9(138)	278.3	0.78	11.03	0.564	0.465
C5C1(138)	390.7	0.47	19.02	0.491	0.488
R1A2(138)	562.9	2.19	8.9	0.64	0.377
R2A3(138)	545.7	1.19	19.88	0.528	0.470
R3A9(138)	538.4	2.31	14.85	0.557	0.422
R4A2(138)	312.8	1.24	8.85	0.555	0.430
R5A3(138)	201.8	0.60	11.49	0.54	0.474
R1B9(138)	721.1	0.80	10.37	0.585	0.462
R2B2(138)	610.1	0.53	7.67	0.492	0.465
R3B5(138)	309.7	2.39	19.92	0.548	0.44
R4B6(138)	334.2	1.22	11.33	0.487	0.446
R5B8(138)	186.8	0.88	16.08	0.566	0.473
R1C8(138)	597.5	0.19	19.89	0.512	0.495
R2C6(138)	736.0	1.14	9.52	0.497	0.440
R3C3(138)	311.3	0.82	18.89	0.517	0.478
R4C7(138)	502.5	0.53	8.67	0.465	0.470
R5C1(138)	214.4	0.84	6.34	0.517	0.434

TABLE 3-5 (Continued)

Sample No.	Principal Stress Different at Failure $(\sigma_1 - \sigma_3)_f$ (kPa)	Volumetric Strain at Failure %	Axial Strain at Failure %	Final Void Ratio e_f	Poisson's Ratio at Failure ν_f
C1A2(69)	859.3	1.04	3.38	0.507	0.346
C2A3(69)	495.0	0.69	7.47	0.532	0.454
C3A7(69)	496.2	0.52	4.906	0.606	0.447
C4A6(69)	143.2	0.65	4.527	0.605	0.428
C5A2(69)	412.3	1.42	10.1	0.433	0.430
C1B1(69)	611.3	0.83	2.76	0.587	0.35
C2B3(69)	330.3	0.88	7.43	0.591	0.441
C4B8(69)	678.4	0.87	5.85	0.499	0.426
C5B3(69)	233.6	0.38	3.45	0.540	0.444
C1C5(69)	685.7	0.73	4.35	0.504	0.416
C1C7(69)	1319.4	0.72	3.28	0.454	0.389
C2C9(69)	657.2	1.46	7.14	0.422	0.398
C2C7(69)	677.2	0.76	3.98	0.55	0.405
C3C3(69)	809.4	0.78	4.60	0.476	0.415
C4C1(69)	281.9	1.02	15.73	0.492	0.468
C5C10(69)	240.3	0.94	6.74	0.570	0.430
R1A7(69)	426.6	0.72	5.18	0.736	0.431
R2A8(69)	381.6	0.98	5.78	0.56	0.415
R3A10(69)	295.9	1.34	7.78	0.577	0.414
R4A7(69)	293.9	0.85	9.05	0.557	0.453
R5A10(69)	404.0	0.61	3.78	0.526	0.42
R1B1(69)	434.4	0.29	6.88	0.629	0.479
R2B7(69)	716.2	0.3	5.6	0.533	0.473
R3B10(69)	391.1	0.57	16.9	0.672	0.483
R4B4(69)	427.0	0.47	6.09	0.525	0.462
R5B3(69)	326.4	0.73	6.4	0.545	0.443
R1C5(69)	607.1	0.22	5.67	0.508	0.48
R2C5(69)	690.6	0.43	4.93	0.536	0.457
R3C1(69)	480.7	-1.26	15.33	0.608	0.541
R4C9(69)	376.1	0.61	7.47	0.493	0.459
R5C9(69)	297.3	0.89	16.9	0.553	0.474

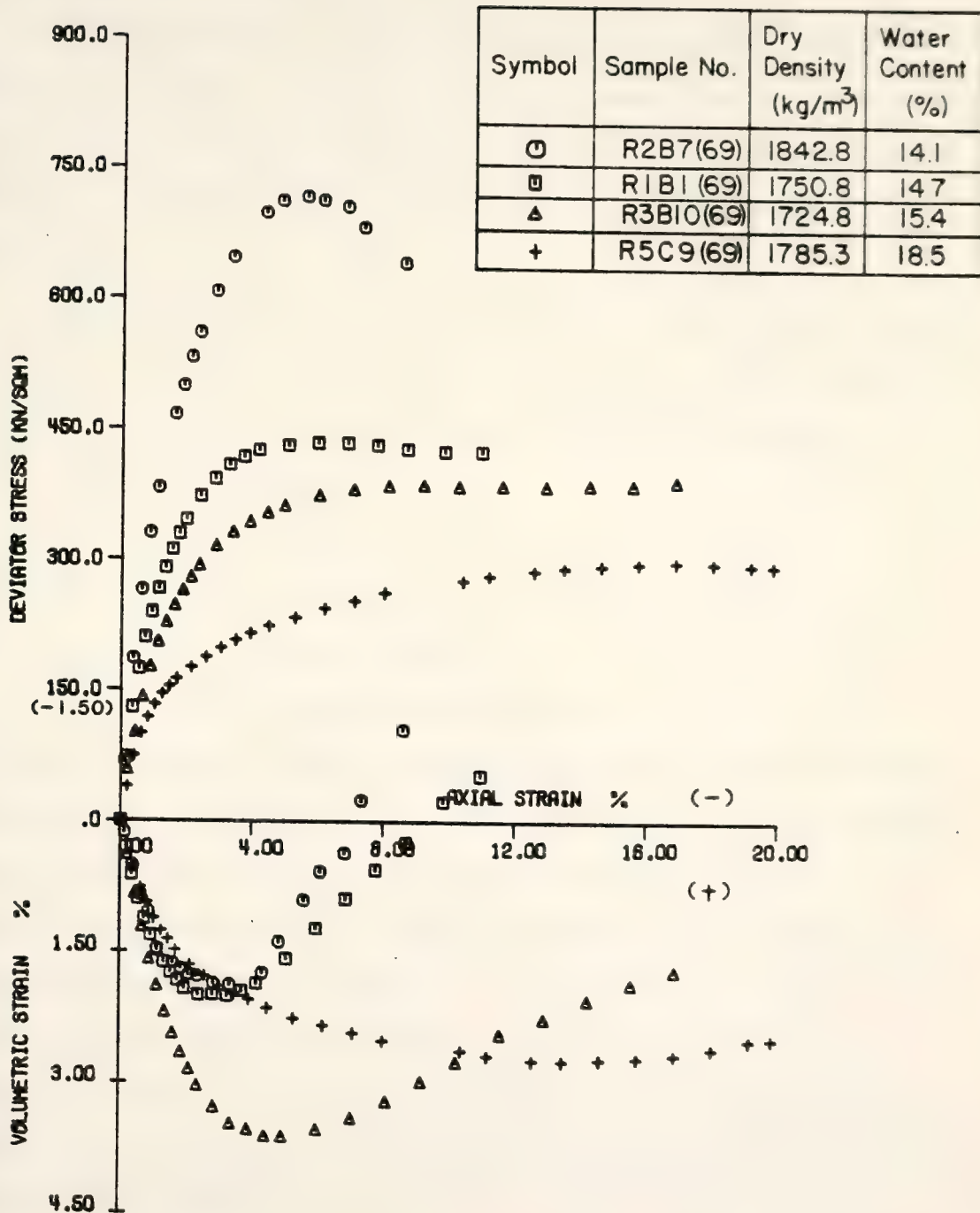


Figure 3-7 Axial Stress and Volumetric Strain Vs. Axial Strain for Sample R2B7, R1B1, R3B10, R5C9

increase in strength at very high strains.

The strain behavior is also dependent on the volume changes that occur in the sample. With low confining pressure, dry-of-optimum samples reach the maximum amount of densification under shear and then begin to dilate. The maximum deviator stress is reached shortly after the dilation begins.

The volume change due to shear seems to be related to the compactive prestress which has been induced in the sample. Lin (1981) developed a compactive prestress regression model for the field compacted St. Croix clay. The prediction model is

$$\hat{P}_s = -160.99 - 0.0063w^2 \cdot P_c + 27.04 P_c^{1/2} \quad (3-1)$$

where

\hat{P}_s = predicted value of compactive prestress, kPa

w = Water content, %

P_c = compaction pressure, kPa

Using the compaction variable values of this study, values of predicted prestress were calculated by Equation 3-1. The value of overconsolidation ratio (OCR) is defined as the ratio of predicted prestress (\hat{P}_s) and confining pressure (σ_c). Figure 3-8 shows the relationship between volumetric strain due to shear up to failure and OCR. It can be seen that the volumetric strain at failure decreases with increasing OCR. Table 3-6, which gives the values of OCR and the volumetric strain at failure and at the end of the test, shows the dilatant behavior for low water content samples with high OCR.

Table 3-7 shows the results of all volume changes during the tests. The higher confining pressures cause more densification to occur in low water content samples, as evidenced by comparison of Figures 3-9 and 3-10. In spite of the poor control over compaction variables in the test

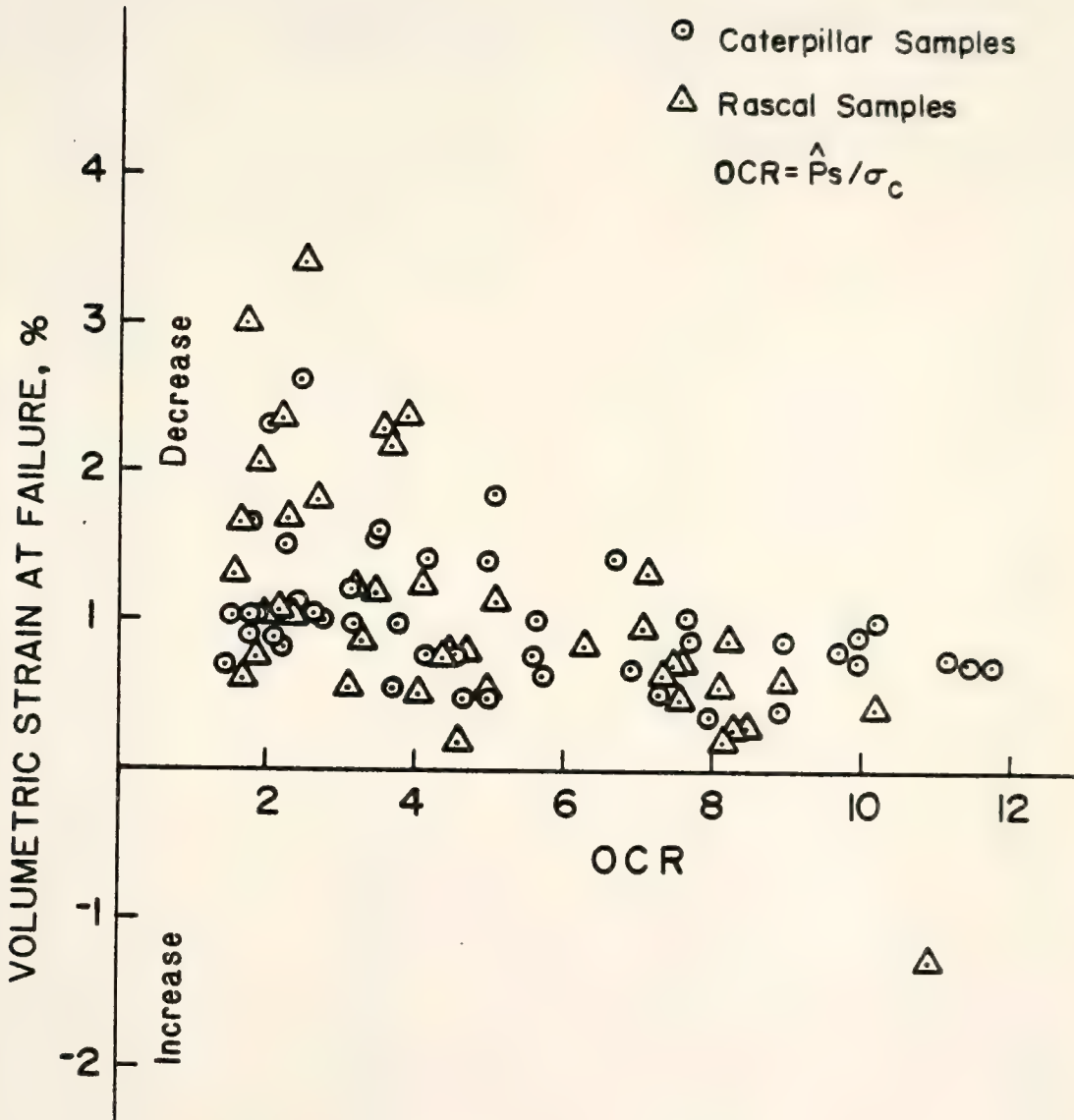


Figure 3-8 OCR Vs. Volumetric Strain Due to Shear Up to Failure

1-2

TABLE 3-6 Values of OCR, Volumetric Strain
at Failure and at End of Test

Sample No.	Volumetric Strain at Failure, %	Volumetric Strain at Test End, %	$\text{OCR} = \frac{\hat{P}_s}{\sigma_c}$
C1A1(276)	1.03	1.02	1.74
C2A6(276)	0.90	0.79	1.76
C3A3(276)	1.67	1.67	1.83
C4A8(276)	0.67	0.67	1.44
C5A1(276)	1.02	1.07	1.58
C1B2(276)	0.81	0.63	2.25
C2B2(276)	1.51	1.89	2.26
C3B8(276)	2.61	2.57	2.42
C4B10(276)	2.32	2.32	2.02
C5B10(276)	1.02	1.02	1.85
C2C6(276)	1.05	1.02	2.63
C3C8(276)	1.0	0.95	2.76
C4C10(276)	0.84	0.84	2.09
C5C4(276)	1.11	1.11	2.42
C1A4(138)	1.62	1.31	3.5
C2A2(138)	0.55	-0.02	3.7
C3A10(138)	1.56	1.37	3.49
C4A1(138)	0.98	0.98	3.13
C5A10(138)	1.21	1.20	3.12
C1B3(138)	0.47	0.16	4.61
C2B9(138)	0.76	0.20	4.48
C3B9(138)	1.42	1.14	4.96
C4B2(138)	0.99	1.01	3.72
C5B9(138)	1.43	1.20	4.14
C1C4(138)	0.79	0.38	5.59
C2C10(138)	1.04	0.80	5.61
C3C2(138)	0.88	0.60	5.05
C4C9(138)	0.78	0.78	4.16
C5C1(138)	0.47	0.47	4.91

TABLE 3-6 (Continued)

Sample No.	Volumetric Strain at Failure %	Volumetric Strain at Test End, %	$\text{OCR} = \frac{\sigma_s}{\sigma}$
R1A2(138)	2.19	2.02	3.67
R2A3(138)	1.19	1.19	3.45
R3A9(138)	2.31	2.30	3.56
R4A2(138)	1.24	1.27	3.12
R5A3(138)	0.60	0.61	3.09
R139(138)	0.80	0.40	4.29
R2B2(138)	0.53	0.38	4.01
R3B5(138)	2.39	2.39	3.83
R4B6(138)	1.22	1.14	4.07
R5B8(138)	0.88	0.88	3.29
R1C8(138)	0.19	0.19	4.59
R2C6(138)	1.14	0.92	5.07
R3C3(138)	0.82	0.82	4.44
R4C7(138)	0.53	0.41	4.95
R5C1(138)	0.84	0.85	4.64
R1A7(69)	0.72	0.06	7.46
R2A8(69)	0.98	0.73	7.01
R3A10(69)	1.34	1.24	7.07
R4A7(69)	0.85	0.78	6.23
R5A10(69)	0.61	0.16	7.3
R1B1(69)	0.29	-0.18	8.23
R2B7(69)	0.3	-0.35	8.41
R3B10(69)	0.57	0.57	8.06
R4B4(69)	0.47	0.13	7.55
R5B3(69)	0.73	0.59	7.52
R1C5(69)	0.22	-0.14	8.12
R2C5(69)	0.43	-0.13	10.16
R3C1(69)	-1.26	-1.26	10.90
R4C9(69)	0.61	0.52	8.94
R5C9(69)	0.89	0.83	8.2

TABLE 3-6 (Continued)

Sample No.	Volumetric Strain at Failure %	Volumetric Strain at Test End, %	$\sigma_{CR} = \frac{\sigma_0}{\sigma}$
C1A2(69)	1.04	0.86	7.6
C2A3(69)	0.69	0.22	6.84
C3A7(69)	0.52	-0.6	7.25
C4A6(69)	0.65	0.68	5.67
C5A2(69)	1.42	1.27	6.62
C1B1(69)	0.83	0.44	9.68
C2B3(69)	0.42	0.06	8.84
C4B8(69)	0.87	0.78	8.91
C5B3(69)	0.38	0.29	7.90
C1C5(69)	0.73	0.10	11.42
C2C9(69)	1.46	1.25	10.68
C2C7(69)	0.76	0.74	9.19
C3C3(69)	0.78	0.28	11.16
C4C1(69)	1.02	1.0	10.14
C5C10(69)	0.94	0.91	9.17
R2A10(276)	1.68	1.75	1.65
R3A1(276)	3.0	3.12	1.70
R4A4(276)	0.61	0.60	1.68
R5A2(276)	1.32	1.32	1.52
R2B10(276)	2.39	2.32	2.13
R3B6(276)	1.70	1.60	2.29
R4B7(276)	1.02	1.08	1.88
R5B9(276)	2.07	2.07	1.87
R1C9(276)	1.83	1.86	2.67
R2C4(276)	1.03	1.03	2.41
R3C10(276)	3.42	3.49	2.49
R4C8(276)	1.07	1.08	2.13
R5C8(276)	0.86	0.92	1.82

TABLE 3-7 Volume Change Data

Symbols in Table:

- V_o = original sample volume prior to test, cm^3
 V_{vo} = original sample volume of voids prior to test, cm^3
 V_{ao} = original sample volume of air prior to test, cm^3
 ΔV_c = change in volume occurring during application of
confining pressure, cm^3
 ΔV_{sh} = change in volume occurring during shear up to failure, cm^3
 V_f = final sample volume after triaxial test (determined by
waxing method), cm^3
 S_f = final degree of saturation, %

Sample No.	V_o	V_{vo}	V_{ao}	ΔV_c	ΔV_{sh}	V_f	S_f
C1A1(276)	185.82	65.17	12.71	0.86	1.93	181.3	95.91
C2A6(276)	189.52	66.05	13.94	1.09	1.73	184.17	85.0
C3A3(276)	175.76	63.34	19.81	2.59	2.98	168.22	76.88
C4A8(276)	193.85	75.61	8.91	1.57	1.29	185.45	99.0
C5A1(276)	183.75	67.68	8.7	1.18	1.96	176.91	96.46
C1B2(276)	189.69	63.27	12.72	0.8	1.97	185.90	84.64
C2B2(276)	193.23	67.48	17.83	1.86	3.61	189.52	76.92
C3B8(276)	190.08	71.25	31.3	4.83	4.88	177.45	67.04
C4B10(276)	186.98	66.09	8.75	1.18	4.31	181.40	94.01
C5B10(276)	190.8	70.72	7.9	1.44	1.93	184.7	96.7
C2C6(276)	187.75	63.62	11.68	0.93	2.08	183.6	86.25
C3C8(276)	182.78	57.77	9.46	1.86	1.90	177.71	90.84
C4C10(276)	184.52	69.3	8.42	2.53	1.53	177.43	97.57
C5C4(276)	194.2	68.26	9.83	0.83	2.15	187.26	94.77
R2A10(276)	187.95	78.17	26.49	4.03	3.22	176.38	82.77
R3A1(276)	189.82	75.02	24.1	3.68	5.80	177.45	81.15

TABLE 3-7 (Continued)

Sample No.	V_o	V_{vo}	V_{ao}	ΔV_c	ΔV_{sh}	V_f	γ
R4A4(276)	186.93	64.61	9.17	1.82	1.20	180.81	94.34
R5A2(276)	191.97	72.11	9.07	1.06	2.52	184.71	96.73
R2B10(276)	182.92	65.92	21.42	1.54	4.48	173.75	77.6
R3B6(276)	198.54	68.12	28.31	1.02	3.37	190.01	65.58
R4B7(276)	191.85	68.34	9.24	0.67	2.06	184.92	95.77
R5B9(276)	189.33	71.32	14.46	2.27	3.88	179.51	92.04
R1C9(276)	195.01	69.67	24.73	1.44	3.63	187.69	70.59
R2C4(276)	184.25	63.28	11.17	0.54	1.9	178.08	90.7
R3C10(276)	192.07	71.55	22.12	3.3	7.14	178.09	84.13
R4C8(276)	192.45	69.32	7.99	0.64	2.08	186.04	96.99
R5C8(276)	192.39	74.59	8.03	2.27	1.74	185.78	97.38
C1A4(138)	198.09	75.96	23.49	2.69	2.56	189.91	75.44
C2A2(138)	173.75	60.41	17.72	1.76	0.05	168.44	76.64
C3A10(138)	176.08	69.04	22.69	4.67	2.37	164.98	76.63
C4A1(138)	187.61	69.69	9.16	0.96	1.78	180.74	95.84
C5A10(138)	191.44	74.13	13.42	1.44	2.28	184.62	87.81
C1B3(138)	186.96	63.72	16.82	0.58	0.23	180.77	80.42
C2B9(138)	185.76	69.95	23.07	1.89	1.07	179.54	71.83
C3B9(138)	202.72	71.25	30.54	3.97	2.27	191.39	65.61
C4B2(138)	185.94	69.58	9.14	0.71	1.83	179.75	94.85
C5B9(138)	205.95	77.23	18.08	2.62	2.52	196.69	85.76
C1C4(138)	174.10	58.50	14.82	1.31	0.57	169.69	79.87
C2C10(138)	200.22	71.87	23.53	1.60	1.68	192.79	73.10
C3C3(138)	169.71	67.48	22.3	3.87	1.16	161.94	73.08
C4C9(138)	202.18	76.91	10.51	0.58	1.54	195.55	93.87
C5C1(138)	195.77	68.32	10.07	1.22	0.94	189.63	93.12
R1A2(138)	187.09	77.1	36.2	3.52	3.99	177.16	58.08
R2A3(138)	192.67	70.65	17.78	1.22	2.51	186.01	82.11
R3A9(138)	191.48	73.94	26.38	1.86	4.49	181.72	72.48
R4A2(138)	193.77	72.81	11.06	1.57	2.35	187.42	91.92
R5A3(138)	191.56	70.01	7.27	2.02	1.11	186.68	95.46

TABLE 3-7 (Continued)

Sample No.	v_o	v_{vo}	v_{ao}	Δv_c	Δv_{sh}	v_f	γ
R1B9(138)	178.28	67.55	25.97	1.15	0.95	173.99	64.2
R2B2(138)	196.21	66.1	9.83	1.07	0.80	193.43	87.89
R3B5(138)	180.86	71.12	20.08	3.58	4.38	172.63	84.94
R4B6(138)	192.5	67.09	14.22	2.59	2.22	185.67	30.65
R5B8(138)	194.13	73.85	7.41	0.10	1.64	188.16	97.51
R1C8(138)	198.07	69.2	9.95	2.14	0.48	192.27	89.72
R2C6(138)	193.2	68.23	18.44	2.59	1.81	185.32	80.11
R3C3(138)	188.75	68.75	11.41	0.70	1.55	181.76	92.37
R4C7(138)	196.48	65.23	10.82	0.29	0.76	191.57	89.05
R5C1(138)	189.40	67.68	12.49	1.44	1.55	183.56	87.67
C1A2(69)	195.67	66.53	21.48	0.22	2.03	189.61	68.67
C2A3(69)	180.96	64.65	12.35	0.35	1.25	177.04	84.51
C3A7(69)	199.22	72.92	22.68	0.54	1.03	196.57	65.58
C4A6(69)	194.54	75.53	7.43	0.28	1.27	189.81	94.67
C5A2(69)	193.4	68.54	9.33	0.58	2.73	189.95	89.12
C1B1(69)	186.0	69.51	9.46	2.56	1.53	181.28	57.0
C2B3(69)	194.76	67.36	29.58	0.54	0.81	189.95	80.55
C3B3(69)	209.44	78.40	16.97	0.32	1.83	205.89	85.69
C4B8(69)	193.0	63.15	9.64	0.23	1.67	189.53	81.77
C5B3(69)	194.44	69.33	11.09	0.0	0.75	191.01	90.42
C1C5(69)	179.53	60.29	7.13	1.13	1.31	175.57	71.86
C1C7(69)	174.23	55.38	15.68	0.0	1.26	170.89	75.7
C2C9(69)	189.59	64.83	17.10	0.0	2.73	186.81	78.5
C2C7(69)	192.58	72.34	15.33	0.74	1.45	185.62	88.93
C3C3(69)	199.94	64.8	13.47	0.95	1.56	194.26	79.82
C4C1(69)	199.06	67.57	9.73	0.41	2.02	194.39	89.43
C5C10(69)	191.88	68.70	8.42	0.90	1.81	189.74	85.94
R1A7(69)	189.82	73.44	32.33	2.87	1.35	188.92	47.97
R2A8(69)	202.58	74.35	20.70	1.73	1.96	195.69	74.07
R3A10(69)	201.24	74.78	22.83	0.63	2.69	195.10	76.52
R4A7(69)	194.02	70.62	7.69	0.0	1.65	191.13	91.56
R5A10(69)	196.82	66.49	17.17	1.1	1.19	194.50	71.95

TABLE 3-7 (Continued)

Sample No.	V_o	V_{vo}	V_{ao}	ΔV_c	ΔV_{sh}	V_f	S_p
R1B1(69)	195.27	72.68	21.41	0.85	0.572	192.29	65.41
R2B7(69)	180.67	61.29	14.32	0.29	0.55	179.71	73.74
R3B10(69)	169.84	64.83	19.51	0.98	1.67	167.38	63.8
R4B4(69)	190.73	67.12	8.50	0.16	0.81	187.16	90.23
R5B3(69)	189.26	68.47	10.78	1.26	1.38	183.19	87.58
R1C5(69)	204.37	69.95	13.09	0.0	0.46	201.21	83.22
R2C5(69)	193.70	65.94	15.31	0.0	0.83	191.77	73.9
R3C1(69)	211.40	75.71	29.45	0.76	-2.02	209.33	56.06
R4C9(69)	183.89	62.42	4.82	0.5	1.13	180.45	96.36
R5C9(69)	196.11	70.57	5.76	0.54	1.74	191.97	95.41

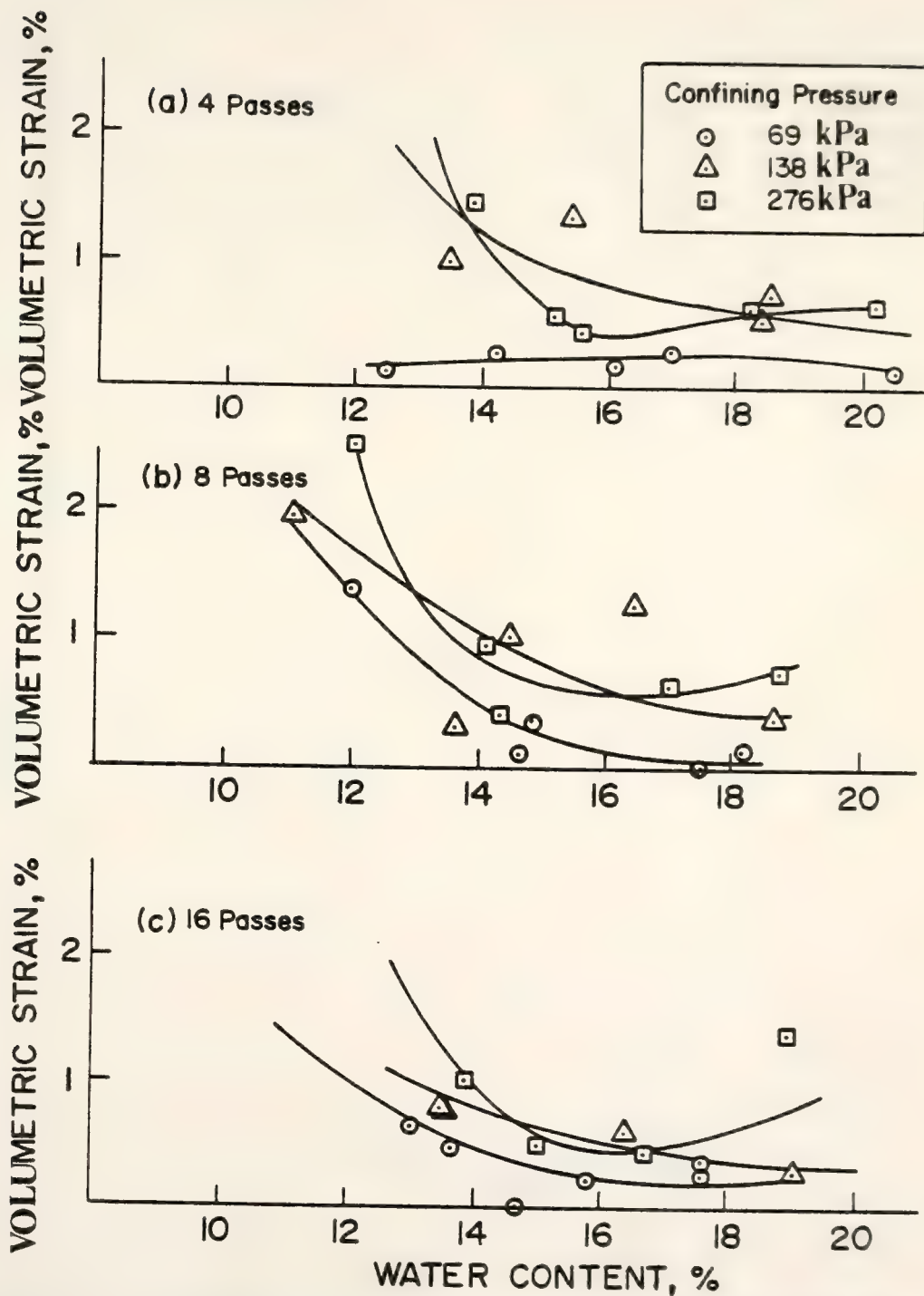


Figure 3-9 Water Content Vs. Volumetric Strain During Application of Confining Pressure for Caterpillar Samples

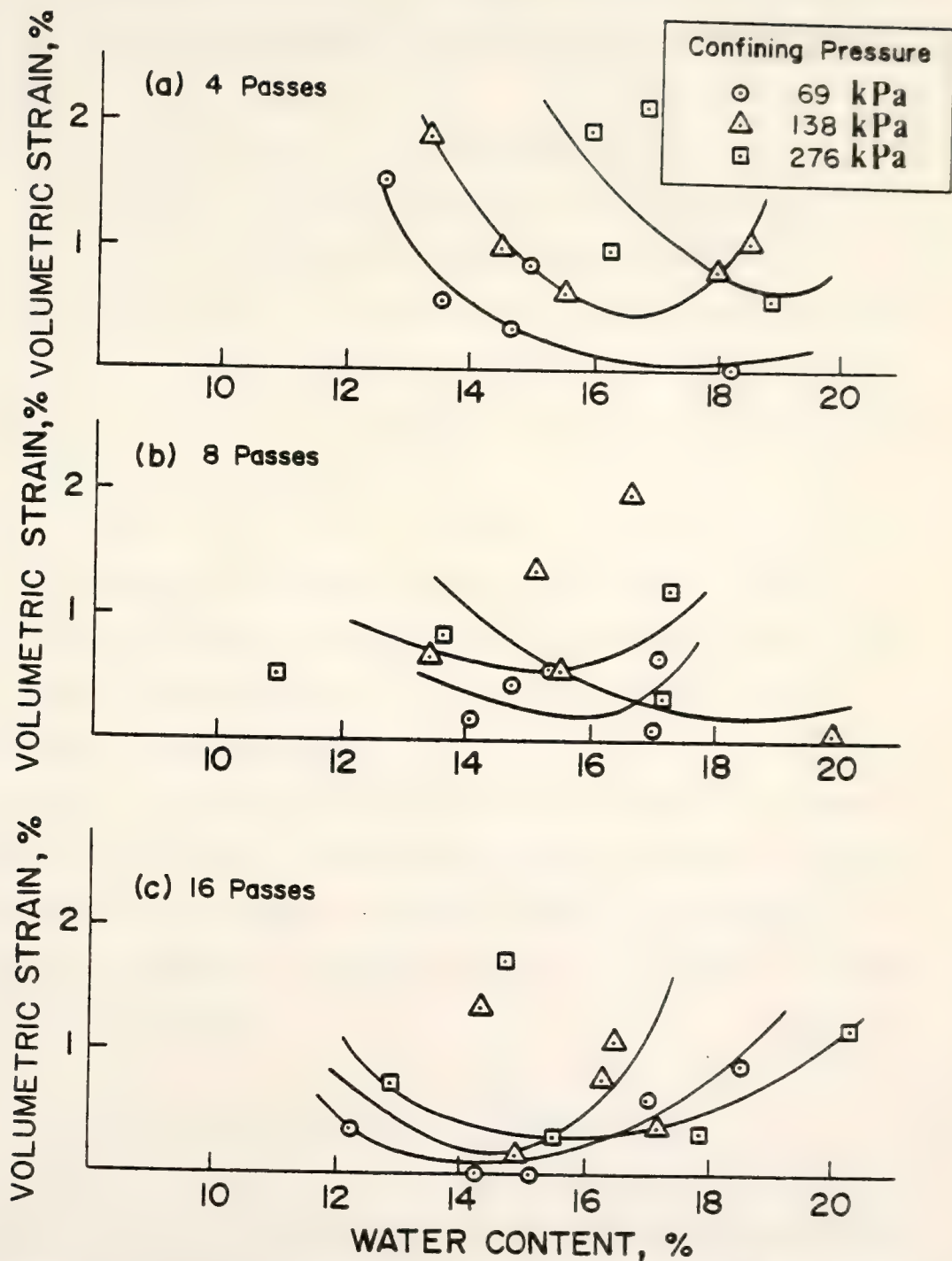


Figure 3-10 Water Content Vs. Volumetric Strain During Application of Confining Pressure for Rascal Samples

pads, it still can be seen that the volumetric strain due to application of confining pressure decreases with water content to a minimum around optimum.

3-1-2.2 The $e_f \sqrt{S_f} - \log (\frac{q_c}{2})$ Relationship

DaCruz (1963) found a linear relationship between the product of void ratio and the square root of degree of saturation at failure ($e_f \sqrt{S_f}$) and the logarithm of one half the stress difference at failure ($\frac{q_c}{2}$). A similar plot of the field compacted St. Croix clay is shown in Figure 3-11. The linear relationship of Figure 3-11 is statistically represented by the equation ($R^2 = 0.66$)

$$\log (\frac{q_c}{2}) = 4.256 - 3.88 e_f \sqrt{S_f} \quad . \quad (3-2)$$

The variabilities in volume change and compressive strength are caused in part by moisture variability and possibly losses during storage. Distinct zones of different water content and large rocks were encountered in some specimens.

Table 3-5 also shows that the values of Poisson's ratio at failure range from 0.35 to 0.54. The values of Poisson's ratio were calculated by assuming the stress-strain curve was a linear elastic response. For dry-of-optimum samples, those values were close to the values of Poisson's ratio in elastic material.

3-1-3 Consolidated-Undrained Shear Strength

The initial dry density-water content relationships for CIU triaxial tests are shown in Figures 3-12 and 3-13. Figure 3-14 shows the joint region of water content and dry density values for CIU triaxial tests. These figures will be a useful reference for subsequent discussions.

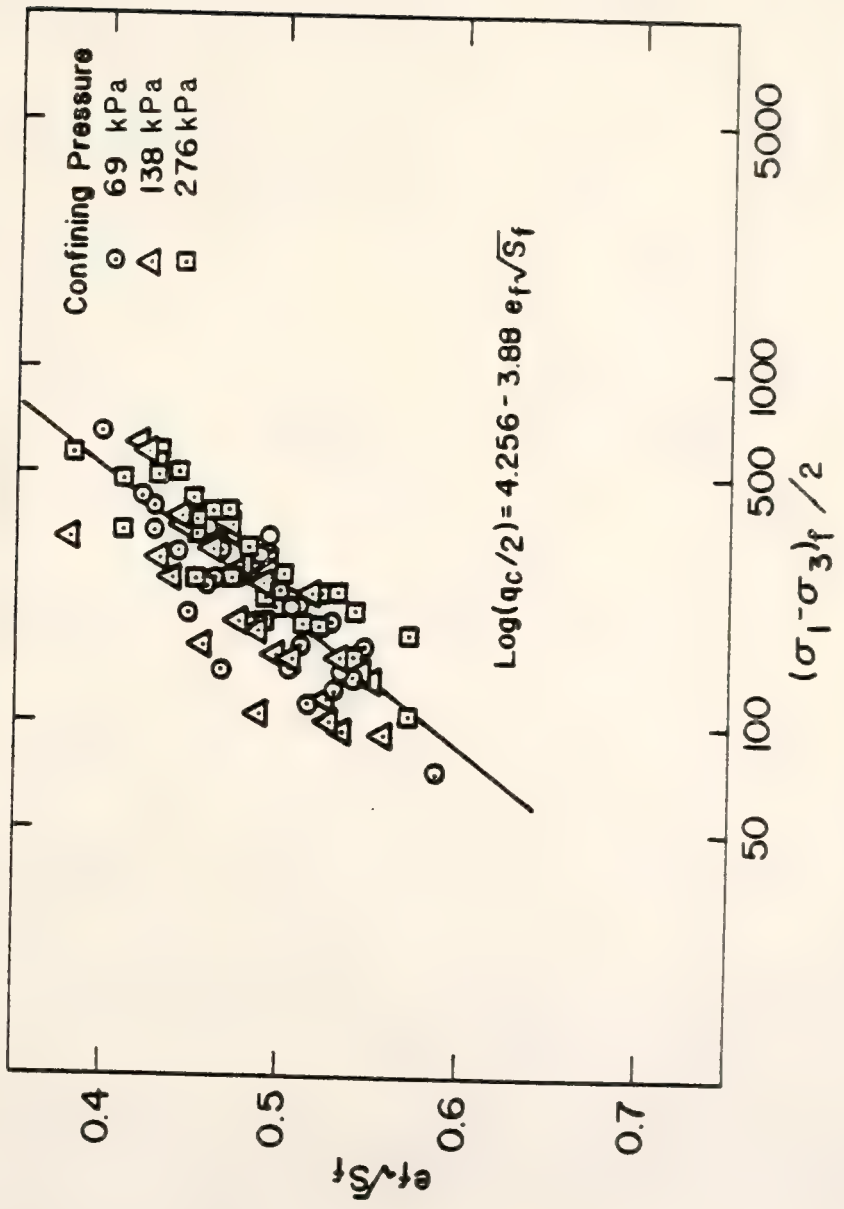


Figure 3-11 Void Ratio Times Square Root of Saturation at Failure Vs. Logarithm of One Half the Compression Strength

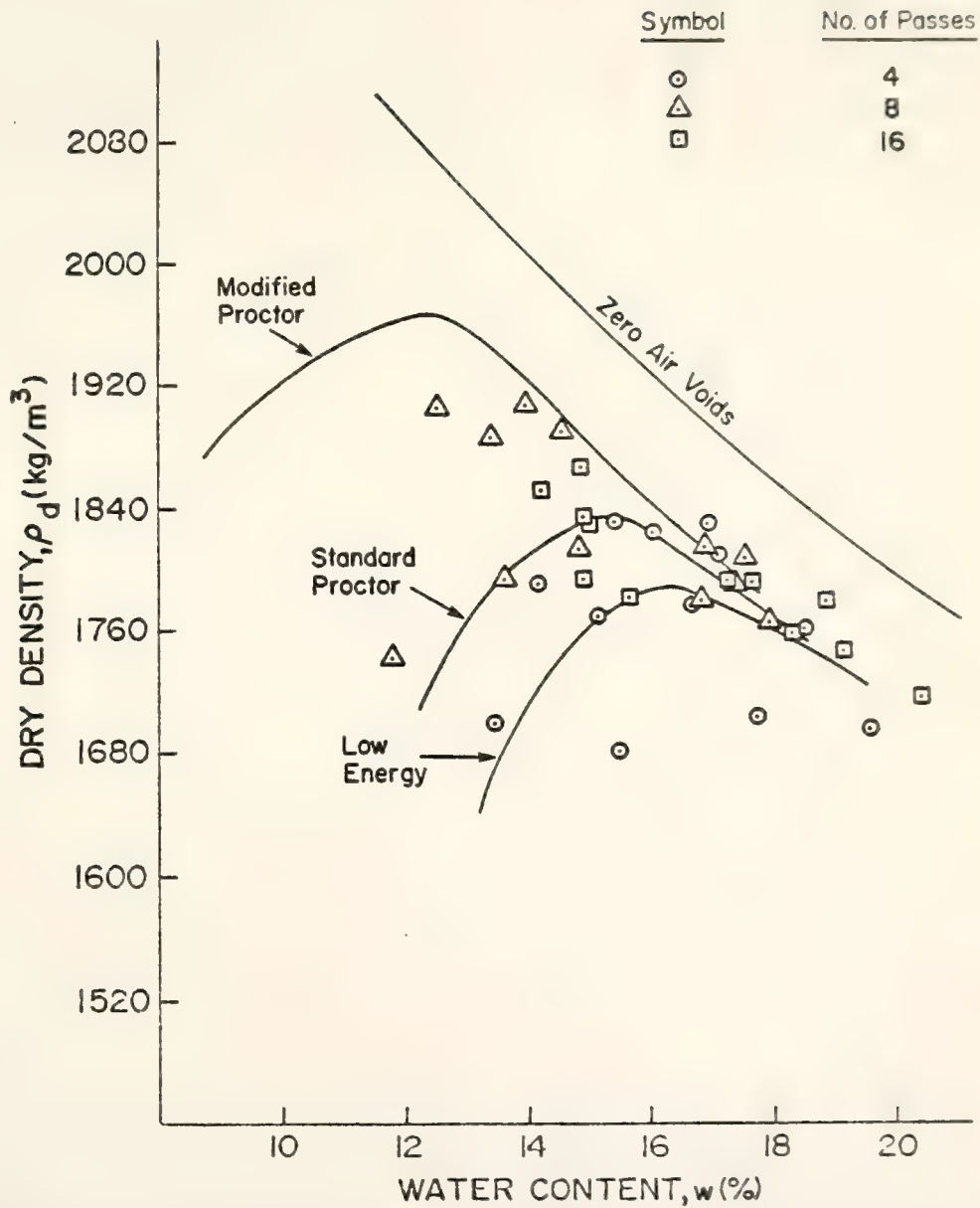


Figure 3-12 Caterpillar Dry Density-Water Content Relationship
Before Test for CIU Triaxial Test Specimens

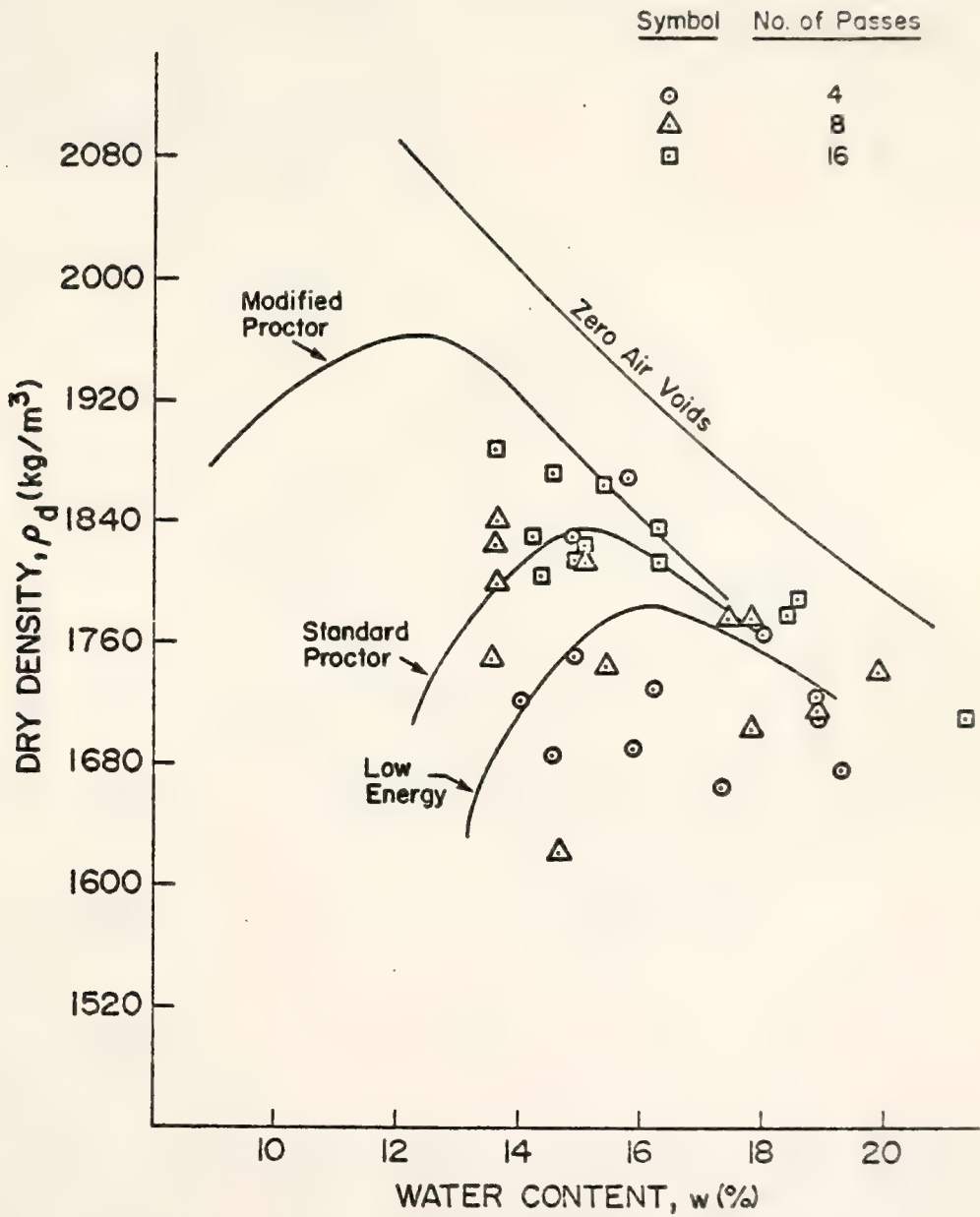


Figure 3-13 Rascal Dry Density-Water Content Relationship Before Test for CIU Triaxial Test Specimens

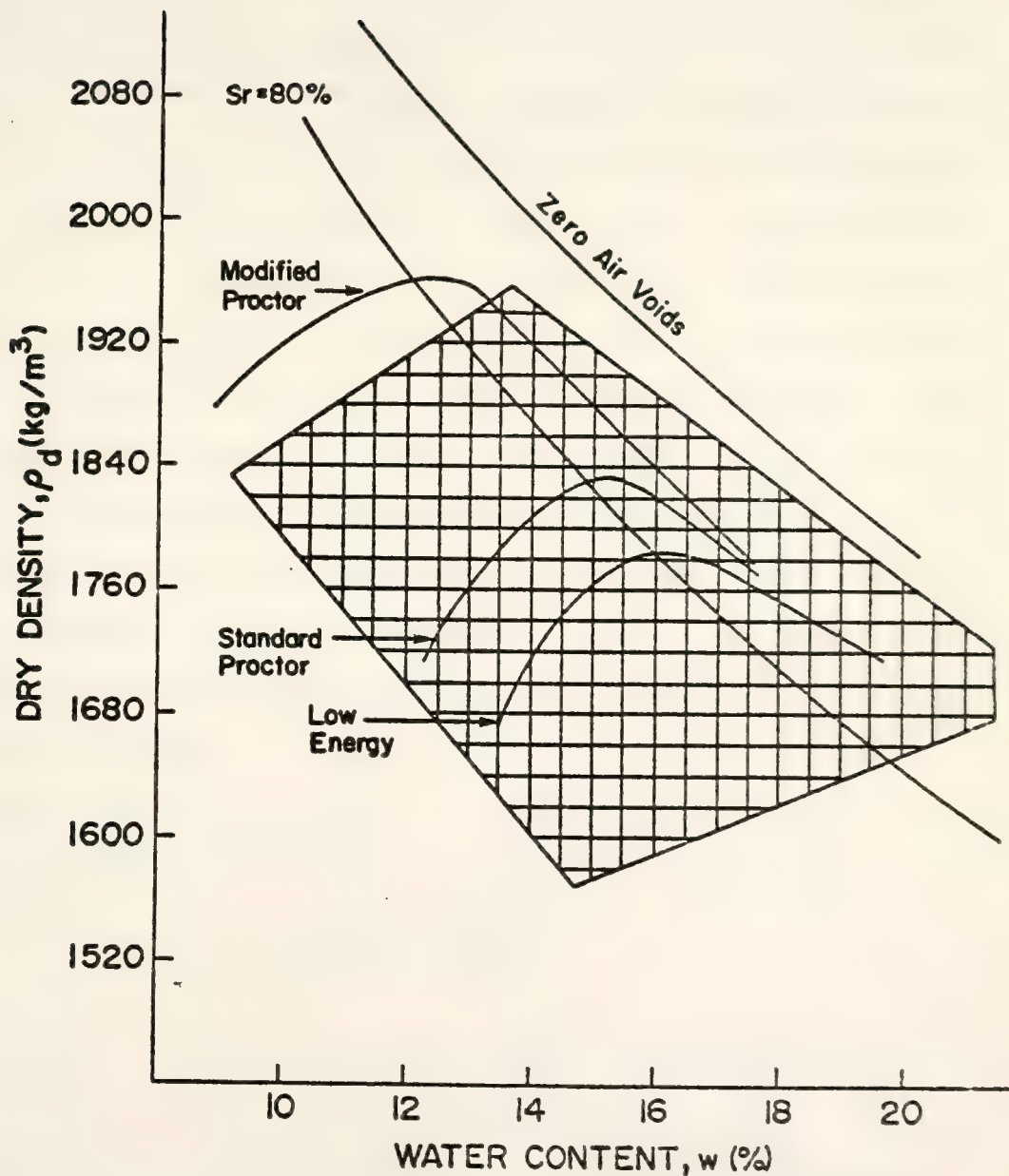


Figure 3-14 Joint Region of Observations for \overline{CIU} Compression Strength Prediction Model

Table 3-8 lists the initial and final degrees of saturation for each of the samples saturated prior to shear. Each initial degree of saturation was obtained through calculations utilizing the specific gravity, the as-compacted moisture content and the dry density. For the calculations of final degree of saturation, the values of moisture content and dry density after shear were determined by weighing the waxed samples in air and in water. The range of the final degree of saturation values is from 97 to 102 percent, with the majority of the values between 98.5 and 100 percent. All of the values of final degree of saturation are measured after the samples has expanded in response to release of the confining pressure and back pressure. The expansion of the sample may cause an inflow of water from the porous stones and drainage line, and a build-up of negative pore pressure. This response usually occurs in samples compacted to high energy levels. It can be seen from Table 3-8 that the final degree of saturation for many higher energy level samples is over 100 percent.

The theoretical back pressures were determined from Figure 2-15A or calculated from the equation (Lowe and Johnson, 1960) below.

$$\Delta u_T = P_i \frac{(S_f - S_i)(1-H)}{1 - S_f(1-H)} \quad (3-2)$$

where

Δu_T = the change in pressure corresponding to

a change in saturation from S_i to S_f

P_i = the initial absolute pressure corresponding to S_i , = 14.7 psi

H = Henry's constant = 0.018 cc of air/per

1 cc of water

TABLE 3-8 Back Pressures Required to Attain the Experimentally Observed Degree of Saturation

Sample No.	S_i (%)	S_f (%)	Theoretical Back Pressure Δu_T (kPa)	Experimental Back Pressure Δu_E (kPa)	Final B Parameter
C1A9(276)	65.6	100.5	1903	897	0.98
C3A5(276)	84.4	98.7	863	897	0.98
C4A4(276)	88.5	98.6	636	897	0.98
C5A5(276)	81.9	102.1	1002	897	1.0
C2B7(276)	74.1	98.4	1433	897	0.98
C1B10(276)	77.9	99.8	1223	897	0.97
C4B9(276)	83.2	102.2	930	897	0.98
C5B6(276)	90.5	100.3	526	897	1.0
C1C9(276)	78.5	100.5	1190	828	0.96
C2C3(276)	94.0	100.9	885	897	0.98
C3C10(276)	74.9	101.2	1389	897	1.0
C4C5(276)	92.6	102.2	410	897	1.0
C2A5(138)	73.5	101.0	1466	897	1.0
C3A1(138)	82.2	100.3	985	759	1.0
C4A5(138)	90.4	99.5	531	897	0.98
C5A7(138)	88.5	99.0	636	897	0.98
C1B8(138)	85.3	100.8	813	897	0.97
C3B6(138)	68.7	100.2	1732	897	1.0
C4B5(138)	77.1	100.0	1267	897	0.98
C5B4(138)	88.5	101.2	636	897	0.98
C2C1(138)	77.6	101.6	1240	897	0.98
C3C1(138)	80.1	101.1	1101	897	0.98
C4C7(138)	89.8	101.6	564	897	0.98
C5C8(138)	87.5	100.2	692	897	0.98
C1A3(65)	58.7	101.0	2285	966	1.0
C2A1(55)	77.8	101.6	1228	966	1.0
C3A9(63)	70.8	101.4	1616	966	1.0
C4A9(69)	84.8	101.2	841	621	0.99
C2B5(69)	83.1	101.4	935	966	1.0

TABLE 3-8 (Continued)

Sample No.	S_i (%)	S_f (%)	Theoretical Back Pressure Δu_T (kPa)	Experimental Back Pressure Δu_E (kPa)	Final B Parameter
C3B2(69)	54.9	98.9	2496	690	0.97
C4B6(69)	87.2	100.5	708	966	0.99
C5B8(83)	86.5	100.8	747	612	0.98
C2C4(70)	80.4	102.1	1085	966	1.0
C3C6(61)	86.5	101.8	747	690	1.0
C4C6(63)	91.4	100.0	476	688	1.0
C5C7(69)	88.7	101.5	625	966	1.0
R1A3(276)	70.5	99.9	1632	897	1.0
R2A7(276)	67.9	98.4	1776	897	0.98
R3A5(276)	63.3	99.5	2031	897	0.98
R5A6(276)	88.3	99.8	647	897	0.98
R2B8(276)	78.2	98.9	1206	897	0.99
R3B8(276)	74.2	99.3	1428	897	0.96
R4B1(276)	72.0	97.0	1549	759	0.93
R5B6(276)	87.4	100.9	697	897	1.0
R1C3(276)	80.0	99.1	1107	897	1.0
R1C10(276)	75.8	98.8	1339	897	0.98
R3C2(276)	77.7	99.8	1234	897	1.0
R5C3(276)	94.5	101.6	304	897	0.97
R2A1(138)	81.3	100.1	1035	897	1.0
R3A3(138)	62.2	99.8	2092	897	1.0
R4A6(138)	79.2	99.0	1151	897	0.98
R5A7(138)	87.0	100.7	719	897	0.98
R2B3(138)	69.3	98.6	1699	897	0.98
R3B7(138)	63.8	100.3	2003	897	1.0
R4B9(138)	85.3	101.8	813	897	0.98
R5B2(138)	56.61	100.4	2401	904	0.99
R2C9(138)	83.3	98.3	941	897	0.98
R3C9(138)	83.8	98.5	896	897	0.98
R4C1(138)	87.2	100.4	708	897	0.96

TABLE 3-8 (Continued)

Sample No.	S_i (%)	S_f (%)	Theoretical Back Pressure Δu_T (kPa)	Experimental Back Pressure Δu_E (kPa)	Final B Parameter
R5C6(138)	90.8	100.4	509	897	0.98
R1A4(69)	71.7	100.6	1566	966	0.98
R2A5(69)	83.9	99.7	891	966	1.0
R3A2(83)	73.9	99.3	1444	684	0.98
R5A8(60)	85.6	98.3	797	690	0.94
R1B10(69)	85.0	99.7	830	966	1.0
R2B9(66)	78.8	99.0	1173	966	1.0
R3B3(69)	71.9	100.0	1555	610	0.98
R5B4(69)	92.5	101.5	415	966	0.99
R2C3(69)	76.7	98.8	1289	966	0.98
R3C5(69)	92.7	101.3	415	966	1.0
R4C6(63)	87.9	98.5	670	690	0.96
R5C4(112)	94.4	99.7	863	710	0.97

S_i = initial degree of saturation

S_f = final degree of saturation

Since a vacuum was applied during the beginning of saturation, the initial absolute pressure may have been less than one atmosphere. The theoretical back pressure in Table 3-8 should be higher than the actually required back pressure. The final degree of saturation, as indicated by the measured B parameters are satisfactory.

3-1-3.1 Volume Change Due to Saturation and Consolidation

The volume changes due to wetting and loading, particularly over the long term, must be taken into consideration in the design of the compacted embankment. These volume changes will produce either embankment settlement or heave. For this study, long-term conditions were simulated in the laboratory by back pressure saturation of the field compacted samples under an isotropic state of stress. The equilibrium percent volume change due to saturation and consolidation ($\Delta V/V_o$) is shown for each sample in Table 3-9. The percent volume change is calculated as $\Delta V/V_o = \frac{\Delta e}{1 + e_o} \times 100\%$, where Δe = change in void ratio from the as-compacted to the saturated-consolidated condition, and e_o = initial void ratio.

The relationship between volume change ($\Delta V/V_o$), initial void ratio (e_o), and the consolidation pressure (σ'_c) is shown in Figure 3-15. From this figure, it can be seen that for a given consolidation pressure, the percent volume change decreases with decreasing initial void ratio. DiBernardo (1979), Johnson (1979), and Lin (1981) obtained similar results for compacted clay from the St. Croix site.

TABLE 3-9 Volume Change Due to Saturation and Consolidation

Sample No.	Initial Void Ratio e_0	Final Void Ratio e_f	Percent Volume Change $\Delta V/V_0$ (%) (+ = Settlement)
C1A9(276)	0.659	0.550	6.57
C3A5(276)	0.529	0.478	3.336
C4A4(276)	0.583	0.542	2.59
C5A5(276)	0.569	0.530	2.486
C1B10(276)	0.480	0.474	0.405
C2B7(276)	0.472	0.440	2.174
C4B9(276)	0.565	0.544	1.342
C5B6(276)	0.542	0.518	1.556
C1C9(276)	0.506	0.500	0.398
C2C3(276)	0.495	0.494	0.067
C3C10(276)	0.555	0.525	1.929
C4C5(276)	0.568	0.538	1.913
C2A5(138)	0.574	0.526	3.05
C3A1(138)	0.523	0.510	0.854
C4A5(138)	0.523	0.495	1.838
C5A7(138)	0.54	0.528	0.779
C1B8(138)	0.476	0.525	3.32
C3B6(138)	0.554	0.480	4.762
C4B5(138)	0.537	0.507	1.952
C5B4(138)	0.535	0.546	-0.717
C2C1(138)	0.562	0.597	-2.241
C3C1(138)	0.523	0.533	-1.97
C4C7(138)	0.596	0.549	2.945
C5C8(138)	0.586	0.557	1.828
C1A3(55)	0.64	0.615	1.524
C2A1(63)	0.637	0.618	1.161
C3A9(69)	0.557	0.547	0.642
C4A9(65)	0.644	0.585	3.589
C2B5(69)	0.47	0.513	-2.925
C3B2(69)	0.60	0.574	1.625

TABLE 3-9 (Continued)

Sample No.	Initial Void Ratio e_o	Final Void Ratio e_f	Percent Volume Change $\Delta V/V_o$ (+ = Settlement)
C4B6(69)	0.558	0.533	1.605
C5B8(83)	0.58	0.576	0.253
C2C4(70)	0.52	0.614	-6.184
C3C6(61)	0.556	0.622	-4.242
C4C6(63)	0.624	0.607	1.047
C5C7(69)	0.556	0.567	-0.707
R1A3(276)	0.592	0.528	4.02
R2A7(276)	0.652	0.543	6.60
R3A5(276)	0.618	0.492	7.787
R5A6(276)	0.50	0.471	1.933
R2B8(276)	0.637	0.580	3.482
R3B8(276)	0.515	0.480	2.31
R4B1(276)	0.528	0.485	2.814
R5B6(276)	0.57	0.544	1.656
R1C3(276)	0.476	0.483	-0.474
R1C10(276)	0.525	0.497	1.836
R3C2(276)	0.536	0.504	2.083
R5C3(276)	0.632	0.588	2.696
R2A1(138)	0.663	0.614	2.946
R3A3(138)	0.653	0.545	6.534
R4A6(138)	0.525	0.491	2.23
R5A7(138)	0.578	0.552	1.648
R2B3(138)	0.549	0.535	0.904
R3B7(138)	0.594	0.540	3.388
R4B9(138)	0.57	0.582	-0.764
R5B2(138)	0.721	0.590	7.641
R2C9(138)	0.489	0.487	0.101
R3C9(138)	0.545	0.530	0.971
R4C1(138)	0.493	0.500	-0.469
R5C6(138)	0.567	0.560	0.447

TABLE 3-9 (Continued)

Sample No.	Initial Void Ratio e_o	Final Void Ratio e_f	Percent Volume Change $\Delta V/V_o$ (%) (+ = Settlement)
R1A4(69)	0.675	0.598	4.597
R2A5(69)	0.631	0.612	1.165
R3A2(83)	0.621	0.585	1.675
R5A8(60)	0.618	0.631	-0.803
R1B10(69)	0.623	0.608	0.924
R2B9(66)	0.537	0.546	-0.586
R3B3(69)	0.599	0.553	2.877
R5B4(69)	0.602	0.585	1.061
R2C3(69)	0.529	0.526	0.196
R3C5(69)	0.56	0.542	1.154
R4C6(63)	0.518	0.521	-0.198
R5C4(112)	0.539	0.547	-0.52

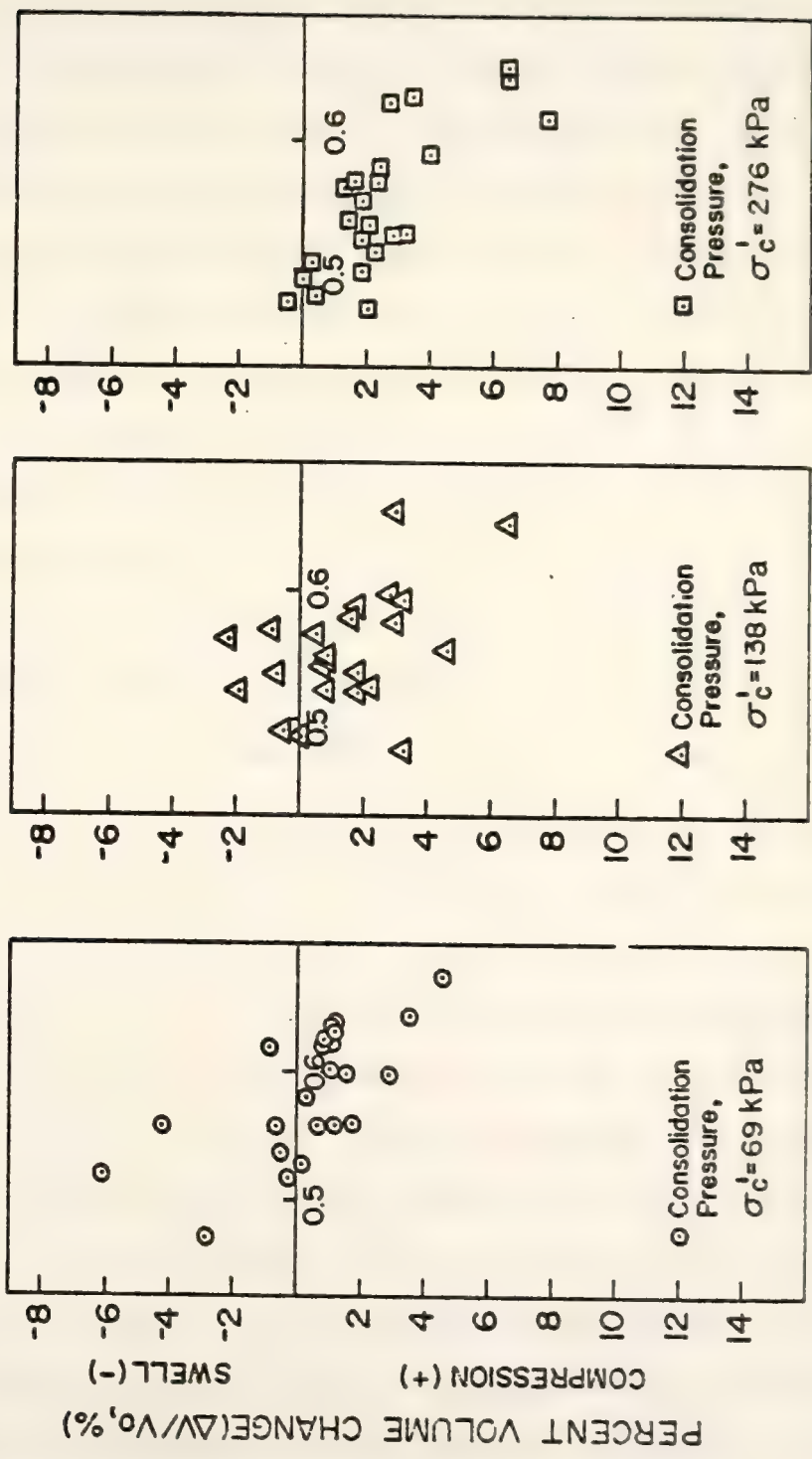


Figure 3-15 Percent Volume Change Upon Saturation Vs. Initial Void Ratio for All Samples

The relationships between the volume change due to saturation and consolidation and consolidation pressure are shown in Figures 3-16 and 3-17. It is observed that the samples with the higher energy level increase in volume (swell) under lower confining pressures, while most samples decrease in volume (settle) under higher consolidation pressures. Apparently in the former case the swelling pressure from the hydrating clay minerals, in conjunction with the reduced effective stress due to saturation, exceeded the confining pressure and resulted in a volume increase. If the confining pressures were sufficient to overcome the swelling tendency, volume reduction occurred.

Compaction moisture content also affects percent volume change due to saturation and consolidation, but trends are difficult to isolate. Holtz and Gibbs (1956) reported for swell tests on compacted clays that increasing the compaction moisture content for a given dry density resulted in decreased percent swell. For this study, most of the samples compacted dry of optimum exhibit percent volume changes more than (less net swell or more net compression) the samples compacted wet of optimum.

The compactive prestress also affects the volume change upon saturation and consolidation. The compactive prestress is a function of compactive pressure. The higher compactive prestress should produce a decrease in initial void ratio. Lin (1981) showed that for a given confining stress, the volume change on wetting decreases with decreasing initial void ratio (more net swell or less net compression). Examination of Figures 3-16 and 3-17 show that percent volume change upon saturation and consolidation are less (more net swell or less net compression) for the Caterpillar than for the Rascal roller at the same confining pressure. Since the Caterpillar roller samples

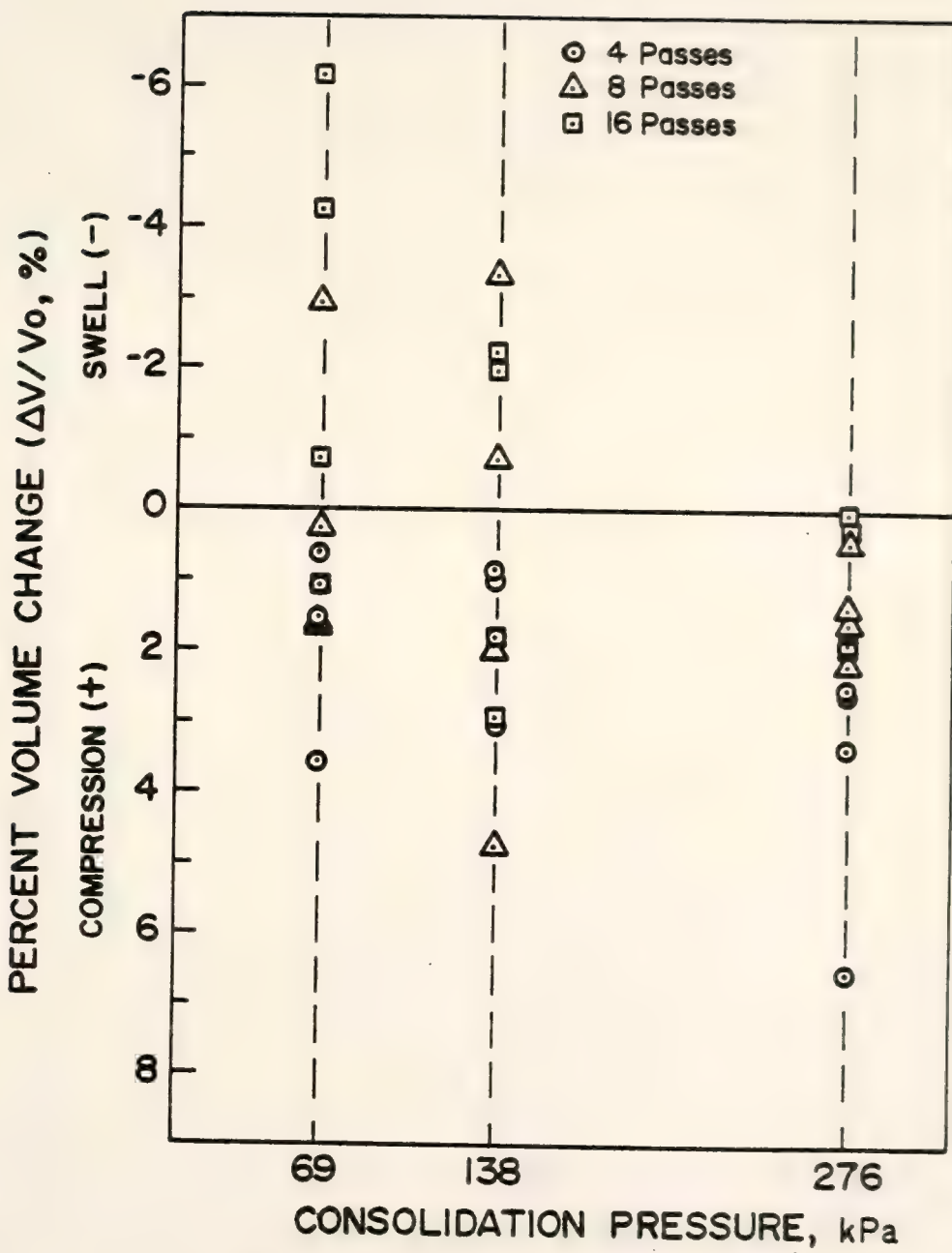


Figure 3-16 Caterpillar Percent Volume Change Upon Saturation and Consolidation Vs. Consolidation Pressure

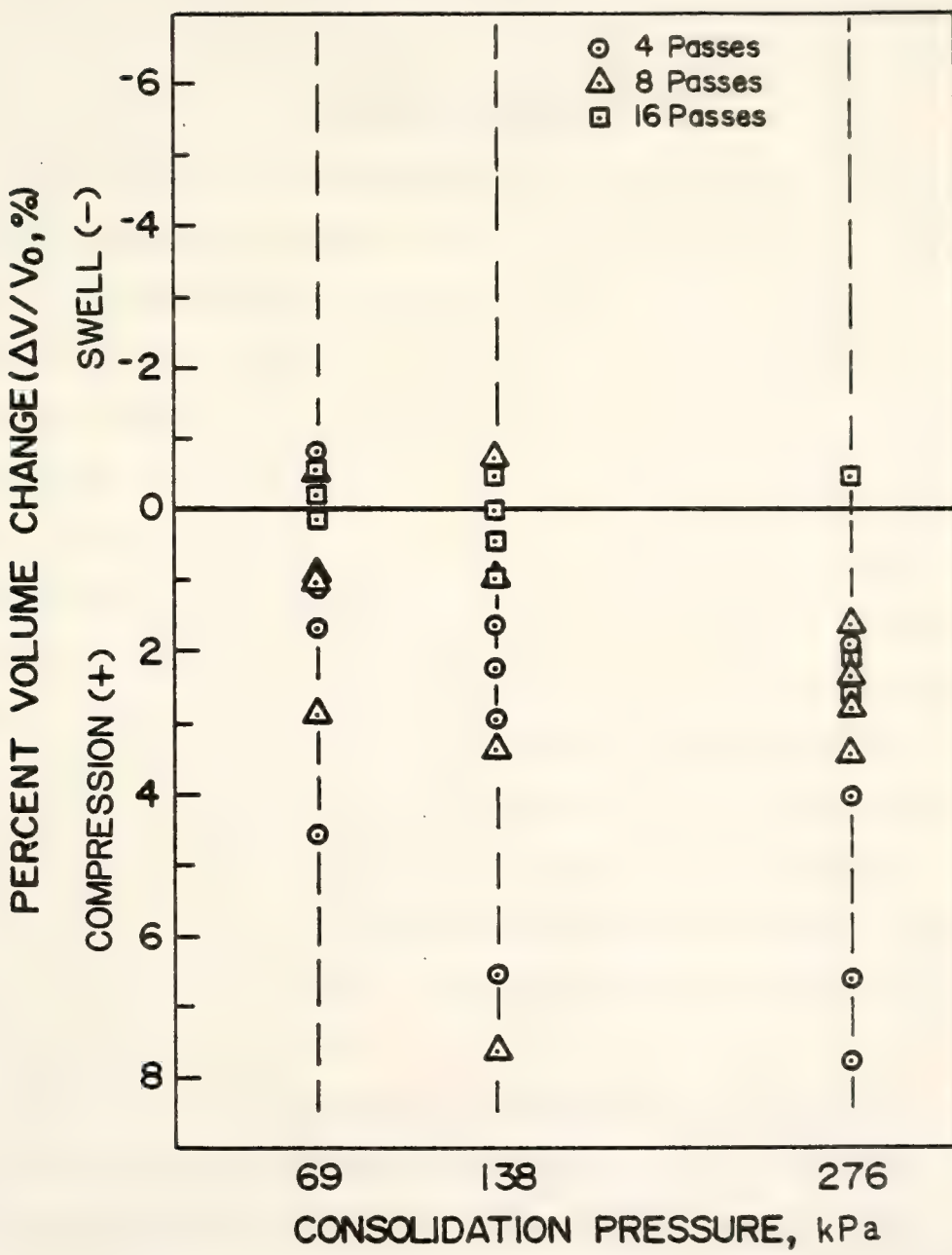


Figure 3-17 Rascal Percent Volume Change Upon Saturation and Consolidation Vs. Consolidation Pressure

have been subjected to a higher compactive pressure, they should have been subjected to a higher compactive prestress than the Rascal samples.

3-1-3.2 Stress-Strain and Pore Water Pressure Response

The typical strain versus stress and pore pressure curves for field compacted samples are shown in Figures 3-18, 19, 20. Figure 3-18 shows the stress-strain curves for high confining pressure (276 kPa) compacted dry and wet of optimum. These curves are classified as either Type I or Type II, in the system of Casagrande and Hirschfeld (1962). All further discussion of "types" of stress-strain curves will be after this system. Type I and Type II curves are well-rounded, with the possible exception of an initial straight line section which terminates before half the maximum shear stress is attained. Figure 3-19 and 3-20 show the curves for samples with low confining pressure (69 kPa) compacted dry and wet of optimum. Compaction dry of optimum produced a Type III stress-strain curve, while compaction wet of optimum produced a Type V curve. Seed and Chan (1959) found similar results. The remainder of the strain versus stress and pore water pressure curves are shown in Figures B1 to B36.

Table 3-10 shows the failure conditions for all CIU tests. It can be seen that the pore pressure and deviator stress at failure increase with increasing final void ratio. Henkel (1956), Bjerrum (1960), and Simons (1960) showed that the magnitude of the A_f value is a function of OCR. The stress versus strain and pore pressure curves for samples C4B6 and C5C7 are shown in Figure 3-21. These two samples have almost the same initial water content, initial dry density, and confinement, but different compactive energy levels. The figure shows that the

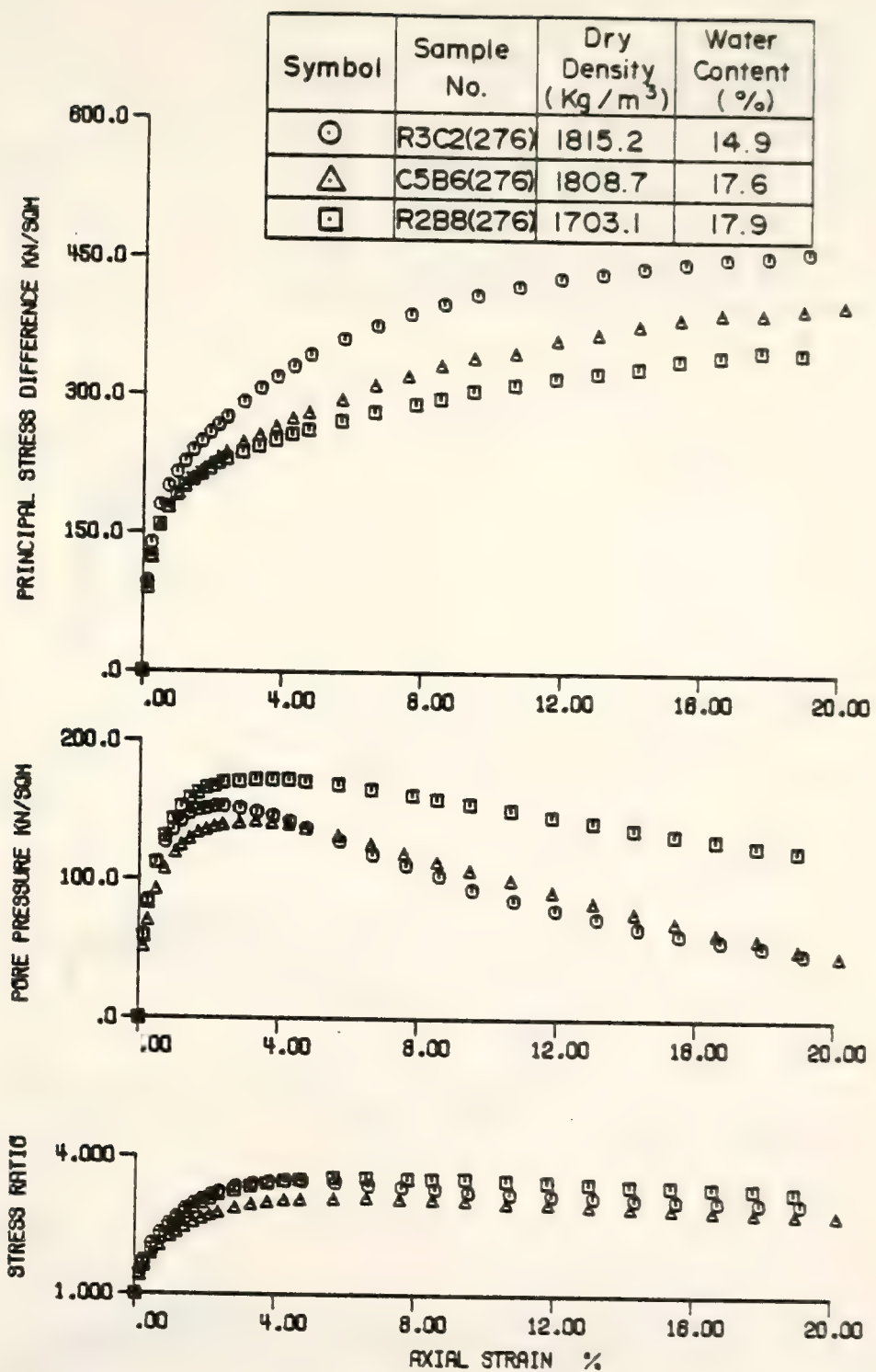


Figure 3-18 CIU Results for Samples R3C2, C5B6, and R2B8

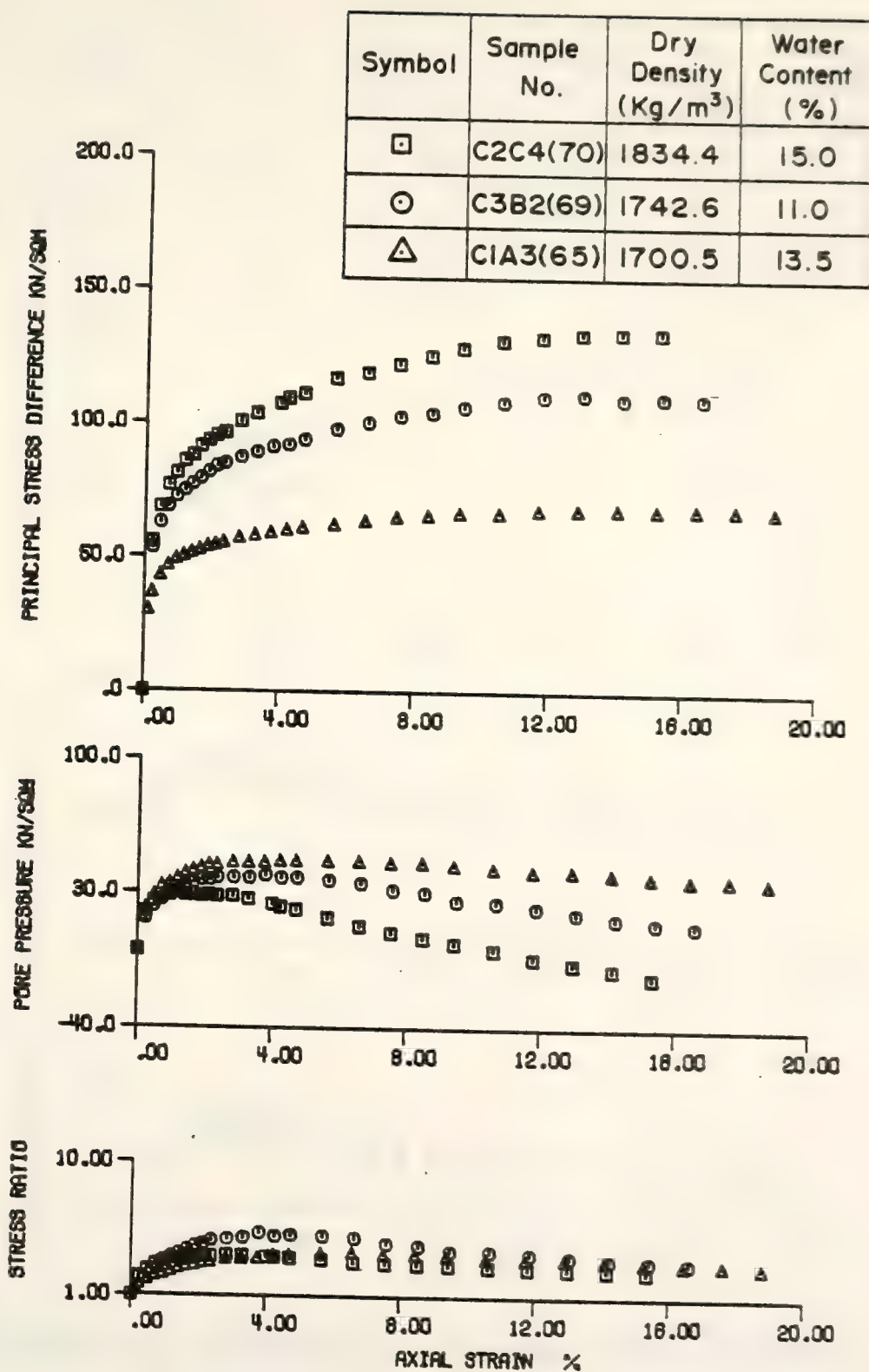


Figure 3-19 CIU Results for Samples C2C4, C3B2, and CIA3

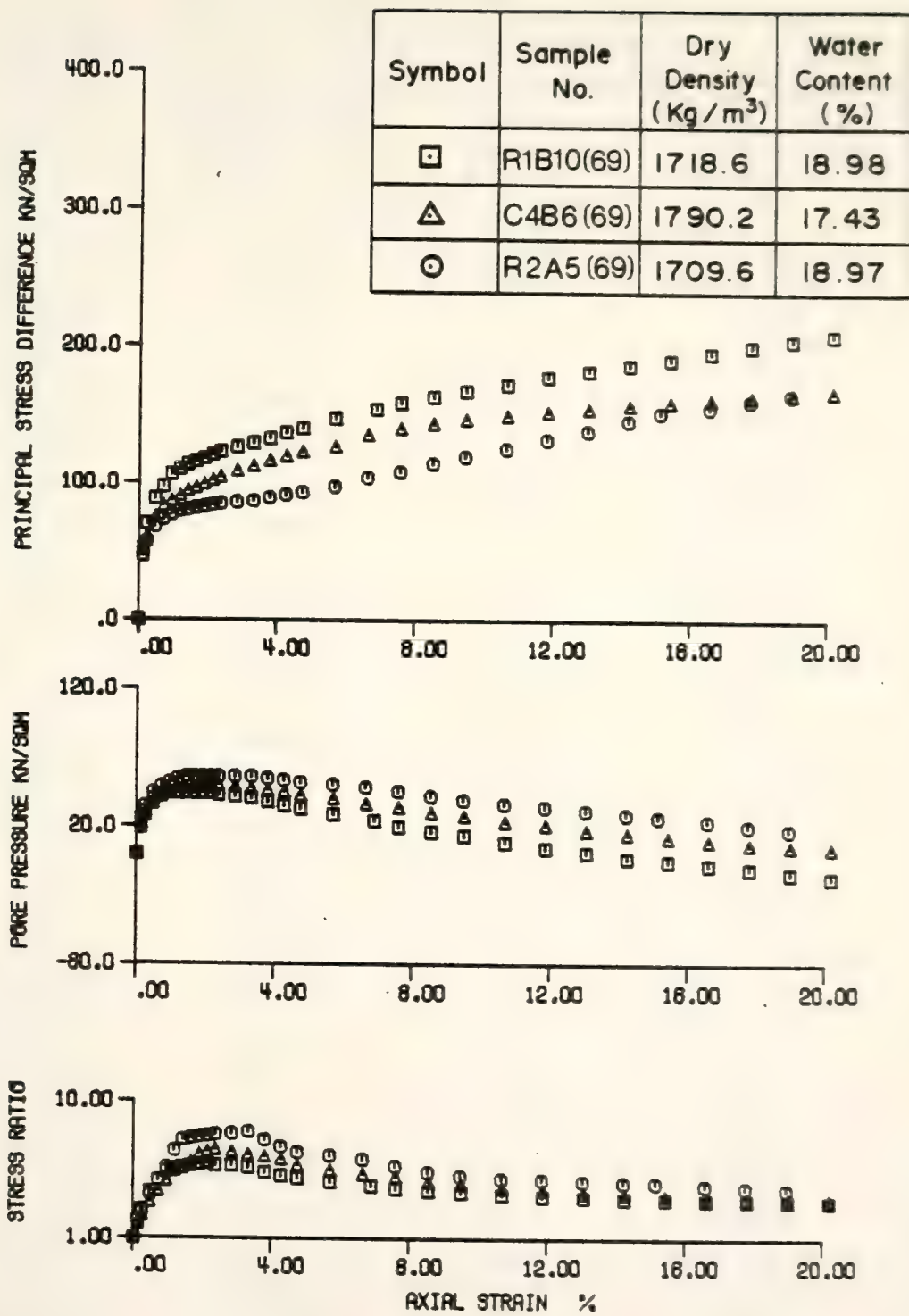


Figure 3-20 CIU Results for Samples R2A5, R1B10, and C4B6

TABLE 3-10 Failure Conditions for Consolidated Undrained Triaxial Tests

Sample No.	Principal Stress Difference at Failure $(\sigma_1 - \sigma_3)_f$ (kPa)	Pore Pressure Change at Failure Δu_f (kPa)	Skempton's A Parameter at Failure A_f	Failure Void Ratio e_f
C1A9(276)	263.0	131.1	0.498	0.550
C3A5(276)	329.7	114.5	0.347	0.478
C4A4(276)	354.4	118.7	0.335	0.542
C5A5(276)	280.2	109.0	0.389	0.530
C1B10(276)	490.2	1.4	0.003	0.474
C2B7(276)	709.3	- 52.4	-0.074	0.440
C4B9(276)	264.9	75.9	0.287	0.544
C5B6(276)	458.7	48.3	0.105	0.518
C1C9(276)	379.0	34.5	0.091	0.500
C2C3(276)	455.8	- 30.4	-0.067	0.494
C3C10(276)	295.1	90.4	0.306	0.525
C4C5(276)	228.4	129.7	0.568	0.538
C2A5(138)	208.6	27.6	0.132	0.526
C3A1(138)	235.5	27.6	0.117	0.510
C4A5(138)	221.6	46.2	0.209	0.495
C5A7(138)	330.6	- 10.4	-0.031	0.528
C1B8(138)	327.5	- 62.8	-0.192	0.525
C3B6(138)	305.7	6.9	0.023	0.480
C4B5(138)	231.4	29.7	0.128	0.507
C5B4(138)	269.6	8.3	0.031	0.546
C2C1(138)	172.8	45.5	0.264	0.597
C3C1(138)	236.3	- 19.3	-0.082	0.533
C4C7(138)	165.9	66.9	0.403	0.549
C5C8(138)	269.4	11.0	0.041	0.557
C1A3(65)	68.8	38.0	0.552	0.615
C2A1(55)	99.6	27.6	0.277	0.618
C3A6(63)	144.6	13.8	0.085	0.547
C4A9(69)	161.5	68.3	0.423	0.585

TABLE 3-10 (Continued)

Sample No.	Principal Stress Difference at Failure $(\sigma_1 - \sigma_3)_f$ (kPa)	Pore Pressure Change at Failure Δu_f (kPa)	Skempton's A Parameter at Failure A_f	Failure Void Ratio e_f
C2B5(69)	246.3	- 56.6	-0.23	0.513
C3B2(69)	111.1	20.0	0.18	0.574
C4B6(69)	167.2	5.1	0.031	0.533
C5B8(83)	195.6	- 12.4	0.063	0.576
C2C4(70)	134.2	- 13.1	-0.098	0.614
C3C6(61)	115.2	2.8	0.024	0.622
C4C6(63)	128.7	31.7	0.247	0.607
C5C7(69)	161.9	- 34.2	-0.211	0.567
R1A3(276)	391.3	118.7	0.303	0.528
R2A7(276)	379.5	125.6	0.331	0.543
R3A5(276)	253.1	144.2	0.57	0.492
R5A6(276)	460.0	41.4	0.09	0.471
R2B8(276)	350.5	125.6	0.358	0.580
R3B8(276)	396.0	73.8	0.186	0.480
R4B1(276)	334.0	91.8	0.275	0.485
R5B6(276)	338.1	72.5	0.214	0.544
R1C3(276)	790.3	-111.1	-0.141	0.483
R1C10(276)	454.2	53.1	0.117	0.497
R3C2(276)	401.7	46.9	0.117	0.504
R5C3(276)	200.2	153.9	0.769	0.588
R2A1(138)	266.4	22.8	0.085	0.614
R3A3(138)	189.2	51.8	0.274	0.545
R4A6(138)	179.2	53.8	0.3	0.491
R5A7(138)	198.9	24.8	0.125	0.552
R2B3(138)	209.8	52.4	0.25	0.535
R3B7(138)	197.6	- 43.3	0.244	0.540
R4B9(138)	228.9	19.3	-0.084	0.582
R5B2(138)	158.1	69.7	0.441	0.590
R2C9(138)	527.1	- 60.0	-0.114	0.487

TABLE 3-10 (Continued)

Sample No.	Principal Stress Difference at Failure $(\sigma_1 - \sigma_3)_f$ (kPa)	Pore Pressure Change at Failure Δu_f (kPa)	Skempton's A Parameter at Failure A_f	Failure Void Ratio e_f
R3C9(138)	248.4	17.9	0.072	0.530
R4C1(138)	353.6	- 78.7	-0.222	0.500
R5C6(138)	298.6	- 23.5	-0.079	0.560
R1A4(69)	98.3	44.9	0.456	0.598
R2A5(69)	164.8	17.9	0.109	0.612
R3A2(83)	134.9	22.1	0.164	0.585
R5A8(60)	106.6	13.1	0.123	0.631
R1B10(69)	208.6	- 16.6	-0.079	0.608
R2B9(69)	253.4	- 19.3	-0.076	0.546
R3B3(66)	117.7	33.8	0.287	0.553
R5B4(69)	110.3	18.6	0.169	0.585
R2C3(69)	244.6	- 20.0	-0.082	0.526
R3C5(69)	153.5	5.5	0.036	0.542
R4C6(63)	165.3	- 4.8	-0.029	0.521
R5C4(112)	205.1	21.4	0.104	0.547

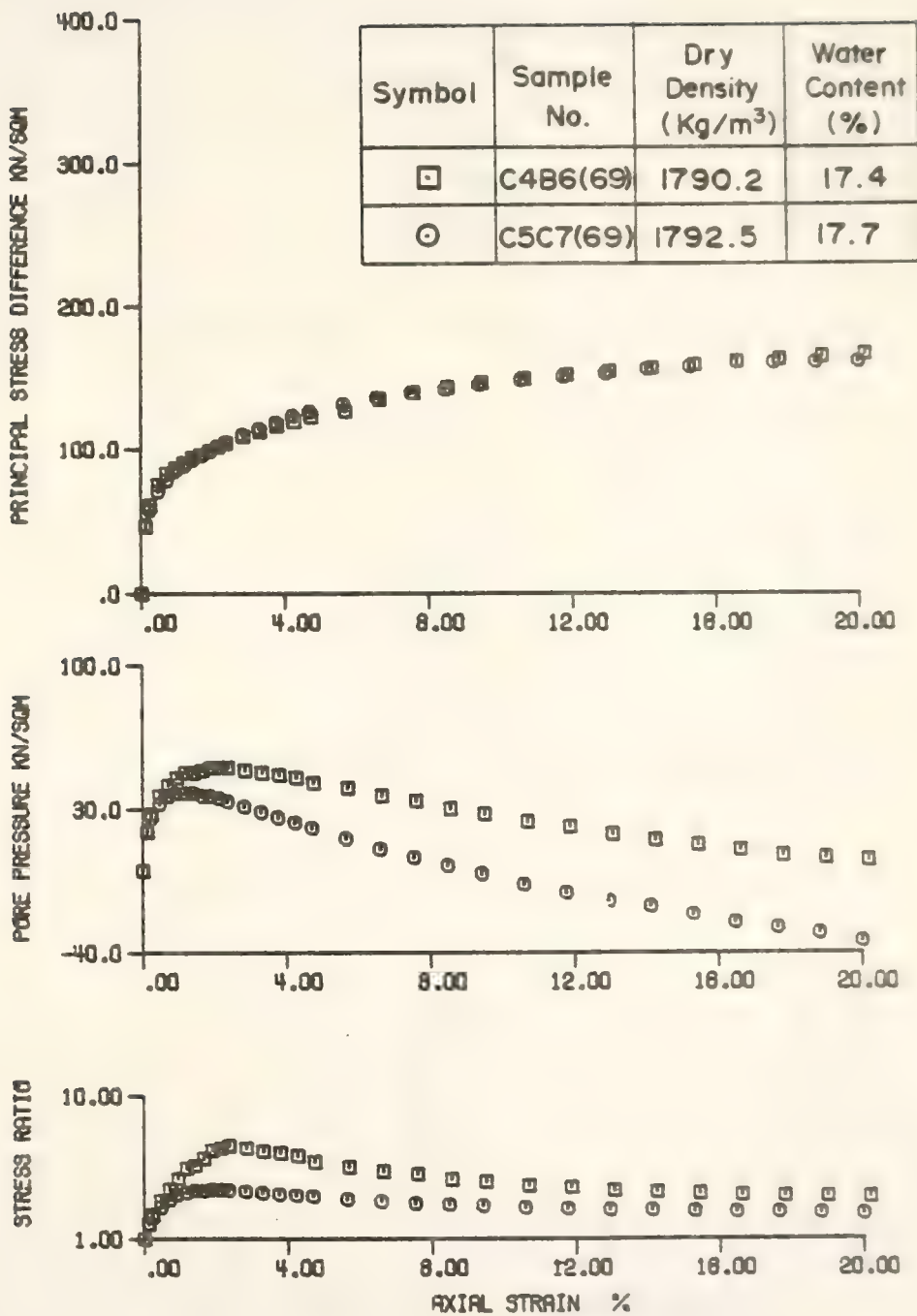


Figure 3-21 CIU Results for Sample C4B6 ,C5C7

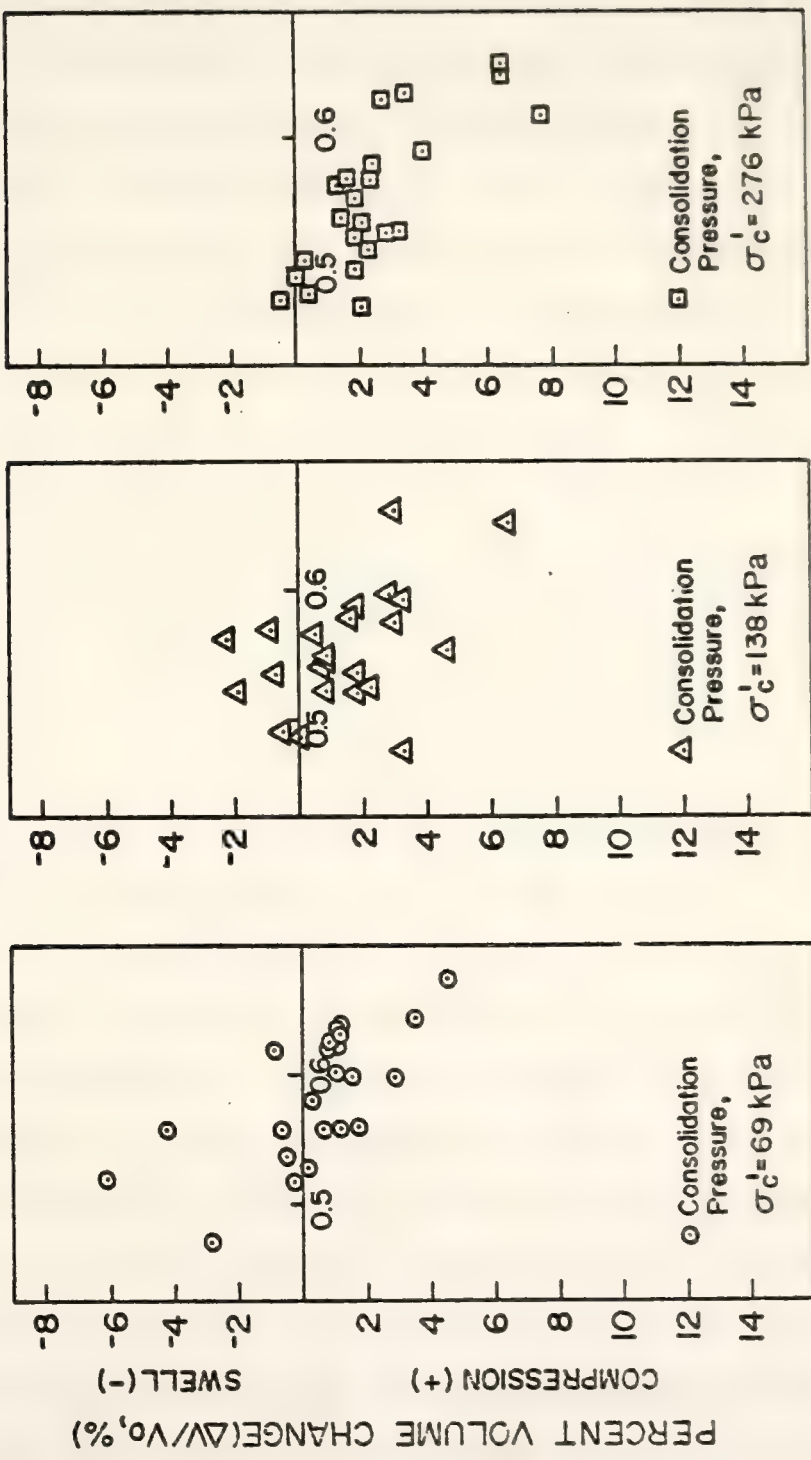


Figure 3-15 Percent Volume Change Upon Saturation Vs. Initial Void Ratio for All Samples

The relationships between the volume change due to saturation and consolidation and consolidation pressure are shown in Figures 3-16 and 3-17. It is observed that the samples with the higher energy level increase in volume (swell) under lower confining pressures, while most samples decrease in volume (settle) under higher consolidation pressures. Apparently in the former case the swelling pressure from the hydrating clay minerals, in conjunction with the reduced effective stress due to saturation, exceeded the confining pressure and resulted in a volume increase. If the confining pressures were sufficient to overcome the swelling tendency, volume reduction occurred.

Compaction moisture content also affects percent volume change due to saturation and consolidation, but trends are difficult to isolate. Holtz and Gibbs (1956) reported for swell tests on compacted clays that increasing the compaction moisture content for a given dry density resulted in decreased percent swell. For this study, most of the samples compacted dry of optimum exhibit percent volume changes more than (less net swell or more net compression) the samples compacted wet of optimum.

The compactive prestress also affects the volume change upon saturation and consolidation. The compactive prestress is a function of compactive pressure. The higher compactive prestress should produce a decrease in initial void ratio. Lin (1981) showed that for a given confining stress, the volume change on wetting decreases with decreasing initial void ratio (more net swell or less net compression). Examination of Figures 3-16 and 3-17 show that percent volume change upon saturation and consolidation are less (more net swell or less net compression) for the Caterpillar than for the Rascal roller at the same confining pressure. Since the Caterpillar roller samples

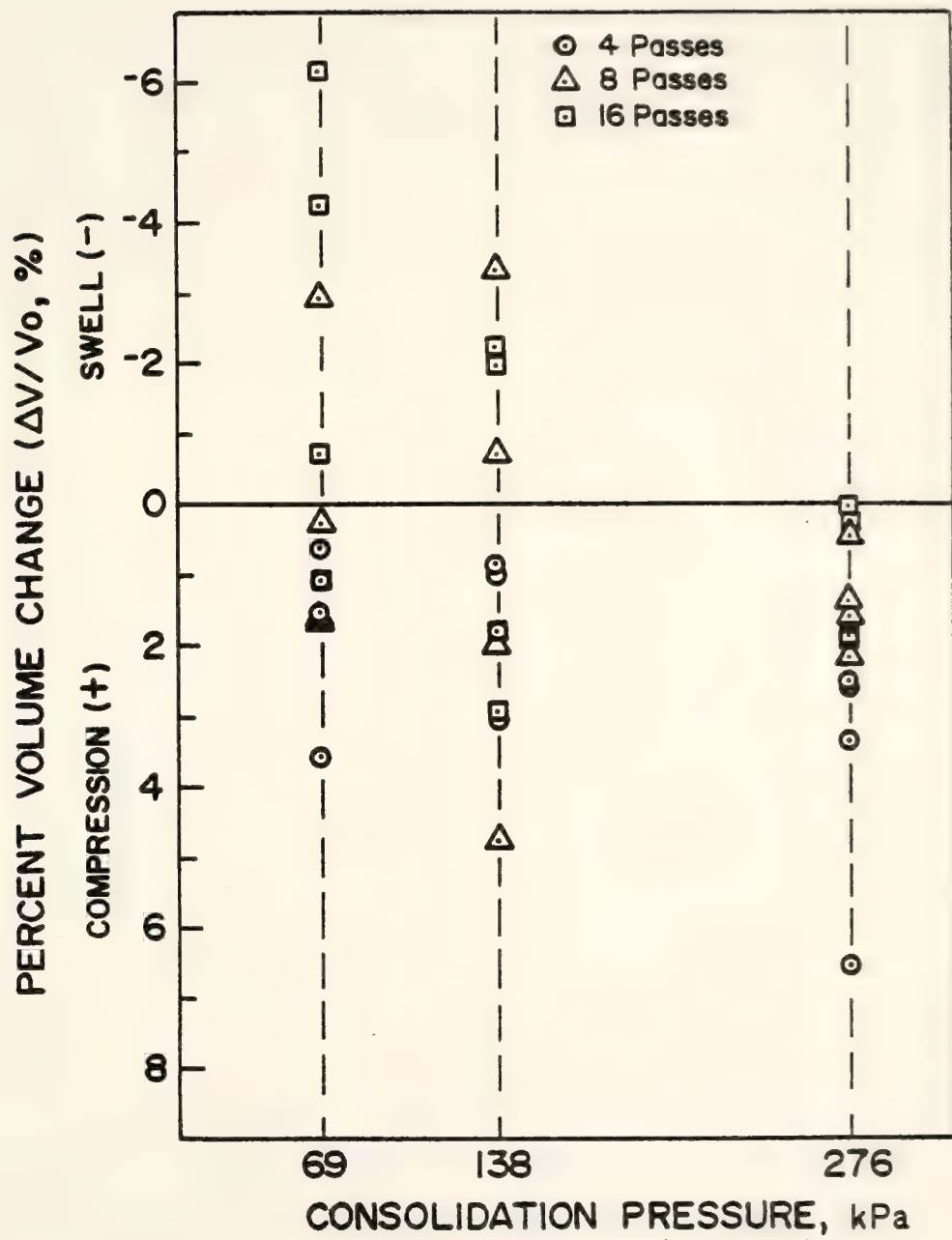


Figure 3-16 Caterpillar Percent Volume Change Upon Saturation and Consolidation Vs. Consolidation Pressure

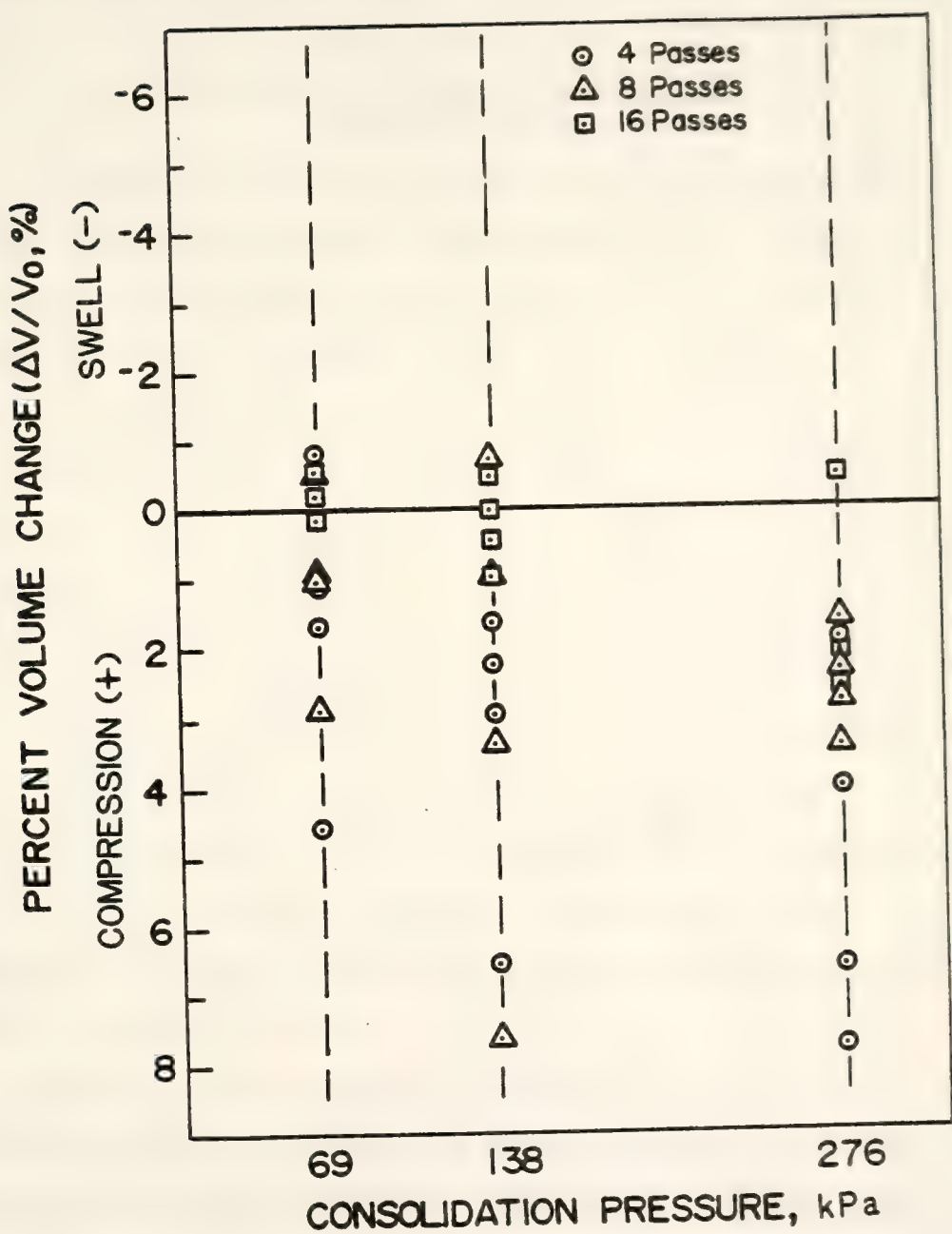


Figure 3-17 Rascal Percent Volume Change Upon Saturation and Consolidation Vs. Consolidation Pressure

have been subjected to a higher compactive pressure, they should have been subjected to a higher compactive prestress than the Rascal samples.

3-1-3.2 Stress-Strain and Pore Water Pressure Response

The typical strain versus stress and pore pressure curves for field compacted samples are shown in Figures 3-18, 19, 20. Figure 3-18 shows the stress-strain curves for high confining pressure (276 kPa) compacted dry and wet of optimum. These curves are classified as either Type I or Type II, in the system of Casagrande and Hirschfeld (1962). All further discussion of "types" of stress-strain curves will be after this system. Type I and Type II curves are well-rounded, with the possible exception of an initial straight line section which terminates before half the maximum shear stress is attained. Figure 3-19 and 3-20 show the curves for samples with low confining pressure (69 kPa) compacted dry and wet of optimum. Compaction dry of optimum produced a Type III stress-strain curve, while compaction wet of optimum produced a Type V curve. Seed and Chan (1959) found similar results. The remainder of the strain versus stress and pore water pressure curves are shown in Figures B1 to B36.

Table 3-10 shows the failure conditions for all CIU tests. It can be seen that the pore pressure and deviator stress at failure increase with increasing final void ratio. Henkel (1956), Bjerrum (1960), and Simons (1960) showed that the magnitude of the A_f value is a function of OCR. The stress versus strain and pore pressure curves for samples C4B6 and C5C7 are shown in Figure 3-21. These two samples have almost the same initial water content, initial dry density, and confinement, but different compactive energy levels. The figure shows that the

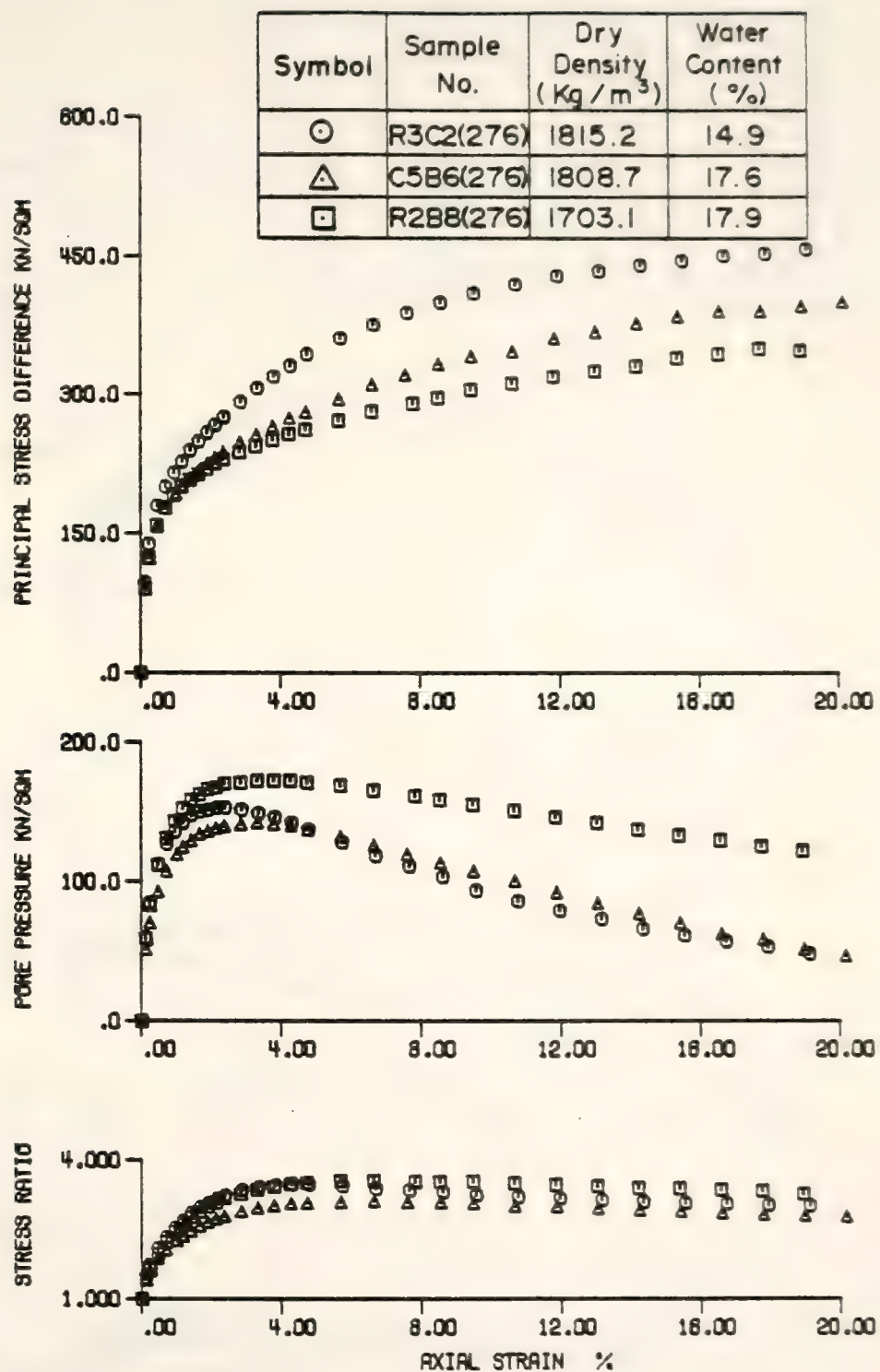


Figure 3-18 CIU Results for Samples R3C2, C5B6, and R2B8

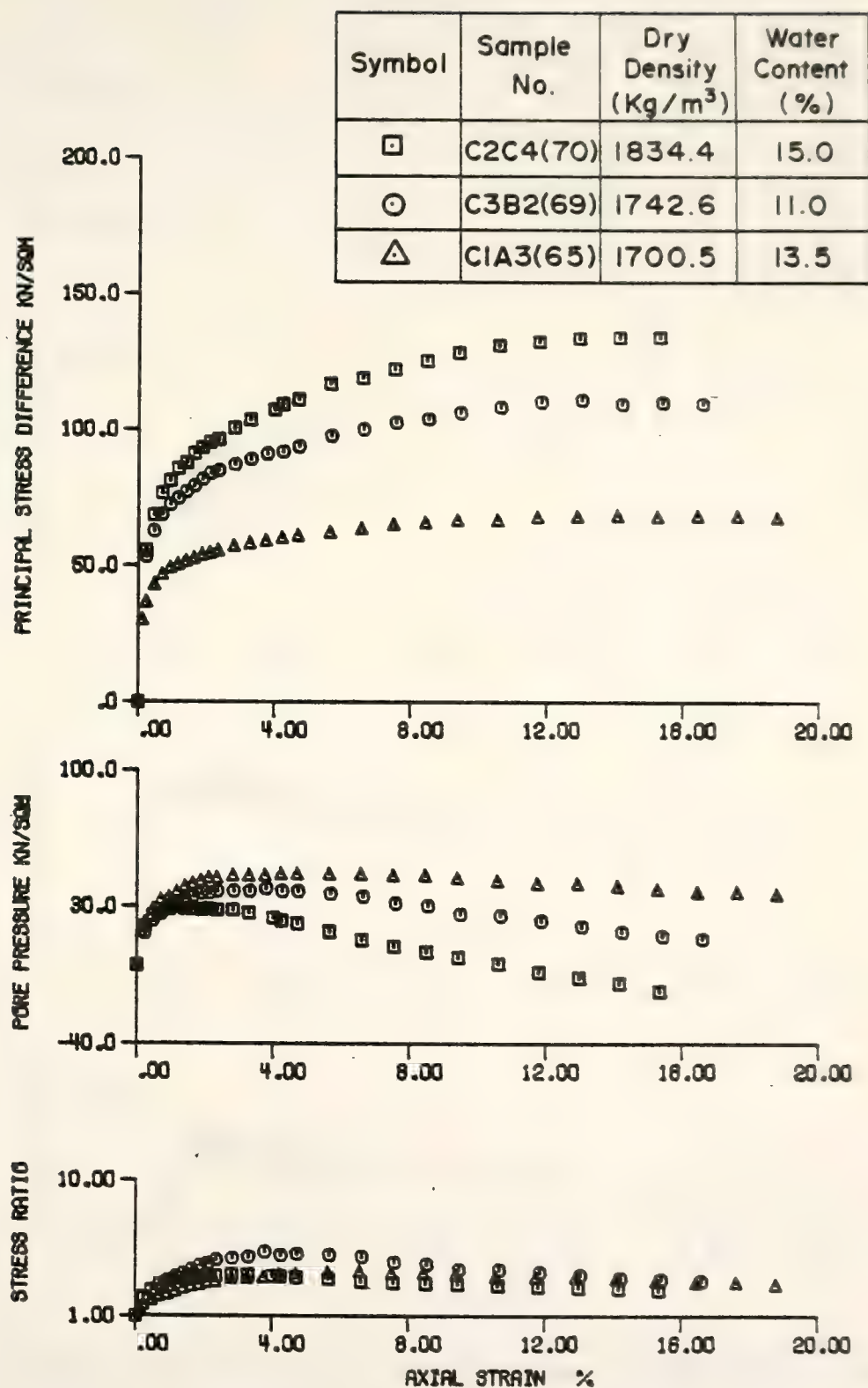


Figure 3-19 CIU Results for Samples C2C4, C3B2, and CIA3

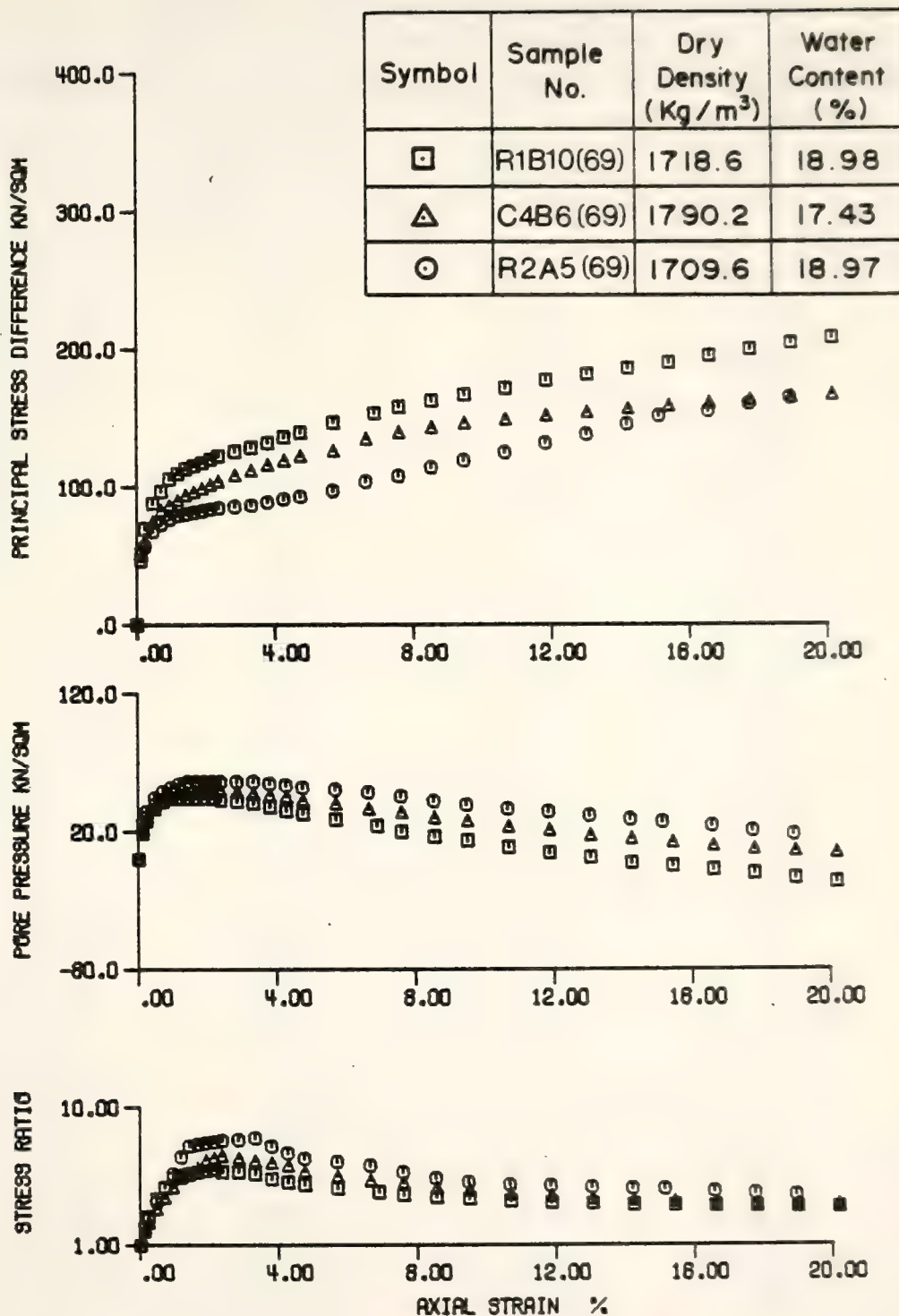


Figure 3-20 CIU Results for Samples R2A5, R1B10, and C4B6

TABLE 3-10 Failure Conditions for Consolidated
Undrained Triaxial Tests

Sample No.	Principal Stress Difference at Failure $(\sigma_1 - \sigma_3)_f$ (kPa)	Pore Pressure Change at Failure Δu_f (kPa)	Skempton's A Parameter at Failure A_f	Failure Void Ratio e_f
C1A9(276)	263.0	131.1	0.498	0.550
C3A5(276)	329.7	114.5	0.347	0.478
C4A4(276)	354.4	118.7	0.335	0.542
C5A5(276)	280.2	109.0	0.389	0.530
C1B10(276)	490.2	1.4	0.003	0.474
C2B7(276)	709.3	- 52.4	-0.074	0.440
C4B9(276)	264.9	75.9	0.287	0.544
C5B6(276)	458.7	48.3	0.105	0.518
C1C9(276)	379.0	34.5	0.091	0.500
C2C3(276)	455.8	- 30.4	-0.067	0.494
C3C10(276)	295.1	90.4	0.306	0.525
C4C5(276)	228.4	129.7	0.568	0.538
C2A5(138)	208.6	27.6	0.132	0.526
C3A1(138)	235.5	27.6	0.117	0.510
C4A5(138)	221.6	46.2	0.209	0.495
C5A7(138)	330.6	- 10.4	-0.031	0.528
C1B8(138)	327.5	- 62.8	-0.192	0.525
C3B6(138)	305.7	6.9	0.023	0.480
C4B5(138)	231.4	29.7	0.128	0.507
C5B4(138)	269.6	8.3	0.031	0.546
C2C1(138)	172.8	45.5	0.264	0.597
C3C1(138)	236.3	- 19.3	-0.082	0.533
C4C7(138)	165.9	66.9	0.403	0.549
C5C8(138)	269.4	11.0	0.041	0.557
C1A3(65)	68.8	38.0	0.552	0.615
C2A1(55)	99.6	27.6	0.277	0.618
C3A6(63)	144.6	13.8	0.085	0.547
C4A9(69)	161.5	68.3	0.423	0.585

TABLE 3-10 (Continued)

Sample No.	Principal Stress Difference at Failure $(\sigma_1 - \sigma_3)_f$ (kPa)	Pore Pressure Change at Failure Δu_f (kPa)	Skempton's A Parameter at Failure A_f	Failure Void Ratio e_f
C2B5(69)	246.3	- 56.6	-0.23	0.513
C3B2(69)	111.1	20.0	0.18	0.574
C4B6(69)	167.2	5.1	0.031	0.533
C5B8(83)	195.6	- 12.4	0.063	0.576
C2C4(70)	134.2	- 13.1	-0.098	0.614
C3C6(61)	115.2	2.8	0.024	0.622
C4C6(63)	128.7	31.7	0.247	0.607
C5C7(69)	161.9	- 34.2	-0.211	0.567
R1A3(276)	391.3	118.7	0.303	0.528
R2A7(276)	379.5	125.6	0.331	0.543
R3A5(276)	253.1	144.2	0.57	0.492
R5A6(276)	460.0	41.4	0.09	0.471
R2B8(276)	350.5	125.6	0.358	0.580
R3B8(276)	396.0	73.8	0.186	0.480
R4B1(276)	334.0	91.8	0.275	0.485
R5B6(276)	338.1	72.5	0.214	0.544
R1C3(276)	790.3	-111.1	-0.141	0.483
R1C10(276)	454.2	53.1	0.117	0.497
R3C2(276)	401.7	46.9	0.117	0.504
R5C3(276)	200.2	153.9	0.769	0.588
R2A1(138)	266.4	22.8	0.085	0.614
R3A3(138)	189.2	51.8	0.274	0.545
R4A6(138)	179.2	53.8	0.3	0.491
R5A7(138)	198.9	24.8	0.125	0.552
R2B3(138)	209.8	52.4	0.25	0.535
R3B7(138)	197.6	- 43.3	0.244	0.540
R4B9(138)	228.9	19.3	-0.084	0.582
R5B2(138)	158.1	69.7	0.441	0.590
R2C9(138)	527.1	- 60.0	-0.114	0.487

TABLE 3-10 (Continued)

Sample No.	Principal Stress Difference at Failure $(\sigma_1 - \sigma_3)_f$ (kPa)	Pore Pressure Change at Failure Δu_f (kPa)	Skempton's A Parameter at Failure A_f	Failure Void Ratio e_f
R3C9(138)	248.4	17.9	0.072	0.530
R4C1(138)	353.6	- 78.7	-0.222	0.500
R5C6(138)	298.6	- 23.5	-0.079	0.560
R1A4(69)	98.3	44.9	0.456	0.598
R2A5(69)	164.8	17.9	0.109	0.612
R3A2(83)	134.9	22.1	0.164	0.585
R5A8(60)	106.6	13.1	0.123	0.631
R1B10(69)	208.6	- 16.6	-0.079	0.608
R2B9(69)	253.4	- 19.3	-0.076	0.546
R3B3(66)	117.7	33.8	0.287	0.553
R5B4(69)	110.3	18.6	0.169	0.585
R2C3(69)	244.6	- 20.0	-0.082	0.526
R3C5(69)	153.5	5.5	0.036	0.542
R4C6(63)	165.3	- 4.8	-0.029	0.521
R5C4(112)	205.1	21.4	0.104	0.547

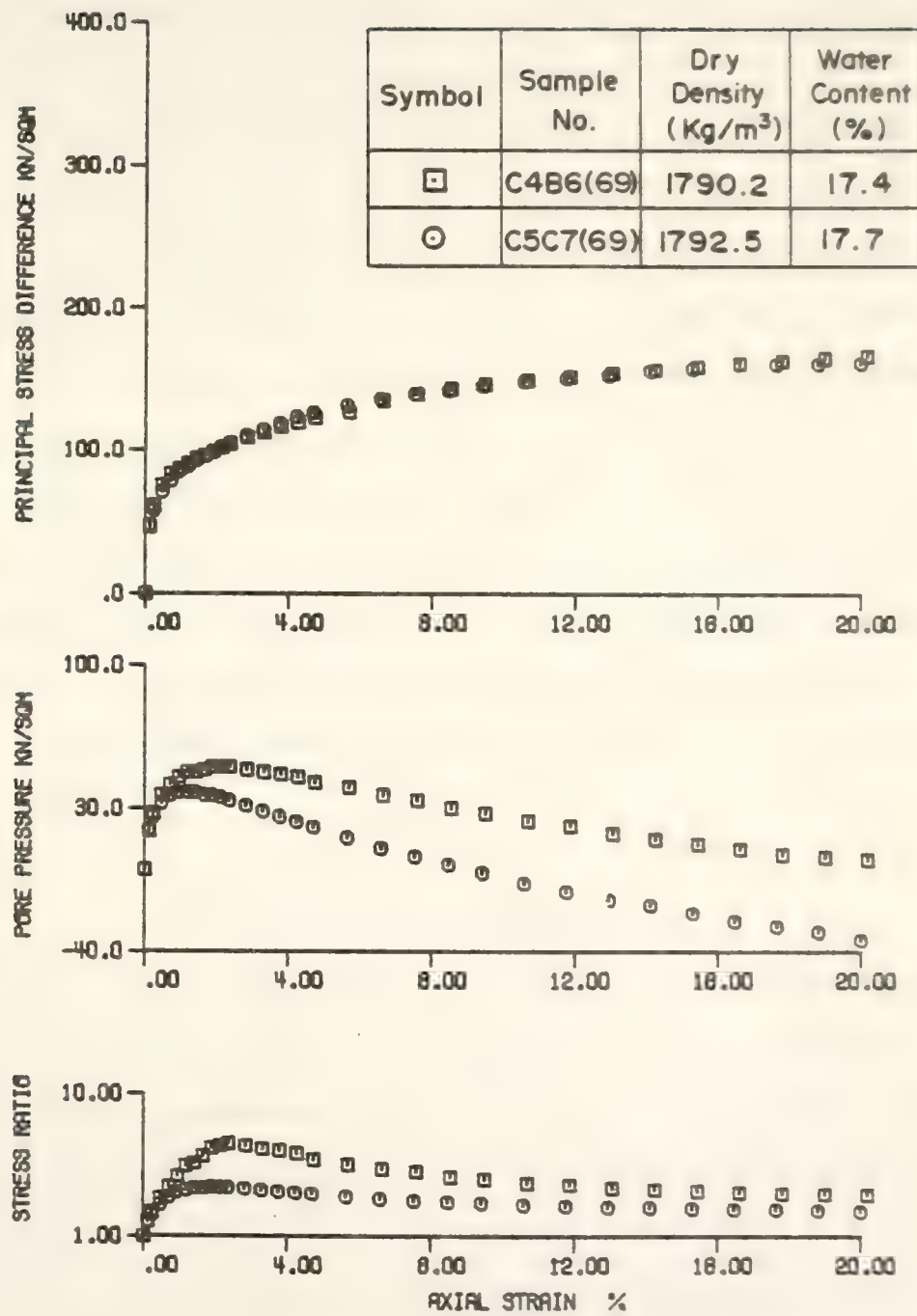


Figure 3-21 CIU Results for Sample C4B6 ,C5C7

deviator stress of both samples are almost identical but the pore pressures are different. Because the higher energy should produce a higher compacted prestress and a higher OCR ($\frac{P_s}{q_c}$), the pore pressures should be smaller, and this is the case.

Figures 3-22 and 3-23 show Caterpillar and Rascal A_f values versus consolidation pressures. The expected trend of a decrease in consolidation pressure with decreasing A_f is not evident for the low consolidation pressure (69 kPa). Johnson (1979) reported that A_f values were not only a function of consolidation pressure, but also a function of dry density and initial degree of saturation.

Since the initial compacted conditions of the samples in this study are so different, trends in the deviator stress and pore pressure are very difficult to determine. The effective stress strength parameters, c' and ϕ' , also cannot be directly obtained from the test data. Therefore, statistical regression analysis is applied to solve these difficulties.

3-2 Statistical Analysis

Regression analysis has become one of the most widely used statistical tools for interpreting multifactor data. It is appealing because it provides a conceptually simple method for investigating functional relationships among variables. The mathematical model used for the response variables in this study is given below:

$$Y_i = \beta_0 + \beta_1 X_1 + \beta_2 X_2 + \dots + \beta_{p-1} X_{p-1} + \epsilon \quad (3-3)$$

where

Y_i = the value of the dependent variable at the i th trial

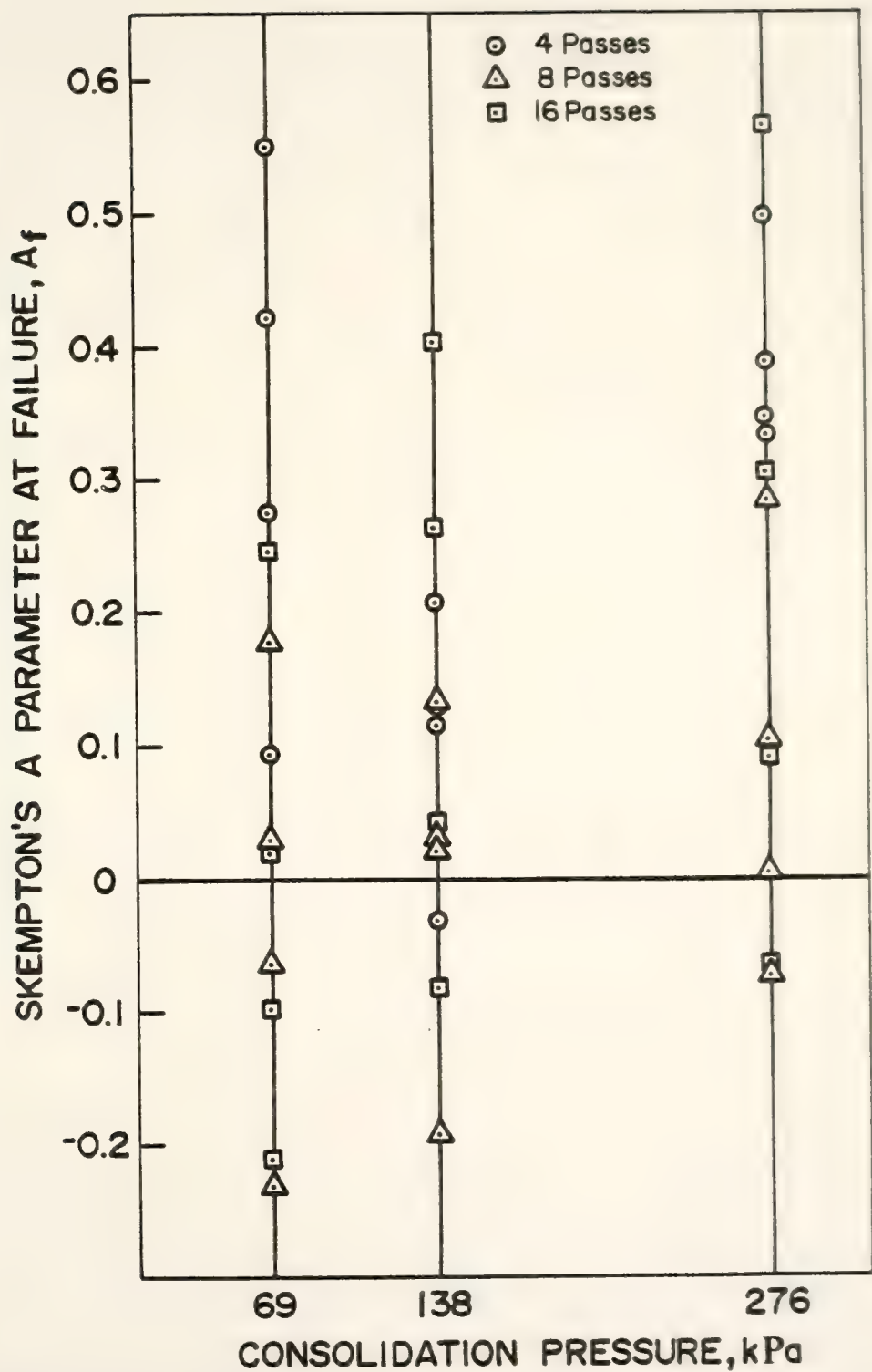


Figure 3-22 Caterpillar A_f Vs. Consolidation Pressure

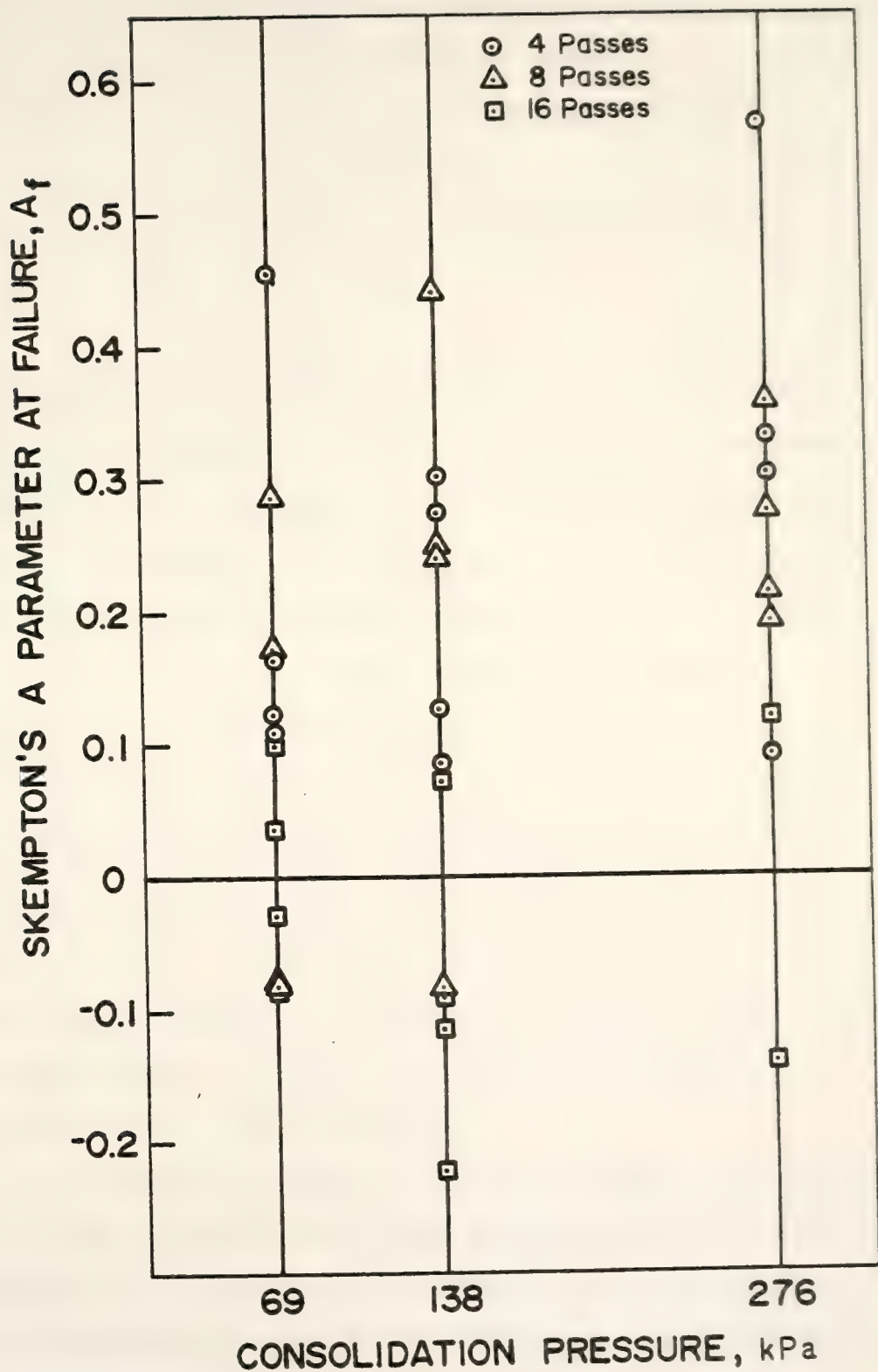


Figure 3-23 Rascal A_f Vs. Consolidation Pressure

β_i = regression parameters that factor
the independent variables

X_i = value of the independent variable
of the ith trial

ϵ_i = random error term with expected value,

$$E(\epsilon_i) = 0$$

$$i = 1, n$$

In general, the least-squares method chooses as the best-fitting model the one which minimizes the sum of squares of the distance between the observed response and those predicted by the fitted model. The better the fit, the smaller will be the deviations of observed from predicted values. The resulting estimated response function can be written as

$$\hat{Y}_i = \hat{\beta}_0 + \hat{\beta}_1 X_1 + \hat{\beta}_2 X_2 + \dots + \hat{\beta}_{p-1} X_{p-1} \quad (3-4)$$

where

\hat{Y}_i = the estimated mean response of Y_i

$1 - \hat{\beta}_0, \hat{\beta}_1, \dots, \hat{\beta}_{p-1}$ = least-squares estimates

Linear regression analysis is a very flexible tool, as variables which correlate nonlinearly can be mathematically transformed to show more linear behavior. Products ($X_1 X_2$), inverses ($1/X$), polynomials (X^n) and logarithms ($\log X$) are the transformations most commonly employed. A major problem is to decide which of these variables, or combinations thereof should be used in the study.

The Statistical Package for the Social Sciences (SPSS, Nie et al., 1975), part of the software library at Purdue University, provided the programs which were utilized in the linear regression analyses. Relevant discussions regarding multiple regression can be found in Neter and Wasserman (1974).

The desired independent variables were first plotted, using the

SPSS routine SCATTERGRAM, versus the dependent variable, and provided quantitative indications of the degree of correlation. The independent variables chosen for future study were those which indicated high linearity during the SCATTERGRAM investigation. Next, the STEPWISE option of the REGRESSION routine was utilized to form multiple linear regression equations from a selected subset of the independent variables. STEPWISE is a SPSS search procedure which progressively adds or removes independent variables during construction of an equation. A variable that entered at an early stage of the correlation may become superfluous at a later stage. To check this possibility, a partial F test for each variable presently in the model is made at each step. The variable is treated as though it were the most recent variable entered, irrespective of its actual entry point into the model. That variable with the smallest nonsignificant partial F statistic is removed. The model is refitted with the remaining variables, the partial F's are obtained and similarly examined, and so on. The whole process continues until no more variables can be entered or removed.

The criteria for selection of a satisfactory multiple regression equation are as follows:

- (1) The coefficient of multiple determination (R^2) must be greater than 0.60.
- (2) The adjusted coefficient of multiple determination (R_a^2) must increase with each additional independent variable entered into the model.
- (3) The overall F-test at the $\alpha = 0.05$ significance level must be satisfied.
- (4) The confidence interval for each $\hat{\beta}_i$ coefficient tested at $\alpha = 0.05$ level must be small and not include zero.

(5) The residuals must be normally distributed random variables.

In this study, if more than one equation satisfied all the above criteria, the final selection was based on the highest values of R^2 and the fewest independent variables.

3-2-1 Density Prediction Models

Table 3-11 lists the basic independent variables used to generate a prediction model for density. It was found that the dry densities wet-of-optimum for both laboratory compacted soil and field compacted soil are independent of compactive effort. Weitzel (1979) developed a prediction model for the wet-of-optimum dry density as below:

$$\hat{\rho}_d = 961.8 + 15564.6/w \quad (3-5)$$

where $\hat{\rho}_d$ = predicted dry density, kg/m^3
 w = water content, %

The prediction model developed for dry density wet-of-optimum of field compacted soil is:

$$\hat{\rho}_d = 1273.05 + 8797.21/w \quad (3-6)$$

The pertinent statistical data for both prediction models are presented in Table 3-12. The coefficients of determination (R^2) for the models are 0.99 and 0.88, respectively.

On the dry side of optimum, the dry density depends very much on compactive effort, as well as moisture content. The dry density regression models dry-of-optimum for field compacted soil and for laboratory compacted soil based on the Weitzel (1979) data are given below:

(a) Laboratory dry density prediction model

TABLE 3-11 Basic Compaction Variables
for Dry Density

Test Pad	No. of Passes	Mean Moisture Content w(%)	Mean Dry Density ρ_d (kg/m ³)	Compactor Foot Pressure P _c (kPa)
R1A	4	14.07	1740.0	780
R2A	4	15.48	1755.3	780
R3A	4	14.91	1754.0	780
R4A	4	17.36	1782.1	780
R5A	4	18.48	1756.7	780
R1B	8	15.27	1773.6	1038
R2B	8	14.77	1810.6	1038
R3B	8	14.31	1806.7	1038
R4B	8	17.03	1789.0	1038
R5B	8	18.12	1736.9	1038
R1C	16	14.18	1835.4	1525
R2C	16	14.07	1839.9	1525
R3C	16	15.4	1803.4	1525
R4C	16	16.38	1816.8	1525
R5C	16	19.18	1740.4	1525
C1A	4	14.54	1771.2	797
C2A	4	15.47	1762.5	797
C3A	4	14.68	1784.3	797
C4A	4	18.51	1745.1	797
C5A	4	17.56	1768.6	797
C1B	8	13.48	1860.1	1204
C2B	8	14.62	1847.3	1204
C3B	8	14.06	1773.7	1204
C4B	8	16.7	1795.2	1204
C5B	8	17.27	1782.9	1204
C1C	16	13.05	1877.4	1771
C2C	16	14.35	1824.7	1771
C3C	16	15.04	1815.5	1771
C4C	16	17.51	1783.8	1771
C5C	16	1757	1791.3	1771

TABLE 3-12 Statistical Data for Density Prediction Models

Wet-of-Optimum Dry Density Models

Statistical Criteria	Laboratory	Field
	$\hat{\rho}_d = 961.8 + 15564.6/w$	$\hat{\rho}_d = 1273.05 + 8797.21/w$
R^2	0.99	0.88
R_a^2	0.99	0.86
Overall F-Test	9779.02	71.19
<u>95% Confidence Interval for Regression Coefficient</u>		
1/w	15236.23, 15892.87	6474.12, 11120.29

All Moisture Dry Density Models

	$\hat{\rho}_d = 1566.38 + 62.45 \sqrt{P_c/w}$ + 0.00214 $\sqrt{P_c} \cdot w^2$ + 0.0031 $w \cdot P_c$ - 2617.4/w	$\rho_d = 1929.68 +$ 211.6 $\sqrt{P_c/w}$ + 0.0016 $\sqrt{P_c} \cdot w^2$ - 0.0096 $w \cdot P_c$ - 6816.83/w
R^2	0.93	0.74
R_a^2	0.92	0.70
Overall F-Test	240.98	17.63
<u>95% Confidence Intervals for Regression Coefficients</u>		
$\sqrt{P_c/w}$	8.39, 116.5	89.16, 334.04
$\sqrt{P_c} \cdot w^2$	-0.011, 0.015	-0.035, 0.038
$w \cdot P_c$	-0.00031, 0.0065	-0.023, 0.0036
1/w	1217.34, 1915.42	-14567.16, 933.49

$$\hat{\rho}_d = 1566.8 + 62.45\sqrt{P_c/w} + 0.00214\sqrt{P_c} \cdot w^2 + 0.0031w \cdot P_c - 2617.4/w \quad (3-7)$$

(b) Field dry density prediction model

$$\hat{\rho}_d = 1929.68 + 211.6\sqrt{P_c/w} + 0.00016\sqrt{P_c} \cdot w^2 - 0.0096w \cdot P_c - 6816.83/w \quad (3-8)$$

The statistical criteria for dry density models are presented in Table 3-12. The range of the field dry density model is shown by the joint region of observations in Figure 3-24. The moisture limits of application of Equations 3-5 and 3-6 are in the range of 19 to 27% and 16 to 20%, respectively.

Figure 3-25 shows the prediction models for the wet-of-optimum dry density for both laboratory and field compacted clay. The trends of the two curves are similar, but the ranges of water content are different. Figure 3-26 shows all moisture-dry density models for laboratory and field compacted St. Croix clay. The field dry-of-optimum dry density prediction model has different trends compared to the laboratory curves. However, the field model is based upon very little data. The moisture limits of application of Equation 3-7 and 3-8 are in the range of 14% to 25% and 12% to 18%, respectively.

3-2-2 As-Compacted Strength Prediction Model

Table 3-13 lists the basic independent variables utilized in the analysis of as-compacted strength (q_c). These basic variables were transformed through the use of square roots, squares, inverses, products and divisions.

Equations (3-9) and (3-10) are the most satisfactory relationships available for the field compacted soil and laboratory compacted soil

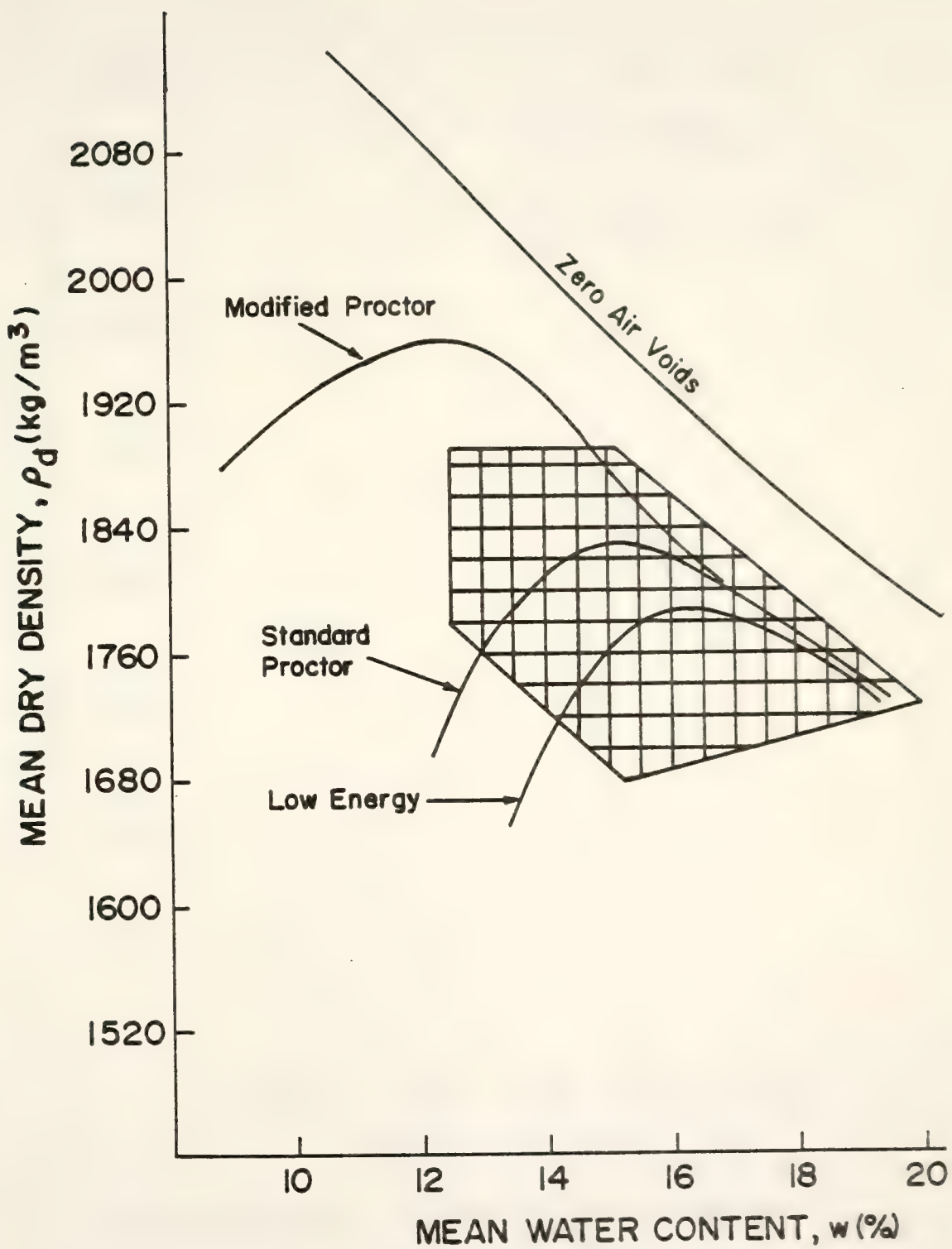


Figure 3-24 Joint Region of Observations for Dry Density Prediction Model

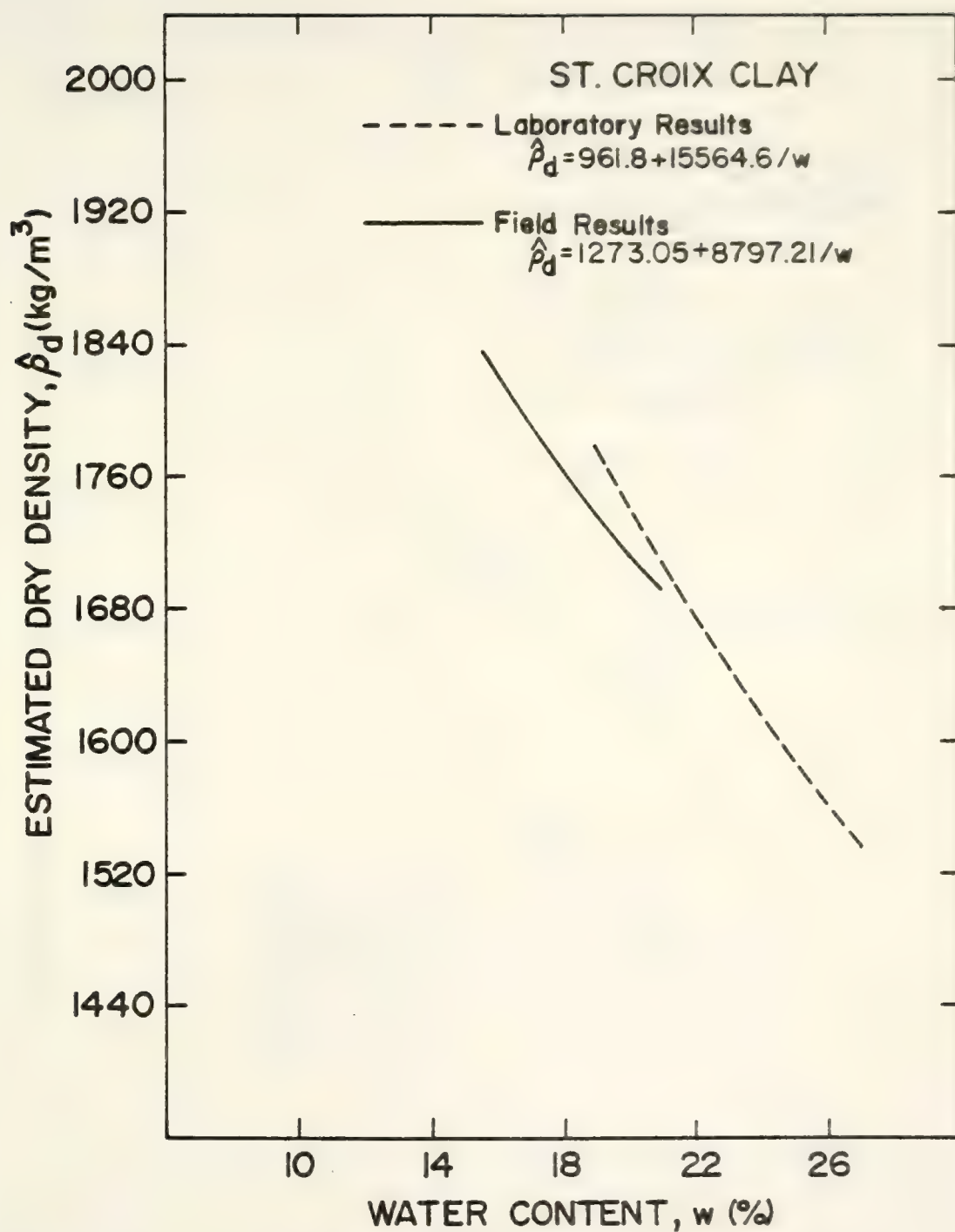


Figure 3-25 Wet-of-Optimum Dry Density Models

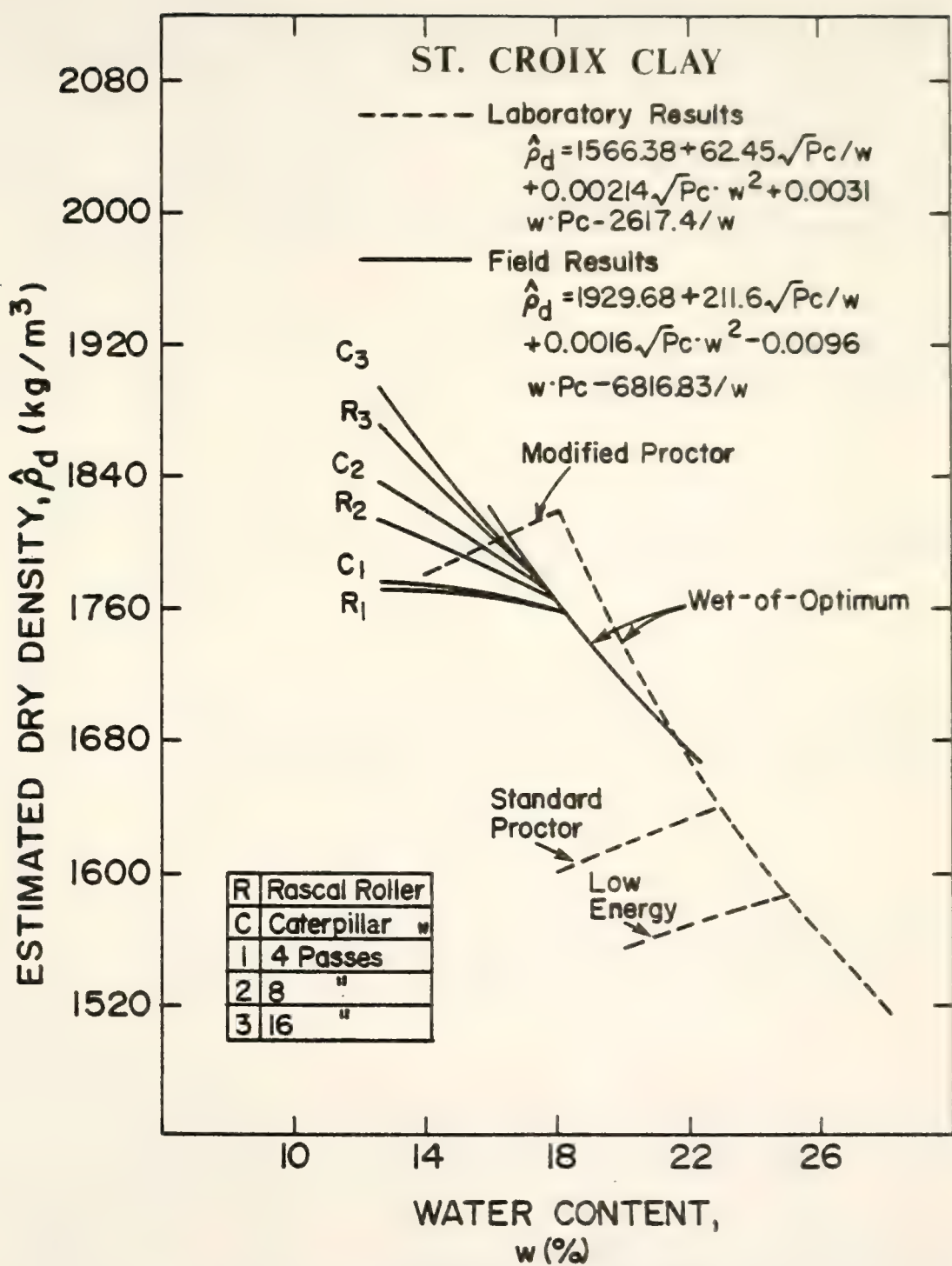


Figure 3-26 All Moistures Dry Density Models

TABLE 3-13 Basic Compaction Variables for As-Compacted Compressive Strength at Failure

Test No.	As-Compacted Compressive Strength At Failure q_c (kPa)	Compaction Moisture Content $w(\%)$	As-Compacted Dry Density ρ_d (kg/m^3)	Compactor Foot Pressure P_c (kPa)	Initial Void Ratio e_o	Initial Saturation $S_i (\%)$	Estimated Compactive Prestress \hat{P}_s (kPa)
C1A1(276)	804.3	15.58	1810.7	797	0.54	80.5	481
C2A6(276)	789.8	15.13	1816.8	797	0.535	78.9	487
C3A3(276)	1005.6	13.88	1783.7	797	0.563	68.7	506
C4A8(276)	235.6	20.22	1701.0	797	0.64	88.2	397
C5A1(276)	378.3	18.21	1761.6	797	0.583	87.2	436
C1B2(276)	1166.9	14.33	1858.6	1204	0.50	79.9	622
C2B2(276)	746.5	14.15	1814.9	1204	0.537	73.6	625
C3B8(276)	959.3	12.05	1743.5	1204	0.60	56.1	667
C4B10(276)	449.6	17.0	1803.0	1204	0.547	86.8	558
C5B10(276)	478.3	18.75	1755.1	1204	0.589	88.8	511
C2C6(276)	685.9	15.0	1843.7	1771	0.513	81.6	726
C3C8(276)	693.6	13.85	1907.3	1771	0.462	83.6	763
C4C10(276)	304.3	18.94	1741.4	1771	0.602	87.9	577
C5C4(276)	624.0	16.63	1808.5	1771	0.542	85.6	683
R2A10(276)	461.7	16.87	1628.9	780	0.712	66.1	454
R2A1(276)	465.8	15.9	1686.6	780	0.654	67.9	470
R4A4(276)	508.6	16.24	1824.9	780	0.528	85.8	465

TABLE 3-13 (Continued)

Test No.	As-Compacted Compressive Strength At Failure q_c (kPa)	Compaction Moisture Content w (%)	As-Compacted Dry Density ρ_d (kg/m^3)	Compactor Foot Pressure P_c (kPa)	Initial Void Ratio e_0	Initial Degree of Saturation S_i (%)	Estimated Compactive Prestress \hat{P}_s (kPa)
R5A2(276)	416.1	18.85	1741.2	780	0.602	87.4	420
R2B10(276)	988.7	13.63	1783.8	1038	0.563	67.5	589
R3B6(276)	1138.8	10.94	1832.0	1038	0.522	58.4	632
R4B7(276)	390.4	17.15	1795.3	1038	0.553	86.5	518
R5B9(276)	532.6	17.27	1738.2	1038	0.604	79.7	515
R1C9(276)	1013.0	12.85	1792.5	1525	0.556	64.5	736
R2C4(276)	855.2	15.44	1831.0	1525	0.523	82.4	666
R3C10(276)	504.9	14.7	1749.9	1525	0.594	69.1	687
R4C8(276)	382.0	17.85	1784.3	1525	0.563	88.5	589
R5C8(276)	211.3	20.25	1707.6	1525	0.633	89.2	501
C1A4(138)	536.3	15.4	1718.9	797	0.622	69.08	483
C2A2(138)	781.1	13.5	1819.4	797	0.533	70.67	511
C3A10(138)	539.4	15.52	1695.7	797	0.645	67.13	481
C4A1(138)	235.6	18.4	1753.1	797	0.591	86.86	432
C5A10(138)	264.7	18.55	1709.2	797	0.632	81.89	430
C1B3(138)	1152.3	13.64	1838.7	1204	0.517	73.61	636
C2B9(138)	691.1	14.51	1738.3	1204	0.604	67.02	613
C3B9(138)	650.1	11.1	1808.2	1204	0.542	57.14	684

TABLE 3-13 (Continued)

Test No.	As-Compacted Compressive Strength At Failure q_c (kPa)	Compaction Moisture Content w (%)	As-Compacted Dry Density ρ_d (kg/m ³)	Compactor Foot Pressure P_c (kPa)	Initial Void Ratio e_0	Initial Degree of Saturation S_i (%)	Estimated Compactive Prestress P_s (kPa)
C4B2(138)	195.3	18.62	1745.4	1204	0.598	86.87	514
C5B9(138)	472.9	16.47	1742.5	1204	0.6	76.59	572
C1C4(138)	1156.7	13.54	1852.1	1771	0.506	74.66	772
C2C10(138)	771.4	13.5	1787.8	1771	0.56	67.26	774
C3C2(138)	546.4	15.84	1680.0	1771	0.66	66.96	697
C4C9(138)	278.3	19.0	1729.9	1771	0.614	86.34	574
C5C1(138)	390.7	16.38	1815.7	1771	0.536	85.26	678
R1A2(138)	562.9	13.33	1639.0	780	0.701	53.05	507
R2A3(138)	545.7	15.53	1766.4	780	0.579	74.83	476
R3A9(138)	538.4	14.5	1711.7	780	0.629	64.32	491
R4A2(138)	312.8	18.3	1740.4	780	0.602	84.8	430
R5A3(138)	201.8	18.5	1769.1	780	0.576	89.6	420
R1B9(138)	721.1	13.46	1732.2	1038	0.61	61.6	592
R2B2(138)	610.1	15.5	1849.5	1038	0.508	85.1	553
R3B5(138)	309.7	16.67	1692.5	1038	0.648	71.8	528
R4B6(138)	334.2	15.11	1816.5	1038	0.535	78.8	601
R5B8(138)	186.8	19.8	1728.0	1038	0.614	90.0	454
R1C3(138)	597.5	16.48	1814.1	1525	0.537	85.6	614

TABLE 3-13 (Continued)

Test No.	As-Compacted Compressive Strength At Failure σ_c (kPa)	Compaction Moisture Content w (%)	As-Compacted Dry Density ρ_d (kg/m ³)	Compactor Foot Pressure P_c (kPa)	Initial Void Ratio e_o	Initial Degree of Saturation S_i (%)	Estimated Compactive Prestress \hat{P}_s (kPa)
R2C6(138)	736.0	14.28	1803.4	1525	0.546	73.0	699
R3C3(138)	311.3	17.13	1772.5	1525	0.573	83.4	613
R4C7(138)	502.5	14.86	1862.3	1525	0.497	83.4	683
R5C1(138)	214.4	16.25	1791.8	1525	0.556	81.5	641
C1A2(69)	859.3	12.5	1840.5	797	0.515	67.7	524
C2A3(69)	495.0	16.12	1792.5	797	0.556	80.9	472
C3A7(69)	496.2	14.25	1768.0	797	0.577	68.9	500
C4A6(69)	143.2	20.52	1706.0	797	0.635	90.2	391
C5A2(69)	412.3	17.0	1800.5	797	0.549	86.4	457
C1B1(69)	611.3	12.0	1746.5	1204	0.597	56.1	668
C2B3(69)	503.8	14.85	1824.2	1204	0.529	78.4	610
C3B3(69)	330.3	18.16	1744.9	1204	0.598	84.7	527
C4B8(69)	678.4	14.64	1876.2	1204	0.486	84.0	615
C5B3(69)	233.6	17.51	1794.4	1204	0.554	88.2	545
C1C5(69)	685.7	13.0	1852.2	1771	0.506	71.68	788
C1C7(69)	1319.4	12.3	1902.4	1771	0.466	73.65	808
C2C9(69)	657.2	14.68	1835.1	1771	0.52	78.81	757
C2C11(69)	677.2	17.54	1741.2	1771	0.602	81.34	634

TABLE 3-13 (Continued)

Test No.	As-Compacted Compressive Strength At Failure q_c (kPa)	Compaction Moisture Content w (%)	As-Compacted Dry Density ρ (kg/m ³)	Compactor Foot Pressure P_c (kPa)	Initial Void Ratio e_0	Initial Degree of Saturation S_i (%)	Estimated Compactive Prestress \hat{P}_s (kPa)
C3C3(69)	809.4	13.63	1884.9	1771	0.48	79.22	770
C4C1(69)	281.9	15.77	1842.1	1771	0.514	85.6	700
C5C10(69)	240.3	17.55	1790.2	1771	0.558	87.75	633
R1A7(69)	426.6	12.66	1709.8	780	0.631	55.98	515
R2A8(69)	381.6	15.0	1765.2	780	0.58	72.16	484
R3A10(69)	295.9	14.69	1752.4	780	0.59	69.47	488
R4A7(69)	293.9	18.27	1773.7	780	0.572	89.11	430
R5A10(69)	404.0	13.56	1846.6	780	0.51	74.18	504
R1B1(69)	434.4	14.74	1750.8	1038	0.583	70.54	508
R2B7(69)	716.2	14.09	1842.9	1038	0.513	76.63	580
R3B10(69)	391.1	15.37	1724.2	1038	0.617	69.9	576
R4B4(69)	427.0	17.0	1807.4	1038	0.543	87.34	521
R5B3(69)	326.4	17.12	1779.8	1038	0.567	84.24	519
R1C5(69)	607.1	15.15	1834.3	1038	0.52	81.49	560
R2C5(69)	690.6	14.2	1839.4	1525	0.516	76.78	501
R3C1(69)	480.7	12.22	1790.1	1525	0.558	61.1	452
R4C9(69)	376.1	17.0	1842.1	1525	0.514	92.23	617
R5C9(69)	291.3	18.5	1785.3	1525	0.562	91.84	510

(Weitzel, 1979), respectively.

(a) Field Compacted Soil:

$$\hat{q}_c = -6980.05 + 636.21w - 8.3w^2 - 0.155 \rho_d \cdot w \\ + 112.1 (1 - S_i/100) \cdot \sqrt{\sigma_3} + 3.6 \rho_d \cdot \sqrt{S_i/w} \quad (3-9)$$

(b) Laboratory Compacted Soil:

$$\hat{q}_c = -1878.2 + 51.54w - 0.06 \rho_d \cdot w + 1.39w^2 \\ + 76.91 (1 - S_i/100) \cdot \sqrt{\sigma_3} + 3.68 \rho_d \cdot \sqrt{S_i/w} \quad (3-10)$$

where \hat{q}_c = estimated compressive strength, kPa

ρ_d = dry density, kg/m^3

S_i = initial degree of saturation, %

w = water content, %

σ_3 = confining pressure, kPa

The statistical data for these two equations are shown in Table 3-14.

The multiple coefficient of determination (R^2) for field compacted soil is 0.72, which is acceptable, but not highly satisfactory.

Since the dry density can be expressed in terms of initial void ratio (e_o) as:

$$\rho_d = G_s \rho_w / (1 + e_o) \quad (3-11)$$

and the initial degree of saturation is related to water content (w) and initial void ratio (e_o) by:

$$S_i = wG_s/e_o \quad (3-12)$$

The strength prediction models can be a function of initial void ratio (e_o), confining pressure (σ_3), and water content (w). Figure 3-27 shows the relationship between the predicted field compressive strength and water content at a constant initial void ratio (or dry density). It can be seen that the predicted field as-compacted strength (\hat{q}_c) increases with increasing confining pressure and decreasing water

TABLE 3-1⁴ Statistical Data for As-Compacted Strength Model

Statistical Criteria	Laboratory	Field
	$d_c = -1878.2 + 51.54 w - 0.06 p_d \cdot v + 1.39 w^2 + 76.91 (1 - S_i/100) \cdot \sqrt{\sigma_3} + 3.68 p_d \cdot \sqrt{S_i/v}$	$d_c = -6980.05 + 636.21 w + 8.3 w^2 - 0.155 p_d \cdot v + 112.1 (1 - S_i/v) \cdot \sqrt{\sigma_3} + 3.6 p_d \cdot \sqrt{S_i/v}$
R^2	0.983	0.72
R_a^2	0.981	0.70
Overall F-Test	832.4	42.8
<u>95% of Confidence Interval for Regression Coefficient</u>		
w	-269.73, 372.8	7.57, 1264.85
w ²	-2.4, 5.18	-16.7, 0.114
p _d w	-0.145, 0.0243	-0.347, 0.038
(1 - S _i /100) $\sqrt{\sigma_3}$	64.76, 89.06	75.11, 149.13
p _d $\cdot \sqrt{S_i/v}$	2.06, 5.3	1.54, 5.65

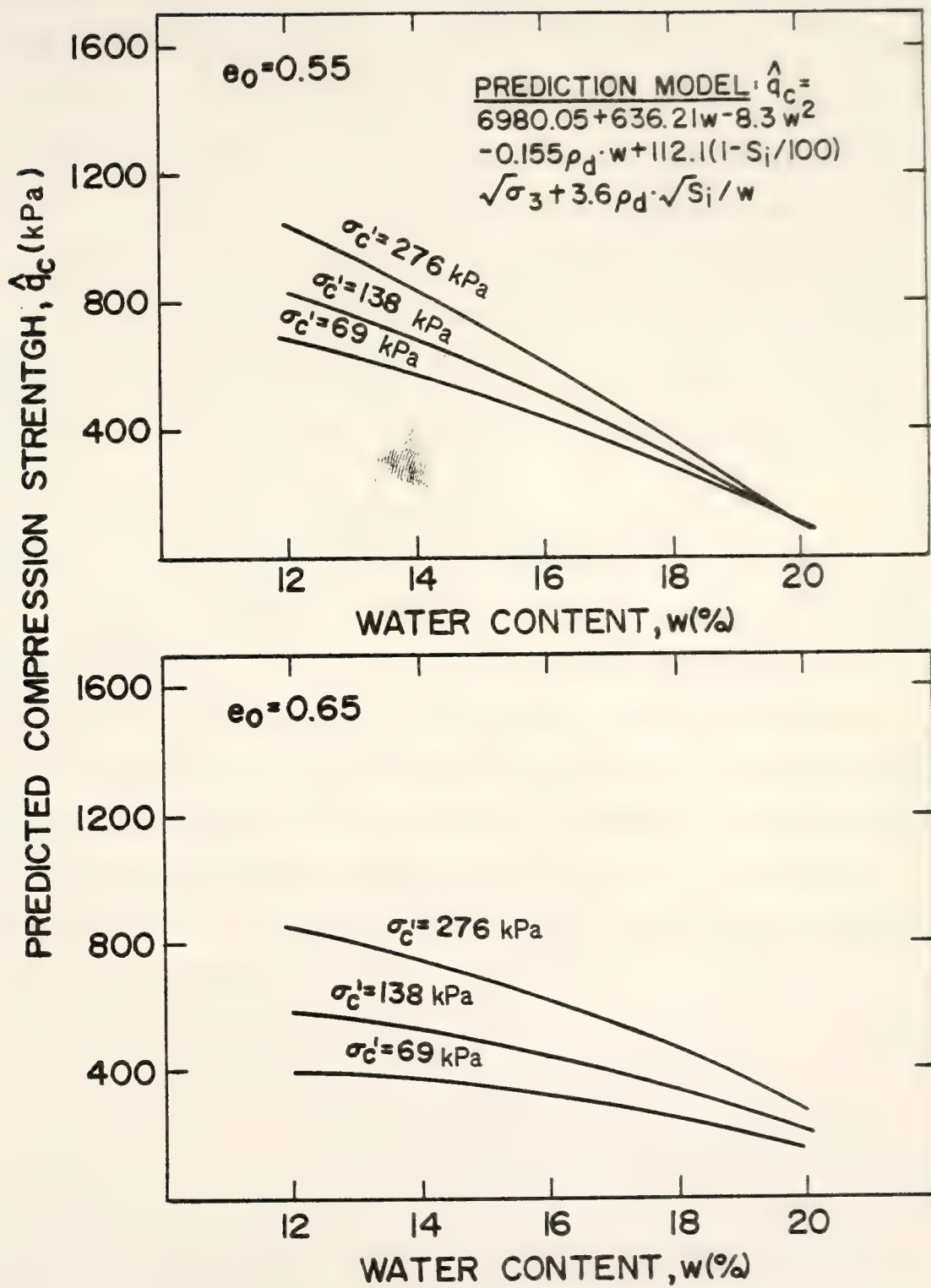


Figure 3-27 Predicted Field As-Compacted Strength-Water Content Relationship at a Constant Initial Void Ratio

content. This is also true for the laboratory as-compacted strength model as shown in Figure 3-28. Figure 3-29 shows that the as-compacted strength of both laboratory and field compacted soils increases with increasing dry density and water content for a given confining pressure until the sample reaches near-saturation at a high water content level.

The joint region of observations for the field strength prediction model is shown in Figure 3-6. Values of the independent variables of water content and dry density should lie in this region. In addition, the range of confining pressure applicable is 69 to 276 kPa.

3-2-3 Prediction Model for Volume Change due to Saturation and Consolidation

The basic independent variables utilized in the analysis of percent volume change due to saturation and consolidation for field compacted soil are listed in Table 3-15. The estimated compactive prestress (\hat{P}_s) values were obtained by inserting the values of compaction moisture content and compactor foot pressure into the predictive model developed by Lin (1981). The final regression models selected for the field compacted soil, and laboratory compacted soil [based on Johnson (1979) data], are given below:

(a) Field Compacted Soil

$$\frac{\Delta V}{V_o} (\%) = -0.166 + 2.47e_o \sqrt{\sigma'_c} - 0.365 \hat{P}_s - 0.00263w \cdot \sigma'_c \quad (3-13)$$

(b) Laboratory Compacted Soil

$$\frac{\Delta V}{V_o} (\%) = -9.4 + 2.9e_o \sqrt{\sigma'_c} - 0.404 \hat{P}_s - 0.00276w \cdot \sigma'_c \quad (3-14)$$

where

$\frac{\Delta V}{V_o}$ (%) = estimated value of percent volume

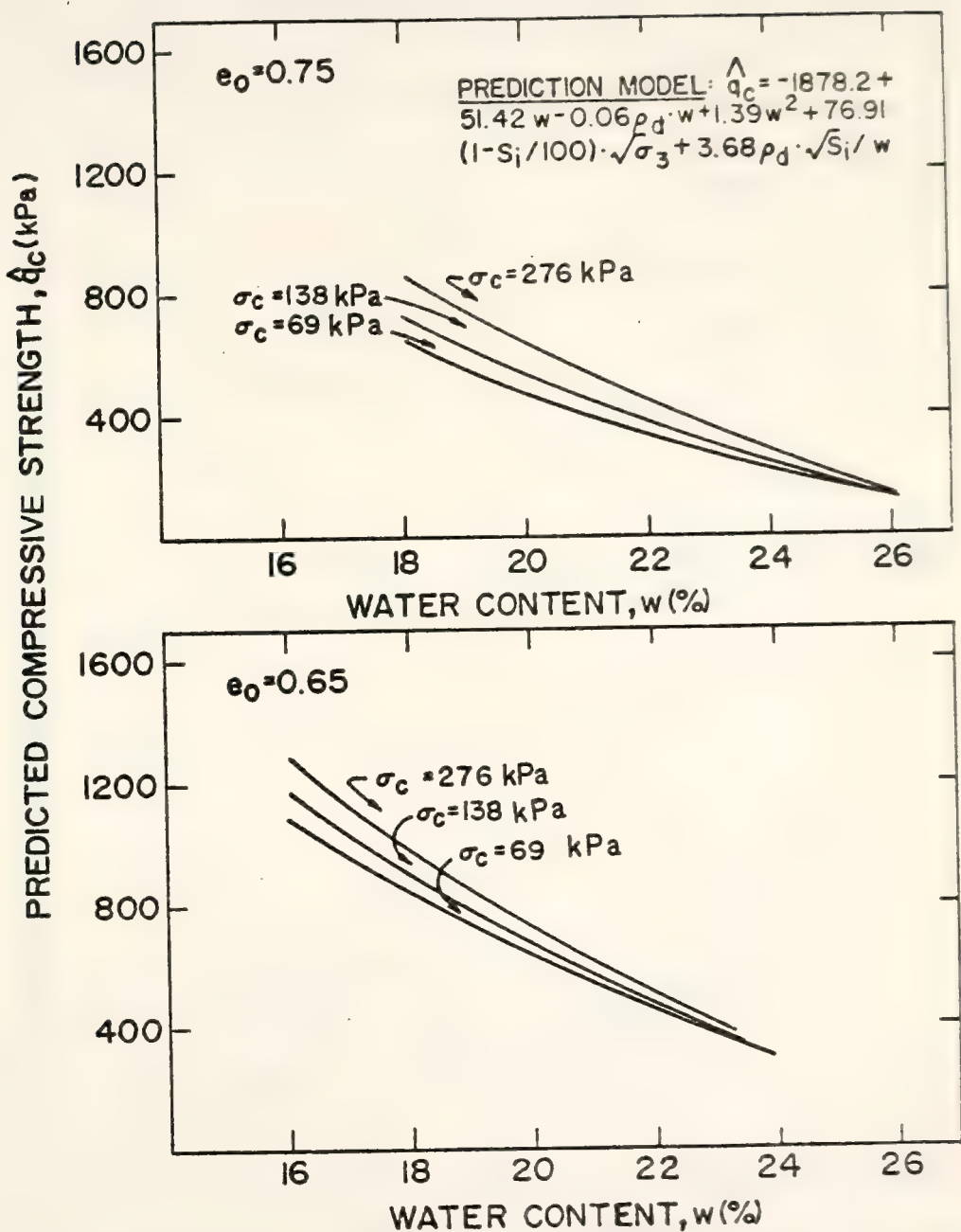


Figure 3-28 Predicted Laboratory As-Compacted Strength-Water Content Relationship at a Constant Initial Void Ratio

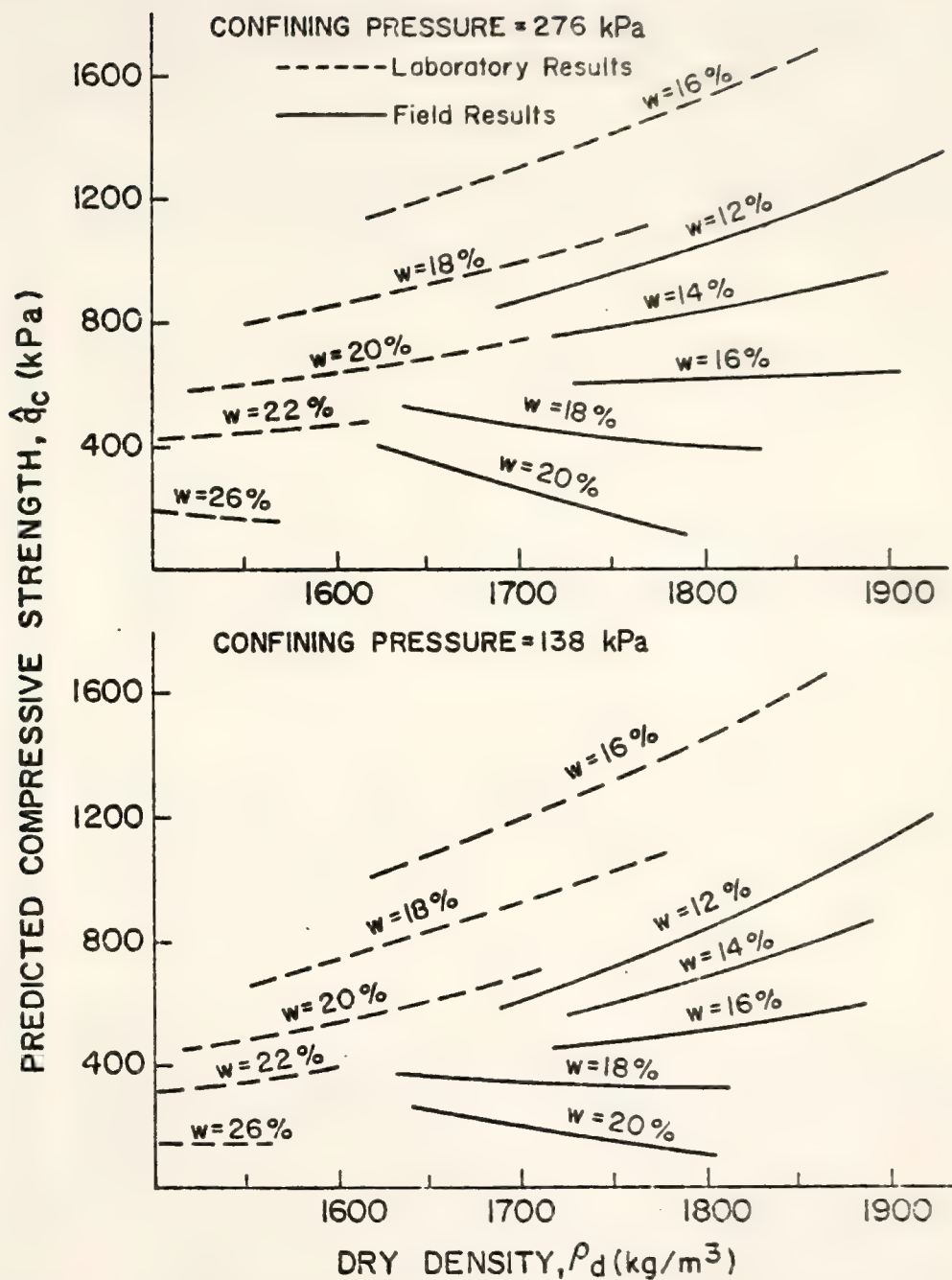


Figure 3-29 Predicted Compressive Strength-Dry Density Relationship at Constant Water Content

TABLE 3-15 Basic Compaction Variables for Percent Volume Change Due to Saturation and Consolidation

Sample No.	Percent Volume Change Due to Saturation And Consolidation $\Delta V/V_0$ (%)	Compaction Moisture Content w (%)	As-Compacted Dry Density ρ_d (kg/m^3)	Compactor Foot Pressure P_c (kPa)	Initial Void Ratio e_0	Estimated Compactive Prestress P_s (kPa)
C1A9(276)	6.57	15.5	1680.98	797	0.659	482
C3A5(276)	3.336	16.01	1824.35	797	0.529	474
C4A4(276)	2.59	18.5	1761.39	797	0.583	431
C5A5(276)	2.486	16.68	1777.89	797	0.569	463
C1B10(276)	0.405	13.4	1884.58	1204	0.480	641
C2B7(276)	2.174	12.53	1895.0	1204	0.472	658
C4B9(276)	1.342	16.84	1781.90	1204	0.565	562
C5B6(276)	1.556	17.58	1808.65	1204	0.542	543
C1C9(276)	0.398	14.23	1851.47	1771	0.506	751
C2C3(276)	0.067	14.89	1865.90	1771	0.495	730
C3C10(276)	1.929	14.9	1793.45	1771	0.555	729
C4C5(276)	1.913	18.86	1779.0	1771	0.568	580
C2A5(138)	3.05	15.13	1771.65	797	0.574	487
C3A1(138)	0.584	15.4	1831.48	797	0.523	483
C4A5(138)	1.838	16.95	1830.91	797	0.523	458
C5A7(138)	0.779	17.12	1811.21	797	0.54	455
C1B8(138)	-3.32	14.54	1889.7	1204	0.476	617
C3B6(138)	4.762	13.64	1794.07	1204	0.554	636

TABLE 3-15 (Continued)

Sample No.	Percent Volume Change Due To Saturation And Consolidation $\Delta V/V_0$ (%)	Compaction Moisture Content w (%)	As-Compacted Dry Density ρ_d (kg/m ³)	Compactor Foot Pressure P_c (kPa)	Initial Void Ratio e_0	Estimated Compactive Prestress \hat{P}_s (kPa)
C4B5(138)	1.952	14.84	1814.10	1204	0.537	610
C5B4(138)	-0.717	16.97	1816.31	1204	0.535	559
C2C1(138)	-2.241	15.64	1784.83	1771	0.562	704
C3C1(138)	-1.97	15.01	1830.96	1771	0.523	726
C4C7(138)	2.945	19.16	1747.62	1771	0.596	567
C5C8(138)	1.828	18.37	1758.83	1771	0.586	600
C1A3(65)	1.524	13.47	1700.52	797	0.64	511
C2A1(55)	1.161	17.76	1703.66	797	0.637	444
C3A9(63)	0.642	14.14	1791.03	797	0.557	502
C4A9(69)	3.589	19.57	1696.52	797	0.644	410
C2B5(69)	-2.925	14.0	1896.83	1204	0.47	629
C3B2(69)	1.625	11.8	1742.59	1204	0.60	672
C4B6(69)	1.605	17.43	1790.24	1204	0.558	547
C5B8(83)	0.253	17.98	1765.29	1204	0.58	532
C2C4(70)	-6.184	14.98	1834.37	1771	0.52	727
C3C6(61)	-4.242	17.24	1792.33	1771	0.556	645
C4C6(63)	1.047	20.44	1717.18	1771	0.624	511
C5C7(69)	-0.707	17.69	1792.15	1771	0.556	609

TABLE 3-15 (Continued)

Sample No.	Percent Volume Change Due to Saturation And Consolidation $\Delta V/V_0$ (%)	Compaction Moisture Content w (%)	As-Compacted Dry Density ρ_d (kg/m ³)	Compactor Foot Pressure P_c (kPa)	Initial Void Ratio e_0	Estimated Compactive Prestress P_s (kPa)
R1A3(276)	4.02	14.96	1751.30	780	0.592	484
R2A7(276)	6.60	15.875	1688.25	780	0.652	470
R3A5(276)	7.787	14.03	1723.62	780	0.618	498
R5A6(276)	1.933	15.83	1859.83	780	0.50	471
R2B8(276)	3.482	17.85	1703.09	1038	0.637	502
R3B8(276)	2.31	13.69	1840.21	1038	0.515	588
R4B1(276)	2.814	13.63	1825.56	1038	0.528	589
R5B6(276)	1.656	17.83	1776.84	1038	0.57	502
R1C3(276)	-0.474	13.64	1889.06	1525	0.476	716
R1C10(276)	1.836	14.26 ^b	1829.04	1525	0.525	700
R3C2(276)	2.083	14.93	1815.17	1525	0.536	681
R5C3(276)	2.696	21.4	1709.13	1525	0.632	455
R2A1(138)	2.946	19.31	1676.98	780	0.663	411
R3A3(138)	6.534	14.55	1686.75	780	0.653	490
R4A6(138)	2.23	14.9	1828.82	780	0.525	485
R5A7(138)	1.648	18.03	1766.74	780	0.578	434
R2B3(138)	0.904	13.64	1799.8	1038	0.549	589
R3B7(138)	3.388	13.57	1749.86	1038	0.594	590
R4B9(138)	-0.764	17.44	1775.65	1038	0.57	511

TABLE 3-15 (Continued)

Sample No.	Percent Volume Change Due to Saturation And Consolidation $\Delta V/V_0$ (%)	Compaction Moisture Content w (%)	As-Compacted Dry Density ρ_d (kg/m^3)	Compactor Foot Pressure P_c (kPa)	Initial Void Ratio e_0	Estimated Compactive Prestress \hat{P}_s (kPa)
R5B2(138)	7.641	14.63	1620.22	1038	0.721	570
R2C9(138)	0.101	14.59	1873.52	1525	0.489	690
R3C9(138)	0.971	16.37	1804.5	1525	0.545	637
R4C1(138)	-0.469	15.41	1867.32	1525	0.493	667
R5C6(138)	0.447	18.45	1779.42	1525	0.567	568
R1A4(69)	4.597	17.34	1664.96	780	0.675	446
R2A5(69)	1.165	18.97	1709.56	780	0.631	417
R3A2(83)	1.675	16.21	1729.49	780	0.621	465
R5A8(60)	-0.803	18.96	1724.07	780	0.618	418
R1B10(69)	0.924	18.98	1718.58	1038	0.623	475
R2B9(66)	-0.586	15.17	1814.14	1038	0.537	560
R3B3(69)	2.877	15.44	1744.51	1038	0.599	554
R5B4(69)	1.061	19.96	1741.02	1038	0.602	450
R2C3(69)	0.196	15.11	1824.35	1525	0.529	676
R3C5(69)	1.154	18.6	1788.72	1525	0.56	563
R4C5(63)	-0.198	16.32	1837.39	1525	0.518	039
R5C4(112)	-0.52	16.3	1812.33	1525	0.539	040

change due to saturation and
consolidation (swell is negative)

e_0 = initial void ratio

σ'_c = isotropic consolidation pressure, kPa

w = water content, %

\hat{P}_s = estimated compactive prestress, kPa

The statistical data for these two models are shown in Table 3-16.

The coefficients of determination (R^2) of 0.95 and 0.72 are excellent and adequate, respectively. The residuals are normally distributed.

Figure 3-30 shows for constant values of initial void ratio that

$\frac{\Delta V}{V_0}$ (%) decreases (more net swell or less net compression), as the estimated compactive prestress increases. The figure also shows that $\frac{\Delta V}{V_0}$ (%) increases (more net compression or less net swell) with increasing confining pressure and decreasing water content. For samples with the same water content and confining pressure, $\frac{\Delta V}{V_0}$ (%) decreases or dry density increases (initial void ratio decreases). This is a result of the greater swell potential of compacted clay at higher densities. The tendency for swelling is evidenced by the negative coefficient for zero confinement (free swell). The highest estimated swell values occur at the lowest confining pressure and the highest compactive prestress (\hat{P}_s), for a given water content and dry density. The same trends also can be obtained from laboratory results (Johnson, 1979) in Figure 3-31.

The usable range of the field percent volume change model is shown by the joint region of observation in Figure 3-14. The dry density can be expressed in terms of initial void ratio by applying Equation 3-11. The range of estimated compressive prestress (\hat{P}_s) is from 400

TABLE 3-16 Statistical Data of the Prediction Models for Percent Volume Change Due to Saturation and Consolidation

Statistical Criteria	Laboratory	Field
	$\hat{\Delta V} / V_0 (\%) = -9.4 + 2.9 e_o \cdot \sqrt{\sigma'_c}$ - 0.404 $\sqrt{\hat{P}_s}$ - 0.00276 $w \cdot \sigma'_c$	$\hat{\Delta V} / V_0 (\%) = -0.66 + 2.47 \cdot e_o \cdot \sqrt{\sigma'_c}$ - 0.365 $\sqrt{\hat{P}_s}$ - 0.00263 $w \cdot \sigma'_c$
R^2	0.95	0.72
R_a^2	0.95	0.70
Overall F-Test	255.04	56.78
<u>95% Confidence Interval for Regression Coefficient</u>		
$e_o \cdot \sqrt{\sigma_c}$	2.47, 3.32	1.97, 2.97
$\sqrt{\hat{P}_s}$	-0.45, -0.36	-0.527, -0.204
$w \cdot \sigma_c$	-0.0034, -0.00215	-0.0033, -0.0019

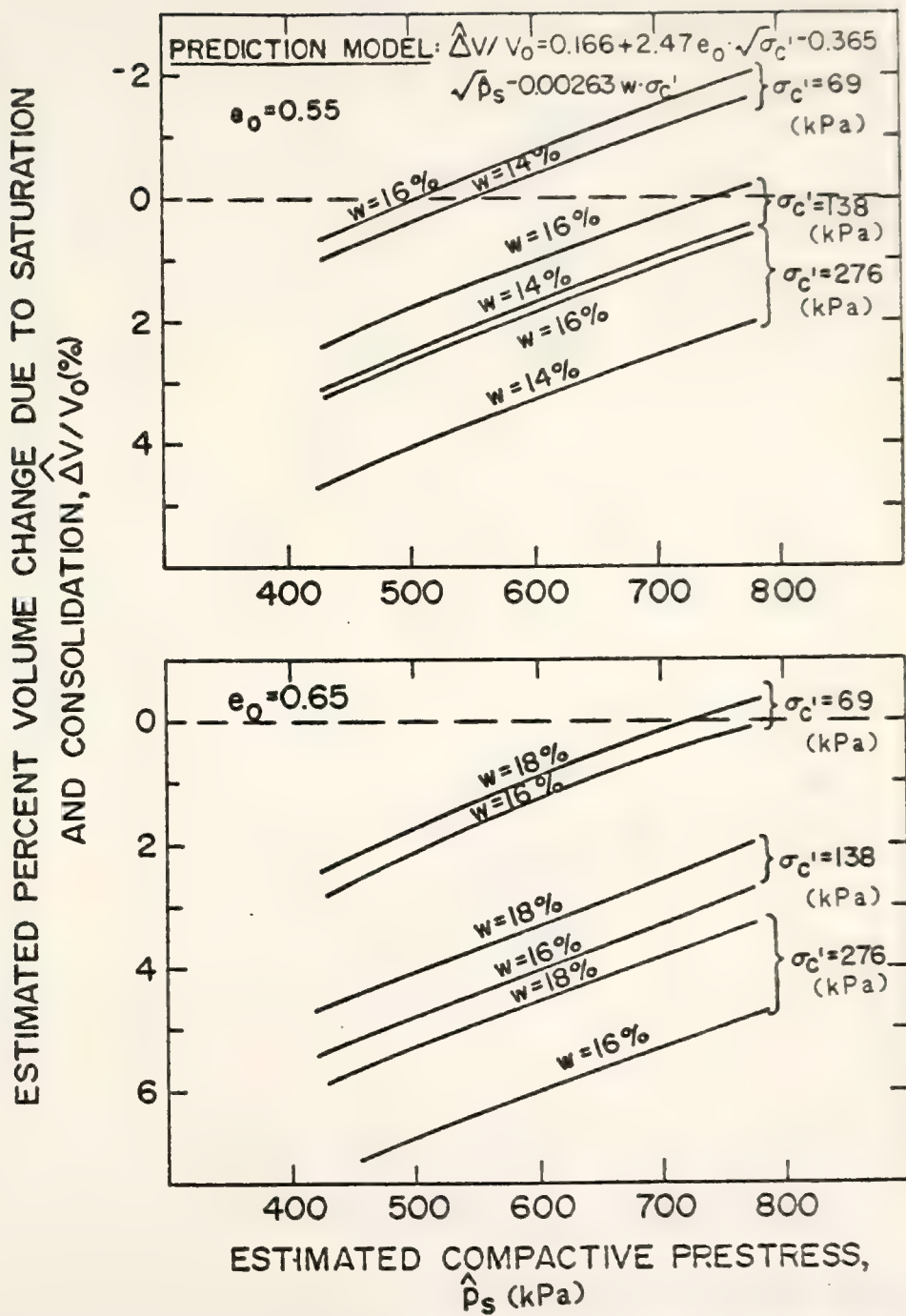


Figure 3-30 Prediction of Field Percent Volume Change Due to Saturation and Consolidation at a Constant Initial Void Ratio

ESTIMATED PERCENT VOLUME CHANGE DUE TO SATURATION AND CONSOLIDATION, $\hat{\Delta}V/V_0(\%)$

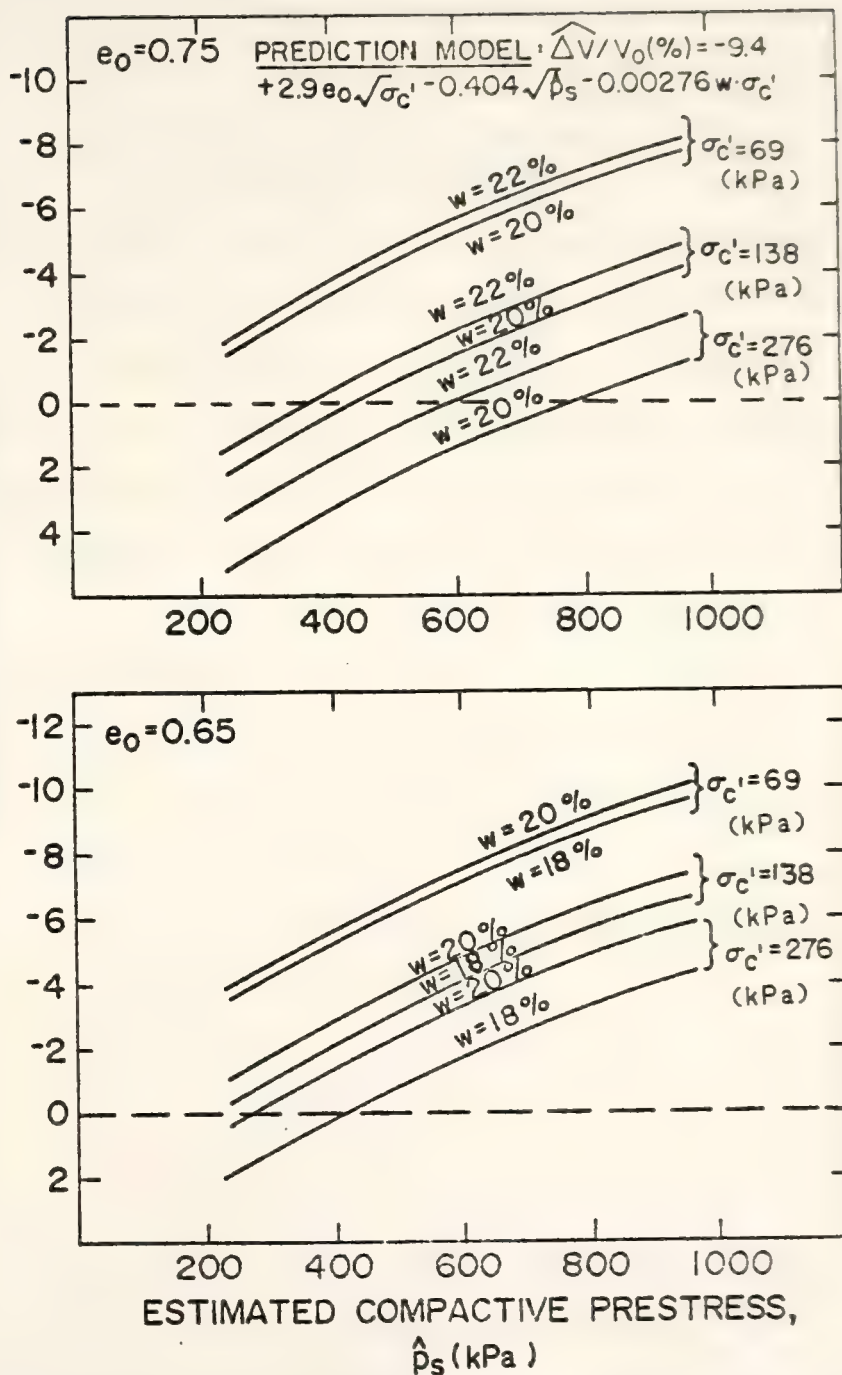


Figure 3-31 Prediction of Laboratory Precent Volume Change Due to Saturation and Consolidation at a Constant Initial Void Ratio

kPa to 750 kPa. It is also required that the consolidation pressure be between 69 kPa and 276 kPa

3-2-4 Prediction Model for Skempton's A Parameter at Failure

Table 3-17 lists the basic independent variables utilized in the analysis of the Skempton's A parameter at failure (A_f) for field compacted soil. For the analysis of A_f , logarithms, square roots and inverses were utilized to transform the basic independent variables. The final regression models selected for the field compacted soil, and laboratory compacted soil [based on Johnson (1979) data], are given below:

(a) Field Compacted Soil

$$\hat{A}_f = 2.05 - 0.73/e_o - 0.232 \times 10^{-4} \rho_d \sqrt{s_i} - 0.382 \log (\text{OCR}) \quad (3-15)$$

(b) Laboratory Compacted Soil

$$\hat{A}_f = 2.34 + 0.56/e_o - 0.189 \times 10^{-3} \rho_d \sqrt{s_i} - 0.246 \log (\text{OCR}) \quad (3-16)$$

where

e_o = initial void ratio

ρ_d = dry density, kg/m³

s_i = initial degree of saturation, %

OCR = the ratio of estimate prestress (\hat{P}_s)

to the isotropic consolidation pressure

$(\sigma'_c) \cdot (\hat{P}_s / \sigma'_c)$

The statistical data for these two equations are shown in Table 3-18.

The multiple coefficient of determination (R^2) for both field compacted soil, 0.72 and 0.63, are low but acceptable. The residuals test satis-

TABLE 3-17 Basic Compaction Variables for Skempton's A Parameter at Failure

Sample No.	A Parameter At Failure A_f	Moisture Content w (%)	As-Compacted Dry Density ρ_d (kg/m ³)	Compactor Foot Pressure P_c (kPa)	Initial Void Ratio e_0	Initial Degree of Saturation S_i (%)	Estimated Compactive Prestress \hat{P}_s (kPa)
CLA3(65)	0.552	13.47	1700.52	797	0.64	58.72	511
C2A1(55)	0.277	17.76	1703.66	797	0.637	77.79	444
C3A9(63)	0.095	14.14	1791.03	797	0.557	70.83	502
C4A9(69)	0.423	19.57	1696.52	797	0.644	84.78	410
C2B5(69)	-0.23	14.0	1896.83	1204	0.47	83.11	629
C3B2(69)	0.18	11.8	1742.59	1204	0.60	54.87	672
C4B6(69)	0.031	17.43	1790.24	1204	0.558	87.19	547
C5B8(83)	-0.063	17.98	1765.29	1204	0.58	86.49	532
C2C4(70)	-0.098	14.98	1834.37	1771	0.52	80.37	727
C3C6(61)	0.024	17.24	1792.33	1771	0.556	86.51	645
C4C6(63)	0.247	20.44	1717.18	1771	0.624	91.39	511
C5C7(69)	-0.211	17.67	1792.15	1771	0.556	88.65	629
R1A3(276)	0.303	14.96	1751.30	780	0.592	70.48	484
R2A7(276)	0.331	15.88	1688.25	780	0.652	67.93	470
R3A5(276)	0.57	14.03	1723.62	780	0.618	63.34	493
R5A6(276)	0.09	15.83	1859.83	780	0.50	88.33	471
R2B8(276)	0.358	17.85	1703.09	1038	0.637	78.18	502
R3B8(276)	0.186	13.69	1840.21	1038	0.515	74.17	533

TABLE 3-17 (Continued)

Sample No.	Skempton's A Parameter At Failure Af	Moisture Content w (%)	As-Compacted Dry Density ρ_d (kg/m ³)	Compactor Foot Pressure P_c (kPa)	Initial Void Ratio e_o	Initial Degree of Saturation S _i (%)	Estimated Compactive Prestress \hat{P}_s (kPa)
R4B1(276)	0.275	13.63	1825.56	1038	0.528	72.02	589
R5B6(276)	0.214	17.83	1776.84	1038	0.57	87.35	502
R1C3(276)	-0.141	13.64	1889.06	1525	0.476	79.95	716
R1C10(276)	0.117	14.26	1829.04	1525	0.525	75.80	700
R3C2(276)	0.117	14.93	1815.17	1525	0.536	77.73	681
R5C3(276)	0.769	21.4	1709.13	1525	0.632	94.47	455
R2A1(138)	0.085	19.31	1676.98	780	0.663	81.26	411
R3A3(138)	0.274	14.55	1686.75	780	0.653	62.17	490
R4A6(138)	0.3	14.9	1828.82	780	0.525	79.18	485
R5A7(138)	0.125	18.03	1766.74	780	0.578	87.03	434
R2B3(138)	0.25	13.64	1799.8	1038	0.549	69.32	589
R3B7(138)	0.244	13.57	1749.86	1038	0.594	63.76	590
R4B9(138)	-0.084	17.4	1775.65	1038	0.57	85.29	511
R5B2(138)	0.441	14.63	1620.22	1038	0.721	56.61	570
R2C9(138)	-0.114	14.59	1873.52	1525	0.489	83.33	690
R3C9(138)	0.072	16.37	1804.5	1525	0.545	83.8	637
R4C1(138)	-0.222	15.41	1867.32	1525	0.493	87.21	607
R5C6(138)	-0.079	18.45	1779.42	1525	0.567	90.81	503

TABLE 3-17 (Continued)

Sample No.	Skempton's A Parameter At Failure A_f	Moisture Content w (%)	As-Compacted Dry Density ρ_d (kg/m^3)	Compactor Foot Pressure P_c (kPa)	Initial Void Ratio e_o	Initial Degree of Saturation S_i (%)	Estimated Compactive Prestress \hat{P}_s (kPa)
R1A4(69)	0.456	17.34	1664.96	780	0.675	71.67	446
R2A5(69)	0.109	18.97	1709.56	780	0.631	83.88	417
R3A2(83)	0.164	16.21	1729.49	780	0.612	73.9	465
R5A8(60)	0.123	18.96	1724.07	780	0.618	85.6	418
R1B10(69)	-0.079	18.98	1718.58	1038	0.623	85.01	475
R2B9(69)	-0.076	15.17	1814.14	1038	0.537	78.82	560
R3B3(66)	0.287	15.44	1744.51	1038	0.599	71.92	554
R5B4(69)	0.169	19.96	1741.02	1038	0.602	92.5	450
R2C3(69)	-0.082	15.11	1824.35	1525	0.529	76.69	676
R3C5(69)	0.036	18.6	1788.72	1525	0.56	92.67	563
R4C6(63)	-0.029	16.32	1837.39	1525	0.518	87.9	0.39
R5C4(112)	0.104	16.3	1812.33	1525	0.539	84.35	640

TABLE 3-18 Statistical Data of the Prediction Model for Skempton's A Parameter at Failure

Statistical Criteria	Laboratory	Field
	$\hat{A}_f = 2.34 + 0.56/e_0 - 0.189 \times 10^{-3} \rho_d \sqrt{s_i} - 0.246 \log(\text{OCR})$	$\hat{A}_f = 2.05 - 0.73/e_0 - 0.232 \times 10^{-4} \rho_d \sqrt{s_i} - 0.382 \log(\text{OCR})$
R^2	0.72	0.63
R_a^2	0.70	0.61
Overall F-Test	32.24	38.44
<u>95% Confidence Interval for Regression Coefficient</u>		
$1/e_0$	0.23, 0.88	-0.98, -0.48
$\rho_d \sqrt{s_i}$	$-0.23 \times 10^{-3}, -0.14 \times 10^{-3}$	$-0.59 \times 10^{-4}, 0.13 \times 10^{-4}$
$\log(\text{OCR})$	-0.37, -0.12	-0.51, -0.26

factorily as being normally distributed.

Figure 3-32 and 3-33 show that for a constant value of initial degree of saturation an increase in the OCR (\hat{P}_s / σ'_c) produces a decrease in \hat{A}_f . This agrees with the results presented by Henkel (1956) for remolded clay. The figures also show that \hat{A}_f increases as initial void ratio increases (or dry density decreases) for a given initial degree of saturation and OCR. This behavior is very similar to that displayed by sand samples sheared at various relative densities. Very loose samples develop positive pore pressure whereas samples at other initial densities develop negative pore pressure during undrained shear. Figure 3-34 and 35 show for constant values of OCR and initial void ratio (or as-compacted dry density) that an increase in initial degree of saturation produces a decrease in \hat{A}_f . It also can be seen that \hat{A}_f decreases as OCR increases, at constant initial void ratio (dry density) and initial degree of saturation.

The range of the field Skempton's A_f parameter model is shown in Figure 3-14. The consolidation pressure must be between 69 kPa and 276 kPa.

3-2-5 Prediction Model for the Effective Stress Parameters, \hat{c}' and $\hat{\phi}'$

Since the initial compacted conditions (water content, dry density, energy level) of the samples from the field test pads were so variable, statistic regression models of soaked strength and pore pressure at failure, shown in Table 3-19, were utilized to calculate p'_f , q_f values. The values of p'_f and q_f are defined as follows:

$$q_f = \frac{(\sigma'_1 - \sigma'_3)_f}{2} = \frac{\hat{q}_u^s}{2} \quad (3-17)$$

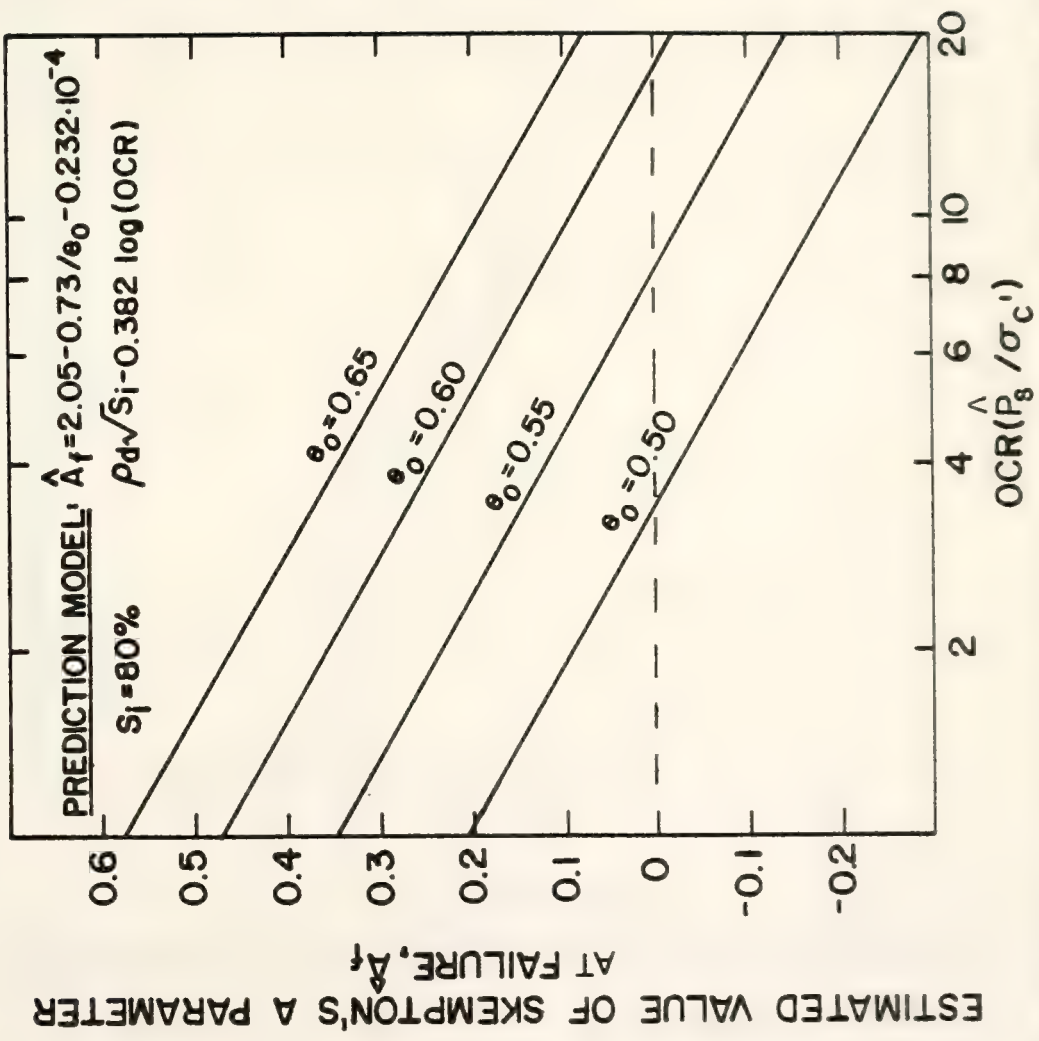
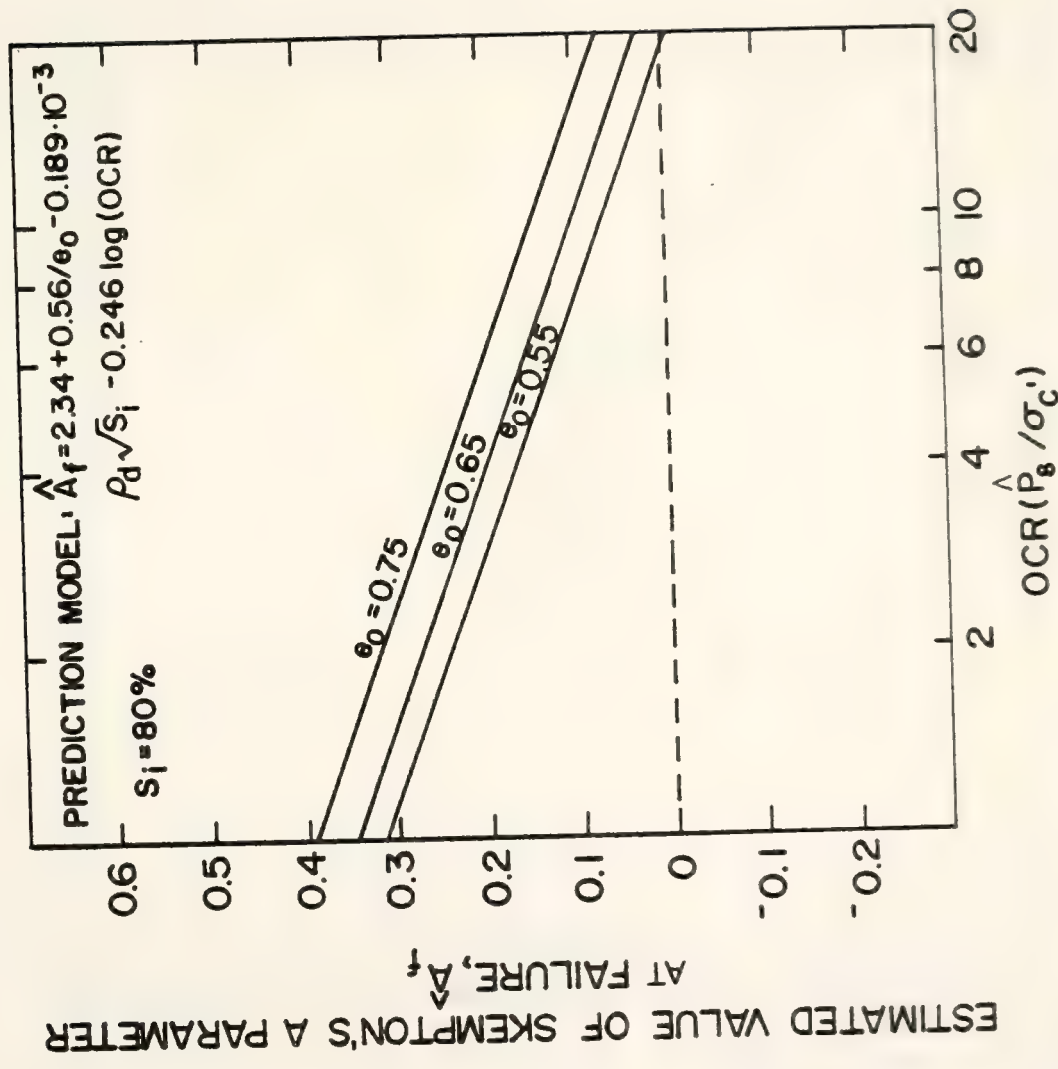


Figure 3-32 Field Skempton's A Parameter at Failure Versus OCR at a Constant Initial Saturation



Figures 3-33 Laboratory Skempton's A Parameter at Failure Versus OCR at a Constant Initial Saturation

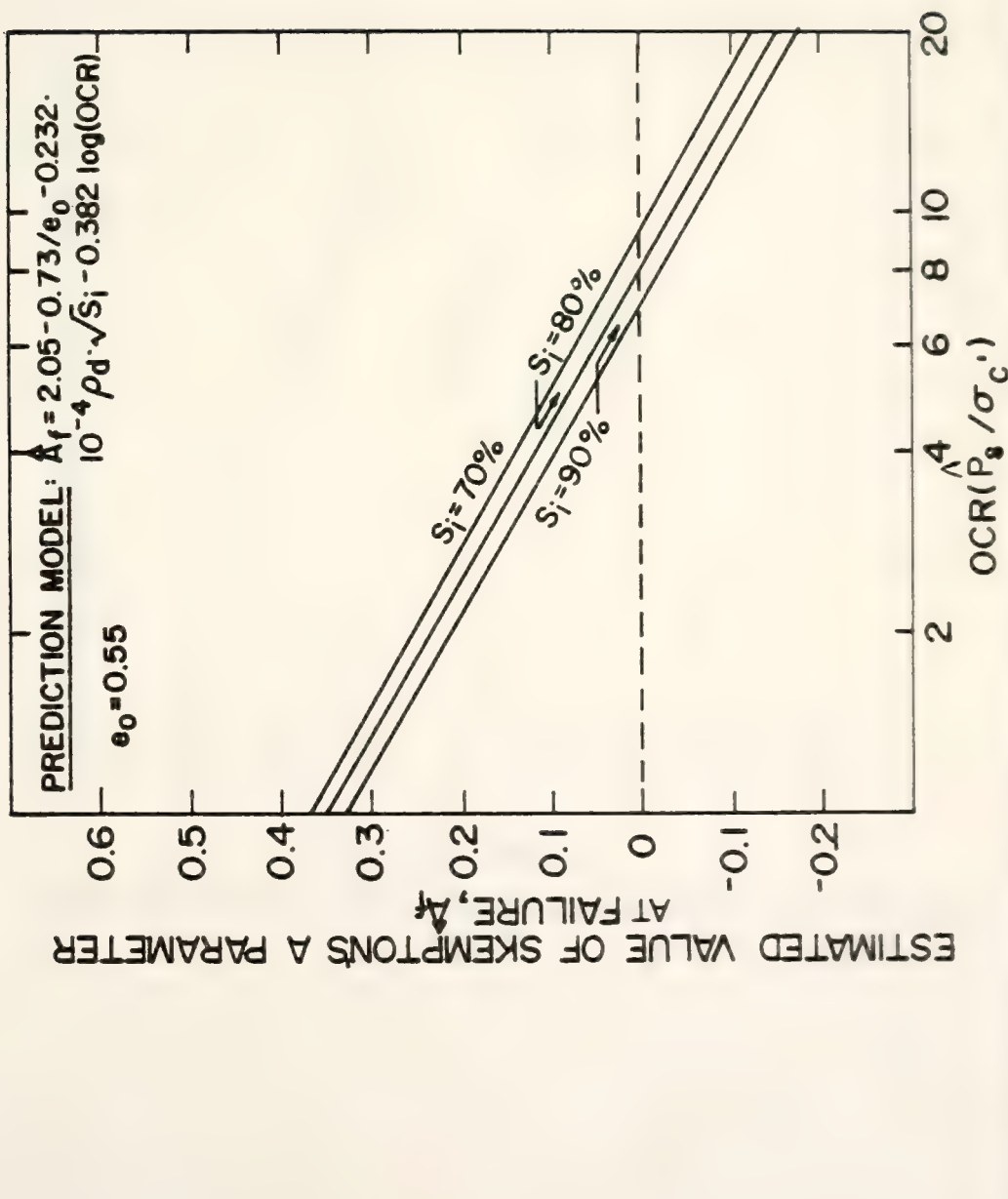


Figure 3-34 Field Skempton's A Parameter at Failure Versus OCR at a Constant Initial Void Ratio

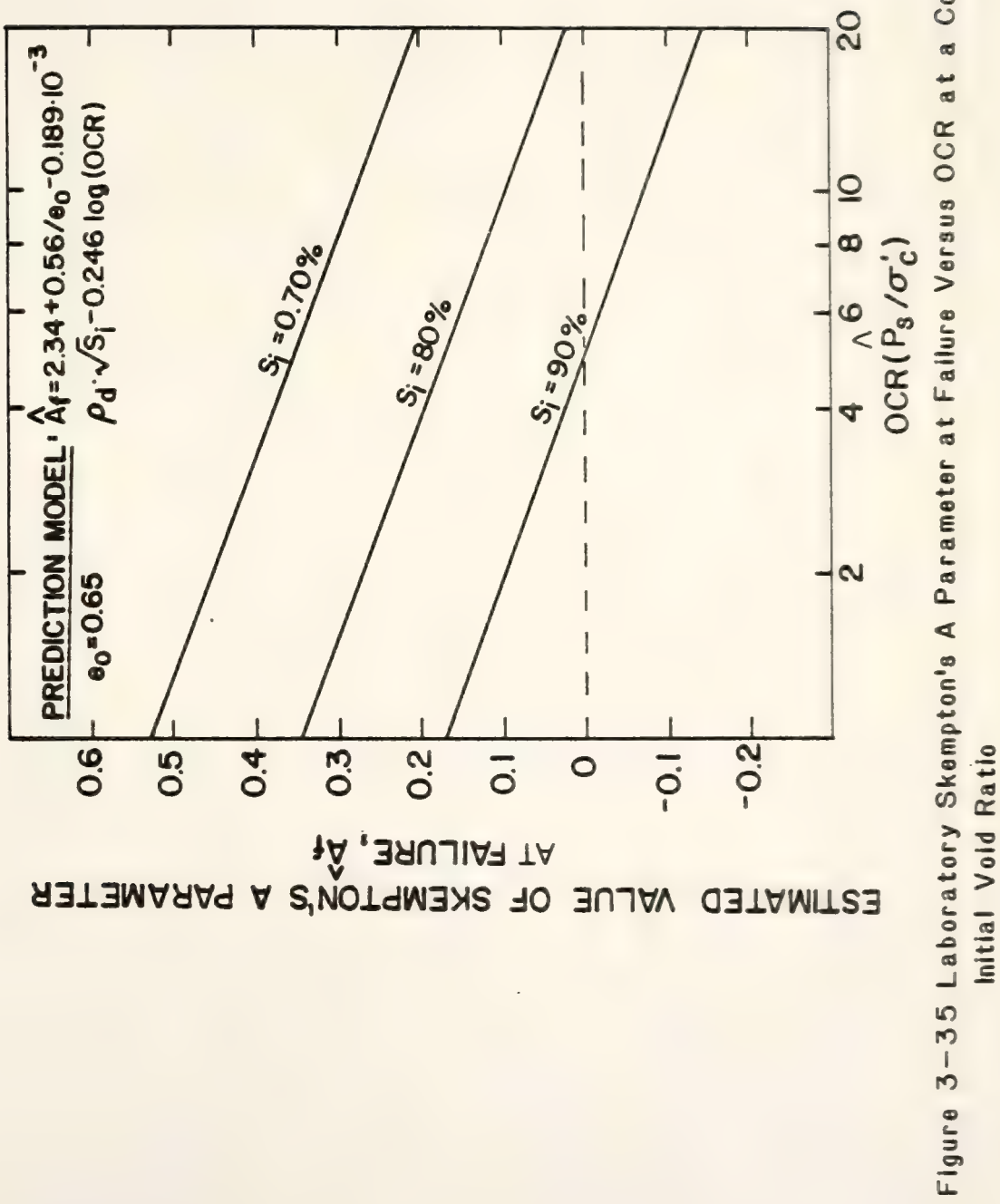


Figure 3-35 Laboratory Skempton's A Parameter at Failure Versus OCR at a Constant Initial Void Ratio

TABLE 3-19 Regression Models for Pore Pressure and Soaked Strength at Failure

Dependent Variable	Type of Roller	Regression Model	R ²
Pore Pressure	Rascal	$\hat{u}_f = 4651.65 + 32.74 e_o \sqrt{\sigma'_c} - 324.32 \log \sigma'_c$ $- 3454.76 e_o - 1345.04/e_o - 11.65 w$ $+ 0.036 w \cdot \sigma'_c + 0.925 \times 10^{-4} \rho_d^2$	0.81
	Caterpillar	$\hat{u}_f = 1925.6 - 521.86/e_o + 0.02 \cdot w \cdot \sigma'_c - 1370.08 e_o$ $- 205.21 \log \sigma'_c + (29.45/e_o) \cdot \sqrt{\sigma'_c}$	0.80
Soaked Strength	Rascal	$\hat{q}_u^s = -12290.64 - 3.24 \sigma'_c \cdot \log e_o + 3248.65/e_o$ $+ 6374.33 e_o + 252.53 w - 4.58 w^2$ $- 9.33 S_i \cdot \log \sigma'_c + 823.04 \log \sigma'_c$	0.83
	Caterpillar	$\hat{q}_u^s = 4079.43 - 6.85 \sigma'_c \cdot \log e_o + 31.29 e_o \cdot \sqrt{\sigma'_c}$ $- 0.0963 w \cdot \sigma'_c + 0.595 w^2 + 1196.2/e_o$ $+ 3162.91 e_o$	0.81

$$p'_f = \frac{(\sigma'_1 + \sigma'_3)_f}{2} = \frac{(\sigma'_1 - \sigma'_3)_f}{2} + (\sigma'_3)_f = \frac{\hat{q}_u^s}{2} + (\sigma'_{3f} - \hat{u}_f) \quad (3-18)$$

where

σ'_1 = the effective major principal stress, kPa

σ'_3 = the effective minor principal stress, kPa

\hat{q}_u^s = estimated compressive strength for

saturated soil, kPa

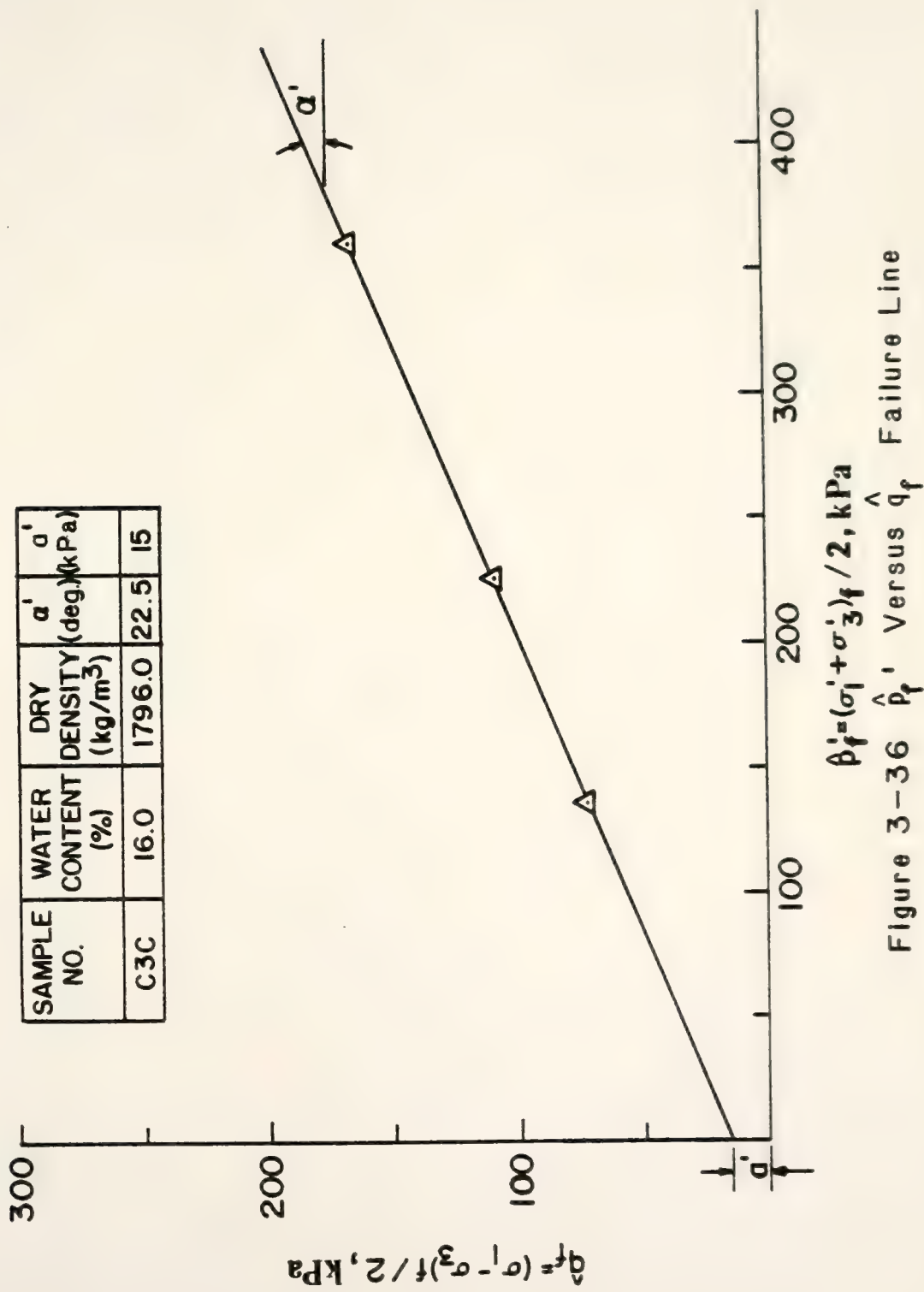
\hat{u}_f = estimated pore pressure at shear failure, kPa

The range of independent variables of dry density and water content are shown in Figure 3-14. The initial void ratio can be expressed in terms of dry density by applying Equation 3-11. The consolidation pressure must be between 69 kPa and 276 kPa

The effective stress strength parameters, c' and ϕ' , were obtained from stress path plots by subjecting the values of \hat{q}_f and \hat{p}_f' for the given water contents and dry densities to simple linear regression analysis. The \hat{p}_f' values were utilized as the independent variable and the \hat{q}_f values as the dependent variable. Examples of the \hat{p}_f' versus \hat{q}_f failure lines are shown in Figures 3-36 and 3-37. The plots for the remainder of the compaction conditions are shown in Figures C1 to C21. The effective stress strength parameters from the stress path plots were determined from equations as:

$$\hat{q}_f' = a' + p_f' \tan \alpha' = c' \cos \phi' + p_f' \sin \phi' \quad (3-19)$$

Table 3-20 lists the basic independent variables utilized in the analysis of the effective stress strength parameters (c' and ϕ') for field compacted soil. The as-compacted dry densities were determined by the field dry density prediction models of Equations 3-6 and 3-8 for the given moisture contents. The most satisfactory regression models de-



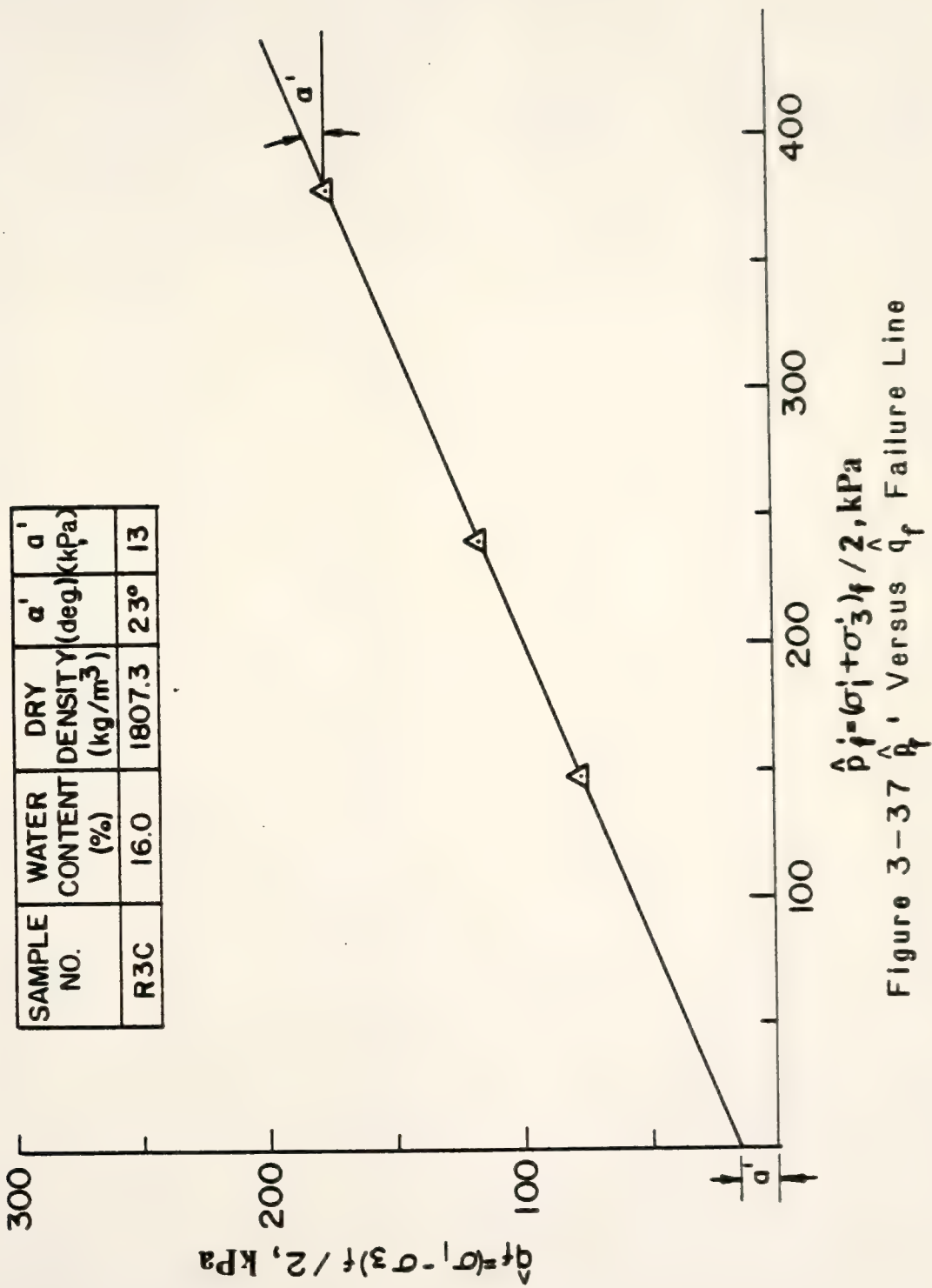


TABLE 3-20 Basic Compaction Variables for the Effective Stress Strength Parameters

Test No.	Estimated Effective Stress Friction Angle, ϕ' (degree)	Estimated Effective Strength Intercept, c' (kPa)	Compaction Moisture Content, w (%)	As-Compacted Dry Density, ρ_d (kg/m^3)	Initial Void Ratio (e_0)
R1A	27.8	0.0	12	1733.0	0.61
R2A	26.4	6.7	14	1753.0	0.591
R3A	24.5	18.7	16	1761.9	0.583
R4A	21.3	35.4	18	1762.2	0.583
R5A	16.1	57.3	20	1756.0	0.508
R2B	27.8	2.3	14	1794.9	0.554
R3B	25.1	16.6	16	1784.7	0.563
R4B	21.3	32.2	18	1767.6	0.578
R5B	21.3	61.2	20	1744.7	0.598
R3C	25.1	14.4	16	1807.3	0.582
R4C	21.3	35.4	18	1763.3	0.582
R5C	14.4	62.0	20	1716.4	0.625
C2A	27.1	2.8	14	1786.0	0.561
C3A	24.5	16.5	16	1762.0	0.583
C4A	20.7	36.4	18	1754.0	0.59
C5A	16.7	55.3	20	1756.0	0.588
C2B	26.4	5.6	14	1827.0	0.526
C3B	24.5	13.7	16	1780.0	0.567
C4B	22.0	32.3	18	1778.0	0.568
C5B	15.5	57.1	20	1760.0	0.585
C3C	24.5	16.5	16	1796.0	0.553
C4C	21.3	34.4	18	1778.0	0.568
C5C	15.5	57.1	20	1762.0	0.583

veloped during statistical analyses of c' and ϕ' are given below:

- (a) Field prediction model for the parameter of c'

$$\hat{c}' = -102.79 + 11.208w + 14.55w \cdot \log e_o \quad (3-20)$$

- (b) Field prediction model for the parameter of ϕ'

$$\hat{\phi}' = 47.56 - 2.112w - 2.625w \cdot \log e_o \quad (3-21)$$

where

\hat{c}' = estimated value of the effective stress

strength intercept, kPa

$\hat{\phi}'$ = estimated value of the effective stress

strength angle, degree

w = compaction moisture content, %

e_o = initial void ratio

The statistical data for these two models are all satisfactory and are shown in Table 3-21. The coefficients of determination of 0.97 and 0.89 indicate that almost all of the variation in the dependent variables are explained by the variables in the models. The residuals also test satisfactorily as being normally distributed.

Figure 3-38 shows that for a constant value of initial void ratio (or dry density), an increase in moisture content produces a decrease in $\hat{\phi}'$ and an increase in \hat{c}' . DiBernardo (1979) and Lin (1981) showed that for a given compaction pressure, an increase in the moisture content resulted in a lower value of compactive prestress. The lower value of compactive prestress gives the lower value of OCR ($\frac{\hat{P}_s}{\sigma'_c}$) and produces the higher pore pressure. With reference to the Mohr-Coulomb failure envelope, when the pore pressure increases, the effective stresses will decrease, and the stress circles will shift toward the origin; this should produce higher \hat{c}' and lower $\hat{\phi}'$ values.

Figure 3-38 shows for a given moisture content that a decrease in

TABLE 3-21 Statistical Data of the Prediction Model for Effective Stress Strength Parameters

Statistical Criteria	$\hat{c}' = -102.79 + 11.21 w + 14.55 w \cdot \log e_0$	$\hat{\phi}' = 47.56 - 2.11 w - 2.63 w \cdot \log e_0$
R^2	0.97	0.89
R_a^2	0.97	0.88
Overall F-Test	340.93	81.9
<u>95% Confidence Interval for Regression Coefficient</u>		
w	9.72, 12.7	-2.7, -1.53
w log e_0	7.46, 21.64	-5.4, 0.13

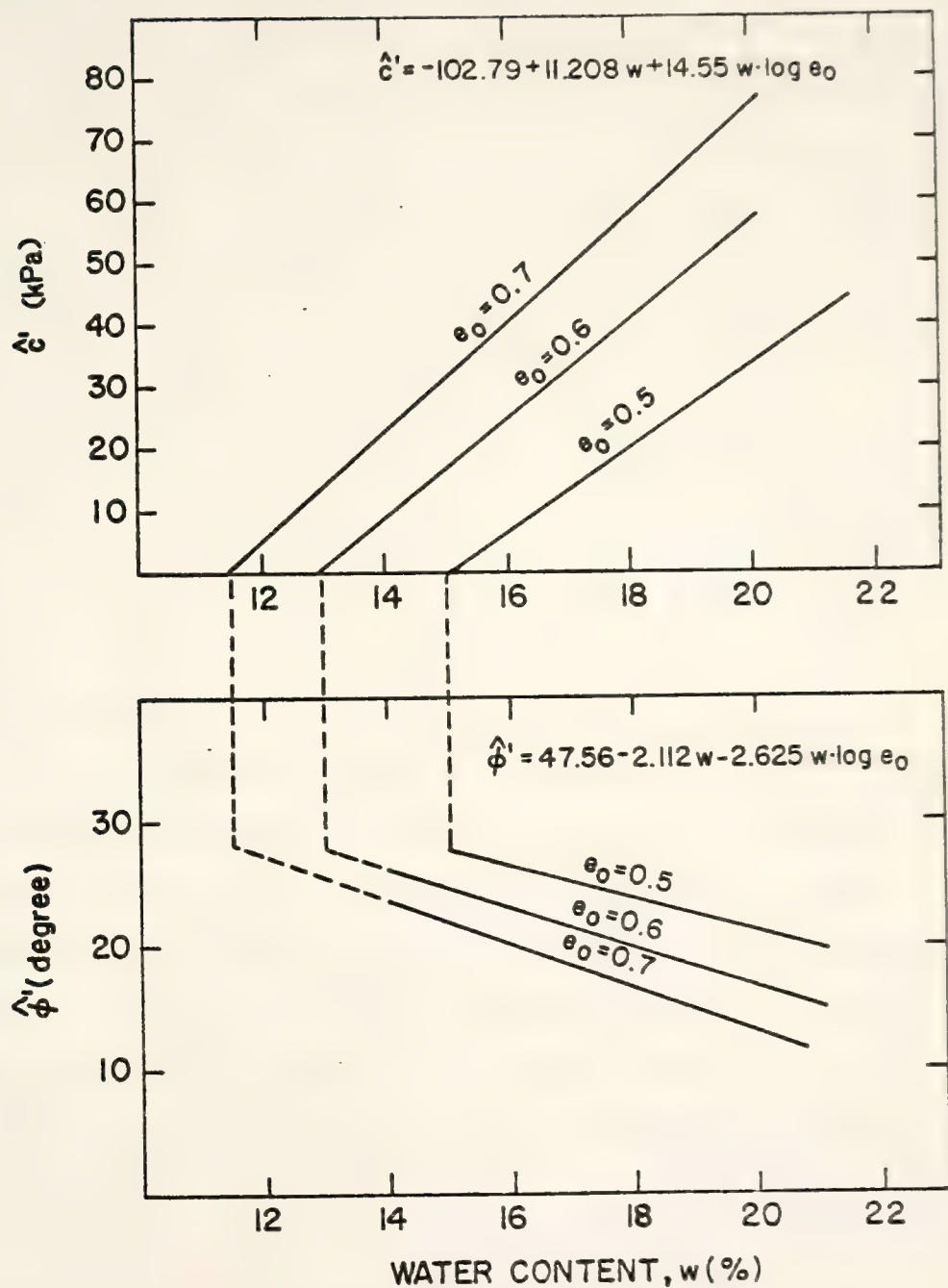


Figure 3-38 Prediction of Field Effective Stress Strength Parameters, \hat{c}' and $\hat{\phi}'$

initial void ratio produces an increase in $\hat{\phi}'$ and a decrease in \hat{c}' . For a constant compacted moisture content, a lower void ratio implies a higher compactive prestress and a higher value of OCR. The lower value of initial void ratio produces higher effective compressive strengths ($2q'_f$). The higher value of OCR produces lower pore pressure. Again, with reference to the Mohr-Coulomb failure envelope, when the pore pressure decreases, the stress circles will shift away from the origin. This produces lower values of \hat{c}' , and the higher effective compressive strength produces higher values of $\hat{\phi}'$.

For laboratory compacted soil, the c' values were small and in the range of 7 to 24 kPa (1 to 3 psi). The values of ϕ' were rather close to each other. Johnson (1978) proposed that the \hat{c}' value be selected at a rough lower bound, e.g., 10 kPa, and $\hat{\phi}' = 20.1^\circ \pm 1.3^\circ$ for all conditions.

All field regression models are summarized in Table 3-22. Once the field initial compaction conditions, such as water content, initial void ratio, energy level, and confining pressure are known, these regression equations can be applied to determine all the dependent variables. For the same initial compaction conditions, the Rascal models will give higher values of as-compacted strength and larger volumetric strains due to saturation and consolidation than the Caterpillar models.

3-3 Application of Results

The initial conditions of compaction may be expressed in terms of the initial void ratio, initial degree of saturation, compaction moisture content, and the specific gravity of the soil. The relationship

TABLE 3-22 Regression Results

Compactor Type	Dependent Variable	Regression Model	R ²
Both Types (Field)	Dry Density (all moisture) Dry Density (wet-of-optimum)	$\hat{\rho}_d = 1929.68 + 211.6\sqrt{P_c/w} + 0.0016\sqrt{P_c \cdot w^2}$ $- 0.0096 w \cdot P_c - 6816.83/w$ $\hat{\rho}_d = 1273.05 + 8797.21 w$	0.74 0.88
Rascal	As-Compacted Strength	$\hat{q}_c = -1310.75 - 117.4 w + 0.23 w^2 + 0.08 \rho_d \cdot w$ $+ 122.77 (1 - S_i/100) \sqrt{\sigma_3} + 1.02 \rho_d \sqrt{S_i/w}$	0.76
Caterpillar		$\hat{q}'_c = -12546.07 + 1432.38 w - 18.76 w^2 - 0.39 \rho_d w$ $+ 114.52 (1 - S_i/100) \sqrt{\sigma_3} + 5.73 \rho_d \sqrt{S_i/w}$	0.75
Both Types (Field)		$\hat{q}_c = -6980.05 + 636.21 w - 8.3 w^2 - 0.155 \rho_d \cdot w$ $+ 112.1 (1 - S_i/100) \cdot \sqrt{\sigma_3} + 3.6 \rho_d \cdot \sqrt{S_i/w}$	0.72
Rascal	Percent Volume Change Due to Saturation and Consolidation	$(\frac{\Delta V}{V})\% = -4.31 + 2.41 e_0 \cdot \sqrt{\sigma'_c} - 0.168 \sqrt{P_s}$ $- 0.286 \times 10^{-2} \cdot w \cdot \sigma'_c$	0.81
Caterpillar		$(\frac{\Delta V}{V})\% = 2.81 + 2.5 \cdot e_0 \sqrt{\sigma'_c} - 0.52 \sqrt{P_s}$ $- 0.25 \times 10^{-2} \cdot w \cdot \sigma'_c$	0.60
Both Types (Field)		$(\frac{\Delta V}{V})\% = -0.166 + 2.47 e_0 \sqrt{\sigma'_c} - 0.365 \sqrt{P_s}$ $- 0.00263 \cdot w \cdot \sigma'_c$	0.72

TABLE 3-22 (Continued)

Compactor Type	Dependent Variable	Regression Model	R ²
Rascal	Skempton's A Parameter at Failure	$\hat{A}_f = 1.92 - 0.55/e_0 - 0.368 \times 10^{-4} \rho_d \cdot \sqrt{S_i}$ - 0.365 log (OCR)	0.60
Caterpillar		$\hat{A}_f = 2.42 - 0.95/e_0 - 0.192 \times 10^{-4} \rho_d \cdot \sqrt{S_i}$ - 0.416 log (OCR)	0.72
Both Types (Field)	Effective Stress Strength Intercept	$\hat{A}_f = 2.05 - 0.73/e_0 - 0.232 \times 10^{-4} \rho_d \sqrt{S_i}$ - 0.382 log (OCR)	0.63
Both Types (Field)		$\hat{c}' = -102.79 + 11.208 w + 14.55 w \cdot \log e_0$	0.97
Both Types (Field)	Effective Stress Strength Angle	$\hat{\phi}' = 47.56 - 2.112 w - 2.625 w \cdot \log e_0$	0.89

between these initial compactive conditions is:

$$S_i e_o = w \cdot G_s \quad (3-22)$$

where

S_i = initial degree of saturation

e_o = initial void ratio

w = compaction moisture content

G_s = specific gravity of the soil

The as-compacted dry density can be expressed in terms of the initial void ratio, as shown by Equation 3-11. From Equation 3-22, the initial void ratio decreases (dry density increases), with decreasing moisture content for a given initial degree of saturation. Compaction at a higher energy level on the dry side results in a higher dry density (lower initial void ratio) at a given compaction moisture content. From Figure 2-2 it can be seen that the range of moisture contents for high compaction energy levels is much lower than for low compaction energy levels. Two different soils compacted at the same energy level and compaction moisture content produce different dry densities. From Figure 2-2 it can be seen that the test pad soil with lower plasticity and a higher density than the laboratory soil with higher plasticity at the same energy level. Thus, the range of compaction moisture contents depends on the level of compaction energy and the plasticity of the soil.

Two methods of prediction are presented herein for prediction of the laboratory control curve of a second soil from the known control curve of a first. Both methods are based on the same concepts.

A. Graphic Superposition Method

Step 1. Translate the dry density-moisture content curve from one soil to another soil at the same laboratory compactive energy

level.

From Figure 2-2, the optimum moisture contents of the soil compacted in the laboratory and the test pad soil are 22% and 15.5% at the same energy level (Standard Proctor). The ratio of these two optimum moisture contents is 0.7. According to Equation 3-22, for a given initial degree of saturation and a given specific gravity, the ratio of the initial void ratios of both soils also equals 0.7. Therefore the regression curves for one soil compacted in the laboratory can be translated to a second soil of differing plasticity (also compacted in the laboratory and at the same energy level) by applying a factor of 0.7 to the compaction water content and initial void ratio. This is not a translation between laboratory and field compaction, but a translation for different soils in laboratory compaction.

Step 2. Applies intuitive judgments to the translated curves for the field soil to account for the variabilities of soil and roller conditions in the field.

B. Statistical Regression Method

Step 1. Get the translation factor due to the difference of soil plasticity. The procedure is the same as Step 1 in Method A. The translation factor of moisture content or initial void ratio for this study is 0.7.

Step 2. Use a statistical method (as shown below) to generate the field compaction curve from laboratory prediction models. Measured field data for field compacted soil is used, the values of which correspond to the translated water contents and initial void ratios.

(a) The wet-of-optimum dry density prediction model

Twelve water contents were selected from within the allowable

range of values, and substituted into Equation 3-5 to generate 12 values of $\hat{\rho}_d$ (laboratory compacted soil). Twelve values of ρ_d (field compacted soil) corresponding to the translated water contents ($0.7 \cdot w_{lab}$) were taken from the field compacted measurements. The statistical regression procedure was then utilized to generate a correlation between the field response ($\hat{\rho}_d$) and the translated laboratory response ($\hat{\rho}_d$).

$$\hat{\rho}_d(\text{field compacted}) = 188.3 + 0.872 \hat{\rho}_d(\text{translated lab compacted}) \quad (3-23)$$

The coefficient of determination (R^2) of 0.88 indicates that almost all of the variation in the dependent variable is explained by the variables in the equation.

(b) The dry-of-optimum dry density prediction model

Because of the scarcity of field compacted samples dry-of-optimum, no correlation between field values and translated laboratory values was possible. Method A is suggested for the prediction of field dry density from translated laboratory dry density data.

The predicted dry density for field compacted and translated laboratory compacted soils both wet and dry of optimum are shown in Figure 4-1.

(c) As-compacted strength prediction model

Seventy-two combinations of water content, dry density, confining pressure, and initial degree of saturation were selected from within the allowable range of values, and substituted into Equation 3-10 to generate 72 values of \hat{q}_c (lab). Seventy-two values of q_c (field) corresponding to the translated water contents and void ratios (which accounts for the soil differences) were taken from the UU data. The

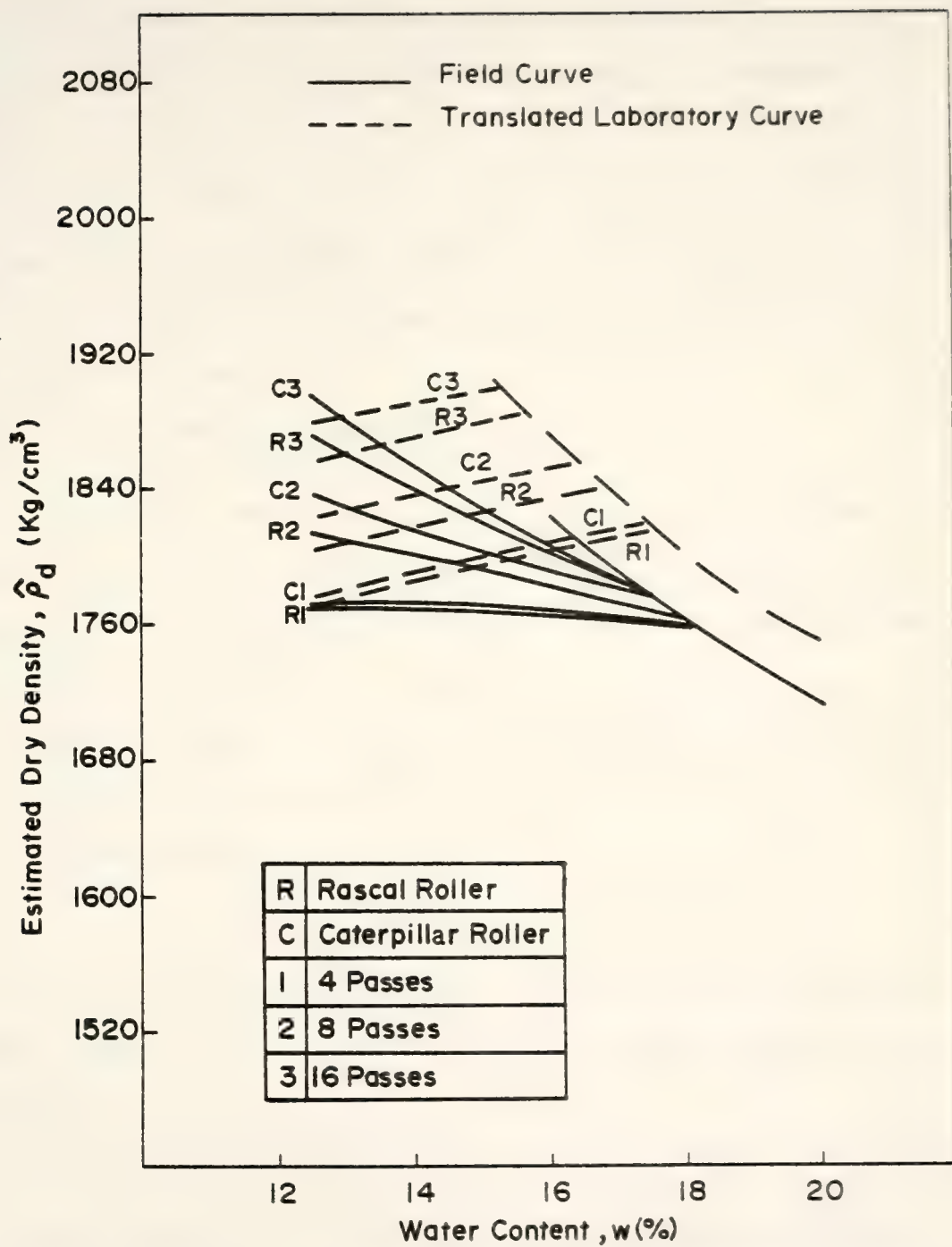


Figure 4-1 The Predicted Dry Density for Field Compacted and Translated Laboratory Compacted Soils.

2/2

correlation between the field response \hat{q}_c and laboratory response \hat{q}_c then was generated by statistical regression analyses procedures as below;

$$\hat{q}_c \text{ (field)} = 174.92 + 0.916 \hat{q}_c \text{ (lab)} \quad (3-24)$$

The coefficient of determination (R^2) of 0.84 indicates that almost all of the variation in the dependent variable is explained by the variables in the equation.

(d) Prediction model for volume change due to saturation and consolidation

Sixty combinations of water content, initial void ratio, confining pressure, and compaction pressure were selected to substitute into Equation 3-14, generating sixty values of $\hat{\Delta V}/V_o$ (lab). The same number of values of $\hat{\Delta V}/V_o$ (field) for translated values of w and e_o were taken from the CIU test data. The correlation between the field response $\hat{\Delta V}/V_o$ and laboratory response $\hat{\Delta V}/V_o$ was found by the statistical regression procedures to be:

$$\hat{\Delta V}/V_o \text{ (field)} = 1.886 + 0.495 \cdot \hat{\Delta V}/V_o \text{ (lab)} \quad (3-25)$$

The coefficient of determination (R^2) of 0.81 indicates that almost all of the variation in the dependent variable is explained by the variables in the equation.

(e) Prediction model for Skempton's A parameter at failure

The correlation between the field compactive prestress (\hat{P}_s) and translated laboratory compactive prestress was determined first by statistical regression procedures as follows:

$$\hat{P}_s \text{ (correct)} = -303.67 + 1.323 \hat{P}_s \text{ (translated lab)} \\ (R^2 = 0.91) \quad (3-26)$$

Fifty-five combinations of water content, initial void ratio, confining pressure, and corrected estimated compactive prestress were selected to substitute into Equation 3-16, generating fifty-five values of \hat{A}_f (lab). The same number of values of \hat{A}_f (field) for translated values of w and e_o were taken from the CIU test data. The correlation between the field response \hat{A}_f and laboratory response \hat{A}_f was generated by statistical regression analyses procedures as below:

$$\hat{A}_f(\text{field}) = 0.223 + 0.66 \hat{A}_f(\text{lab}) \quad (3-27)$$

The coefficient of determination (R^2) of 0.69 is low but acceptable.

(f) Prediction model for the effective stress parameters, c' and ϕ'

Since the c' and ϕ' values for laboratory compacted soil and field compacted soil were very close to each other, no correlations between the field responses and laboratory responses were possible. The field responses \hat{c}' , $\hat{\phi}'$ can best be estimated by substituting the estimated initial field compacted conditions into Equations 3-20 and 3-21.

(g) Example problem

Given -- in a laboratory Standard Proctor test:

- 1) Dry density-moisture content curves for both test pad and laboratory soils as shown in Figure 2-2;
- 2) $G_s = 2.79$, $w = 24\%$.

Required--

- (i) Estimate the field dry density for roller foot compaction pressure (P_c) = 800 kPa.
- (ii) Estimate the field as-compacted strength and its corresponding water content and dry density at a depth of cover of 7.0 m in a compacted embankment.

(iii) Estimate the field volumetric strain at 7.0 m due to saturation and consolidation.

(iv) Estimate the value of A_f at 7.0 m caused by undrained shear of this saturated and consolidated soil.

For (i), the translation ratio is 0.7 ($= 15.5\%/22\%$). The laboratory dry density can be determined from the laboratory prediction model, Equation 3-5, as $\hat{\rho}_d$ (lab soil) = 1610.3 kg/m^3 ($e_o = 0.73$). The translated laboratory compacted dry density is 1845.6 kg/m^3 ($e_o = 0.7 \times 0.73 = 0.511$). From Equation 3-23, the field dry density can be calculated as 1798.0 kg/m^3 . The corresponding field water content is 17% ($0.7 \times 24\%$).

For (ii), the initial degree of saturation (S_i) can be obtained from Equation 3-22. $S_i = w \cdot G_s/e_o = 92\%$. The laboratory as-compacted strength can be determined from the laboratory prediction model, Equation 3-10, as \hat{q}_c (lab) = 281.2 kPa . The field as-compacted strength from Equation 3-24, is 432.4 kPa which corresponds to field compactive conditions of $w = 17\%$ (0.7×24), $e_o = 0.51$ (0.7×0.73), $\sigma_c = 138 \text{ kPa}$, and $S_i = 92\%$.

For (iii), the laboratory volumetric strain due to saturation and consolidation can be determined from the laboratory prediction model, Equation 3-14, as $\Delta V/V_o$ (lab) = 1.93% . The field volumetric strain due to saturation and consolidation from Equation 3-25, is 2.84% , which corresponds to the field compactive conditions of $w = 17\%$, $e_o = 0.51$, $S_i = 92\%$, $\sigma'_c = 138 \text{ kPa}$ and $P_c = 800 \text{ kPa}$.

For (iv), the value of A_f for laboratory compacted soil can be determined by Equation 3-16, or A_f (lab) = 0.21 . The value of A_f for field compacted soil from Equation 3-27 is 0.36 which corre-

sponds to the field compactive conditions of $w = 17\%$, $e_o = 0.51$, $S_i = 92\%$, $\sigma'_c = 138 \text{ kPa}$ and $P_c = 800 \text{ kPa}$.

This method also can be applied starting with given field initial conditions. The laboratory translated water content and void ratio can be obtained by using the reciprocal of the translation factor, and these can be inserted in the laboratory prediction model. The field prediction dependent variables can then be determined by using appropriate equation, viz., 3-23, 3-24, 3-25, or 3-27.

4- CONCLUSIONS AND RECOMMENDATIONS

4-1 Conclusions

The as-compacted and saturated undrained strengths of a field compacted medium plastic St. Croix clay have been examined in this study. The statistical predictions accomplished in this study were coupled with those from preceding laboratory studies (Weitzel, 1979 and Johnson, 1979) to produce predictions of field compacted responses from laboratory compacted behavior.

From the UU and CIU triaxial tests performed on samples of field compacted, medium plastic St. Croix clay, the following conclusions may be drawn:

- (1) The soil used in the field test pads was of lower plasticity than that used in the laboratory studies. The moisture-density curves are displaced in an expected fashion.
- (2) The magnitude of field compacted dry density is influenced by both compaction water content and compactive effort for dry-of-optimum moisture contents.
- (3) The dry density of wet-of-optimum field compacted soil is a function of water content but not of compactive energy.
- (4) The as-compacted strength (q_c) of the field compacted soil increases with increasing confining pressure and dry density, and with decreasing water content until the samples reaches near-saturation. This parallels the laboratory results of Weitzel (1979) (Figure 3-29).

- (5) The volume change occurring during shear for as-compacted samples are significant, especially for samples of low water content and low dry density. The volumetric strain at failure decreases with increasing OCR (\hat{P}_s/σ_c'). The volumetric strain due to application of the confining pressure decreases to a minimum with water contents about the optimum value (Figures 3-8, 3-9, and 3-10).
- (6) The volume change due to saturation and consolidation ($\Delta V/V_o$, %) increases (more net compression or less net swell) with increasing confining pressure and decreasing water content for a given dry density. An increase in as-compacted dry density for constant values of initial degree of saturation and consolidation pressure produces a decrease in volume change ($\Delta V/V_o$, %) due to saturation and consolidation (Figures 3-15 and 3-30).
- (7) Lower confining pressures and higher estimated compactive prestress for a given water content and dry density produces a greater swell potential for the field compacted St. Croix clay (Figure 3-30).
- (8) Skempton's A parameter at failure is a function of initial void ratio and OCR (\hat{P}_s/σ_c'). \hat{A}_f decreases as OCR increases for constant values of initial void ratio (or dry density) and degree of saturation (Figures 3-32 and 3-34).
- (9) An increase in e_o for constant values of S_i and OCR produces an increase in \hat{A}_f (Figure 3-32).
- (10) A decrease in S_i for constant e_o and OCR produces an increase in \hat{A}_f (Figure 3-34).

- (11) The predicted effective stress strength parameters, c' and ϕ' , are function of compaction water content and initial void ratio. For a constant value of initial void ratio (or dry density), an increase in water content produces a decrease in ϕ' and an increase in c' (Figure 3-38).
- (12) Statistically valid prediction models for dry density, as-compacted strength, percent volume change due to saturation and consolidation, Skempton's A parameter at failure, and effective stress strength parameters c' and ϕ' were formulated for field compacted St. Croix clay (Table 3-22).
- (13) The prediction equations developed herein are generally similar to those of an earlier study for laboratory compacted St. Croix clay (Weitzel, 1979 and Johnson, 1979).
- (14) Two methods were developed for the predictions of field compacted relationships from laboratory tests. The first step is to translate the laboratory compacted relations to those appropriate for the soil involved in the field compaction. The translation factor is the ratio of Standard Proctor optimum moisture content values.
- (15) Applying the translation factor allows the selection of appropriate values for the statistical development of Equations 3-23, 3-24, 3-25, and 3-27. These equations predict the field compacted dry density at wet-of-optimum, the field compacted as-compacted strength, the field compacted volume change due to saturation and consolidation, and

Skempton's A parameter at failure, all from testing of laboratory compacted soil. A graphic superposition method is suggested for the prediction of field dry density at dry-of-optimum, from laboratory tests.

4-2 Recommendations for Future Research

- (1) If sample volume changes in the triaxial test are to be measured by the volume of the displaced cell water, improvements in the current triaxial design are required to minimize leakage.
- (2) A study of the K_o values for field compacted samples is needed. Strength responses for K_o consolidated samples can then be determined, and compared with the isotropic consolidation behavior.
- (3) Improvements in the present methods of predicting field compactive energies are needed for commonly used rollers. Correlations between field compactive energy, laboratory compactive energy, and dry density can then be developed for typical soils.
- (4) One additional clay should be experimentally studied by procedure similar to those presented herein. A material of lacustrine origin is recommended.
- (5) A simplified compacted clay model can be formulated from these and similar studies, and this should be accomplished. This model will have somewhat reduced credentials with respect to the statistical ones reported above, but will be more simple and acceptable in engineering practice.

BIBLIOGRAPHY

BIBLIOGRAPHY

Abeysekera, R. A. (1978), "Stress Deformation and Strength Characteristics of a Compacted Shale", Ph.D. Thesis, Purdue University, West Lafayette, Indiana, May, 420 pp. (Also Joint Highway Research Project Report No. 77-24).

Abeysekera, R. A., Lovell, C. W. and Wood, L. E. (1978), "Stress-Deformation and Strength Characteristics of a Compacted Shale", Papers of the Conference on Clay Fills, Institution of Civil Engineers, London, England, Nov., pp. 1-14.

Abeysekera, R. A. and Lovell, C. W. (1981), "Volume Changes in Compacted Clays and Shales Upon Saturation", Transportation Research Record 790, pp. 67-73.

Ahmed, S., Lovell, C. W. and Diamond, S. (1974), "Pore Size and Strength of Compacted Clay", Journal of the Geotechnical Engineering Division, ASCE, Vol. 100, No. GT4, pp. 407-425.

Aitchison, G. D. (1965), Panel Discussion in Session 2, Proceedings, 6th International Conference on Soil Mechanics and Foundation Engineering, Montreal, Vol. III, pp. 318-321.

Aitchison, G. E. (1973), Part 2 of the General Report for Main Session 4, Proceedings, 8th International Conference on Soil Mechanics and Foundation Engineering, Moscow, Vol. III, pp. 161-190.

Akai, K. (1963), "The Effect of Back Pressure on the Consolidation and the Shear of an Undisturbed Saturated Clay", Proceedings of the Second Asian Regional Conference on Soil Mechanics and Foundation Engineering, Vol. 1, Japanese Society of Soil Mechanics and Foundation Engineering, Tokyo, pp. 105-107.

Allam, M. M., and Sridharan, A. (1980), "Influence of the Back Pressure Technique on the Shear Strength of Soils", Geotechnical Testing Journal, Vol. 3, No. 1, March, pp. 35-40.

Barden, L., Madedor, A. , and Sides, G. R. (1969), "Volume Change Characteristics of Unsaturated Clay", Journal of the Soil Mechanics and Foundations Division, ASCE, Vol. 95, No. SM1, Proc. Paper 6338, Jan., pp. 33-52.

Barden, L, and Sides, G. R. (1970), "Engineering Behavior and Structure of Compacted Clay", Journal of Soil Mechanics and Foundations Division, ASCE, Vol. 96, No. SM4, July, pp. 1171-1200.

Bhasin, R. N. (1975), "Pore Size Distribution of Compacted Soils After Critical Region Drying", Ph.D. Thesis, Purdue University, West Lafayette, Indiana, May, 222 pp. (Also Joint Highway Research Project Report No. 75-3)

Bishop, A. W., Alpan, I., Blight, G. E. and Donald, I. B. (1960), "Factors Controlling the Strength of Partly Saturated Cohesive Soils", Research Conference on Shear Strength of Cohesive Soils, ASCE, Boulder, Colorado, pp. 503-532.

Bishop, A. W. and Bjerrum, L. (1960), "The Relevance of the Triaxial Test to the Solution of Stability Problems", Research Conference on Shear Strength of Cohesive Soils, ASCE, Boulder, Colorado, pp. 437-501.

Bishop, A. W. and Henkel, D. J. (1962), The Measurement of Soil Properties in the Triaxial Test, 2nd edition, Edward Arnold, London, 228 pp.

Bjerrum, L. and Simons, N. E. (1960), "Comparison of Shear Strength Characteristics of Normally Consolidated Clays", Research Conference on Shear Strength of Cohesive Soils, ASCE, Boulder, Colorado, pp. 711-762.

Black, D. K. and Lee, K. L. (1973), "Saturating Laboratory Samples by Back Pressure", Journal of the Soil Mechanics and Foundation Division, ASCE, Vol. 99, No. SM1, pp. 75-93.

Blight, G. E. (1963), "The Effect of Non-Uniform Pore Pressure on Laboratory Measurements of the Shear Strength of Soils", Laboratory Shear Testing of Soils, STP No. 361, American Society for Testing and Materials, pp. 173-184.

Brand, E. W. (1975), "Back Pressure Effects on the Undrained Strength Characteristics of Soft Clay", Soils and Foundations, Vol. 15, No. 2, pp. 1-16.

Burland, J. B. (1964), "Effective Stresses in Partly Saturated Soils", Correspondence, Geotechnique, Vol. 14, No. 1, pp. 64-68.

Casagrande, A. and Hirschfeld, R. C. (1960), "First Progress Report on Investigation of Stress-Deformation and Strength Characteristics of Compacted Clays", Harvard Soil Mechanics Series, No. 61, Cambridge, Massachusetts, 45 pp.

Casagrande, A. and Hirschfeld, R. C. (1962), "Second Progress Report on Investigation of Stress-Deformation and Strength Characteristics of Compacted Clays", Harvard Soil Mechanics Series, No. 65, Cambridge, Massachusetts, 39 pp.

Casagrande, A. and Poulos, S. J. (1964), "Fourth Report on Investigation of Stress-Deformation and Strength Characteristics of Compacted Clays", Harvard Soil Mechanics Series, No. 74, Cambridge, Massachusetts, 82 pp.

Chan, C. K. and Rivard, P. J. (1963), "The Effect of Test Techniques on the Shear Strength of Western Canadian Clays", Laboratory Shear Testing of Soils, STP No. 361, American Society for Testing and Materials, pp. 492-500.

Chan, C. K. and Duncan, J. M. (1967), "A New Device for Measuring Volume Changes and Pressures in Triaxial Tests on Soils", Materials Research and Standards, Vol. 7, No. 7, pp. 312-314.

Channey, R. C., Stevens, E. and Sheth, N. (1979), "Suggested Test Method for Determination of Degree of Saturation of Soil Samples by B Value Measurement", Geotechnical Testing Journal, Vol. 2, No. 3, Sept., pp. 158-162.

Coleman, J. D. (1962), "Stress-Strain Relations for Partly Saturated Soil", Correspondence to Geotechnique, Vol. 12, No. 4, pp. 348-350.

Conlin, M. F. (1972), "Shearing Properties of Compacted Specimens of Taylor Marl Clay as Determined in an Unconsolidated-Undrained Triaxial Test", M.S. Thesis, University of Texas, Austin, Texas, 106 pp.

Croney, D., Coleman, J. D. and Black, W. P. M. (1958), "The Movement and Distribution of Water in Soil in Relation to Highway Design and Performance", Highway Research Board, Special Report No. 40, Washington, D. C.

DaCruz, P. T. (1963), "Shear Strength Characteristics of Some Residual Compacted Clays", 2nd Pan-Am Conference on Soil Mechanics and Foundation Engineering, Vol. 1, pp. 73-102.

Diamond, S. (1971), "Microstructure and Pore Structure of Impact Compacted Clays", Clays and Clay Minerals, Vol. 19, pp. 239-249.

DiBernardo, A. (1979), "The Effect of Laboratory Compaction on the Compressibility of a Compacted Highly Plastic Clay", MSCE Thesis, Purdue University, West Lafayette, Indiana, May, 187 pp. (Also Joint Highway Research Project Report No. 79-3)

Essigmann, M. F. (1976), "An Examination of the Variability Resulting from Soil Compaction", MSCE Thesis, Purdue University, West Lafayette, Indiana, August, 108 pp. (Also Joint Highway Research Project Report No. 76-28)

Fredlund, D. G. (1975), "A Diffused Air Volume Indicator for Unsaturated Soils", Canadian Geotechnical Journal, Vol. 12, No. 4, pp. 533-539.

Fredlund, D. G. and Morgenstern, N. R. (1976), "Constitutive Relations for Volume Change in Unsaturated Soils", Canadian Geotechnical Journal, Vol. 13, No. 3, pp. 261-276.

Fredlund, D. G. and Morgenstern, N. R. (1977), "Stress State Variables for Unsaturated Soils", Journal of the Geotechnical Engineering Division, ASCE, Vol. 103, No. GT5, pp. 447-466.

Garcia-Bengochea, I. (1978), "The Relation Between Permeability and Pore Size Distribution of Compacted Clayey Silts", MSCE Thesis, Purdue University, West Lafayette, Indiana, 170 pp. (Also Joint Highway Research Project Report No. 78-4).

Gibson, R. E. and Henkel, D. J. (1954), "Influence of Duration of Tests at Constant Rate of Strain on Measured Drained Strength", Geotechnique, Vol. IV, No. 1, pp. 6-15.

Henkel, D. J. (1956), "The Effect of Overconsolidation on the Behavior of Clays During Shear", Geotechnique, Vol. 6, No. 4, pp. 139-150.

Henkel, D. J. and Sowa, V. A. (1963), "The Influence of Stress History on Stress Paths in Undrained Triaxial Tests on Clay", Laboratory Shear Testing of Soils, STP No. 361, American Society for Testing and Materials, pp. 280-291.

Hilf, J. W. (1956), "An Investigation of Pore Water Pressure in Compacted Cohesive Soils", Technical Memorandum 654, United States Dept. of Interior Bureau of Reclamation, Denver, Colorado.

Hilf, J. W. (1975), "Compacted Fill", Chapter 7 of Foundation Engineering Handbook, edited by H. F. Winterkorn and H. Y. Fang, Van Nostrand-Reinhold Co., New York, pp. 244-311.

Hodek, R. J. (1972), "Mechanism for the Compaction and Response of Kaolinite", Ph.D. Thesis, Purdue University, West Lafayette, Indiana, December 269 pp. (Also Joint Highway Research Project Report No. 72-36).

Hodek, R. J. and Lovell, C. W. (1979), "A New Look at Compaction Processes in Fills", Bulletin of the Association of Engineering Geologists, Vol. CVI, No. 4, Fall, pp. 487-499.

Hodek, R. J. and Lovell, C. W. (1980), "Soil Aggregates and Their Influence on Soil Compaction and Swelling", Transportation Research Record 733, TRB, pp. 94-99.

Hogentogler, C. W. (1936), "Essentials of Soil Compaction", Proceedings of the Highway Research Board, Vol. 16, pp. 309-316.

Holtz, R. D. and Krizek, R. J. (1971), "Effects of Stress Path and Overconsolidation Ratio on the Shear Strength of a Kaolin Clay", Proceedings of the Fifth Regional Conference for Africa on Soil Mechanics and Foundation Engineering, Luanda, Angola, Vol. I, August, pp. 3-17 to 2-35.

Holtz, R. D. and Kovacs, W. D. (1981), An Introduction to Geotechnical Engineering, Prentice-Hall, Inc., 733 pp.

Holtz, W. G. and Gibbs, H. J. (1956), "Engineering Properties of Expansive Clays", Transactions, ASCE, Paper No. 2814, pp. 641-663.

Holtz, W. G. and Ellis, W. (1964), "Comparison of the Shear Strength of Laboratory and Field Compacted Soils", Laboratory Shear Testing of Soils, STP No. 361, American Society for Testing and Materials, pp. 280-291.

Jennings, J. E. and Burland, J. B. (1962), "Limitations of the Use of Effective Stress in Partly Saturated Soils", Geotechnique, Vol. 12, No. 2, pp. 125-144.

Johnson, A. W. and Sallberg, J. R. (1960), "Factors that Influence Field Compaction of Soils and Compaction Characteristics of Field Equipment", Highway Research Board, Bulletin 272, Washington, D. C., 206 pp.

Johnson, J. M. (1979), "The Effect of Laboratory Compaction on the Shear Behavior of a Highly Plastic Clay After Saturation and Consolidation", MSCE Thesis, Purdue University, West Lafayette, Indiana, 271 pp.
(Also Joint Highway Research Project Report No. 79-7)

Ladd, C. C. (1964), "Stress-Strain Behavior of Saturated Clay and Basic Strength Principles", Research Report, R64-17, Department of Civil Engineering, Massachusetts Institute of Technology, April, 70 pp.

Lade, P. V. and Hernandez, S. B. (1977), "Membrane Penetration Effects in Undrained Tests", Proceedings Paper 12758, Journal of the Geotechnical Engineering Division, ASCE, Vol. 103, No. GT2, Feb., pp. 109-125.

Lambe, T. W. (1958), "The Structure of Compacted Clay", Journal of the Soil Mechanics and Foundations Division, ASCE, Vol. 84, No. SM2, pp. 1654-1 to 1654-34.

Lambe, T. W. (1958), "The Engineering Behavior of Compacted Clay", Journal of the Soil Mechanics and Foundations Division, ASCE, Vol. 84, No. SM2, pp. 1655-1 to 1655-35.

Lambe, T. W. (1960), "A Mechanistic Picture of Shear Strength in Clay", Proceedings of Research Conference on Shear Strength of Cohesive Soils, ASCE, Boulder, Colorado, pp. 555-580.

Lambe, T. W. and Whiteman, R. V. (1969), Soil Mechanics, Wiley, New York, 553 pp.

Lee, K. L. and Haley, S. C. (1968), "Strength of Compacted Clay at High Pressure", Journal of the Soil Mechanics and Foundations Division, ASCE, Vol. 94, No. SM6, Nov., pp. 13-3-1332.

Lee, K. L., Morrison, R. A. and Haley, S. C. (1969), "A Note on the Pore Pressure Parameter B", Proceedings Mechanics and Foundation Engineering, Mexico, Vol. 1, pp. 231-238.

Leonards, G. A. (1955), "Strength Characteristics of Compacted Clay", Transactions, ASCE, Vol. 120, Paper No. 2780, pp. 1426-1449.

Leonards, G. A. (1962), "Engineering Properties of Soils", Chapter 4 of Foundation Engineering, edited by G. A. Leonards, McGraw-Hill, New York, pp. 66-240.

Lin, P. S. (1981), "Compressibility of Field Compacted Clay", Ph.D. Thesis, Purdue University, West Lafayette, Indiana, August, 154 pp. (Also Joint Highway Research Project Report No. 81-14)

Lowe, J. and Johnson, T. C. (1960), "Use of Back Pressure to Increase Degree of Saturation of Triaxial Test Specimens", Research Conference on Shear Strength of Cohesive Soils, ASCE, Boulder, Colorado, pp. 819-836.

Lovell, C. W. and Johnson, J. M. (1980), "Shearing Behavior of Compacted Clay After Saturation", Laboratory Shear Strength of Soil, ASTM, STP 740, Sept. 1981, pp. 277-293.

Matyas, E. L. and Radhakrishna, H. S. (1968), "Volume Change Characteristics of Partially Saturated Soils", Geotechnique, London, England, Vol. XVIII, No. 4, Dec., pp. 432-448.

Marsal, R. T. and Resines, J. S. (1960), "Pore Pressure and Volumetric Measurements in Triaxial Compression Tests", Research Conference on Shear Strength of Cohesive Soils, ASCE, Boulder, Colorado, pp. 965-983.

Menzies, B. K. (1975), "A Device for Measuring Volume Change", Geotechnique, Vol. 25, No. 1, pp. 133-134.

MIT (1963), "Engineering Behavior of Partially Saturated Soils", Research Report R63-26, Soil Engineering Division, Publication No. 134, 68 pp.

Mitchell, J. K. (1976), Fundamentals of Soil Behavior, Wiley, New York, 422 pp.

Mitchell, R. J. and Burns, K. N. (1971), "Electronic Measurement of Changes in the Volume of Pore Water During Testing of Soil Samples", Canadian Geotechnical Journal, Vol. 8, No. 2, pp. 341-345.

Neter, J. and Wasserman, W. (1974), Applied Linear Statistical Models, Richard D. Irwin, Inc., Homewood, Illinois, 842 pp.

Nie, N. H., Hall, C. H., Jenkins, J. G., Steinbrenner, K. and Bent, D. H. (1975), Statistical Package for the Social Sciences, 2nd edition, McGraw-Hill, New York, 675 pp.

O'Connor, M. J. and Mitchell, R. J. (1978), "Measuring Total Volumetric Strains During Triaxial Tests on Frozen Soils: A New Approach", Canadian Geotechnical Journal, Vol. 15, No. 1, pp. 47-53.

Olson, R. E. (1963), "Effective Stress Theory of Soil Compaction", Journal of the Soil Mechanics and Foundations Division, ASCE, Vol. 89, No. SM2, pp. 27-45.

Olson, R. E. and Langfelder, L. J. (1965), "Pore Pressures in Unsaturated Soils", Journal of the Soil Mechanics and Foundations Division, ASCE, Vol. 91, No. SM4, pp. 127-150.

Olson, R. E. (1960), "The Migration of Pore Fluid During Shear in Consolidation-Undrained Triaxial Tests", Research Conference on Shear Strength of Cohesive Soils, ASCE, Boulder, Colorado, pp. 1043-1049.

Olson, R. E. and Kiefer, M. L. (1963), "Effect of Lateral Filter Paper Drains on the Triaxial Shear Characteristics of Soils", Laboratory Shear Testing of Soils, STP No. 361, American Society for Testing and Materials, pp. 482-491.

Parcher, J. V. and Lin, P. C. (1965), "Some Swelling Characteristics of Compacted Clays", Journal of the Soil Mechanics and Foundations Division, ASCE, Vol. 91, No. SM3, pp. 1-17.

Peterson, J. L. (1975), "Improving Embankment Design and Performance: Prediction of As-Compacted Field Strength by Laboratory Simulation", Joint Highway Research Project Report No. 75-22, Purdue University, 94 pp.

Perloff, W. H. and Baron, W. (1976), Soil Mechanics, Ronald Press, New York, 745 pp.

Price, J. T. (1978), "Soil Compaction Specification Procedure for Desired Field Strength Response", MSCE Thesis, Purdue University, West Lafayette, Indiana, 151 pp. (Also Joint Highway Research Project Report No. 78-7)

Proctor, R. R. (1933), "Fundamental Principles of Soil Compaction", Engineering News-Record, Vol. III, No. 9, August 31, Sept. 7, 21, and 28. pp. 241-248, pp. 286-289, pp. 348-351, and pp. 372-376.

Reed, M. A., Lovell, C. W., Altschaeffl, A. G., and Wood, L. E. (1979), "Frost Heaving Rate Predicted from Pore-Size Distribution", Canadian Geotechnical Journal, Vol. 16, No. 3, pp. 463-472.

Richardson, A. M. and Whitman, R. V. (1963), "Effect of Strain Rate Upon Undrained Shear Resistance of a Saturated Remolded Fat Clay", Geotechnique, Vol. 13, No. 4, pp. 311-324.

Rowe, P. W. and Barden, L. (1964), "Importance of Free Ends in Triaxial Testing", Journal of the Soil Mechanics and Foundations Division, ASCE, Vol. 90, No. SM1, pp. 1-27.

- Rowlands, G. O. (1972), "Apparatus for Measuring Volume Change Suitable for Automatic Logging", Geotechnique, Vol. 22, No. 3, pp. 525-526.
- Rutledge, P. C. (1947), "Cooperative Triaxial Shear Research Program", Progress Report on Soil Mechanics Fact Finding Survey, Corps of Engineers, U.S. Department of the Army, Waterways Experiment Station, Vicksburg, Mississippi, 155 pp.
- Scott, J. C. (1977), "Examination of the Variability of the Soaked Strength of a Laboratory Compacted Clay", MSCE Thesis, Purdue University, West Lafayette, Indiana, 97 pp. (Also Joint Highway Research Project Report No. 77-8).
- Seed, H. B. and Chan, C. K. (1959), "Structure and Strength Characteristics of Compacted Clays", Journal of the Soil Mechanics and Foundations Division, ASCE, Vol. 85, No. SM5, pp. 87-128.
- Seed, H. B. and Chan, C. K. (1957), "The Thixotropic Characteristics of Compacted Clays", Journal of the Soil Mechanics and Foundations Division, ASCE, Vol. 83, SM4, pp. 1427-1435.
- Seed, H. B., Mitchell, J. K. and Chan, C. K. (1960), "The Strength of Compacted Cohesive Soils", Research Conference on Shear Strength of Cohesive Soils, ASCE, Boulder, Colorado, pp. 877-964.
- Seed, H. B., Woodward, R. J. and Lundgren, R. (1962), "Prediction of Swelling Potential for Compacted Clays", Journal of the Soil Mechanics and Foundations Division, ASCE, Vol. 88, No. SM3, June, pp. 53-87.
- Selig, E. T. (1971), "Unified System for Compactor Performance Specification", Paper No. 710727, Society of Automotive Engineers, September, pp. 1-12.
- Simons, N. E. (1960), "The Effect of Overconsolidation on the Shear Strength Characteristics of an Undisturbed Oslo Clay", Research Conference on the Shear Strength of Cohesive Soils, ASCE, Boulder Colorado, pp. 747-763.
- Skempton, A. W. (1954), "The Pore Pressure Coefficients A and B", Geotechnique, Vol. 4, No. 4, pp. 143-147.
- Sridharan, A. (1968), "Some Studies on the Strength of Partly Saturated Clays", Ph.D. Thesis, Purdue University, West Lafayette, Indiana, 179 pp.
- Sridharan, A., Altschaeffl, A. G. and Diamond, S. (1971), "Pore Size Distribution Studies", Journal of the Soil Mechanics and Foundation Division, ASCE, Vol. 97, No. SM5, pp. 771-786.

APPENDICES

NOTE: The following Appendices are not included in this copy of the Report:

	<u>Pages</u>
Appendix A - Results from UU Test	219-25.
Appendix B - Results from <u>CIU</u> Test	259-290
Appendix C - ϕ'_f versus q_f Failure Lines	291-311

Persons desiring a copy of any or all of the above indicated Appendices may obtain a copy for the cost of duplication upon request to:

Joint Highway Research Project
Civil Engineering Building
Purdue University
West Lafayette, Indiana 47907

Terdich, G. M. (1981), "Prediction and Control of Field Swell Pressure of Compacted Medium Plastic Clay", MSCE Thesis, Purdue University, West Lafayette, Indiana, March, 171 pp. (Also Joint Highway Research Project Report No. 81-4)

Wahls, H. E., Fisher, C. P. and Langfelder, L. J. (1966), "The Compaction of Soil and Rock Materials for Highway Purposes", Report No. FHWA-RD-73-8, Federal Highway Administration, Washington, D. C., 457 pp.

Waterways Experiment Station (1949), "Soil Compaction Investigation: Compaction Studies on Silty Clay", Report No. 2, Tech. Memo. No. 3-271, U.S. Corps of Engineers, Vicksburg, Mississippi, 49 pp.

Weitzel, D. W. (1979), "The Effect of Laboratory Compaction on the Unconsolidation-Undrained Strength Behavior of a Highly Plastic Clay", MSCE Thesis, Purdue University, West Lafayette, Indiana, Sept., 218 pp. (Also Joint Highway Research Project Report No. 79-11)

Whitman, R. V. (1960), "Some Consolidations and Data Regarding the Shear Strength of Clays", Research Conference on the Shear Strength of Cohesive Soils, ASCE, Boulder, Colorado, pp. 581-614.

White, D. M. (1980), "The Fabric of a Medium Plastic Clay Compacted in the Laboratory and in the Field", MSCE Thesis, Purdue University, West Lafayette, Indiana, August, 101 pp. (Also Joint Highway Research Project Report No. 80-10)

Wissa, A. E. (1969), "Pore Pressure Measurement in Saturated Stiff Soils", Journal of the Soil Mechanics and Foundations Division, ASCE, Vol. 95, No. SM4, pp. 1063-1073.

Yoshimi, Y. and Osterberg, J. D. (1963), "Compression of Partially Saturated Cohesive Soils", Journal of the Soil Mechanics and Foundations Division, ASCE, Vol. 89, SM4, pp. 1-23.

APPENDIX D

List of Negative Numbers for Photographs

Figure No.	Negative No.
2-7	81189
2-8	81190
2-9	78492-2
2-13	78289-42A

COVER DESIGN BY ALDO GIORGINI